ORNL/TM-13594

Advanced Industrial Materials (AIM) Program
Office of Industrial Technologies
Energy Efficiency and Renewable Energy
U.S. Department of Energy (DOE)

Advanced Industrial Materials (AIM) Program

Annual Progress Report

FY 1997

Date Published: May 1998

Coordinated by Peter Angelini
Compiled by LSD/Toxicology and Risk Analysis Section
Oak Ridge National Laboratory

Prepared by the Oak Ridge National Laboratory
Oak Ridge, Tennessee 37831
for the U.S. Department of Energy
under contract number DE-AC05-96OR22464

DISCLAIMER

Portions of this document may be illegible electronic image products. Images are produced from the best available original document.

TABLE OF CONTENTS

ADVANCED INTERMETALLICS/METALS AND COMPOSITES (Continued)

NEW MATERIALS AND PROCESSES

NEW MATERIALS AND PROCESSES (Continued)

POLYMERS

INTRODUCTION

Introduction to the Advanced Industrial Materials (AIM) Program
Office of Industrial Technologies
Fiscal Year 1997

C. A. Sorrell, Program Manager

The Advanced Industrial Materials (AIM) Program is a part of the Office of Industrial Technologies (OIT), Energy Efficiency and Renewable Energy, U.S. Department of Energy (DOE). The mission of AIM is to "support development and commercialization of new or improved materials to improve energy efficiency, productivity, product quality, and reduced waste in the major process industries." Program investigators in the DOE National Laboratories are working closely with approximately 100 companies, including 11 partners under Cooperative Research and Development Agreements. Research and development is being performed in a wide variety of materials technologies, including metallic and intermetallic alloys, ceramic and metal matrix composites, polymers, inorganic membrane materials, and coatings.

OIT has embarked on a fundamentally new way of working with industries—the Industries of the Future (IOF) strategy—concentrating on the major process industries that consume about 90% of the energy and generate about 90% of the waste in the industrial sector. These are the aluminum, chemical, forest products, glass, metalcasting, and steel industries. OIT has encouraged and assisted these industries in developing visions of what they will be like 20 or 30 years into the future, defining the drivers, technology needs, and barriers to realization of their visions. These visions provide a framework for development of technology roadmaps and implementation plans, some of which have been completed. OIT then provides cost shared support for research and development of needs identified in the roadmaps and is working with other government agencies to leverage that funding. Since the IOF strategy was undertaken, other industries that serve the six IOFs in a crosscutting way have completed or are working on visions and roadmaps. These include the forging, heat treating, welding, and carbon products industries. These industries are also invited to form partnerships with the IOFs and respond to solicitations for research and development proposals.

The AIM Program supports IOF by conducting research and development on materials to solve problems identified in the roadmaps. This is done by National Laboratory/industry/university teams with the facilities and expertise needed to develop new and improved materials. Each project in the AIM Program has active industrial participation and support.

Assessments of materials needs and opportunities in the process industries are an on-going effort within the program. These assessments are being used for program planning and priority setting, followed by support of work to satisfy those needs. All the industries have identified materials as critical, particularly for high-temperature strength, corrosion resistance, and wear resistance. Also important from the energy efficiency viewpoint are membranes, catalytic membranes, and reactors for separations, both for processing and waste reduction. AIM focuses, therefore, on high-temperature materials, corrosion resistant materials, wear resistant materials, strong polymers, coatings, and membrane materials for industrial applications.

Recently AIM provided funding to designate the Metals Processing Laboratory User Center (MPLUS) at Oak Ridge to solve materials problems for the IOFs. To date, more than 60 projects have been completed or are in progress, with about 20 more potential projects being planned. Industry and university participants are unanimous in their praise and appreciation for MPLUS. An additional benefit to industry is that access to MPLUS also provides access to the other user centers at Oak Ridge. When funding reaches a satisfactory level, the plan is to refer potential users to other National Laboratories, as appropriate, and to provide funds to those Laboratories to work with the users.

This year, FY 1998, two of the projects initiated and supported by AIM are being funded by the Chemical Industry Team. In addition, funding for three AIM projects has been designated for materials for the glass industry. These examples show clearly that project selection in the AIM Program are relevant to the Industries of the Future, and every effort will be made to select and fund projects with a high probability that they will eventually be taken over by the IOF teams in order to ready the technologies for demonstration in industrial environments.

The success of AIM can be best illustrated by a statement made by the Panel on Intermetallic Alloy Development, Committee on Industrial Technology Assessment, National Materials Advisory Board, in their report, *Intermetallic Alloy Development: a Program Evaluation, 1997*. Although the statement was made about only one part of AIM at Oak Ridge, a good case can be made for applying it to the entire Program and to the other participating Laboratories. The quote is: "Work by the ORNL Metals Processing Lab and their technical support of industrial product development have been very important. The AIM Program strategy, the IOF focus, MPLUS, and changes in licensing strategy have established a framework for developing technologies that can be commercially successful."

ADVANCED CERAMICS AND COMPOSITES

HIGH TEMPERATURE PARTICLE FILTRATION TECHNOLOGY

T.M. Besmann
Metals and Ceramics Division
Oak Ridge National Laboratory
P.O. Box 2008, Oak Ridge, Tennessee 37831

C. A. Hall
Dow Corning Corporation
4770 Highway 42 E
Carrolton, Kentucky 41008

INTRODUCTION

Dow Corning Corporation is a market leader in the production of dimethyldichlorosilane (DDS) which is utilized as an intermediate in a wide variety of silicone products. In Carrollton, Kentucky, they currently operate the largest plant of its type for the production of DDS, housing several generations of production streams. The facility could benefit substantially both in process stream efficiency and effluent clean-up from improved high-temperature filtration technology. The current project is therefore designed to assess the applicability of high temperature filter materials developed by various commercial concerns.

TECHNICAL PROGRESS - FY 1997

During this period a furnace system was modified to allow exposure of filter samples to simulated environments in the Dow Corning DDS process (Figure 1). The furnace system and gas delivery system have been built. The mass flow controllers have been calibrated for their respective gas flow rates. The peristaltic pump has been calibrated for proper delivery of liquid. The heating tapes and the primary heating mantle on the water evaporator and their respective controllers have been calibrated. The furnace elements and their respective controllers have been tested and calibrated. The mixed gas has been directed through the heated water evaporator, and the amount of water vapor driven off has been measured and calibrated for the thermal oxidizer simulation. The vacuum system has been checked for leaks. An argon line has been added to the DDS delivery system. The methyl chloride line has been diverted into the DDS flashpot to act as a carrier gas.

In order to prevent the liquid DDS from condensing back out in the exhaust lines, and since we only had one source cylinder of liquid DDS, we fabricated a condensing vessel to collect the liquid DDS on the exhaust end. This reclaimed DDS was then transferred back into the original source cylinder and sent to Dow Corning Corporation for analysis and disposal.

Due to the magnitude of demand for liquid DDS for the planned test matrix, several options and ideas for recycling the used DDS have been discussed with Dow Corning staff. We propose to collect the DDS on the exhaust end and transfer it to the source cylinder once it has been depleted. This recycling of DDS will ensure efficiency in completing the test matrix, especially when we begin to run the long-term, 1000-hour tests. Switching out cylinders, shipping used DDS to Dow Corning Corporation, and waiting on fresh DDS from Dow Corning Corporation proved to be impractical. We plan to extract a sample of the DDS after 100 hours of recycling and send it to Dow Corning Corporation for analysis.

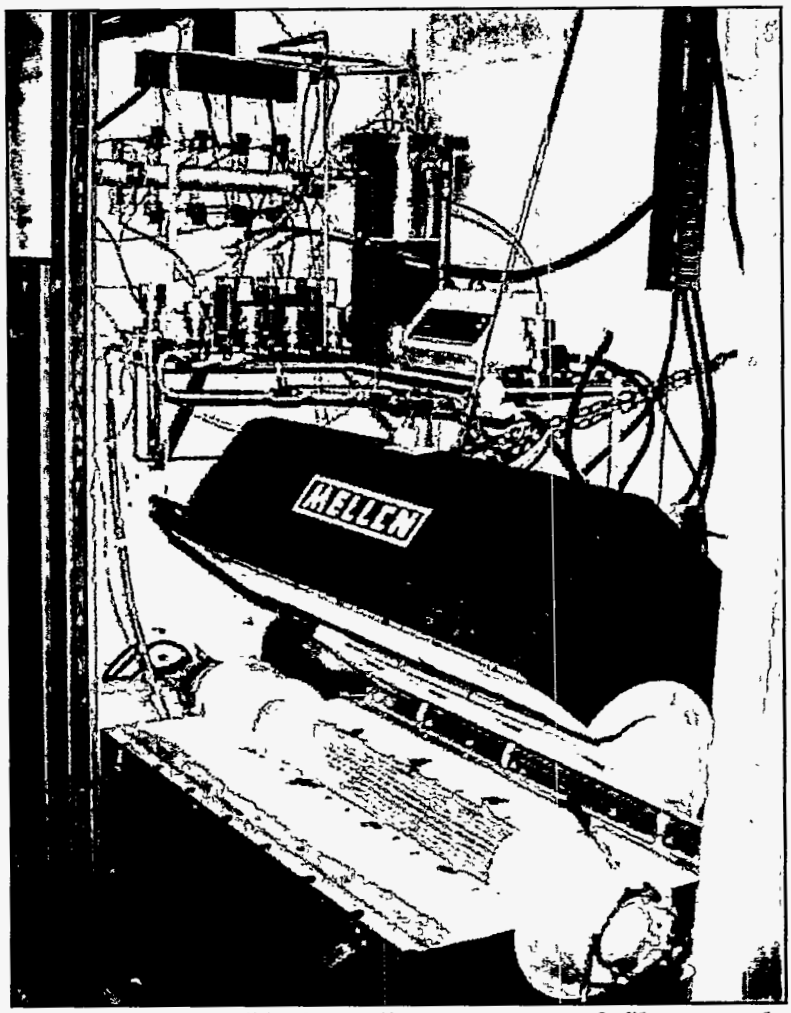

Figure 1. Furnace system modified to allow exposure of filter samples to simulated environments in the Dow Corning DDS process.

We have replaced the stainless steel (SS) end caps with Hastelloy B-2 end caps because of the corrosive nature of the thermal oxidizer tests. Prior to these successful fluidized bed reactor tests, we tried a thermal oxidizer simulation test and found major problems with clogged SS tubing and valves and severe corrosion on the SS end caps. We also redesigned the point of introduction of HCl into the system to help solve the problem.

The two environments consist of the following:

- Fluidized Bed Reactor - 290°C, 50 Vol. % DDS, 50 Vol.% Methylsilane, 1 l/min flow rate

- Thermal Oxidizer - 1000°C, 74 Vol. % N_2, 8 Vol. % O_2, 6 Vol. % CO_2, 10 Vol. % H_2O, 1 Vol. % HCl, 1 l/min flow rate

Samples of filter materials have been acquired from eight companies:

3M Company
DuPont Lanxide Inc.
McDermott Industries
Pall Corporation
Techniweave Inc.
Smart Ceramics Inc.
Amercom Inc.
Blasch Inc.

These companies provided a total of 13 different filter media that included carbon, silicon carbide, oxide ceramics, and metal alloys. All the samples were in the form of rings 2.5 cm in height obtained from candle filter shapes.

Unexposed samples (three) of each material were subjected to a burst test. The test consisted of filling the volume of the ring with elastomer and bursting the sample by applying pressure to the elastome with a plunger in test frame. Displacement was measured via sensors on the circumference of the ring and burst pressure was recorded. The same test was applied to samples that were exposed to the process environments.

The fluidized bed environment testing for a 24h period was completed for all the sample types (three of each). These were then destructively tested as described above. Interestingly, almost none of the samples indicated strength loss as a result of the exposure. Thermochemical computations to determine predicted negative interactions and theoretical recession rates were performed for all the material types with the exception of the metals. The results indicated that the carbon and silicon carbide-based materials were stable in the environment, yet the oxides were indicated to react

extensively. The recession rates were not experienced experimentally; however, likely due to the slow kinetics at the relatively low temperature of 240°C.

INDUSTRIAL INPUT AND TECHNOLOGY TRANSFER

This project is performed as a Cooperative Research and Development Agreement with Dow Corning. Information is shared with Dow Corning regarding the stability of the filters in their environments.

ESTIMATED ENERGY SAVINGS

Potentially 12 trillion Btu/y by the year 2010.

Research performed at the Oak Ridge National Laboratory, sponsored by the U.S. Department of Energy, Assistant Secretary for Energy Efficiency and Renewable Energy, Office of Industrial Technologies, Advanced Industrial Materials Program, and Continuous Fiber Ceramic Composite Program; and Fossil Energy, under contract DE-AC05-96OR22464 with Lockheed Martin Energy Research Corporation.

MEMBRANE SYSTEMS FOR ENERGY EFFICIENT SEPARATION OF LIGHT GASES

D. J. Devlin, T. Archuleta, and R. Barbero
Los Alamos National Laboratory
MS E549, MST-7
PO. Box 1163
Los Alamos New Mexico 87545

N. Calamur and M. Carrera
Amoco Research Center
P.O Box 3011
Naperville, Illinois 60566-7011

INTRODUCTION

Ethylene and propylene are two of the largest commodity chemicals in the United States. and are major building blocks for the petrochemicals industry. These olefins are separated currently by cryogenic distillation which demands extremely low temperatures and high pressures. Over 75 billion pounds of ethylene and propylene are distilled annually in the United States at an estimated energy requirement of 400 trillion BTU's. Non-domestic olefin producers are rapidly constructing state-of-the-art plants. These energy-efficient plants are competing with an aging US. olefins industry in which 75% of the olefins producers are practicing technology that is over twenty years old. New separation opportunities are therefore needed to continually reduce energy consumption and remain competitive. Amoco has been a leader in incorporating new separation technology into its olefins facilities and has been aggressively pursuing non-cryogenic alternatives to light gas separations. The largest area for energy reduction is the cryogenic isolation of the product hydrocarbons from the reaction by-products, methane and hydrogen. This separation requires temperatures as low as -150°F and pressures exceeding 450 psig. This CRADA will focus on developing a capillary condensation process to separate olefinic mixtures from light gas byproducts at temperatures that approach ambient conditions and at pressures less than 250 psig; this technology breakthrough will result in substantial energy savings. The key technical hurdle in the development of this novel separation concept is the precise control of the pore structure of membrane materials. These materials must contain specially-shaped channels in the 20-40A range to provide the driving force necessary to remove the condensed hydrocarbon products. In this project, Amoco is the technology end-user and provides the commercialization opportunity and engineering support. LANL provides the material development expertise that is critical for achieving the desired product separation.

TECHNICAL PROGRESS - FY 1997

Summary

The development of thin films with controlled pore size in the nanometer range is an objective of this program. The separations approach is based on the capillary condensation of hydrocarbons in 1- to 5-nm pores. Figure 1 illustrates one version of the concept.

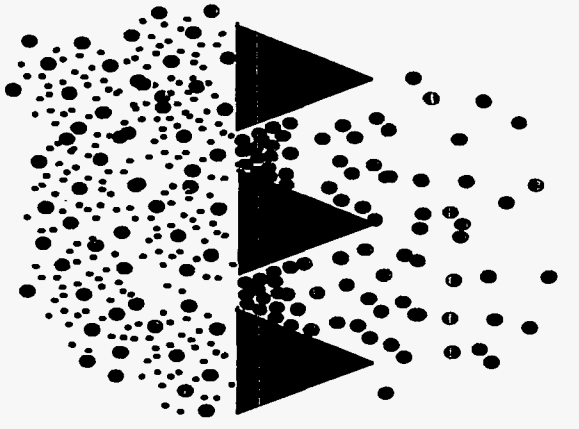

Figure 1. Illustration of capillary condensation of hydrocarbons in a porous substrate.

In this approach a feed consisting of hydrocarbon and hydrogen gas pass over the up stream side of the membrane. Preferential condensation of the hydrocarbon in the pores occurs blocking them with hydrocarbon and restricting flow of hydrogen. The hydrocarbon is transported through tapered pores and evaporated on the large-pore-diameter side leaving a hydrogen rich feed. The actual operating conditions will depend on the pore size, geometry and membrane permeability.

Thin film deposition by evaporation and sputter techniques can result in porous microstructures. This is a problem which effects thin film properties such as electrical conductivity and represents a limitation to these techniques when applied to complex geometric structures. For the development of porous structures this effect can be used to our advantage. These microstructures typically consist of columnar grains separated by porous regions. The structures are dependent on a number of deposition parameters such as substrate temperature, deposition rate, ambient atmosphere, angle of incidence, and energy of depositing flux. Porous structures are generally observed for conditions where the surface mobility of depositing atoms is limited. It is found in many examples that the direction of columnar growth is related to the angle of incidence according to the relationship known as the tangent rule:

direction of columnar growth is related to the angle of incidence according to the relationship known as the tangent rule:

$$\tan(\beta)=1/2\tan(\alpha) \qquad (1)$$

Where α is the angle between the surface normal and the direction of the vapor flux and β is the angle between the surface normal and growth direction, Figure 2. While this exact relation does not always hold, it is universally found that the angle β is less than α. The effect is a consequence of a process known as "self shadowing"(1-3).

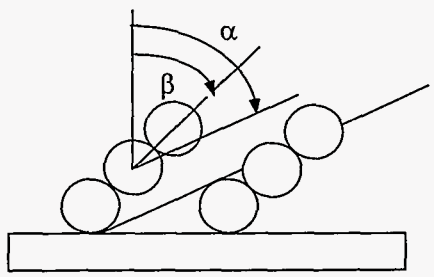

Figure 2. Self shadowing of vapor flux during oblique angle deposition. α is the angle of the incoming beam and β is the direction of columnar grain growth.

This occurs when deposited atoms exposed to the incoming vapor flux shield the substrate or unoccupied sites from direct impingement. When the surface mobility is low such that rearrangement to fill the shielded sites is not possible, columnar grains form.

The dimensions of the pore in simplistic terms is dependent on the incident angle and size of the shadowing adatom, cluster or nuclei. Crystallographic effects can also be important in defining the grain structure. Substrate temperature and therefore mobility will effect nuclei size and rearrangement. Also the energy and distribution of the atomic flux, and degree of thermalization of the beam is important. For carbon materials sputter deposited at room temperature the surface mobility is low.

Simulation studies using SIMBAD^{TM} thin film process simulator are shown in Figure 3.

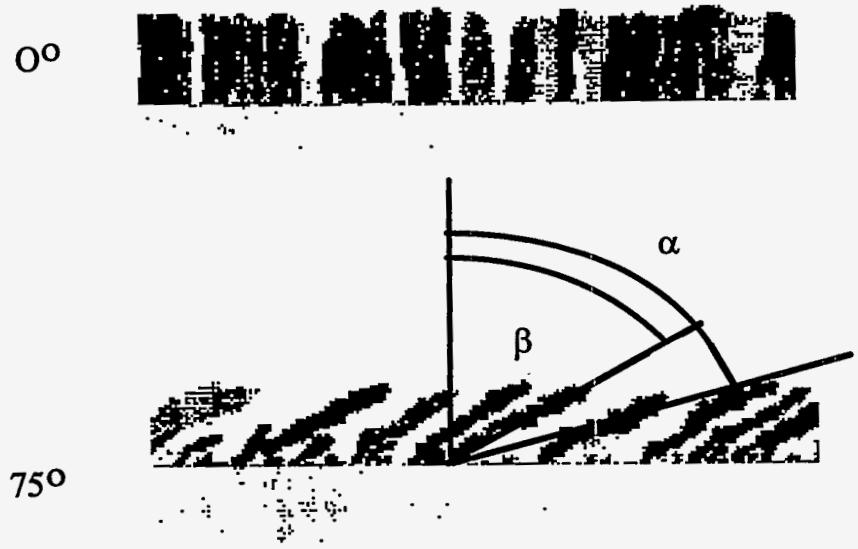

Figure 3. Simulations showing the effect of the angle of incidence of incoming vapor flux on the microstructure of films. a) Deposition at normal incidence producing a dense film. b) Deposition at an oblique angle resulting in a porous film.

When the angle of incidence is 0° (i.e., the flux is normal to the surface) a dense columnar film is produced. At an angle of 75° a porous columnar structure is produce obeying the tangent rule. A comparison of the TEM micrograph of an oblique angle evaporated film to a simulation under similar experimental conditions is shown in Figure 4.

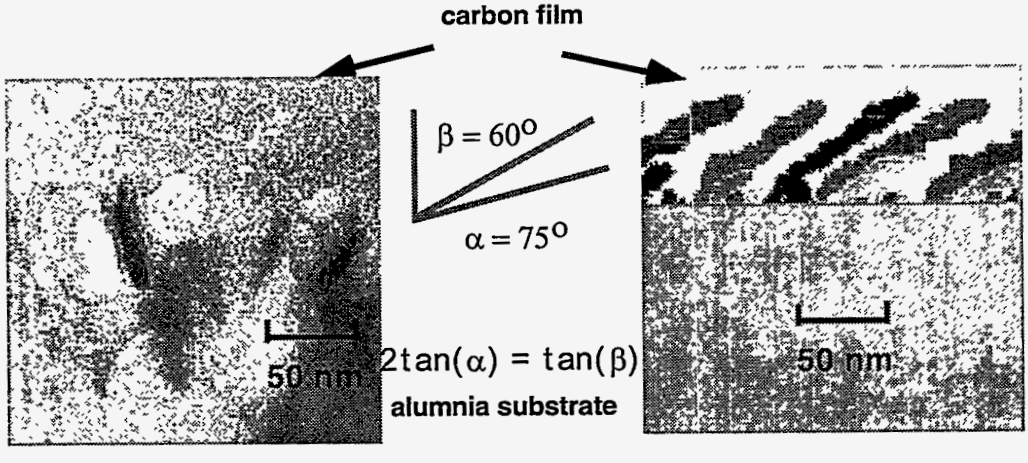

Figure 4. Comparison of thin film deposition process simulation to TEM micrograph of evaporated carbon film.

The simulation predicts the correct angle of the growth of the carbon grains. Furthermore, it is in reasonable agreement with the pore size and grain size observed in the TEM. For the sputtered films we will need to model vapor flux transport from the magnetron source. The code has the capability of modeling angular distributions of flux from a planar magnetron. This is expected to give closer agreement to results obtained for sputter deposited films which do not strictly follow the tangent rule.

Processing

The fine pore side of an alumina Anodisc™ filter provides a suitable substrate for the deposition of carbon films with a 4- to 5-nm pore dimension. Films were deposited with a 10 cm. diameter RF powered magnetron sputter gun in a high vacuum system. The arrangement is illustrated in Figure 5.

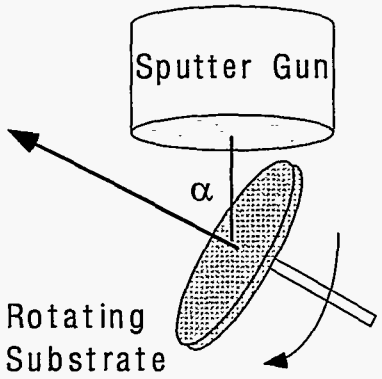

Figure 5. Illustration of the oblique angle deposition arrangement used in this study.

Substrates were set at an angle with respect to the gun and rotated. Rotation of the stage improved uniformity and altered the microstructure. Typical sputter conditions were argon pressures of 0.1 to 0.3 Pa and RF power of 90 watts. Deposition rates were on the order of 100 nm/hr and angle of incidence varied from 0 to 85°. Figure 6 shows a typical microstructure produced by this deposition technique. Pores are on the order of 5 nm as discussed in more detail in previous reports [Advanced Industrial Materials (AIM) Program Annual Progress Report].

Figure 6. TEM micrograph showing the effect of rotating the substrate during deposition at an angle of 85°.

A vacuum manipulator for in-situ variation of the deposition angle is installed. The objective is to vary the incident angle of the sputter beam to effect the self shadowing and produce a tapered pore structure. A number of membranes have been prepared. The deposition conditions were the same as above. The angle was varied as follow 85° for 15 min., 80° for 15 min., and 75° for 15 min. Samples are being tested at Amoco in the new capillary condensation cell.

Capillary Condensation Unit

Amoco has designed, constructed, and commissioned through a three-stage safety review a capillary condensation cell for the testing of these membranes. The system does have the capability of a full analysis of permeate gas and permeability in multicomponent systems over a wide range of operating conditions from subambient to elevated temperatures and high pressures. The details of the system are proprietary. This unit will provide data on the performance of these membranes and fundamental information on important aspects of condensed phases in small pores.

RESULTS

A laboratory screening apparatus was constructed at Amoco whereby the membrane(s) was supported horizontally on a porous stainless steel disk and held between sealing surfaces from above and below. Provisions were made for measured amounts of two gas mixtures to be mixed through a static mixer and brought along the axis of the membrane onto the superior surface of the membrane. The membrane having been primed with a suitable liquid, condensed the gas components of lower volatility within its pores and

transferred them across the membrane. Noncondensed materials were allowed to exist through a bubbler filled with vacuum pump oil. A stream of nitrogen gas was heated and swept along the inferior surface of the membrane to provide the heat of vaporization to the lower volatility compounds being transferred across the membrane. This stream was passed through a carbon dioxide/acetone cold trap to recondense the compound which had been transferred. Gas samples were taken of the streams before and after contact with the inferior membrane surface. These were analyzed by gas chromatography on a chromatograph equipped with both a flame ionization detector and a thermal conductivity detector. the former was used to detect hydrocarbons the latter was used to detect fixed gases such as helium, hydrogen, carbon oxides, nitrogen, oxygen and methane.

n-Butane and iso-Butane from methane and hydrogen

Feed gases of compositions given in Tables 1 and 2 were swept across the superior surface of the membrane at a flow rate of 0.1 SCFM. The membrane was primed with toluene, and warm nitrogen gas was swept across the inferior surface. Chromatographic analysis of feed and permeate are shown in Tables 1 and 2.

Table 1. Separation of n-Butane from Hydrogen, Methane and Argon.

Component	*Feed (mole %)*	*Permeate (mole%)*
Hydrogen	5.26	0.00
Nitrogen	1.31	82.74
Methane	21.03	0.00
Argon	37.01	0.00
Carbon dioxide	1.12	0.00
n-Butane	34.23	12.24
Toluene	0.04	4.92

The results of Table 1 demonstrate the selective transfer of n-butane across the membrane to the exclusion of hydrogen, methane and argon.

Table 2. Separation of Iso-Butane from Hydrogen, Methane and Argon.

Component	*Feed (mole %)*	*Permeate (mole %)*
Hydrogen	5.49	0.00
Nitrogen	1.37	73.13
Methane	21.95	0.19
Argon	38.62	0.00
Carbon dioxide	1.12	0.00
Ethane	0.02	
Propane	0.25	0.09
iso-Butane	32.23	19.80
n-Butane	0.06	1.36
Toluene	0.00	5.43

The results of Table 2 demonstrate the selective transfer of iso-butane across the membrane to the exclusion of hydrogen and methane.

A final example demonstrates the separation of ammonia from nitrogen. A 10 vol% mixture of ammonia-balanced nitrogen was passed across the superior side of the membrane at a flow of 0.1 SCFM. The membrane was primed with water and warn nitrogen passed across the inferior side. The permeate stream was bubbled through a 0.1 N solution of HCl. Titration of this solution with NaOH was used to determine the amount of ammonia which permeated the membrane. The results showed that 48% of the ammonia in the feed was transferred across the membrane.

REFERENCES

A. G. Dirks and H. J. Leamy, "Columnar Microstructures in Vapor Deposited Thin Films," *Thin Solid Films*, 47 (1977) 219-233.

K. H. Muller, "Dependence of thin film microstructure on deposition rate by means of computer simulation," *J Appl. Phys.* 58(7),1 2573 (1985).

R. Messier, A. P. Giri, and R. A. Roy, "Revised structure zone model for thin film physical structure," *Vac Sci. Technol.* A, 2, 2, 500 (1984).

D. Devlin, T. Archuleta, R. Barbero, N. Calamur, and M. Carrera, "Membrane Systems for Energy Efficient Separation of Light Gases," *AIM Program Annual Progress Report p135. 1997.*

MILESTONES

A method for developing carbon pores for capillary condensation of hydrocarbons has been devised. The use of oblique angle sputter techniques to develop thin films with controlled pore size has been demonstrated. Separation of butane gases from streams containing methane argon and hydrogen has been demonstrated.

PUBLICATIONS

"Dynamics of Chemical Vapor Infiltration in Carbon Fiber Bundles", R. P. Currier, D. J. Devlin and J. Morziski. *J. Adv. Mater.* (1996), 27(4), 13-24.

"Membrane Systems for Energy Efficient Separation of Light Gases," D. Devlin, T. Archuleta, R. Barbero, N. Calamur and M. Carrera. *AIM Program Annual Progress Report*, p135 (1997).

PRESENTATIONS

AIM Annual Meeting June 16-18, 1997, Albuquerque, New Mexico.

HONORS AND REWARDS

None.

PATENTS/DISCLOSURES

"Membranes for Separation of Light Gases," D. J. Devlin, T. Archuleta, Docket #S-87-264 filed June 24, 1997.

"Energy Efficient Separation of Light Gases by Capillary Condensation," N. Calamur, M. E. Carrera Docket # 35,028 filed Disclosure, August 14, 1995.

LICENSES

None.

INDUSTRIAL INPUT and TECHNOLOGY TRANSFER

This effort will continue in 1998 as a joint research effort under the CRADA with Amoco's Olefins R&D group. Amoco will develop characterization capabilities and design criteria for the membrane systems. With their guidance we will develop the materials and processing for the fabrication of these membranes. Amoco's goal is to scale this system for use in a pilot plant.

COST SHARING

Amoco will cost share with in kind funds and capital investment exceeding the present DOE allocation.

ESTIMATED ENERGY SAVINGS

Initial economic analyses have shown that the commercialization of this novel separation concept could result in an energy reduction potential of 5 trillion BTUs per year for an olefins complex: this corresponds to a potential annual savings of nearly $8 million.

HIGHLIGHTS

A method for developing carbon pores for capillary condensation of hydrocarbons has been devised. Initial experiments demonstrate the separation of hydrocarbons using these membranes. Applications have been submitted for patents.

METALLIC AND INTERMETALLIC-BONDED CERAMIC COMPOSITES

P. F. Becher and C. G. Westmoreland
Metals and Ceramics Division
Oak Ridge National Laboratory
Oak Ridge, Tennessee 37831-6068

INTRODUCTION

The purpose of this task is to establish a framework for the development and fabrication of intermetallic-bonded ceramic matrix composites with improved fracture toughness and temperature capability. The incorporation of intermetallic phases that plastically deform in the crack-tip region and thus dissipate strain energy, will result in an increase in the fracture toughness of the composite as compared to the monolithic ceramic. It is intended that such ceramic matrix composites will be used over a temperature range from 20°C to 800-1200°C for advanced applications in the industrial sector. In order to systematically develop these composites, the influence of composition and processing on the resultant properties have been undertaken.

TECHNICAL PROGRESS – FY 1997

The microstructure of aluminide-bonded ceramics can have a significant effect on their mechanical properties. It is well known that reducing the grain size of the matrix can be used to increase the fracture strength of ceramics. A similar trend is noted in the Ni_3Al-bonded carbides where finer grain size was achieved by decreasing the processing temperature. The materials processed at 1200°C for one hour exhibited a fine TiC grain size while those processed at 1400°C exhibited considerably more grain growth. In addition, measurements were made on the rise in the fracture resistance with crack extension in the Ni_3Al-bonded TiC composites with different TiC grain sizes. A finer TiC matrix grain size can also increase the fracture resistance of these composites.

Further improvements in the reduction of the matrix grain size can also be achieved by use of finer TiC powders. In support of this direction, collaborations were established with the task on "New Method for Synthesis of Metal Carbides, Nitrides, and Carbonitrides"[a] (presented in this Annual Report) to examine the processing and properties of composites produced from nano-sized carbide powders using the Melt-Infiltration Sintering (MIS) process. This study examined the influence of powder characteristics on formation of dense intermetallic-bonded carbides. The intermetallic phase was Ni_3Al that has been successfully employed to fabricate dense composites by the MIS process. Some of the characteristics of the three TiC powders are listed in Table 1.

[a] Prof. R. Koc, Southern Illinois University, funded under the AIM program.

The fabrication procedure consisted of cold pressing a disk-shaped sample in a steel die using a uniaxial stress of 70 MPa. The sample was subsequently cold isostatically pressed at ~320 MPa. The sample was then placed in an alumina crucible and an appropriate amount of Ni3Al powder was placed on the top surface of the sample. The crucible with a alumina cover was then placed in a graphite resistance heated furnace. The furnace chamber was evacuated to ~0.1 Pa vacuum prior to heating the sample to 1350°C or 1400°C. The heating cycle and temperatures are similar to those used to prepared composites from commercial TiC powders.

Table 1. TiC Powder Characteristics. Data supplied by Prof. Koc, Southern Illinois University.

Identification	*Surface Area* m^2/g	*Total Carbon Content, Wt. %*	*Oxygen Content Wt. %*
TiC-31	7	18.4	2.14
TiC-32	20	19.9	1.97
TiC-34	49	24	1.25

When sintered at 1350°C for 1 hr, the composite using the TiC-31 powder exhibited evidence of considerable wetting by the Ni3Al but was not fully dense. When sintered at 1400°C for 1 hour, the composite was at least 98% of theoretical density. Sintering at 1350°C with the TiC-32 powder produced a fragmented TiC preform that was not wetted by the Ni3Al melt. Similarly, use of the TiC-34 powder did not result in wetting by the Ni3Al melt at 1350°C. It appeared that there might have been some wetting of the surface of the TiC-34 preform by the Ni3Al melt. As a result, a sintering run was conducted at 1400°C in an attempt to improve the wetting. This was unsuccessful.

These initial studies illustrate the difficulty of wetting preforms of submicron-sized TiC powders having differing carbon contents. Only in the case of TiC powder (TiC-31) with the lower surface area (somewhat larger particle size) and lower total carbon content was wetting by the Ni3Al and full densification achieved. A submicron TiC grain size was found in this composite in subsequent scanning electron microscopy observations.

These initial results do not independently address the influence of the TiC stoichiometry or free carbon content on the wetting behavior. Additional studies will be needed to evaluate such effects. Such understanding is critical in the development of intermetallic-bonded carbides that have very fine grain size pertinent to the evolution of very tough, very strong composites and will be addressed in future studies.

PUBLICATIONS

Journals

K. P. Plucknett, P.F. Becher, and S.B. Waters, "Flexure Strength Behavior of Melt-infiltration Processed TiC/Ni3Al Composites,"*J. Am. Ceram. Soc.*, accepted.

K. P. Plucknett, P.F. Becher and R. Subramanian, "Melt-infiltration Processing of TiC/Ni3Al Composites," *J. Mater. Res.*, 12(10) 2515-2517 (1997).

P. F. Becher and K. P. Plucknett, "Properties of Ni3Al-Bonded TiC," *J. Eur. Ceram. Soc.*, in press.

Other Publications

T. N. Tiegs, K. P. Plucknett, P. A. Menchhofer and P. F. Becher, "Development of Nickel Aluminide Cermets," pp. 339-357 in *Proc. International. Symp. Nickel and Iron Aluminides*, ASM International, Metals Park, Ohio (1997).

J. H. Schneibel, R. Subramanian, K. B. Alexander, and P. F. Becher, "Processing and Properties of FeAl-Bonded Composites," pp. 329-37 in *Proc. International Symp. on Nickel and Iron Aluminides: Processing, Properties, and Applications*, ASM International, Materials Park, Ohio (1997).

PRESENTATIONS

"Properties of Ni3Al-Bonded Titanium Carbide Ceramics," Paul F. Becher, Kevin P. Plucknett, Terry N. Tiegs, Joachim H. Schneibel, and Ramesh Subramanian, Annual Meeting of the American Ceramic Society, Cincinnati, Ohio (May 1997).

HONORS AND AWARDS

None.

PATENTS/DISCLOSURES

Patent application of invention disclosure entitled "Method of Making Sintered Ductile Intermetallic-Bonded Ceramic Composites" (ERID-0133, ESID 1751-X) is being drafted. This activity was stimulated by interest in these materials expressed by both X-Form Corporation and Kennametal.

LICENSES

None.

INDUSTRIAL INPUT AND TECHNOLOGY TRANSFER

Interactions with LTV Steel Company concerning their interest in materials for bearing and rolls have been used for hot-dip galvanizing bath facilities; intermetallic-bonded carbides were supplied for their evaluation. Samples were also provided to Reynolds Metals, Cummins Engines, Kennametal, and Thixomat. A data book detailing properties of various aluminide-bonded carbides and borides has been prepared and distributed to various interested industrial contacts.

NEW METHODS FOR SYNTHESIS OF METAL CARBIDES, NITRIDES AND CARBONITRIDES

R. Koc, C. Meng, and D. B. Hodge
Department of Mechanical Engineering and Energy Processes
Southern Illinois University
Carbondale, Illinois 62999

P. F. Becher and T. N. Tiegs
Metals and Ceramics Division
Oak Ridge National Laboratory
Post Office 2008, Oak Ridge, Tennessee 37831

INTRODUCTION

The objective of this project is to develop a new synthesis method using a carbothermic reduction reaction of carbon coated precursors for producing high purity, submicron, non-agglomerated powders of metal carbide, metal nitride and metal boride systems. A further objective is to demonstrate the advantages of the process and provide information on the applicability of the process for producing related advanced ceramic powders. During the FY 1997 phase of the project, steps are taken to investigate the effect of carbon content in the precursor on the properties of resulting TiC powders, and applicability of the process for producing WC and TiB_2 powders. A total of 3,240 grams of submicron TiC powders with desired properties have been produced with a combined effort of Southern Illinois University and Advanced Refractory Technologies, Inc. (D. Bray and R. Hexemer) and supplied to ORNL (Dr. P.F. Becher), 3M Ceramic Technology Center (Dr. C. Shaklee), and Greenleaf (Dr. C.K. Jun) for evaluation.

TECHNICAL PROGRESS - FY 1997

A novel synthesis process using carbon-coated oxide precursors was developed under the Advanced Industrial Materials (AIM) Program for producing high purity, submicron, non-agglomerated and low cost powders of metal carbide, metal nitride and metal boride systems. The process is patented (U.S. Patent No. 5,417,952) and it utilizes a carbothermic reduction reaction of novel coated precursors (1,2). The precursors are derived from an oxide of related cation and a hydrocarbon gas and provides high contact area between the reactants. This yields a better distribution of carbon within the oxide and inhibits the agglomeration among the oxide particles, resulting in a more complete reaction and a purer product at a comparatively low temperature.

This program has demonstrated the capability of producing high purity, high surface area, low cost titanium carbide (TiC), tungsten carbide (WC), and titanium diboride (TiB_2) powders utilizing the carbon coating process. From a technical standpoint, the carbon coating process is a leap forward in the technology for producing nonoxide advanced ceramic powders. This technology improves energy efficiency because it does not require high reaction temperatures for production of these powders. [3,4,5].

By reaction of the carbon-coated titania particles at 1550°C, submicron TiC powders were synthesized during the first year of the project. Depending on the carbon content in the coated titania precursor, TiC powder was produced with different stoichiometries (different amount of oxygen and free carbon) and morphologies (particle shape, agglomeration). During the FY 1997 time period, steps were taken to produce submicron TiC powders with desired stoichiometries by optimizing the amount of carbon in coated titania precursors. The produced submicron TiC powders with desired stoichiometries were supplied to 3M Ceramic Technology Center (Drs. C. Shaklee and V. Nehring - 1,500 grams), to Greenleaf Inc. (Dr. C.K. Jun - 1,500 grams) and to ORNL (Dr. P.F. Becher - 240 grams) for evaluation and fabrication of TiC-based composites.

The densification of TiC with different carbon content has been studied using Ni as a binder in flowing 10% H_2-Argon gas at 1500°C. Density of 98% TD was obtained for TiC (30F)-3wt.%Ni. Dr. Becher and his group at ORNL also had success obtaining wetting of the TiC (30F) powder by Ni_3Al alloy, thus achieving a dense composite. More importantly, the majority of final TiC grain size in the composite was ≤ 1 μM. These results suggest that the produced submicron TiC powders using the new process will result in the development and fabrication of TiC components and composites with superior mechanical and electrical properties.

The applicability of the process for producing submicron WC and TiB_2 have also been investigated. The advantages of the process have been demonstrated. The developed process was capable of producing high quality WC and TiB_2 powders suitable for making ceramic materials and composites-highly pure powder with submicrometer particles. The produced powders were characterized using X-ray diffraction (XRD), BET surface area analyzer, Transmission Electron Microscopy (TEM) and chemical analysis (oxygen and carbon). The produced submicron 50 grams of TiB_2 powders in addition to 1,500 grams of TiC powder were supplied to 3M Ceramic Technology Center (Dr. C. Shaklee) for evaluation.

MILESTONES

1. Production of Submicron TiC Powders with Desired Stoichiometries

A rotating coating apparatus consisting of 10-cm-ID x 35-cm-long stainless steel vessel was used for preparing the carbon coated titania (TiO_2 -P25 Degussa Corporation, Ridgefield Park, NJ) precursors. About 200 grams of TiO_2 powders were placed in the vessel. The vessel was evacuated, purged with argon, and evacuated again. Then the vessel was heated to 550°C, kept at this temperature for 30 minutes, and filled with propylene gas until the pressure reached 50 psi. After approximately 5 minutes the remaining gas was released and the vessel was filled with fresh propylene. This is continued until the required carbon is deposited. Precursors 30F, 32F and 34F containing 30.95 wt.%, 32 wt.% and 34 wt.% carbon were prepared, respectively.

Figure 1 shows bright field TEM micrograph of the carbon coated titania precursor (32F). As shown in the figure, a very uniform circumferential carbon coating (bright area due to low atomic weight of carbon) on titania particle surfaces is apparent. This shows the effectiveness of the carbon coating process (on titania surfaces) by the pyrolysis of C_3H_6 gas at 550°C. XRD pattern of the carbon-coated titania precursor (32F) is shown in Figure 2. In the figure, the absence of crystalline carbon phases implies that the deposited carbon in Figure 1 has an amorphous (pyrolytic) structure. The BET surface area of the produced precursors were measured to be 44 m^2/g, 45 m^2/g and 46 m^2/g after being coated with 30.95 wt%, 32 wt%, and 34 wt% carbon, respectively. These results showed that a uniform, highly porous and low density carbon coating can be deposited at 550°C on TiO_2 particles by pyrolyzing C_3H_6 gas.

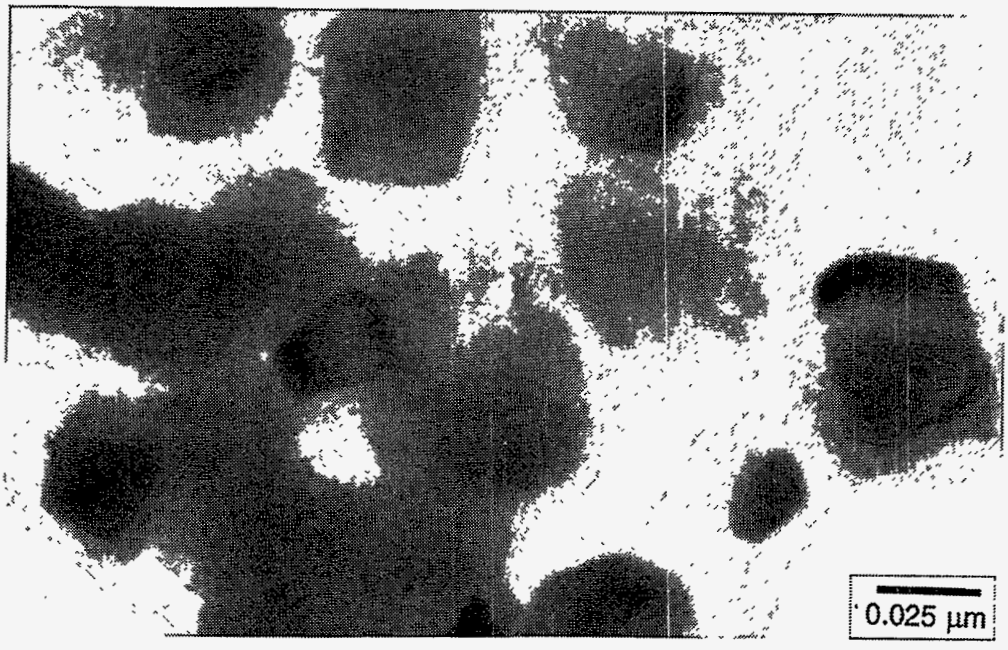

Figure 1. TEM micrograph of the carbon-coated titania precursor (32F).

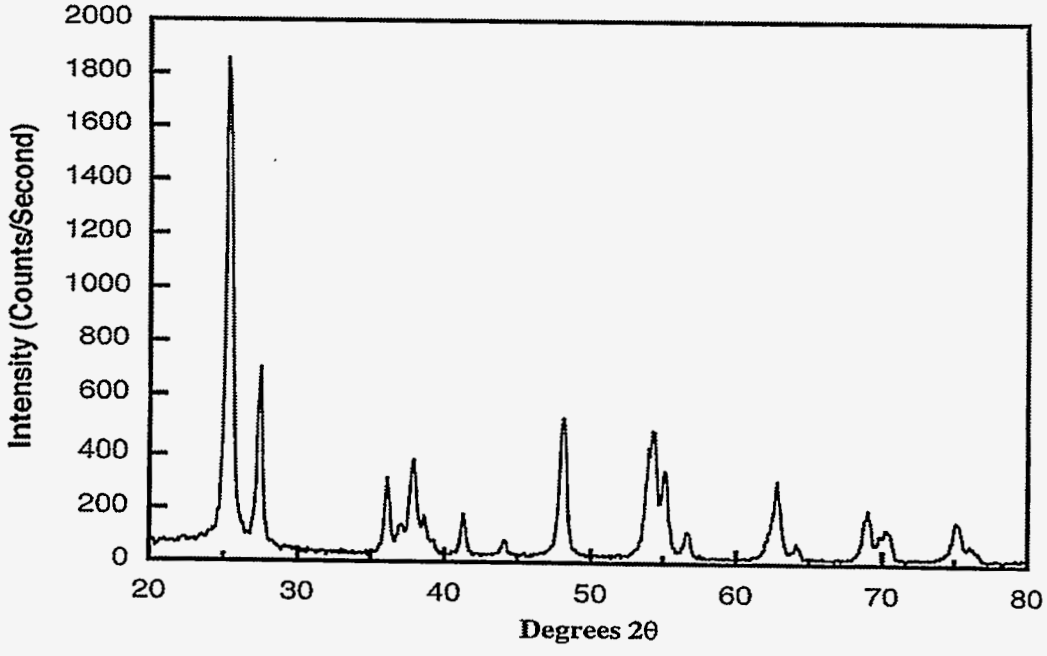

Figure 2. XRD pattern of the carbon- coated titania precursor (32F).

The carbon coated all three titania precursors with different initial carbon content and were subjected to 1550°C for 4 hours in an inert atmosphere (Argon) to produce TiC powders. The tube furnace (Model CTF 17/75/300, Carbolite, Sheffield) with ID of 70 mm was used for producing the powders. A heating rate of 4°C/min. and cooling rate of 4°C/min. were used. A flowing stream of Ar at 1LPM was supplied during the whole experiment. Table 1 provides the summary of the comparison between commercially available TiC (High Vacuum Grade A.H.C. Stark) powder with the TiC powders produced (containing different initial carbon content in the precursors) using the developed process.

Table 1. Properties of the produced TiC powders and comparison with commercially available TiC.

	Initial Carbon 30.95 wt%-30F	**Initial Carbon 32 wt%-32F**	**Initial Carbon 34 wt%-34F**	**H.C. Starck High Vacuum Grade A**
Particle Size, μM, From TEM	**~0.2**	**~0.2**	**~0.2**	**1 - 1.5**
Surface Area, BET, m^2/G	**8**	**30**	**48**	**2 - 3.5**
Total Carbon, wt%, LECO C200	**19.3**	**22.1**	**25**	**20 - 21**
Total Oxygen, wt%, LECO RO416DR	**1.45**	**1.12**	**0.98**	**0.7**
Lattice Parameter, a_o, Å calculated	**4.3296**	**4.3280**	**4.3352**	**4.331**

TEM was used to investigate the particle size, size distribution, particle morphology and degree of agglomeration as a function of total carbon. Figure 3 is a TEM micrograph of TiC produced from the precursor 30F. The particles are agglomerated and range from 0.1μM. Figure 4 is a TEM micrograph of TiC produced from the precursor 32F. The particles shown in the micrograph are uniform with the exception of the unreacted carbon. As can be seen from Figure 5, the amount of free carbon present in TiC produced from the precursor 34F increased. However, the TiC powders are loosely agglomerated with the

from the precursor 34F increased. However, the TiC powders are loosely agglomerated with the particles being mostly spherical. These results show that the TiC oxygen content decreased and total carbon content increased with increasing the initial carbon amount in the precursors. The degree of agglomeration was also decreased with increased carbon content in the precursors.

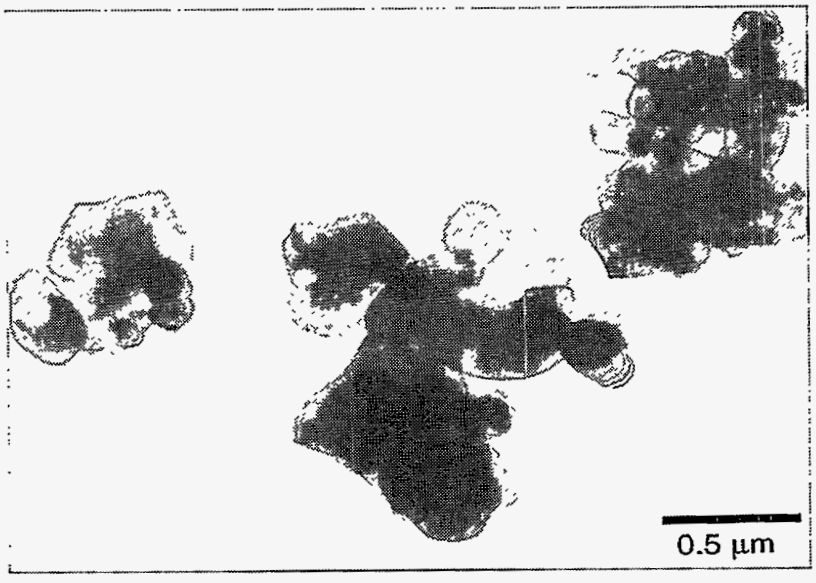

Figure 3. TEM micrograph of TiC powder product synthesized at 1550°C for four hours in flowing argon atmosphere (using the precursor 30F).

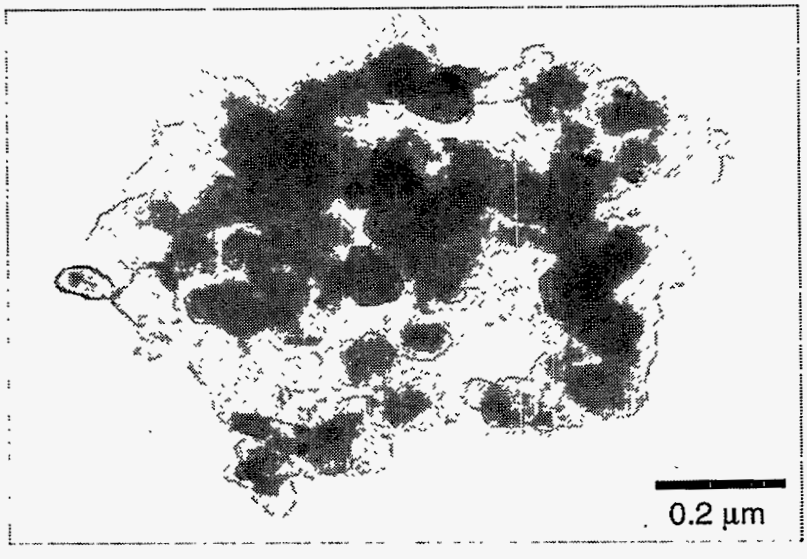

Figure 4. TEM micrograph of TiC powder product synthesized at 1550°C for four hours in flowing argon atmosphere (using the precursor 32F).

Sintering studies were done in flowing 10% H_2-Ar gas at temperature of 1500°C using Ni as a binder. A density of above 99% theoretical was achieved with the 20 wt.% Ni for TiC-T30 powders. Significant improvements in densification were observed with decreasing free carbon content in the TiC powders. Scanning electron micrographs of the polished surfaces of specimen sintered at 1500°C for 2 hours in flowing 10%H_2-Ar gas is given in Figure 6. Microstructure development, the level of densification and amount of liquid phase can be observed from this photomicrograph. The microstructure and amount of liquid phase control the properties of TiC-Ni composites. A fine grain size with a narrow size distribution is most useful for milling, cutting and wear applications.

2. Production of WC Powders Using the New Process

The importance of WC is well known in machining, cutting, grinding, drilling, and hard facing [6,7]. It is widely used in the manufacture of dies, cutting tools, mining tools and other wear parts. WC powder used for the manufacture of these structural components should be free of di-tungsten carbide (W_2C), presence which is objectionable because of its poor mechanical properties. Powders with varying carbon content can cause instability during sintering if not properly compensated for by uniformly blending in carbon. Powders within homogeneous microstructure are believed to be detrimental to the consistent performance of sintered cemented WC components. In homogeneity is caused by the presence of coarse grains which have been found to adversely affect the strength properties and cause poor uneven surface conditions after sintering.

The conventional process for making WC powders consists of a solid state carburization of tungsten powder (W). In this process WC particle size is controlled by the starting tungsten powder. Tungsten particle growth is affected by a water vapor deposition reaction which occurs in the reaction powder bed. High hydrogen flow rates are required to eliminate grain growth in the particles. Lso, the produced powder, has to be milled to fine size before further processing. Altogether, production of tungsten powder itself is expensive. Carburization of tungsten does not yield WC powder directly. The resultant powder is a mixture of carbides and it has to be further treated to produce pure WC powder [8].

The potentially advantageous method to produce WC powder is from tungsten oxide. Fine powder can be produced because tungsten grain growth reactions are minimized in this process. Processes patented for the production of WC powder from its oxide were either time consuming, involving several repetitive processing steps, or requiring controlling of reaction atmospheres [9].

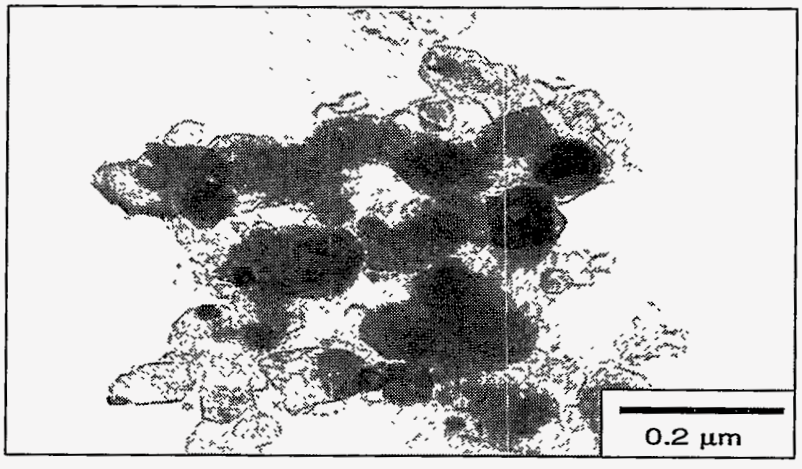

Figure 5. TEM micrograph of TiC powder product synthesized at 1550°C for 4 hrs in flowing argon atmosphere (using the precursor 34F).

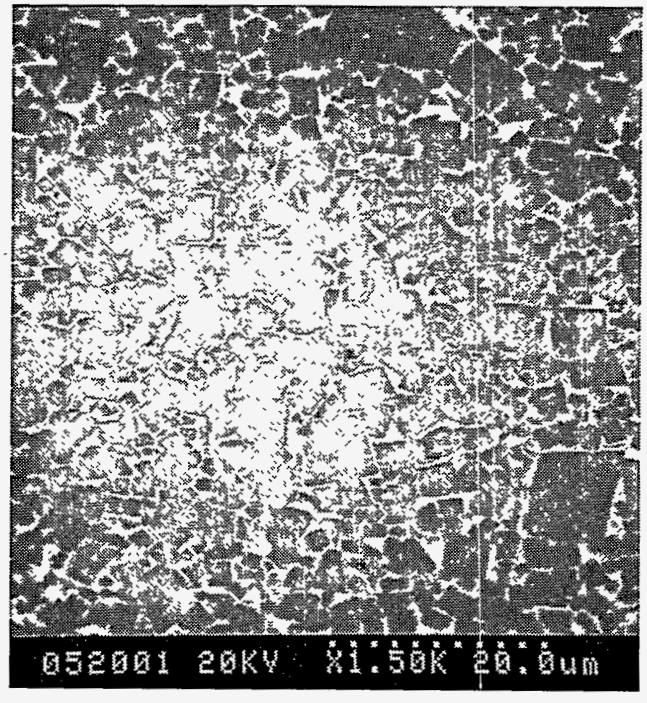

Figure 6. SEM micrograph of TiC-20wt.% Ni cermets sintered at 1500°C for 2 hrs in flowing 10% H_2-Ar atmosphere.

Various attempts made in the past to produce WC powder directly from tungsten oxide have not been successful on an industrial scale. Problems encountered in the past were: 1) controlling the carbon content in the final product, 2) controlling the grain size and grain size distribution of WC, and 3) inability to produce pure WC powder in a single treatment. Reaction mechanisms involved in this process were complex and were not investigated in detail in the past. We have studied the reduction mechanism of tungsten oxides in detail and developed a new process to produce high quality WC powder [10]. The present invention is based on the carbon coating process with some novel changes. Southern Illinois University is currently in the process of completing patent application for the process. We have been working with Kennametal Inc., and Fansteel Inc., to transfer the technology.

The new method based on carbon coating method is capable of producing high-quality powders suitable for making cemented carbide components. The powders produced were phase pure and were synthesized at temperatures as low as 1100°C. It is possible to produce phase pure powders in inert atmosphere using this process. The main advantage of this process is its capability to produce high-quality powders at low temperatures in less times minimizing the production cost. Carbon coating is essential only in the beginning of the reduction process. Because it provides intimate contact between the reactants, and hence guarantees continuous supply of carbon monoxide at later stages of reduction for gas phase reduction. This enhances reduction rates and minimizes reduction temperature and time resulting in formation of fine tungsten particles. XRD patterns in Figure 7 show the formation of WC powders synthesized in a tube furnace from the novel precursors at various temperatures. Presence of fine particles of tungsten increases the diffusion rates and helps in the formation of pure tungsten monocarbide. The reaction path was similar to that of conventionally prepared precursors but the reduction occurred at much lower temperature.As a result, high-quality WC powder was produced from the novel precursors by treating at 1400°C for two hours in flowing 10% H_2-Argon atmosphere. The produced WC powders possess the following properties:

- single phase WC (with no traces of W_2C)
- total carbon and oxygen contents with ~6.5 wt% and ~0.2 wt.%, respectively
- BET surface are of 3 m^2/g
- loosely agglomerated powder which breaks up into well-dispersed particles after 30 minutes of milling in a tungsten carbide ball mill
- produced WC powder wa sintered to above 90% theoretical density using 10 wt.% Co metal powder by heat treating for one hour at 1400°C in 10% H_2-Ar atmosphere

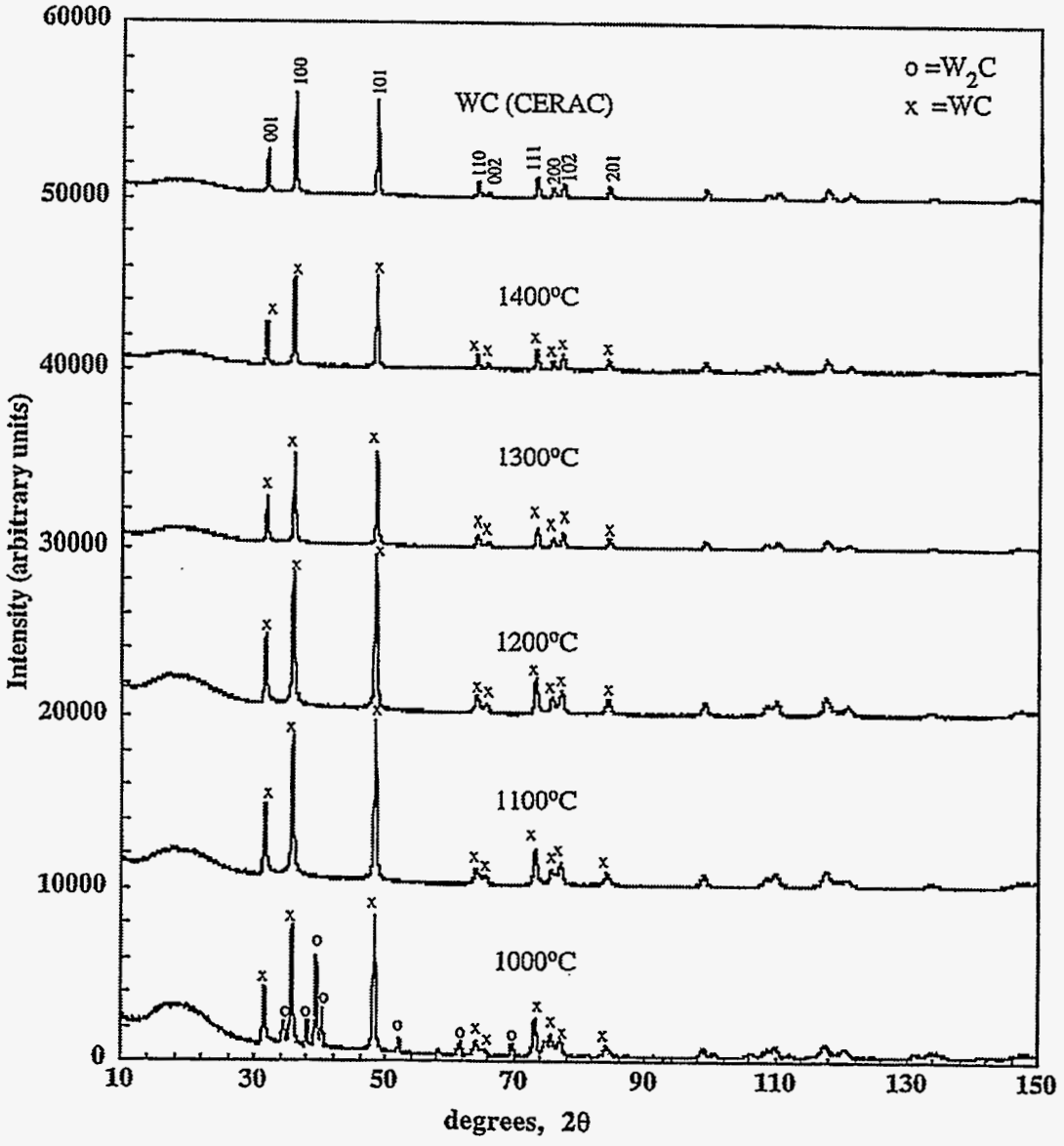

Figure 7. XRD patterns of WC powders synthesized at 1000-1400°C for 2 hrs in flowing 10% H_2-Ar atmosphere.

Following is Table 2 providing comparison of properties of WC powder produced from the new process and the commercial WC powder.

Table 2. Comparison of WC Powder Characteristics.

Powder Properties	Best Powder Available (CERAC)	Powder Produced from the New Process
BET Surface Area, m^2/g	1.7	3.0
Total Carbon, wt.%	6.15	6.3
Free Carbon, wt.%	0.05	0.2 max.
Total Oxygen, wt.%	0.2	0.1-0.2 max.
Impurities (Fe, Al, Mo, Ni)	0.02	N/A

TEM micrograph of the WC produced from the new process is shown in Figure 8. Comparison of the WC powder morphology with that of commercial CERAC WC powder shown in Figure 9.

Figure 8. TEM micrograph of WC powder produced from the novel precursors at 1400°C for 2 hrs in flowing 10 % H_2-Ar atmosphere.

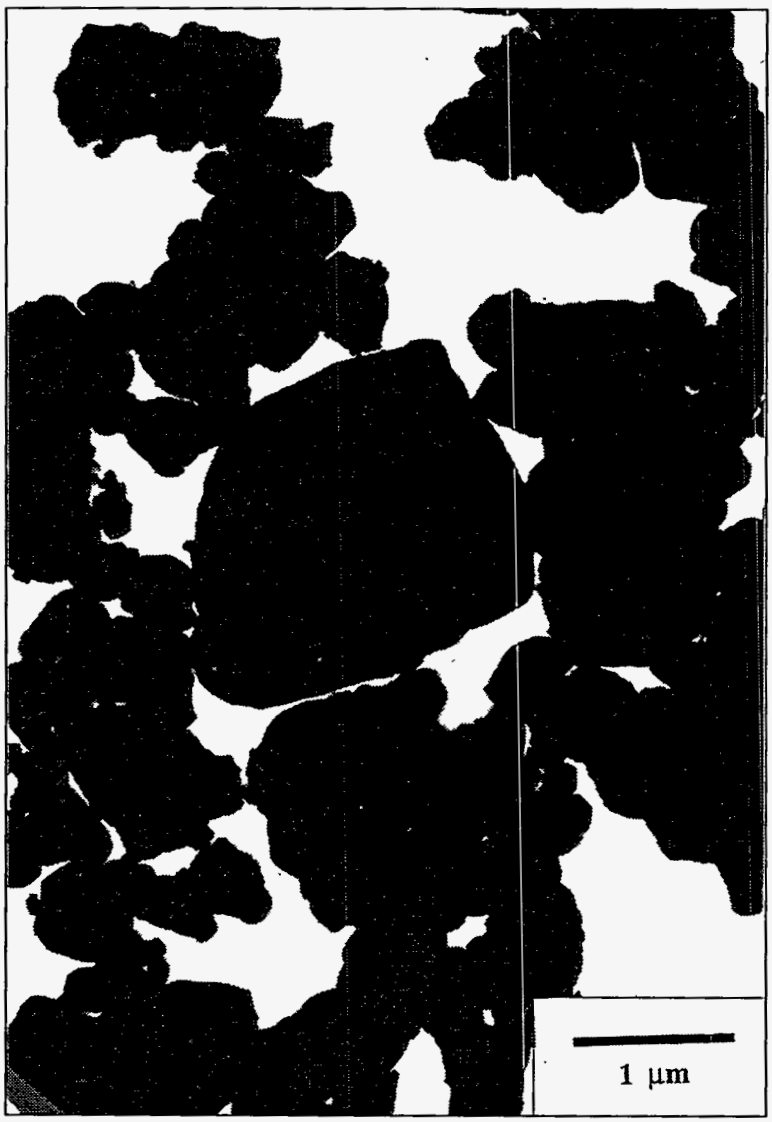

Figure 9. TEM micrograph of the CERAC-WC commercial powder (for comparison).

ACKNOWLEDGMENT

This research was sponsored by the U.S. Department of Energy, Office of Industrial Technologies, as part of the Advanced Industrial Materials Program, under contract DE-AC05-84OR21400 with Lockheed Martin Energy Research Corporation.

REFERENCES

1. R. Koc and G. Glatzmaier, "Process for Synthesizing Titanium Carbide, Titanium Nitride and Carbonitride", U.S. Patent No: 5,417,952, (1995).

2. R. Koc and J. S. Folmer, "Synthesis of Submicron Titanium Carbide Powders," *The Journal of American Ceramic Society,* 80, 4, 952-56, (1997).

3. R. Koc, "Kinetics and Phase Evolution During Carbothermal Synthesis of Titanium Carbide from Carbon Coated Titania," *Journal of the European Ceramic Society,* Vo. 17, Iss. 11, 1309-1315, (1997).

4. R. Koc, "Kinetics and Phase Evolution During Carbothermal Synthesis of Titanium Carbide from Ultrafine Titania/Carbon Mixture," accepted for publication in *the Journal of Materials Science,* (February 1997).

5. R. Koc and J. S. Folmer, "Carbothermal Synthesis of Titanium Carbide Using Ultrafine Titania Powders," *the Journal of Materials Science,* Vol. 32, No: 12, 3101-3111, (1997).

6. L. E. Toth, "Transition Metal Carbides and Nitrides," (1971)

7. M. George and S. Januszkiewicz, "New Materials for Fluorosulfonic Acid Electrolyte Fuel Cells", Energy Research Corporation, Final Technical Report, 1-47, (June 1977).

8. G. Leclercq, M. Kamal, J. M. Giraudon, P. Devassine, L. Feigenbaum, L. Leclercq, A. Frennet, J.M. Bastin, A. Lofberg, S. Decker, and M. Dufour, "Study of the Preparation of Bulk Powder Tungsten Carbides by Temperature Programmed Reaction with CH_4+H_2 Mixtures", *Journal of Catalysis*, 158, 142-169, (1996).

9. C. J. Terry and J. D. Frank, "Macrocrystalline Tungsten Monocarbide Powder and Process for Producing", U.S. Patent 4,834,963, (1989).

10. R. Koc and S. K. Kodambaka, "Method for Producing Tungsten or Tungsten Monocarbide Powders", ROI filed at SIUC, (1996).

PUBLICATIONS

Journal

R. Koc and J.S. "Folmer,Synthesis of Submicron Titanium Carbide Powders", *The Journal of American Ceramic Society,* 80, 4, 952-56, (1997).

R. Koc, "Kinetics and Phase Evolution During Carbothermal Synthesis of Titanium Carbide from Carbon Coated Titania," Journal of the European Ceramic Society, Vo. 17, Iss. 11, 1309-1315, (1997).

R. Koc, "Kinetics and Phase Evolution During Carbothermal Synthesis of Titanium Carbide from Ultrafine Titania/Carbon Mixture," accepted for publication in the *Journal of Materials Science*, (February 1997).

R. Koc and J. S. Folmer, "Carbothermal Synthesis of Titanium Carbide Using Ultrafine Titania Powders," the *Journal of Materials Science*, Vol. 32, No: 12, 3101-3111, (1997).

Other

R. Koc and J.S. Folmer, A New Method for Synthesis of Submicron TiC Powders, the Ceramic Engineering and Science Transactions, Vol. 79, 19-26, (1996).

PRESENTATIONS

R. Koc, S. Cattamanchi and S. Kaza, "Synthesis of Submicron Silicon Nitride Powders," presented at *ACS 99th Annual Meeting*, Paper No: SIII-003-97, Cincinnati, Ohio, May 4-7, 1997.

S. Cattamanchi and R. Koc, "Carbothermal Synthesis of Beta SiC Powders using Carbon Coated Colloidal Silica," presented at *ACS 99th Annual Meeting*, Paper No: SIII-028-97, Cincinnati, Ohio, (May 4-7, 1997).

R. Koc and S. Cattamanchi, "Synthesis of SiC Powders," presented at *ACS Meeting on Composites, Advanced Ceramics, Materials and Structures,* Paper No: SI-0035-97F, Abstract Book p. 34, Cocoa Beach, Florida, (January 12-16, 1997)

R. Koc, "Kinetics and Phase Evaluation During Carbothermal Synthesis of TiC," presented at *ACS Meeting on Composites, Advanced Ceramics, Materials and Structures,* Paper No: SI-0036-97F, Abstract Book, p. 35; Cocoa Beach, Florida, (January 12-16, 1997).

S. K. Kodambaka and R. Koc, "Synthesis of Submicron Tungsten Monocarbide Powders Using a Novel Tungsten Trioxide Precursors," presented at *ACS Meeting on Composites, Advanced Ceramics, Materials and Structures,* Paper No: SI-0034-97F, Abstract Book, p. 34; Cocoa Beach, Florida (January 12-16, 1997).

R. Koc, "Sintering of Submicron TiC Powders Using Ni," *University of Missouri-Rolla,* Missouri, Invited Talk (October 23, 1997).

HONORS AND AWARDS

R&D 100 for the Development of Method for Making Silicon Carbide Powder, Award Winning Team, Rasit Koc, Greg C. Glatzmaier, Kent Scholl, Mark Anselmo, Jack Sibold (1995).

Federal Laboratory Consortium Award for Technology Transfer, Award Winning Team, Rasit Koc, Greg C. Glatzmaier, Kent Scholl, Mark Anselmo, Jack Sibold (1996).

PATENTS/DISCLOSURES

R. Koc and G. Glatzmaier, "Process for Synthesizing Titanium Carbide, Titanium Nitride and Carbonitride," U.S. Patent No: 5,417,952.

R. Koc and S. K. Kodambaka, "Process for the Production of Tungsten or Tungsten Monocarbide Powders," Patent application is in process.

LICENSES

ART Inc. has licensed the SiC patent to produce SiC powders.
Greenleaf Inc. is in process of licensing TiC patent.
Kennametal Inc. is in process of licensing WC technology.

INDUSTRIAL INPUT AND TECHNOLOGY TRANSFER

Advanced Refractory Technologies (ART), Inc.

We have been collaborating with ART in producing SiC powders using the new process. We are also supplying carbon coated titania precursors for the production of larger quantities of submicron TiC powders.

3M Ceramic Technology Center

The personnel at 3M are interested in the results of our program with respect to materials application in write-read devices and wear-resistant composites. We have supplied 3M with materials and consultation for their particular needs.

Greenleaf Corporation

The personnel at Greenleaf have a Al_2O_3-TiC processing program in which they are making use of submicron TiC powders produced from the program.

Oak Ridge National Laboratory (ORNL)

The personnel at ORNL have a TiC-Intermetallic composite program which is directed at developing composites with superior properties for cutting tool applications than the WC-Co currently being used.

ESTIMATED ENERGY SAVINGS

This technology will improve energy efficiency when compared the conventional ones because it does not require high reaction temperatures for production of these powders.

PROCESS SIMULATION FOR ADVANCED CERAMICS PRODUCTION: 1. Process Simulation for Advanced Composites Production 2. Development of Advanced Energy-Efficient Coatings for Sun-Belt Low-E Applications

M. D. Allendorf, S. M. Ferko, S. K. Griffiths,
A. McDaniel, R. H. Nilson, and D. R. Hardesty
Sandia National Laboratories
Livermore, California 94551-0969

INTRODUCTION

The objective of this project is to improve the efficiency and lower the cost of chemical vapor deposition (CVD) processes used to manufacture advanced ceramics by providing the physical and chemical understanding necessary to optimize and control these processes. Project deliverables include: numerical process models; databases of thermodynamic and kinetic information related to the deposition process; and process sensors and software algorithms that can be used for process control. Target manufacturing techniques include CVD fiber-coating technologies (used to deposit interfacial coatings on continuous fiber ceramic preforms), chemical vapor infiltration, thin-film deposition processes used in the glass industry, and coating techniques used to deposit wear-, abrasion-, and corrosion-resistant coatings for use in the pulp and paper, metals processing, and aluminum industries.

Experimental measurements are performed under realistic processing conditions to obtain gas-phase concentrations, precursor decomposition kinetics, and deposition rates, using Sandia's high-temperature flow reactor (HTFR) equipped with mass spectrometric and laser diagnostics. In addition, advanced characterization methods such as high-resolution transmission electron microscopy and energy-dispersion spectroscopy are used to characterize the microstructure and composition of reactor deposits. Computational tools developed through extensive research in the combustion field are employed to simulate the chemically reacting flows present in typical industrial reactors.

Currently, this project includes two industrial collaborations. First, joint work with DuPont Lanxide Composites (DLC; Newark, DE) is directed toward development of a process model for simulating, optimizing, scaling, and controlling boron nitride (BN) fiber-coating processes used in the manufacturing of fiber-reinforced composites. Second, research performed in collaboration with Libbey-Owens-Ford Co. (LOF; a major manufacturer of float glass located in Toledo, OH) is directed toward development of

new CVD methods for depositing coatings on glass. Work with LOF is performed under a CRADA.

Project Tasks

Six tasks for FY 1997 are defined as follows:

Task 1. Characterization of reactor deposition chemistry

Task 2. Simulation of reactor fluid dynamics and mass transport

Task 3. Implementation of strategies for process design, optimization, and operation

Task 4. Development of process-control sensors

Task 5. Chemical kinetics of precursor systems for float-glass coating

Task 6. *In-situ* process-control sensors for float-glass coating

Tasks 1-4 are conducted in conjunction with DLC; Tasks 5 and 6 are part of the CRADA with LOF. This report contains no proprietary information.

TECHNICAL PROGRESS - FY 1997

Summary

Process Simulation for Advanced Composites Production

Development of a comprehensive analytical model of boron nitride (BN) fiber-coating processes was completed. Analysis of an extensive database of information supplied by DLC concerning BN preform coating runs was also initiated. A subset of these data that includes approximately forty separate coating runs was used to more accurately establish three parameters used in the model that were initially obtained from literature sources or were fit to very limited data. A report describing model results in detail was written; normalized variables are used in the discussion so that model predictions can be extended to a range of chemical-vapor infiltration (CVI) fiber-coating processes. The model was used to identify labor-saving strategies for optimizing both fiber-coating and preform-densification processes. Implementation of these strategies is estimated to have saved DLC approximately $1M in process-development costs.

Development of Advanced Energy-Efficient Coatings for Sun-Belt Low-E Applications

Investigations using theoretical and experimental methods necessary for understanding the factors affecting CVD of indium tin oxide (ITO) on float glass were begun in FY 1997, the first year of this CRADA. Significant results were obtained in four areas: (1) A database of thermochemical properties for gas-phase species relevant to this process was developed using empirical correlations to estimate molecular heats of formation. *Ab-initio* electronic-structure methods were also explored as possible routes to more accurate thermochemistry; (2) Three possible systems for delivering low-vapor-pressure ITO precursors to the HTFR for subsequent experiments were constructed and tested: (3) Pyrolysis rates for trimethylindium (TMI) and a proprietary precursor were measured in the HTFR, using a molecular-beam mass spectrometer (HTFR/MS) system to monitor precursor decomposition and product formation. The data provide insight into the thermal stability of these compounds and the effects of heterogeneous processes on the observed rates. Kinetics of bimolecular reactions between the precursors and other components of the process gases, such as oxygen, were also explored; and, (4) A laboratory system for evaluating spectroscopic methods for their potential as on-line process monitors was constructed. Investigations in all four areas are expected to continue in FY 1998.

MILESTONES AND PROGRESS

Task 1. Characterization of reactor deposition chemistry

All work originally planned for this task was completed in FY 1997. The primary activities this year consisted of writing several publications to bring the results obtained in FY 1996 into the open literature (for a list, see the end of this report). These included works describing a database of thermodynamic properties for gas-phase species predicted by *ab-initio* quantum-chemistry techniques and two articles describing HTFR investigations of the reaction between the BN precursors BCl_3 and NH_3.

As will be seen from results described in Task 2 below, analysis of the BN coating data provided by DLC indicates that increasing the NH_3 concentration increases the BN deposition rate. This contradicts the prediction of our model, which assumes that a rapid gas-phase reaction converts BCl_3 and NH_3 to a single species that is responsible for BN coating formation:

$$BCl_3 + NH_3 \leftrightarrow Cl_2BNH_2 + HCl \qquad (1)$$

$$Cl_2BNH_2 \rightarrow BN(solid) + 2\ HCl \qquad (2)$$

As a result, we plan some new experiments and modeling under this task in FY 1998, which will hopefully resolve this issue. Results of these investigations will be used to revise the current BN coating model so that it correctly predicts the behavior with regard to the NH_3 concentration.

Task 2. Simulation of reactor fluid dynamics and mass transport

Work under this task can be divided into two primary areas. First, development of an analytical model that predicts fiber-coating rates as a function of key process variables was completed. Second, analysis of a large body of experimental results obtained in DLC fiber-coating reactors to obtain more accurate values of important model parameters was initiated.

Summary of analytical model results

The objectives of this work are to: (1) complete mathematical development of the analytical model begun in FY 1996, (2) analyze model predictions in detail and understand their implications for fiber coating, and (3) identify strategies for improving the operation of DLC's coating operations.

Due to its complexity we will not present an in-depth description of the model here. Briefly, we derived analytical expressions describing the reactor conditions that give the maximum centerline deposition rate for a first-order deposition reaction involving a single gas-phase reactive species. These expressions account for both diffusive and advective transport and both ordinary and Knudsen diffusion. For ease of analysis, all process variables are normalized to form non-dimensional variables. This makes the predictions of the model much more accessible to the user since the results can be easily applied to any chemical vapor infiltration (CVI) fiber-coating process. A detailed description of the model can be found in a report compiled this year (see Reference 1 under "Publications" below). This report also provides an in-depth discussion of model predictions and suggests labor-saving strategies for optimizing both fiber-coating and preform-densification processes. Copies of the report can be obtained free of charge by contacting the authors.

In the discussion below, the following non-dimensional variables are defined as follows:

ξ	Normalized preform thickness
Ψ^*	Normalized reaction yield (i.e., the amount of reactant converted to solid in the deposition reaction. Also corresponds to the amount of gas-phase products produced by the deposition reaction).
p^*	Normalized reactor pressure

T^*	Normalized reactor temperature
β	Deposition (Thiele) modulus (the ratio of the deposition rate on preform fiber
β	surfaces to the rate of reactant diffusive transport)
U	Deposition uniformity, defined as the thickness of the BN coating at the center of the preform divided by the mean value
S^{**}	Normalized deposition rate
Kn	Knudsen number (ratio of mean-free path in the gas to preform pore size)

Key results of this investigation are summarized below:

- The optimum processing conditions (i.e., those for which the centerline deposition rate is a maximum) for coating a ceramic-fiber preform are a function of only two dimensionless parameters: the normalized preform thickness (ξ) and the normalized reaction yield (Ψ^*). This highlights the relative importance of advective transport away from the preform center due to the evolution of product gases from the deposition reaction.

- The optimum pressure is obtained in closed form. Its value is proportional to the activation energy of the deposition reaction and inversely proportional to the characteristic preform pore size. The optimum pressure does not depend on the preform thickness, specific surface area, or effective diffusivity, nor does it depend on the reaction yield.

- The optimum temperature and maximum centerline deposition rate depend strongly on the preform thickness. Surprisingly, the deposition modulus β and deposition uniformity U at the optimum conditions are nearly independent of the thickness for a given normalized reaction yield. This provides a simple means of identifying optimum conditions for preforms of different thicknesses, once the optimum conditions are known for a single case. Thus, the optimum temperature for a new thickness is obtained when the deposition uniformity is the same as the for the known case, as determined either experimentally or by using a simple algebraic relation to give the same value of β for the new preform thickness.

- The conditions giving rise to the maximum centerline deposition rate do not yield the maximum rate at the preform surface, nor do they yield the maximum mean deposition rate. This is shown in Figure 1, where the centerline, surface, and mean normalized deposition rates are shown as a function of T^*. We see that both the surface and mean rates increase smoothly with increasing temperature, while the centerline rate exhibits a maximum.

- The optimum deposition conditions occur when the normalized centerline reactant fraction (equivalent to U) and deposition uniformity are about 0.25, regardless of the preform thickness. Calculations of the optimum normalized conditions are shown in Figure 2 for a range of normalized preform thicknesses. The plot shows that β and U at the optimum conditions vary by only about 15% as the ξ varies by nearly ten orders of magnitude. This result provides a simple and practical method of determining the optimum temperature.

- Optimum values for β, U, and S^{**} decrease as the reaction yield Ψ^* increases. The sample results in Figures 1 and 2 are for the special case in which no gas-phase products are produced by the deposition reaction. To examine the effect of the generation of gas-phase products on the optimum processing conditions, we also computed the optimum conditions over a range of values of Ψ^*. These results are shown in Figure 3. This single figure gives the optimum conditions for nearly the full range of both Ψ^* and ξ. We see that the optimum values of β, U, and the maximum centerline deposition rate (labeled as S^{**} in Figure 3) all decrease significantly with increasing values of Ψ^*. The reason for this is that positive values of Ψ^* correspond to a net production of gas by the deposition reaction and a corresponding flow away from the center toward the preform surface. This outward flow impedes the inward diffusion of the reactive species, giving rise to lower uniformity, lower reactant concentrations at the preform center, and correspondingly lower centerline deposition rates. This increased resistance to diffusion therefore requires a reduced temperature to maximize the centerline deposition rate.

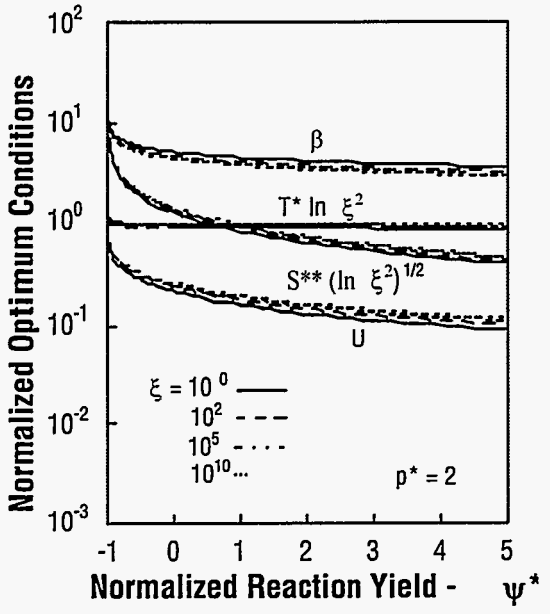

Figure 1. Surface, mean and centerline deposition rates. For a given pressure, the maximum centerline deposition rate occurs at a specific temperature and corresponding value of the deposition modulus.

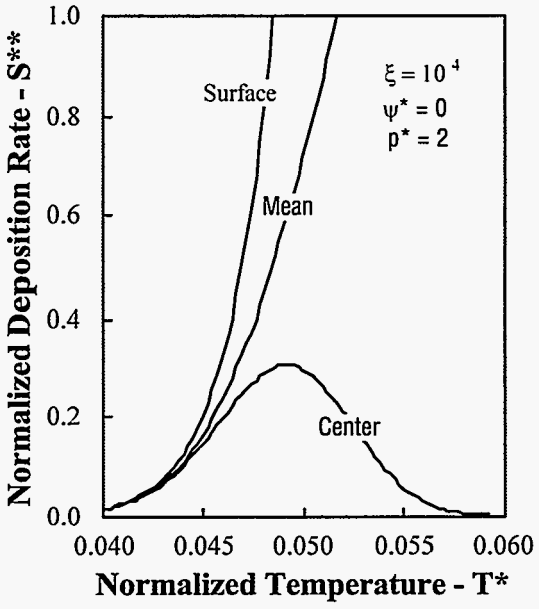

Figure 2. Normalized optimum conditions as a function of the normalized preform thickness. The optimum deposition uniformity U is insensitive to preform thickness.

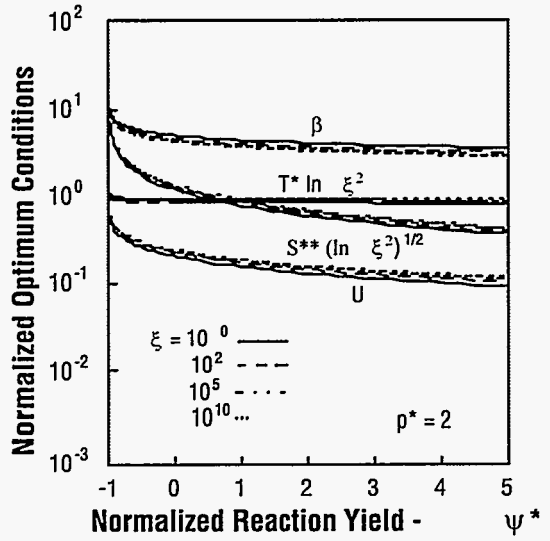

Figure 3. Normalized optimum conditions as a function of normalized reaction yield. Larger reaction yields require slightly lower temperatures and give significantly reduced maximum deposition rates.

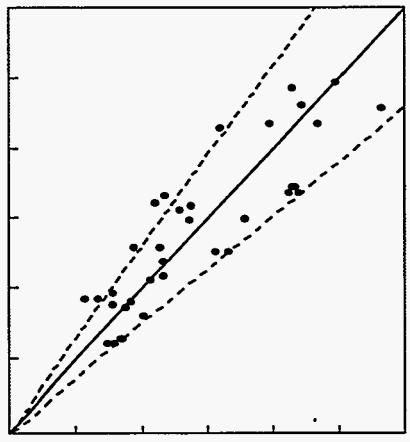

Figure 4. Comparison of measured and predicted weight gains. The solid line corresponds to exact agreement, while the dashed lines indicate the ± 30% boundaries.

- The model suggests a simple strategy for optimizing fiber-coating processes to obtain a given value of U. Conditions yielding the maximum centerline deposition rate yield U of only about 25%. That is, the deposition rate at the preform surface is roughly four times that at its center. Since this is probably not acceptable for some coating applications, we also examined the influence on the optimum conditions of a constraint on the deposition uniformity. We find that the optimum pressure in this constrained maximization of the centerline deposition rate is the same as that obtained in the unconstrained case. This result suggests that a good strategy for optimizing fiber coating processes is to fix the pressure at the optimum value and then vary only the temperature or temperature history to obtain the desired final state of the preform. Using this strategy, the time-consuming process of empirically varying both the pressure and temperature to produce at once both the desired uniformity and maximum deposition rate can be avoided.

Analysis of BN coating data provided by DLC

DLC provided an extensive database of information concerning the manufacturing of BN preform coatings. A subset of these data (approximately 40 separate coating runs) was analyzed to more accurately establish three parameters used in our model of the fiber-coating process. These parameters were previously determined from literature values or were fit to the very limited data that were available initially. The three parameters are: (1) the activation energy for BN deposition; (2) the sticking coefficient for the BN gas-phase precursor (assumed to be Cl_2BNH_2); and, (3) the tortuosity, which is a correction to the binary diffusivity that accounts for flow through the preform. Fitting these parameters to the expanded data set yields values of 54 kJ mol^{-1} K^{-1}, 0.0045, and 7.7. The high quality of the fit is evident from Figure 4, which compares the measured weight gain of the preform with the value computed by the model. The solid line represents perfect agreement, while the dashed lines show the boundaries representing □ 30% deviation from the correct value. We conclude from this plot that the deviations in the model are comparable to differences in data for identical process runs, i.e., to the uncertainty in the available data.

Using the new fit parameters, we can predict coating uniformities for the various process runs included in the subset of the database. Figure 5 compares predicted and measured values of the uniformity *U* as a function of the deposition modulus. The plot shows that model predictions are consistent with the trend displayed by the data, despite considerable uncertainties in the measured values. For these data, the measured centerline coating thickness varies by a factor of two between identical parts, while the thickness across the surface of the preform also varies by a factor of two from edge to edge, due to the presence of holes in the plates used to clamp the preform.

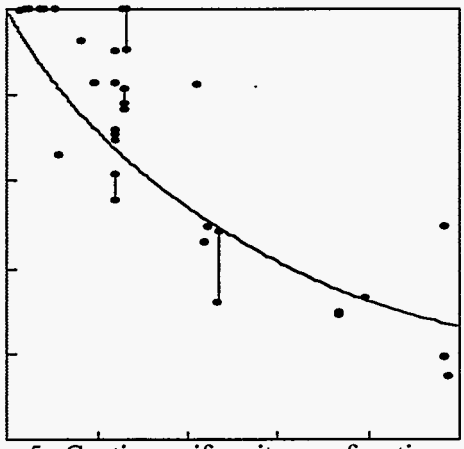

Figure 5. Coating uniformity as a function of deposition modulus.

Although the results of this fitting process yield a model that successfully predicts several trends in the data obtained from DLC's reactor, our more detailed analysis reveals several inconsistencies that require further investigation in order to fully prove the model. These include: an activation energy for BN deposition that is considerably smaller than the value reported in the literature; deposition rates measured in one small reactor that are about a factor of two smaller than those obtained in another under otherwise comparable conditions; BN deposition rates that increase with the ammonia concentration, which is the opposite of the trend predicted by the model; and a stronger-than-expected dependence of the deposition rate on pressure. Given the complexity of the commercial reactors from which the data used in the fit were taken, these discrepancies are not surprising. However, it is important that some understanding of their cause be determined, so that the model can be made as generic as possible. Consequently, we plan additional experiments and modeling in FY 1998 that we expect will shed light on the origin of these differences between observation and model prediction.

Task 3. Implementation of strategies for process design, optimization, and operation

Several strategies for optimizing the fiber-coating process used by DLC are suggested by our model, as described above and in earlier reports. One prediction of the model suggests that lowering the deposition temperature and raising the pressure from their present values should increase the coating uniformity and the deposition rate. Dr. Craig Shumaker at DLC conducted several experiments in which lower temperatures were used to deposit BN on fiber preforms. The results indicate that the uniformity did indeed increase, as did the reactor yield (i.e., the percentage of good parts). These data confirm our predictions that deposition uniformity depends *only* on the temperature, while the deposition rate depends on both the temperature and pressure.

Task 4. Development of process-control sensors

The need to develop sensors for monitoring the BN deposition process was discussed during a visit by project leader Mark Allendorf to DLC's facility in Newark, Delaware. Initially, it was thought that improvements in coating uniformity and minimization of

deposition times would require periodic changes in deposition temperature and pressure during the production run, control of which would be facilitated by the use of on-line sensors monitoring the deposition process. However, current modeling results indicate that this is not necessary. In addition, our improved understanding of the process chemistry has also improved considerably and suggests that it is unlikely that gas-phase species that could be used to measure the progress of deposition will be detectable in the downstream process gases. In the DLC reactor most of these species are removed before they reach a point in the downstream piping where they could be detected. For these reasons, we believe it is neither necessary nor productive to attempt to develop on-line sensors for this process and suggest that no further efforts be expended on this task.

Task 5. Chemical kinetics of precursor systems for float-glass coating

The objective of this task is to develop an understanding of the important chemical phenomena occurring during CVD of indium tin oxide (ITO). This knowledge is essential to the development of a stable process producing high-quality, defect-free coatings. Little is known about the thermodynamics and kinetics of the chemical reactions that occur during deposition. Consequently, our investigations in this task include experiments, theory, and modeling aimed at developing chemical mechanisms that can be used to determine precursor stability under various operating conditions and to predict the evolution of the gas-phase during processing. Principal results are summarized below.

Thermochemistry

Reliable thermodynamic data are unavailable for most gas-phase species relevant to the CVD of indium-containing compounds. Data that are available from standard sources are summarized in Table 1. For these species, we converted the reported thermodynamic data from tabular form to useful polynomial fits that are readily used by Sandia computer models. For molecules for which there are no data, we estimated heats of formation by comparing values for similar compounds and trends exhibited by the series of analogous Group III compounds containing boron, aluminum, and gallium. These data are also given in Table 1. *Ab initio* calculations were then conducted to predict vibrational frequencies needed to predict heat capacities and entropies.

Since the uncertainty associated with the estimated values in Table 1 is rather high in some cases, we are developing theoretical methods for predicting these quantities. A search of available basis sets for *ab initio* calculations identified only one basis set that is both appropriate for indium compounds and sufficiently small to be computationally practical. This is the Stevens/Basch/Krauss/Jasien/Cundari -21G ECP Basis, which is available from the Pacific Northwest Laboratories. Preliminary results, in which we used this basis set to predict atomization energies, suggest that it may be possible to improve

the accuracy of the data shown in Table 1 using these methods. Work in this area will continue in FY 1998.

Table 1. Heats of formation for gas-phase species relevant to ITO CVD.

Species	ΔH°_{298}	Species	ΔH°_{298}
In[1]	57.53	$In(CH_3)_2$ [2]	53.4
InOH[1]	-29.74	$In(OH)(CH_3)$ [2]	-20.8
InO[1]	34.89	$In(OH)_2$ [2]	-95
In_2O[1]	-8.31	CH_3 [4]	34.9
In(s,l) [1]	0	OH [4]	9.5
$In(CH_3)_3$[3]	41.1		
$In(OH)(CH_3)_2$ [2]	-20.7		
$In(OH)_2(CH_3)$ [2]	-82.3		
$In(OH)_3$ [2]	-144		

[1] L. V. Gurvich et al. *Thermodynamic Properties of Individual Substances*, CRC Press (Boca Raton), 1994. [2] Estimate, this work. [3] W. D. Clark, S. J. W. Price *Can J. Chem.* **46**, 1633 (1968). [4] *JANAF Thermochemical Tables.*

Vapor delivery systems for indium-containing precursors

Delivery of the vapors of indium-containing precursors to the HTFR for experimentation is challenging since all compounds of interest are solids with low vapor pressures. This year we tested three delivery systems, including: (1) a system built by J. C. Schumacher Inc. and originally designed for delivery of low-vapor-pressure liquids; (2) a temperature-controlled vaporizer designed to improve on limitations of the commercial system and built at Sandia; and (3) a direct-liquid-injection (DLI) system made by MKS Instruments. Of the three, the DLI system is the most promising, as it can achieve the highest delivery rates and does not require prolonged storage of precursors at elevated temperature in order to elevate their vapor pressure. We are also experimenting with methods for forming some precursors *in situ*. This avoids many of the difficulties associated with handling the compounds, since compounds such as trimethylindium (TMI), which have relatively high vapor pressures, can be used as the indium source.

Kinetics of precursor pyrolysis

Knowledge of the thermal stability of coating precursors is of great importance to the design of new CVD processes, since it can affect aspects of the design such as residence time within heated lines, long-term storage temperatures, and gas-phase particle nucleation. This year's investigations focused on two compounds: trimethylindium (TMI) and a proprietary precursor developed by LOF. Results of the TMI investigations are described here. Previous investigations in the literature suggest that TMI decomposes by sequential loss of methyl groups:

$$In(CH_3)_3 \leftrightarrow In(CH_3)_2 + CH_3 \quad (3)$$
$$In(CH_3)_2 \leftrightarrow InCH_3 + CH_3 \quad (4)$$
$$InCH_3 \leftrightarrow In + CH_3 \quad (5)$$

This year, we conducted a series of HTFR experiments to probe these reactions and determine the overall rate of TMI decomposition as a function of temperature. Results of these investigations are summarized below:

- The mass spectrum of TMI was recorded and is shown in Figure 6. The figure shows that the parent ion ($In(CH_3)_3^+$) is not observed, which proved to be the case at all ionization energies used (20-70 eV). This complicates the interpretation of pyrolysis data, since the strongest ion signal (m/e 145), may correspond to either the reactant or the product $In(CH_3)_2$. Evidence from the literature suggests that the concentration of $In(CH_3)_2$ should be very low.

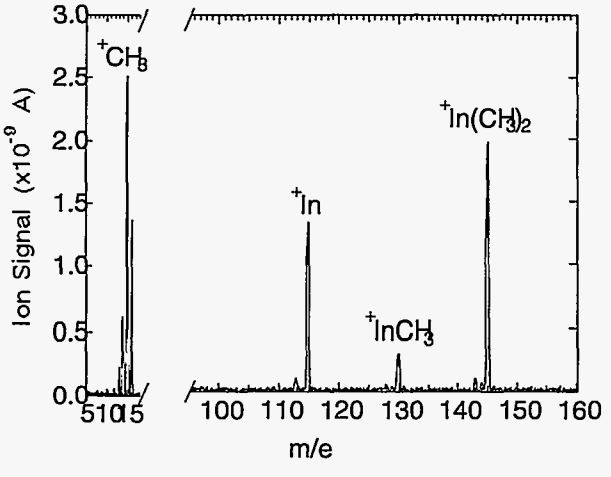

Figure 6. Mass spectrum of trimethylindium.

- The rate of TMI decomposition and formation of products were measured in the HTFR from 523 K to 698 K at a total pressure of 10 Torr. Typical results are shown in Figure 7. The decomposition of TMI is strongly temperature dependent and produces methane and ethane as the two principal products. Addition of an excess of the radical scavenger toluene had no effect on the measured rate, suggesting that radical-chain mechanisms do not affect the measured rate under the conditions of our experiments.

• Non-linearity in the curves shown in Figures 7 and 8 was shown to be primarily caused by non-uniform temperature profiles in the HTFR. This non-uniformity is caused by the use of a water-cooled injector, which is required since TMI is thermally unstable. This curvature invalidates the linear least-squares analysis (Figure 8, dashed line) normally applied to determine rate constants (normally, the rate constant is simply the slope of the line fit to the data). Consequently, we developed a new analytical method for extracting rate constants from HTFR data that uses a non-linear least-squares fitting routine to fit the predictions of a comprehensive model (Sandia's CRESLAF code) of the reactor. CRESLAF simulates the flow of reacting gases through a tube using the boundary-layer approximations and can account for the non-uniform axial temperature profile. A typical fit obtained in this manner is shown in Fig. 8 (solid line). Using this method, we obtained a rate constant $k_3(s^{-1}) = 7.00x10^{15}exp(-46,170/RT)$ for Reaction 3, which agrees reasonably well with the limited data available in the literature for this reaction (Figure 9).

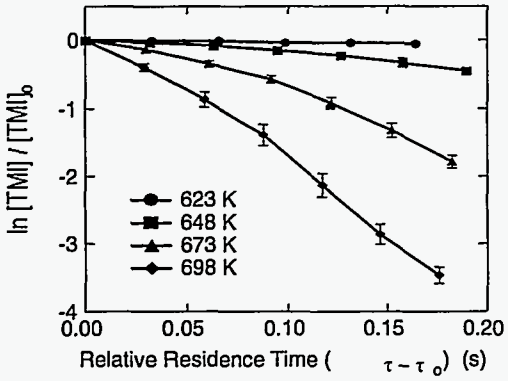

Figure 7. Temperature dependence of TMI concentration as a function of residence time. model.

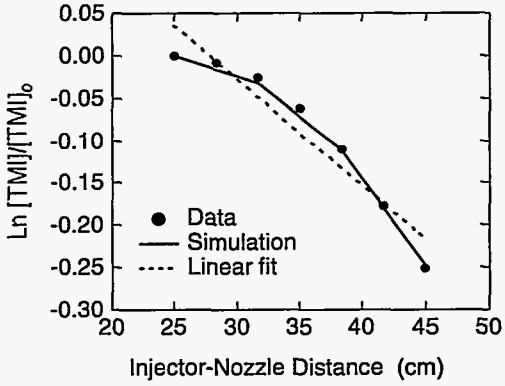

Figure 8. 648 K data from Fig. 7 fit by linear least-squares method using the CRESLAF model.

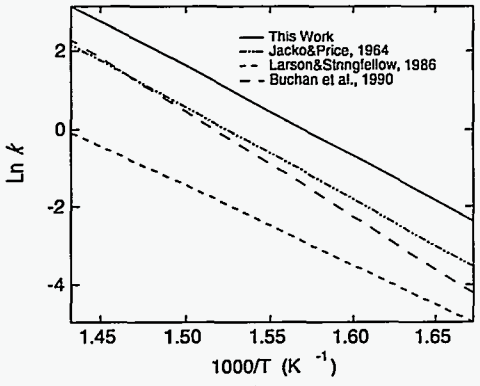

Figure 9.Comparison of literature rate expressions for TMI pyrolysis with results of this work.

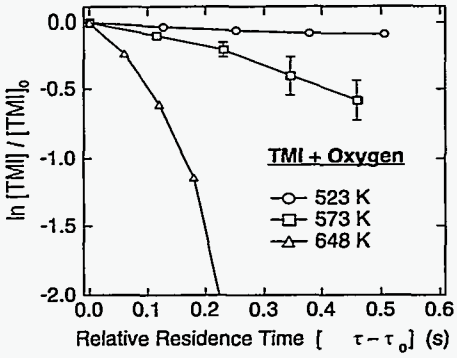

Figure 10. Decay of the TMI signal as a function of the relative residence time at a reactor pressure of 20 Torr.

A valuable feature of this new approach to the analysis of flow-reactor data is that it enables one to measure a reaction's temperature dependence by conducting a single experiment, rather than a series of experiments at different temperatures. This is possible because the gases are exposed to a range of temperatures as they travel through the HTFR and the analysis does not assume that the temperature profile is uniform. Thus, when one would like to obtain a broad picture of a molecule's reactivity, activation energies for a series of related reactions could be obtained (e.g., TMI + NH_3, PH_3, or AsH_3) with a relatively small number of experiments.

Kinetics of TMI oxidation

Understanding the reactions between indium-containing precursors and oxygen is clearly of importance for the formation of ITO, since oxygen is a major component of the reactant gases. An investigation of the reaction between TMI and O_2 in the HTFR showed that this chemistry is quite complex. Except for the observation that TMI reacts readily with O_2, thereby increasing its rate of decay at pyrolysis temperatures (Figure 10), the experimental results are difficult to interpret and point to possible heterogeneous mechanisms. No volatile product species were detected from which to formulate a governing equation, making the analysis even more difficult. Investigations of this system will continue in FY 1998; experiments will be conducted using other oxygen-containing reactants, such as water vapor, whose chemistry is expected to be less complex but which should shed light on the TMI+O_2 reaction.

Task 6. In-situ process-control sensors for float-glass coating

Construction of a test cell for process diagnostics

Although the HTFR is an excellent tool for investigating complex chemical reactions, its complexity makes it difficult to quickly obtain qualitative information. It is also not an ideal environment for testing diagnostic techniques with potential for process control, due to the limited access to the heated flow tube. To overcome these limitations, we constructed a heated test cell (depicted in Figure 11) that will be equipped with an off-the-shelf residual gas analyzer and a Fourier transform infrared spectrometer. The unit is designed for flexibility, so that we can change from one chemical system to another with little downtime. The unit will allow us to evaluate sensor/control schemes based on the analysis of gas-phase constituents.

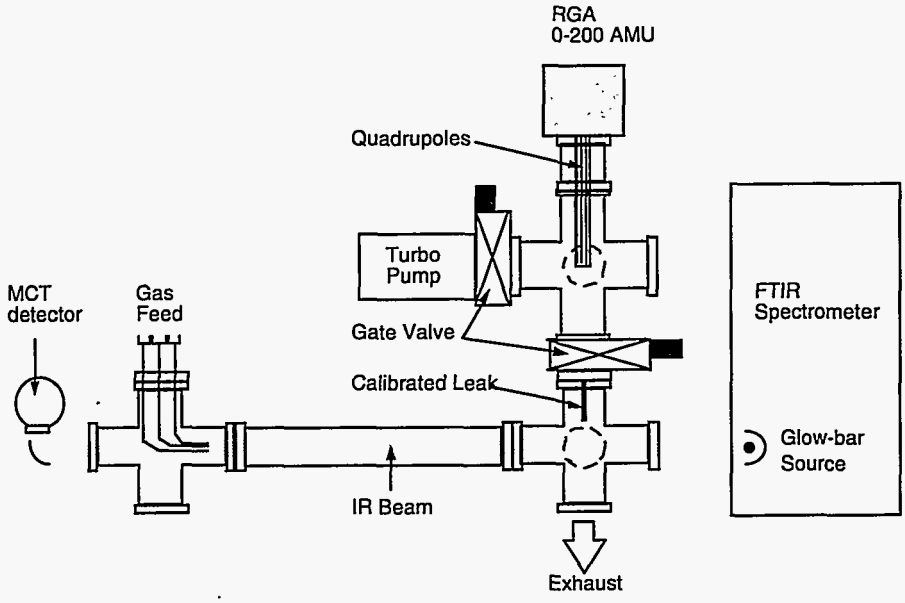

Figure 11. Schematic of diagnostics test cell.

PUBLICATIONS

S. K. Griffiths and R. H. Nilson, "Optimum Conditions for Composites Fiber Coating by Chemical Vapor Infiltration," submitted to *J. Electrochem. Soc.*, 1997. Also Sandia National Laboratories Report SAND97-8255, (1997).

M. D. Allendorf and C. F. Melius, "Thermochemistry of Molecules in the B-N-H-Cl System: *Ab Initio* Predictions Using the BAC-MP4 Method," *J. Phys. Chem. A*, **101** (1997), 2670.

F. Teyssandier and M. D. Allendorf, "Thermochemistry and Kinetics of Gas-Phase Reactions in the Ti-Cl-H System," submitted to *J. Electrochem. Soc.*, (1997).

A. H. McDaniel and M. D. Allendorf, "A Flow-Tube Investigation of the High-Temperature Reaction Between BCl_3 and NH_3," submitted to *J. Phys. Chem.*, (1997).

F. Teyssandier and M. D. Allendorf, "Thermodynamics and Kinetics in the Ti-Cl-H System," accepted for publication in *Fourteenth Int. Symp. Chem. Vapor Dep.*, The Electrochemical Society Proceedings Series, Vol 97-25, p. 15, (1997).

C. F. Melius and M. D. Allendorf, "Quantum Chemistry: A Review of *Ab Initio* Methods and Their Use in Predicting Thermochemical Data for CVD Processes," *Fourteenth Int. Symp. Chem. Vapor Dep.*, The Electrochemical Society Proceedings Series, Vol 97-25, p. 1, (1997).

A. H. McDaniel and M. D. Allendorf, "The Reactions of BCl_3 and NH_3 Relevant to the CVD of Boron Nitride," *Fourteenth Int. Symp. Chem. Vapor Dep.*, The Electrochemical Society Proceedings Series, Vol 97-25, p. 40, (1997).

S. K. Griffiths and R. H. Nilson, "Conditions for Maximum Centerline Deposition Rates in Composites Fiber Coating by Chemical Vapor Infiltration," *Fourteenth Int. Symp. Chem. Vapor Dep.*, The Electrochemical Society Proceedings Series, Vol 97-25, p. 544, (1997).

PRESENTATIONS

M. L. Chase, D. Hildenbrand, and M. D. Allendorf, "Thermodynamic Properties of Boron," poster presented at *High Temperature Materials Chemistry IX*, Penn. State University, (May 19-23, 1997).

M. D. Allendorf, R. M. McCurdy and P. Gerhardinger, "Development of Advanced Energy-Efficient Coatings for Low-E Sunbelt Applications," poster presented at *Second OIT/Expo*, Arlington, Virginia, (February 1997).

M. D. Allendorf and C. Shumaker "Development of Process Models for Advanced Fiber-Preform Coating Technologies," poster presented at *Second OIT/Expo*, Arlington, Virginia, (February 1997).

M. D. Allendorf and C. B. Schumaker, "Process Simulation for Advanced Composites Production and Glass Process Development," Annual Review, DOE/Advanced Industrial Materials Program, Albuquerque, New Mexico, (June 1997).

HONORS AND AWARDS

E. Karl Bastress Award, given to Mark Allendorf by Sandia National Laboratories "for technical accomplishments and leadership that have established a strong and effective coupling of Sandia's interdisciplinary fundamental research on high-temperature chemical synthesis of advanced materials with the U.S. ceramics, composites, and glass manufacturing industries."

PATENTS/DISCLOSURES

None during this reporting period.

LICENSES

None during this reporting period.

INDUSTRIAL INPUT AND TECHNOLOGY TRANSFER

DLC shared a large body of data on fiber coating obtained in their reactors with Sandia to assist in the verification of the model developed in this project. Sandia developed strategies for process optimization specific to DLC's fiber-coating reactors and developed a parameterized model for use by DLC based on their processing data.

COST SHARING

LOF provided $180 K of direct and in-kind cost sharing to support investigations of float-glass coating chemistry. DLC provided $85 K of in-kind cost-sharing to support fiber-coating modeling efforts.

ESTIMATED ENERGY SAVINGS

The availability of low-cost, fiber-reinforced composites will have a major impact on both energy consumption and pollutant production in energy-intensive industries. For example, it is estimated that widespread use of ceramic composites will result in energy savings of up to 0.52 Quads/year in gas turbines, 0.5 Quads/year in high-pressure heat exchangers, 0.1 Quads/year in hot-gas cleaning systems, and 0.5 Quads/year in radiant burners (such as those used in the metals and glass industries (all figures courtesy of the DOE/Continuous Fiber Ceramic Composites Program). These energy savings and emission reductions can be achieved primarily through process operation at higher temperatures, where fuel combustion is more efficient.

In North America, 2.6 Million tons/year of float glass are used in residential and commercial construction. Use of so-called "low-E" (for "low emissivity") coatings on this glass can dramatically improve the energy efficiency of this material. New coatings developed in this project will save 1.4×10^{19} Btu/year when installed in place of clear glass windows.

Research performed at Sandia National Laboratories, California, sponsored by the U.S. Department of Energy, Assistant Secretary for Energy Efficiency and Renewable Energy, Office of Industrial Technologies, Advanced Industrial Materials Program, and the Glass Industry Vision Team.

SYNTHESIS AND PROCESSING OF COMPOSITES BY REACTIVE METAL PENETRATION

R. E. Loehman and K. G. Ewsuk
Sandia National Laboratories
Albuquerque, New Mexico 87185

A. P. Tomsia
Pask Research and Engineering
Berkeley, California 94720

W. G. Fahrenholtz
University of New Mexico
Albuquerque, New Mexico 87106

INTRODUCTION

Development of improved products and processes often requires new and improved materials. Ceramic-metal composites are better than conventional materials for many applications because of their high stiffness-to-weight ratios, good fracture toughness, excellent high-temperature stability, and because their electrical and thermal properties can be varied through control of their compositions and microstructures. However, despite a lot of development effort, ceramic composites are still too expensive for many applications and they have not demonstrated sufficient reliability for wide commercial use. Results obtained previously in this project have shown that reactive metal penetration is a practical method for making ceramic and metal-matrix composites to near-net shape with control of both compositions and microstructures. Making parts to near net shape is a significant advantage because it reduces costly and energy intensive grinding and machining operations, and minimizes finishing wastes. Thus, reactive metal penetration is attractive as an economical process for making many of the advanced ceramic composites that are needed for light-weight structural and wear applications for transportation and energy conversion devices. The most promising composite compositions to date consist of Al and Al_2O_3 or Al, Al_2O_3 and $MoSi_2$. One spin-off of this work is development of a deep understanding of reactions between molten metals and ceramics. Promotion of reactions leads to composite material applications. Knowing how to minimize reactions leads to applications as refractories, containers, and die materials for the metal processing industries. Whether for the composites themselves or for the insight it gives into improving refractories, this work should be of particular interest to the aluminum industry.

The goals of this ceramic-metal composite research and development program are to:
(1) identify compositions favorable for making composites by reactive metal penetration; (2) understand the mechanism(s) by which these composites are formed; and, (3) control and optimize the process so that composites and composite coatings can be made economically; and 4.) apply to R&D results to problems of interest to industry.

Over the past two years the program has had a second part, performed under subcontract by SRI International. The SRI effort is concerned with making composite coatings, especially corrosion-resistant coatings on metals, by pyrolysis of preceramic polymers blended with metal or ceramic powders. Those coatings have advantages in engineering applications because they can protect metals such as aluminum and mild steel from corrosive environments. In addition, they are stable at high temperatures and may increase surface hardness. The preceramic polymer serves both as a high temperature polymeric binder and, after pyrolysis, as a ceramic matrix. The composite coatings are applied by simple deposition techniques such as brushing, spraying, rolling, or dipping. The technique is a relatively low cost way to make durable coatings, but it requires further development to improve the processing conditions and coating uniformity, and to evaluate properties.

The goals of the preceramic polymer research effort are to:

(1) identify feasible compositional systems for making composite coatings with good corrosion resistance;
(2) evaluate the corrosion resistance in severe environments; and
(3) to optimize formulation, deposition, and curing processes, especially low temperature processes

TECHNICAL PROGRESS - FY 1997

Summary

This past year we developed a mechanistic model for composite formation that explains several important features: (1) the rapid, linear kinetics of formation for temperatures below about 1100°C; (2) the decrease in reaction rate above 1100°C; and, (3) the effect of Si concentration in the Al on reaction kinetics. The key to developing the model was availability of new microstructural information from transmission electron microscopy (TEM) studies done in collaboration with Professor Ping Lu of New Mexico Tech.

Previous kinetic studies showed that the thickness of the composite layer produced by Reaction 1 increases in direct proportion to time.

$$8\ Al + 3\ Al_6Si_2O_{13} \rightarrow 13\ Al_2O_3 + 6\ Si \qquad (1)$$

Analysis of reaction rate data showed that below 900°C, Reaction 1 does not proceed due to poor wetting and kinetic limitations. Above 1100°C, the reaction is rapid initially, but it stops after a brief period of a few minutes where the growth kinetics are linear. As shown in Figure 1, TEM micrographs of the aluminum-mullite interface show that the reaction front in quenched specimens does not contain any silicon after heating at 900°C,

whereas a lot of it is present in samples heated at 1100°C. The model explaining this difference is based on the fact that the activation energy for forming Si by Reaction 1 is much greater than the activation energy for Si diffusion in Al. Thus, at 900°C silicon production at the interface is much slower than its transport away from the reaction front, but because of the steep temperature dependence of Reaction 1, by 1100°C the rates are approximately comparable (see Figure 2). Above 1100°C, silicon production is much faster than its transport, causing silicon to build up near the reaction front, which inhibits further reaction. The rapid, linear growth period is observed when the composite formation reaction is controlled by the Si transport rate. The observed time of the linear growth period decreases from 250 minutes at 1100°C to less than a minute at 1250°C. Above 1250°C, the reaction zone is too thin to be detected by optical microscopy. One practical consequence of our model is that it has allowed us to construct a process diagram showing the time-temperature combinations where the reactive metal penetration (RMP) reaction between aluminum and mullite has favorable rates (see Figure 3).

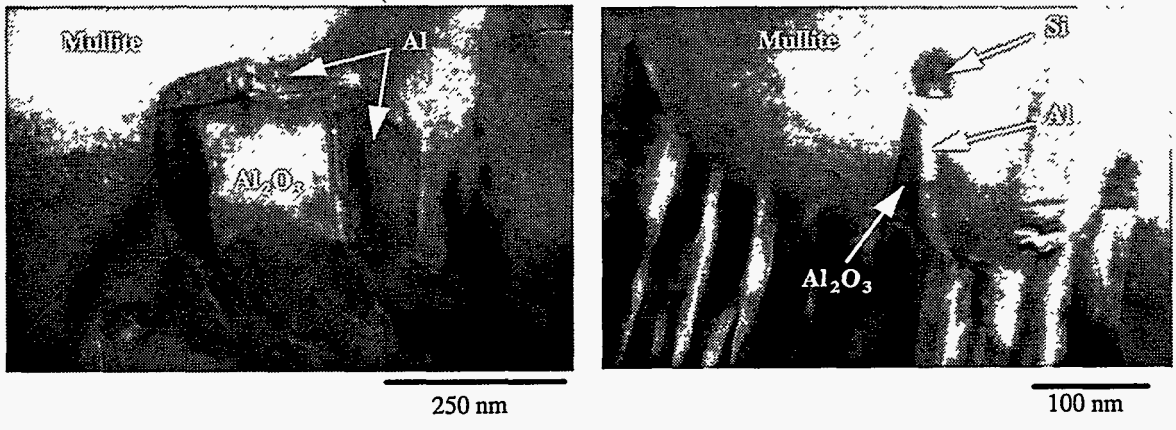

Figure 1. TEM micrographs of the aluminum mullite reaction interface after reaction at (a) 900°C for 10 minutes; (b) 1100°C for 10 minutes.

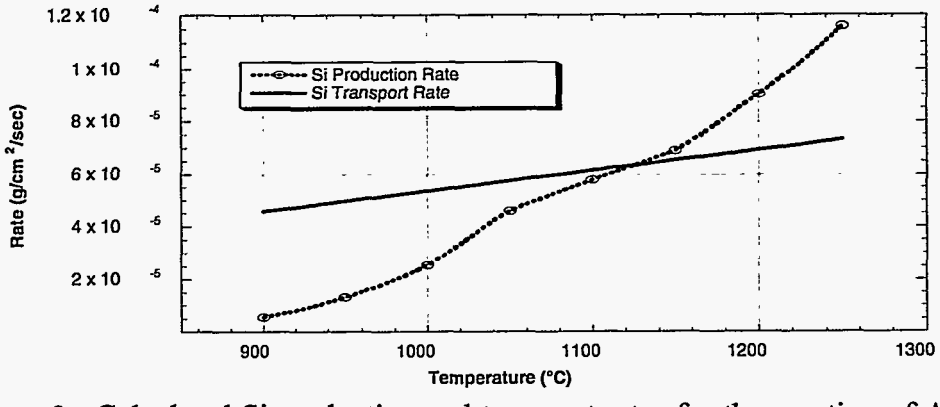

Figure 2. Calculated Si production and transport rates for the reaction of Al and mullite as a function of reaction temperature.

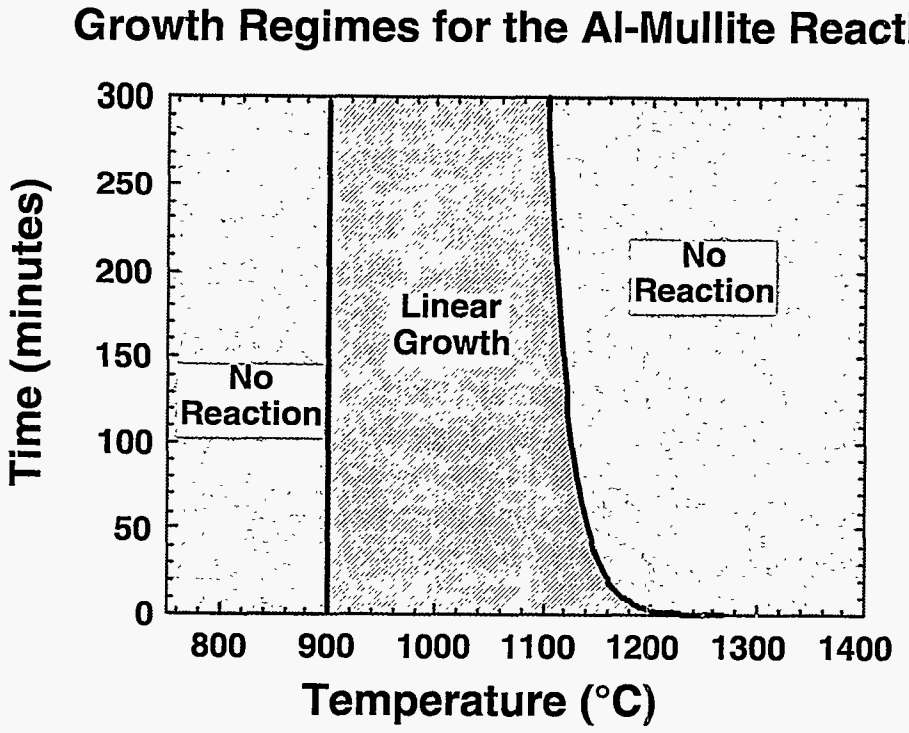

Figure 3. RMP processing map detailing the time-temperature response of the Al-mullite reaction.

Our understanding of metal-ceramic reactions has led to study of other composites where in situ synthesis might be attractive. For example, molybdenum intermetallic compounds, most notably $MoSi_2$ and Mo_5Si_3, are candidates for use in high temperature, oxidizing environments. However, monolithic molybdenum intermetallics have low strength and toughness below their brittle to ductile transition (BDT) temperatures, and a high creep rate above the BDT. To overcome these limitations, the use of ceramic-intermetallic composites has been proposed for some applications. Alumina is an ideal choice for a second phase because of its thermodynamic stability in contact with many molybdenum compounds, its high strength, its creep resistance, and its thermal expansion match with $MoSi_2$. Conventional composite synthesis from alumina and $MoSi_2$ powders requires extreme processing conditions such as hot pressing above 1600°C or plasma spraying. Synthesis by in situ methods such as reactive metal penetration and reactive hot pressing are attractive alternatives because of lower processing temperatures and the potential for ambient pressure densification. Last year we investigated the thermodynamics of reactions in the Mo-Al-mullite system and began developing some processing procedures. This year we optimized the processing to make three composites in three different families: Al_2O_3-$MoSi_2$, Al_2O_3-$Mo(Si_{0.93}Al_{1.43})$, and Al_2O_3-$Mo(Si_{0.93}Al_{1.43})$-Mo_3Al_8. $Mo(Si_{0.93}Al_{1.43})$ was included because it is the only reported ternary compound in the Mo-Al-Si system. The density, Young's modulus, four-point bend strength, and fracture toughness of the three different composites were

evaluated. These composites were found to have excellent strength and stiffness at room temperature.

Low-cost preceramic binders mixed with a broad range of fillers can be applied to metals as composite coatings that adhere well and are very corrosion resistant. The concept is based on the use of a mixture of preceramic polymers, ceramic powders, and metal powders that react after heating to make durable coatings. Such formulations, when heated above 450°C, yield ceramic or metal/ceramic composite coatings, some with near zero shrinkage. At lower temperatures, an inorganic-organic hybrid material (90% and above is inorganic) coating is formed from the highly cured polymer and the filler powders. When applied to aluminum, steel, and other metals, these coatings are very adherent, withstand wear, and are thinner than coatings from conventional, corrosion resistant paints. In addition, VOC's are reduced and the coatings are resistant to HCl and long-term, salt spray exposure.

Task 1. Evaluate Reactions and Mechanisms of Composite Formation in the Al/Mullite System

Recently collected microstructural information has given us new insight into the reaction between aluminum and mullite. In a collaboration with Professor Ping Lu of New Mexico Tech, we used TEM to analyze aluminum-mullite reaction couples. Previously we showed that the reaction layer thickness increases linearly with time over a range of temperatures and that its rate is a strong function of temperature, with an activation energy of ~90 kJ/mole and a penetration rate of 6 mm/hour at 1100°C. As the temperature increases above 1100°C, the linear growth period becomes progressively shorter and eventually stops. The duration of linear growth decreases from 250 minutes for reaction at 1100°C to less than a minute for reaction at 1250°C (Table 1). Until recently, this rapid decrease in growth kinetics was not understood.

Table 1. Duration of linear composite growth as a function of temperature for the reactive metal penetration of mullite by aluminum.

Reaction Temperature	Reaction Layer Thickness	Reaction Rate	Time of Linear Growth (min)
1150°C	2.4 mm	6.0 mm/hr	25 min
1200°C	0.6 mm	7.8 mm/hr	5 min
1250°C	0.1 mm	10.0 mm/hr	0.6 min

Figure 1 shows TEM micrographs of the Al-mullite reaction interface after reaction at 900°C and 1100°C. After reaction at 900°C, the reaction front does not contain any silicon. This suggests that the rate at which silicon is removed from the reaction front is much greater than the rate at which it is produced by Reaction 1. TEM micrographs such as that presented in Figure 1 show that after reaction at 1100°C for 10 minutes there is a significant amount of silicon present at the reaction front. For this to occur, the silicon transport rate must be at least a little slower than the silicon production rate. Kinetic data show that the reaction proceeds for ~4 hrs at 1100°C before the reaction slows, implying that it takes that long for the silicon concentration at the reaction front to reach saturation. At higher reaction temperatures, the duration of the linear growth decreases until, at 1300°C and above, the reaction stops so soon that there is almost no detectable reaction layer. Our most recent results indicate that, when it precipitates, silicon stops the RMP reaction by forming a diffusion barrier at the aluminum-mullite reaction interface. Silicon is thermodynamically stable with both mullite and the reacting metal so once it forms there is no tendency for further reaction.

To gain further insight into the reaction mechanism, we calculated the rate of Si production at the reaction front from our measured penetration rates. We then calculated the Si removal rate by diffusion using literature values of the Si diffusion coefficient and diffusion activation energy for the particular microstructure observed at the Al-mullite reaction front. The calculated rates of Si production and transport are compared in Figure 2 as a function of temperature. A comparison of these rates shows that, as suggested by the TEM results, Si transport is faster than Si production in the linear growth regime that occurs at reaction temperatures between 900°C and 1100°C. In this temperature range, Si concentration at the reaction front remains relatively low. As the reaction temperature increases, the Si production rate increases faster than does Si transport. This more rapid increase in Si production is due to a significantly higher activation energy of ~100 kJ/mole for Si production compared to only ~20 kJ/mole for Si transport. Earlier we showed that the extent of reaction between mullite and Al-Si alloys at 900-1100°C decreases with increasing Si content in the alloy and that there is no reaction between mullite and molten Al saturated with Si. The calculated magnitudes and temperature dependences of the Si production and transport rates support the reaction mechanism described above that was based solely on kinetic and microstructural data.

The kinetic data have been used to construct a time-temperature-reaction map that defines the time-temperature combinations where the RMP reaction mechanism described above is operative (Figure 3). Below 900°C, the reaction is kinetically limited and therefore it does not proceed at an appreciable rate.

Phase equilibrium diagrams provide a wealth of useful information for processing ceramics. Our work on ceramic-metal reactions has not previously benefited from this approach because few ternary diagrams exist for the systems we have studied. Recently, we acquired a versatile software package (MTDATA, AEA Software, Pittsburgh,

Pennsylvania) that calculates equilibrium phase diagrams from available thermodynamic data. In the past year, we used MTDATA to calculate ternary equilibrium diagrams for several systems of interest to RMP composite processing. We compared calculated diagrams with published binary and ternary diagrams to evaluate the accuracy of the program. The ability to calculate equilibrium diagrams is giving us a great deal of information on reaction paths, and it will aid in screening potential reaction systems. The utility of the approach is discussed below in terms of the Al-Ti-O phase diagram.

Task 2. Evaluate Other Ceramic-metal Systems

Work this past year concentrated on further investigations of in situ formation of metal-ceramic composites containing structural intermetallic phases. The compositions of particular interest to us are those made according to Reactions 2-4 :

$$3\ Mo + 8\ Al + 3\ Al_6Si_2O_{13} \rightarrow 13\ Al_2O_3 + 3\ MoSi_2 \quad (2)$$
$$6.5\ Mo + 17.3\ Al + 3\ Al_6Si_2O_{13} \rightarrow 13\ Al_2O_3 + 6.5\ MoSi_{0.93}Al_{1.43} \quad (3)$$
$$9.5\ Mo + 25.3\ Al + 3\ Al_6Si_2O_{13} \rightarrow 13\ Al_2O_3 + 6.5\ MoSi_{0.93}Al_{1.43} + Mo_3Al_8 \quad (4)$$

We made the composites by reactive sintering or reactive hot pressing of powders that were mixed either by ball milling or by attritor milling. The two mixing methods yielded powders that produced composites with significantly different properties. Table 2 lists the hot pressing temperatures, final densities, and four-point bend strengths for all three compositions and both mixing methods. Not only did the attritor milled powders press to higher relative densities, but the composites made from them had higher strengths. Table 3 lists other mechanical properties for each of the three3 composites prepared from attritor milled precursor powders. The microstructures of the composites produced from the two powders were different as well. Optical micrographs, shown in Figure 4, compare the microstructures of Al_2O_3-$MoSi_2$ composites hot pressed from ball milled and attritor milled Mo, Al, and mullite powders that were batched according to Reaction 2. For composites produced from ball milled powders, the $MoSi_2$ phase is in the form of large, isolated particles that are typically greater than 100 μm in diameter. For Al_2O_3-$MoSi_2$ composites made from attritor milled powders, the $MoSi_2$ phase is in the form of thin, elongated bands that have an average thickness of ~10 μm. In both cases the $MoSi_2$ phase was produced by in situ reaction that required interdiffusion and rearrangement of the starting powders, which might have been expected to have a stronger effect on microstructure than powder mixing. Attritor milled powders batched and hot pressed according to Reactions 3 and 4 produced composites in which the ceramic and intermetallic phases are interpenetrating and co-continuous. These composites showed a smaller, but still noticeable decrease in the size of the interconnected ligaments when prepared from the attritor milled precursor powder.

Table 2. Hot pressing temperature, density, and four-point bend strength of composites prepared by hot pressing Mo, Al, and mullite powders mixed by ball milling or attritor milling.

Composite Phases	Al_2O_3 $MoSi_2$		Al_2O_3 $MoSi_{0.93}Al_{1.43}$		Al_2O_3 $MoSi_{0.93}Al_{1.43}$ Mo_3Al_8	
Mixing Method	Ball Mill	Attritor	Ball Mill	Attritor	Ball Mill	Attritor
Temperature(°C)	1450	1450	1450	1450	1450	1400
Relative Density (%)	87	93	90	93	97	98
Strength (MPa)	139	467	196	238	310	321

Table 3. Mechanical properties of composites prepared by hot pressing attritor milled Mo, Al, and mullite powders.

	Al_2O_3 $MoSi_2$	Al_2O_3 $MoSi_{0.93}Al_{1.43}$	Al_2O_3 $MoSi_{0.93}Al_{1.43}$-Mo_3Al_8
Toughness ($MPa \cdot m^{1/2}$)	2.8	3.5	5.2
Young's Modulus (GPa)	382	300	325
Hardness (GPa)	12.8	9.7	10.4

Compared to composites prepared from ball milled powder, we believe the properties of composites prepared from attritor-milled powders are better due to their higher relative densities and their finer, more homogeneous microstructures, The improved composite microstructure is attributed to better mixing and a finer ultimate particle size for the attritor milled precursor powders. Other researchers working on reaction bonding of aluminum oxide (RBAO) have shown that attritor milling is necessary to achieve the desired mixing and precursor powder morphology required for successful reaction bonding. Our powders were not milled under the extreme conditions employed for RBAO processing, but even mild attritor milling leads to better mixing than ball milling. Improved mixing should also benefit other composites prepared by reactive hot pressing such as Al_2O_3-Ti and Al_2O_3-Ni.

We used our newly-acquired capabilities in computational thermodynamics to investigate several systems that might be favorable for RMP processing. Figure 5 shows a ternary phase diagram calculated for the Al-Ti-O system at 1200°C using the MTDATA program. The diagram is consistent with published binary phase diagrams. As an example, using the calculated diagram, the products and reaction paths can be predicted for the reaction of Al and TiO_2 or Al and Al_2TiO_5, two systems we investigated earlier in the program. If Al is in contact with TiO_2 at 1200°C, the diagram shows that the equilibrium products should be Al_2O_3, TiO, and TiAl. The Gibbs energy for this reaction is -317 kJ/mole of Al_2O_3 at 1200°C. If the only reaction product of the oxidation of Al is Al_2O_3, then TiO_2 must be reduced through its sub-oxides to TiO in order to conserve mass. Some of the TiO then reacts with Al, forming TiAl and additional Al_2O_3. The ternary phase diagram shows that, at equilibrium, the product of the reduction of Al_2TiO_5 by Al will also be Al_2O_3, TiO, and TiAl. The Gibbs energy for this reaction is -85 kJ/mole. However, the ternary phase diagram suggests that the first stable reduction product of Al_2TiO_5 and Al has to be TiO_2, not TiO. Calculating the Gibbs' energy for this reaction shows that it is not favorable; i.e., there is a positive □G. Thus, Al in contact with Al_2TiO_5 is metastable. This prediction is consistent with experimental results showing that Al will react with TiO_2, but there is no significant reaction in the Al-Al_2TiO_5 system.

Task 5. Evaluate Ceramic-Metal Composite Microstructure and Properties

This task was successfully completed for composites in the Al_2O_3-Al system in FY96 and work was directed elsewhere in this reporting period. As our mechanistic studies identify other favorable systems for making composites we will introduce them into this task.

Task 7. Development of Commercial Collaborations

This past year we devoted a lot of effort negotiating a three-way CRADA among Sandia, the Reynolds Metals Co., and the A.P. Green Co. in the area of improved refractories for aluminum reprocessing, a subject to which our knowledge of Al-ceramic reactions has considerable relevance. The joint work statement for the CRADA was being evaluated by the DOE Albuquerque Area Office when we learned that the part of Reynolds we were dealing with had been sold and all of our contacts were leaving the company. Thus, we have had to put the CRADA on hold temporarily while we and A.P. Green seek another partner or group of partners from the aluminum industry. Those discussions are underway.

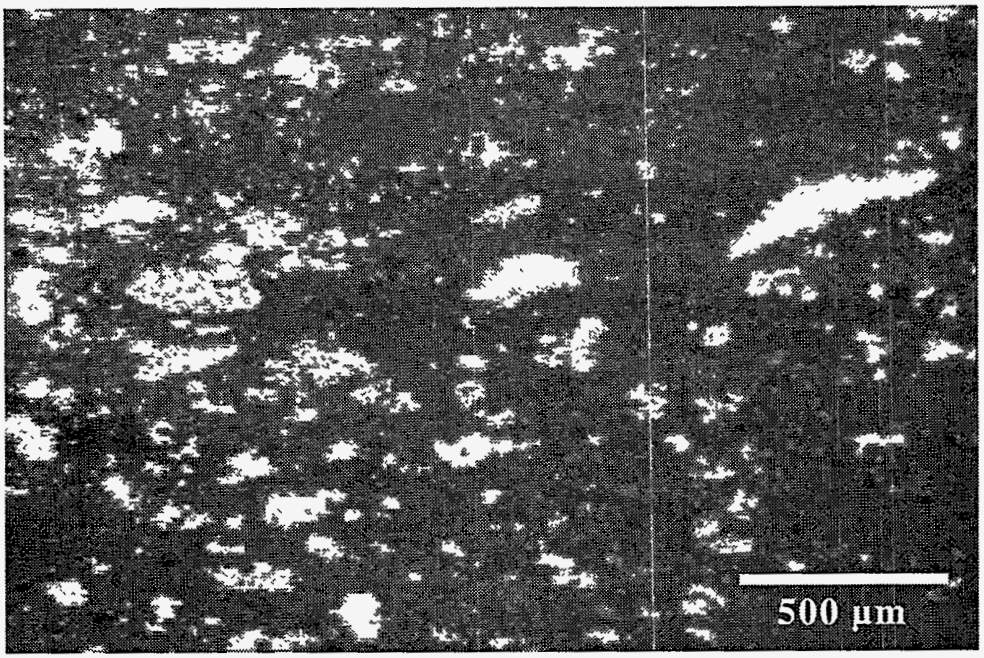

a

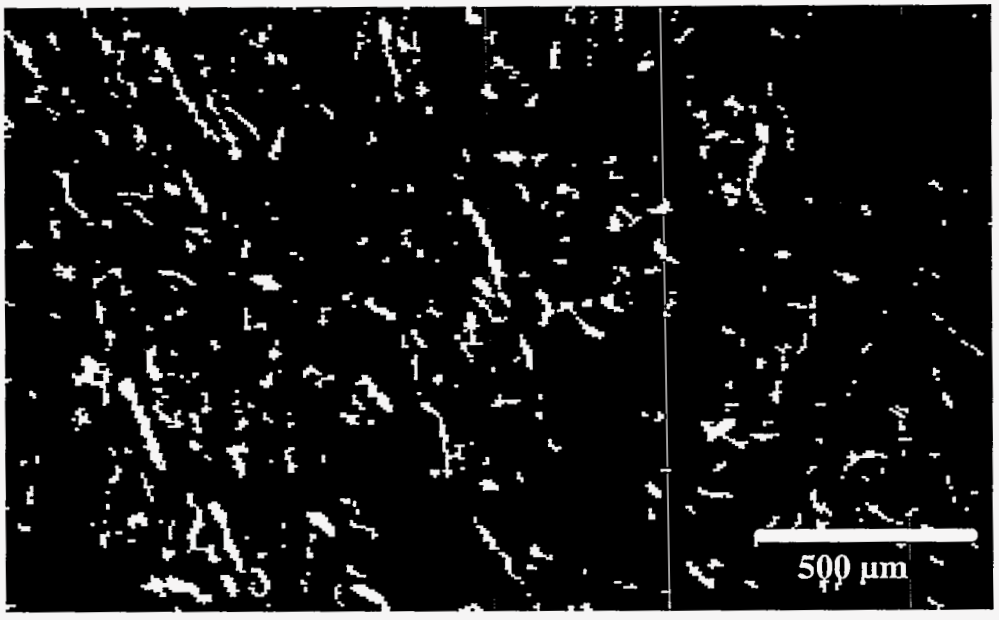

b

Figure 4. Optical micrographs of Al_2O_3-$MoSi_2$ composites prepared by reactive hot pressing of Mo-Al-mullite powders mixed by (a) ball milling, and (b) attritor milling.

We continue providing samples and information to companies who are evaluating our composites for their applications. For example, we provided samples to StratEdge Corporation for testing as thermal management components in electronic packages.

SRI has made presentations on their composite coatings results to Sherwin Williams, AISI, Loctite, Honeywell, ACC, Conversion Technology, and Azure Capital Corporation.

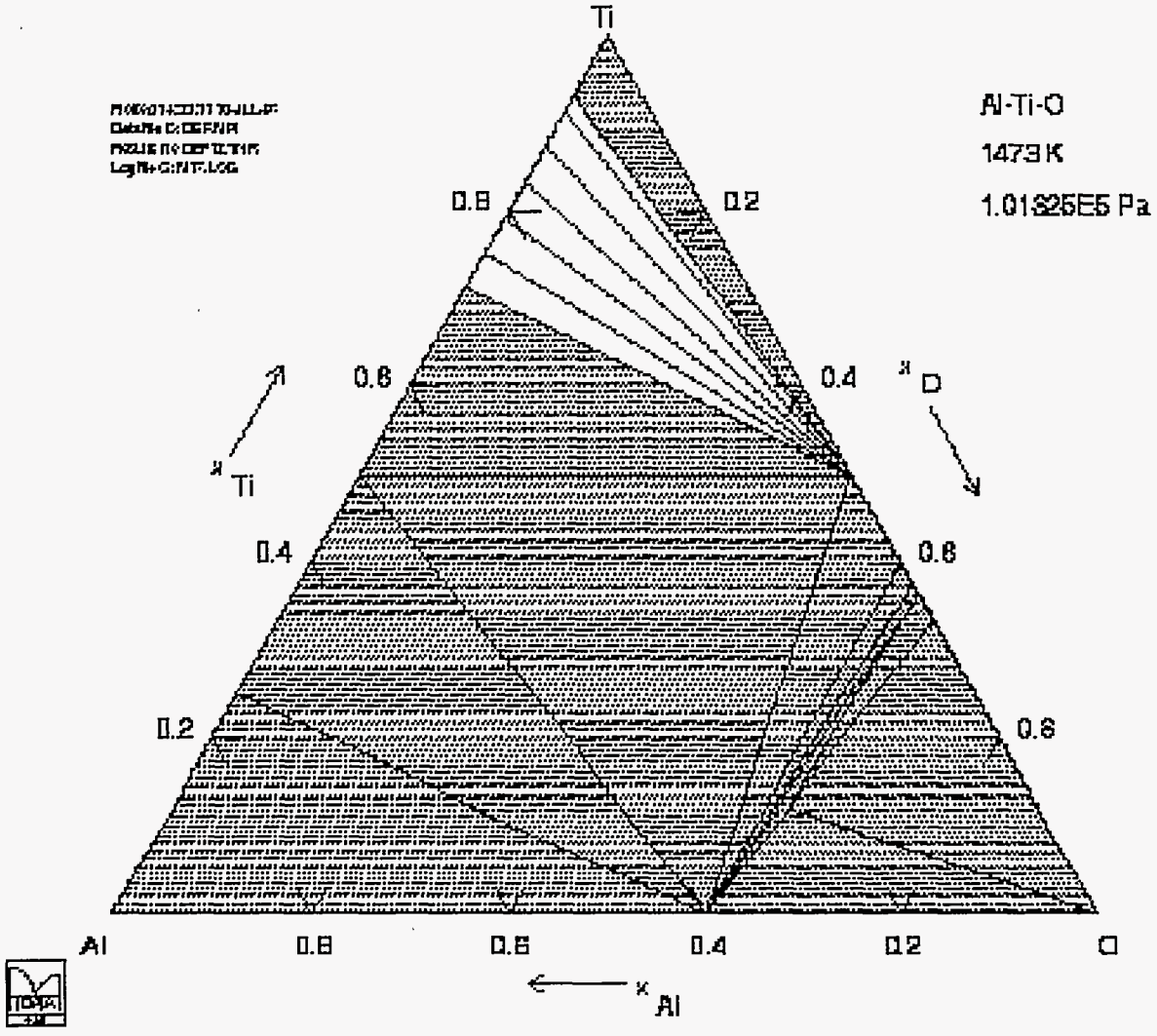

Figure 5. Ternary phase diagram for the Al-Ti-O system calculated using MTDATA software.

Task 8. Protective Coatings on Metals (Summary of SRI Results; S. Johnson and Y. Blum, SRI International)

Results during the second year of this project indicated that coatings based on a broad range of fillers mixed into low-cost preceramic binders can be applied to metals, adhere well, and are very corrosion resistant. The concept is based on the use of a mixture of preceramic polymers, ceramic powders, and metal powders. Such a formulation, if heated above 450°C, will yield ceramic or metal/ceramic composite coatings, some with near zero shrinkage. At lower temperatures, an inorganic-organic hybrid coating is formed from the highly cured polymer and the filler powders. When applied to aluminum, steel,

and other metals, these coatings are very adherent, withstand wear, and allow the use of thinner coatings than with conventional, corrosion resistant paints. VOCs have been reduced. In addition, the coatings are resistant to HCl and long-term, salt spray testing.

Modification of the polymer has indicated that curing can be carried out at room temperature, making the process very attractive to industry. Discussions have been held with various industrial representatives regarding testing of coatings an possible applications. SRI's spin-off company, 4C Technologies, is actively marketing the technology to industry.

More detailed information on these results are available in the reports SRI has submitted on their subcontract work.

PUBLICATIONS

Journals

W. G. Fahrenholtz, K. G. Ewsuk, R. E. Loehman, and P. Lu, "Kinetics of Ceramic-Metal Composite Formation by Reactive Metal Penetration," accepted for publication in J. Amer. Ceram. Soc.

E. Saiz and A. P. Tomsia, "Kinetics of Metal-Ceramic Composite Formation by Reactive Penetration of Silicates with Molten Aluminum," submitted for publication in J. Amer. Ceram. Soc., (February 1997).

W. G. Fahrenholtz, D. T. Ellerby, and K. G. Ewsuk, "Forming Controlled Composition Al_2O_3-Al Composites by Reactive Metal Penetration of Dense Aluminosilicate Preforms," submitted to J. Amer. Ceram. Soc., (June 1997).

Proceedings

R. E. Loehman, K. G. Ewsuk, W. F. Fahrenholtz, and B. B. Lakshman, "Ceramic-Metal Composite Formation by Reactive Metal Penetration," in *Proc. Ceramic and Metal Matrix Composites CMMC96*, M. Fuentes, J.M. Martinez-Esnaola, and A.M. Daniel, eds.,Trans Tech Publications, Zurich (1997), pp. 431-438.

W. G. Fahrenholtz, K. G. Ewsuk, A. P. Tomsia, and R. E. Loehman "Reaction Mechanisms and Microstructures of Ceramic-Metal Composites made by Reactive Metal Penetration," to be published in *Ceramic Microstructures 96*, A.P. Tomsia and A. Glaeser, eds, Plenum Publishers.

PRESENTATIONS

Oral Presentations

W. G. Fahrenholtz, K. G. Ewsuk, and R. E. Loehman, "$MoSi_2$-Based Composites Prepared By Reactive Hot Pressing," presented at the 1996 New Mexico Section Meeting of the American Ceramic Society and Materials Research Society, Albuquerque, New Mexico (October 28, 1996).

W. G. Fahrenholtz, R. E. Loehman, and K. G. Ewsuk, "Forming Multicomponent Ceramic-Metal Composites By Reactive Metal Penetration," presented at the 1996 Fall Meeting of the Basic Science Division of the American Ceramic Society, San Antonio, Texas (October 31 - November 2, 1996).

W. G. Fahrenholtz, K. G. Ewsuk, and R. E. Loehman,"In-Situ Formation of Molybdenum Silicides in Ceramic-Metal Composites," presented at the 21st Annual Cocoa Beach Conference and Exposition. on Composites, Advanced Ceramics, Materials, and Structures, Cocoa Beach, Florida (January 12-16, 1997).

K. G. Ewsuk, W. G. Fahrenholtz, and R. E. Loehman, "Controlling Metal-Ceramic Reactions in Composite Fabrication and Al Processing," presented at the DOE Office of Industrial Technologies 2nd Annual Industrial Energy Efficiency Symposium and Exposition, Arlington, Virginia (February 24-26, 1997).

R. E. Loehman, K. G. Ewsuk, W. G. Fahrenholtz, and P. Lu, "Mechanisms of Forming Ceramic-Metal Composites By Reactive Metal Penetration," presented at the 99th Annual Meeting of the American Ceramic Society, Cincinnati, Ohio (May 4-7, 1997).

W. G. Fahrenholtz, K. G. Ewsuk, and R. E. Loehman, "Alumina-Molybdenum Silicide Composites Formed By Reactive Hot Pressing," presented at the 99th Annual Meeting of the American Ceramic Society, Cincinnati, Ohio (May 4-7, 1997).

R. E. Loehman, K. G. Ewsuk, W. G. Fahrenholtz, and A. P. Tomsia, "Synthesis and Processing of Composites by Reactive Metal Penetration," presented at the Advanced Industrial Concepts (AIC) Materials Program Annual Progress Review for FY 1996, Sandia National Laboratories, Albuquerque, New Mexico (June 24-26, 1996).

H. P. Chen, Y. D. Blum, S. M. Johnson, and C. Kanazawa, "Corrosion Resistant and High Temperature Coatings from Preceramic Polymers," presented at the 49th Pacific Coast Regional Meeting of the American Ceramic Society, San Francisco, California (October. 13-15, 1997).

D. T. Ellerby, R. K. Bordia, K. G. Ewsuk, R. E. Loehman, and W. G. Fahrenholtz, "Mocrostructure Control of Al/Al_2O_3 Composites Formed by Reactive Metal Penetration," presented at the 49th Pacific Coast Regional Meeting of the American Ceramic Society, San Francisco, CA (October 13-15, 1997).

R. E. Loehman, K. G. Ewsuk, W. G. Fahrenholtz, and J. J. Walker, "Chemical Effects in the Wetting of Ceramics by Molten Metals," presented at the 49th Pacific Coast Regional Meeting of the American Ceramic Society, San Francisco, California (October. 13-15, 1997).

W. G. Fahrenholtz, K. G. Ewsuk, and R. E. Loehman, "Processing and Properties of $MoSi_2$-Al_2O_3 Composites Formed by Reactive Hot Pressing," presented at the 49th Pacific Coast Regional Meeting of the American Ceramic Society, San Francisco, California, (Oct. 13-15, 1997).

HONORS AND AWARDS

None this reporting period.

PATENTS/DISCLOSURES

None this reporting period.

LICENSES

None this reporting period.

INDUSTRIAL INPUT, TECHNOLOGY TRANSFER, AND OTHER INTERACTIONS

Collaboration with other researchers

We are continuing our collaboration with A.P. Tomsia of Lawrence Berkeley Laboratory. Dr. Tomsia is the co-discoverer of reactive metal penetration and has contributed significantly in the past to its understanding and development. Dr. Eduardo Saiz is a visiting scientist working with Dr. Tomsia on the project and supported by LBL. Dr. Tomsia's participation is supported by internal funds from LBL.

Professor Ping Lu of New Mexico Institute of Mining and Technology is supported on a subcontract to the project to provide TEM analysis of reaction zones and other structural information on reaction mechanisms. Tiangao Du is a graduate student at the New Mexico Tech who is completing a master's thesis on reactive metal penetration under the direction of Professor Lu. Professor Raj Bordia of the University of Washington has provided a graduate student to work on the project during the past three summers at the Advanced Materials Laboratory and throughout the rest of the year at the University of Washington.

Dr. Sylvia Johnson and Dr. Yigal Blum worked on a subcontract to the project to evaluate oxidation- and corrosion-resistant coatings on steel and Al. The coatings are made by full or partial pyrolysis of mixtures of organo-metallic polymers, metal powders and ceramic additives, as described above.

ADVANCED INTERMETALLICS/METALS AND COMPOSITES

ADVANCED MATERIALS FOR HIGH TEMPERATURE LIQUID METAL CORROSION AND EROSION RESISTANCE

M. Trkula, M. A. Nastasi, K. C. Walter, and D. W. Carroll

Materials Science and Technology Division
P.O. Box 1663, MS-E549
Los Alamos National Laboratory
Los Alamos, New Mexico 87545

INTRODUCTION

We are developing novel coating technologies and surface engineering to develop erosion resistant, thermodynamically stable, and highly adherent conformal coatings on die materials used to cast aluminum and other metals. A fundamental component of this work is the combination of several areas of Los Alamos expertise that will allow us to engineer the surface and coating at an unprecedented level. Specifically, we will combine low-temperature, organometallic chemical vapor deposition (OMCVD) with plasma immersion ion processing (PIIP). In aluminum casting, high production rates and use of aluminum-silicon alloys leads to corrosion and erosion of the die which leads to premature die failure. Currently, there exists little that can be done to address this problem. Die cast aluminum is designed heavier than required to extend die lifetime. This leads to scrap aluminum, energy waste, and lower productivity. The "Aluminum Industry: Industry/Government Partnerships for the Future" specifically calls out enhanced coating technologies under their Enabling Technologies. The successful development of novel coating technologies directly addresses four research needs of the metal casting industry. Coatings that are adherent, wear-resistant, and non-reactive with the molten metal will allow improved dimensional control of castings and casting quality which may reduce or eliminate the need for post-casting finishing. Improved dimensional control allows the production of castings with thinner walls. This reduces the use of raw materials and, more importantly, reduces the weight of cast products. By successfully developing coatings to provide extended die-casting die life, one reduces the number of production stoppages (increasing productivity and domestic competitiveness), energy consumption (by avoiding molten metal remelt after changing out a die), and the environmental impact of die-casting (by eliminating the need for release agents that may contaminate cooling water).

TECHNICAL PROGRESS - FY 1997

This project is a new start as of the fourth quarter for FY 1997. We focused our efforts on materials synthesis and characterization of two materials of primary interest in aluminum casting, namely AlN and B_4C.

1. Background

In considering die surface compatibility with molten aluminum, a search of the literature suggests a large number of refractory carbides, nitrides, borides, and oxides as potential candidates. A metric for a coating is the thermal shock parameter. The thermal shock parameter, S, is given by

$$\frac{E\Delta\alpha}{(1-\nu)\kappa},$$

where; E is the modulus of the coating, $\Delta\alpha$ is the difference in coefficient of thermal expansion (CTE) between the coating and substrate, ν is Poison's ratio and κ is the thermal conductivity of the coating. To obtain a large value of S and, therefore, good thermal shock performance, one desires a low modulus, small difference in CTE, and high thermal conductivity. Low modulus is generally at odds with high hardness and subsequently good wear properties. Furthermore, high modulus coatings are typically low-fracture-toughness materials prone to brittle fracture particularly in tension. For wear properties, high modulus is required but improvements in fracture toughness are possible with composite coatings. A high CTE is desirable to match that of tool steels (which range from 11 to 13 x 10^{-6} K^{-1}) and minimize $\Delta\alpha$. High thermal conductivity is very desirable. In addition to its importance in reduced thermal shock effects, it is significant in terms of temperature control of dies in operation.

Several materials stand out as potentially superior candidates. However, no one material is the clear choice. Considering the above analysis, we chose to investigate AlN, B_4C, ZrB_2 and TiB_2 for our initial studies. Below, we report our results for AlN and B_4C.

2. Materials Synthesis

We produce thin-film coatings of AlN by low-temperature OMCVD. The deposition system is a cold-wall vertical reactor. We control the gas flows with precision mass flow controllers. Temperatures are monitored with type K thermocouples. The thermocouples provide a feed back signal for active temperature control. The aluminum precursor is tris(dimethylamido) aluminum. The aluminum precursor is held at 84°C and the vapor is

swept with a flow of 150 sccm of helium. This is mixed with NH_3 flowing at 150 sccm. All experiments were at a total pressure of 1.0 torr. We performed a series of depositions at different temperatures on both silicon and steel substrates. All depositions gave a lustery film. Details of the experiments are in Table 1.

Table 1. Deposition conditions for AlN.

Run	substrate	Temperature (C)	deposition time (min)
AlN2	Si	422	12
AlN3	steel	362	24
AlN4	steel	423	24
AlN5	Si	302	12

Amorphous boron carbide coatings were deposited on steel using a PIIP process. The steel coupons (1" x 2" x 0.5") were mechanically polished to a mirror finish. The coupons were introduced into the PIIP chamber and sputter cleaned in 20 mtorr argon at 1.4 kW of rf power to the plasma sources and a 2 kV bias with a 50 μs pulse width at a 4 kHz pulse frequency. The incident ion dose for the cleaning was 3.6×10^{17}. The boron carbide was deposited using a pulsed glow discharge method of generating the plasma. Plasma conditions were 4 kV bias with a 30 μs pulse width at a 4 kHz pulse frequency. The deposition was run for 6 hours at 20 mtorr total gas pressure. The gas mixture consisted of diborane (B_2H_6) diluted in helium and acetylene (C_2H_2).

3. Material Characterization

Compositions of the samples were measured by simultaneous elastic recoil detection (ERD) and Rutherford backscattering spectroscopy (RBS). The ERD provides information about the hydrogen concentration, and RBS measures all other elements heavier than helium. The analysis used the 3 MeV tandem accelerator at the Los Alamos Ion Beam Materials Laboratory. A 2 MeV He+ beam occurs on the sample at an angle of incidence of 7°. Helium ions elastically backscattered at an angle of 167° are detected by a silicon surface-barrier detector connected to standard pulse-counting electronics. Hydrogen elastically recoiled from the sample at an angle of 30° is detected by a similar detector. A piece of mylar 8-m thick is placed in front of the detector to block scattered helium ions.

We use nanoindentation to measure the elastic modulus of the materials. The nanoindenter only travels 10% of the sample thickness to avoid substrate effects. From the load displacement curve, we calculate elastic modulus and hardness.

Pin-on-disk wear tests were performed using a smooth, 6-mm-dia. 52100 ball, 50% relative humidity, loads from 0.2 to 0.4 N, a Hertzian contact stress from 360 to 460 MPa, 120 rpm, and a track diameter of 3 mm. The coefficient of friction was calculated by measuring the tangential force on the pin through a load cell.

Figure 1 shows the RBS spectra for AlN sample AlN2. Analysis of the data indicates the AlN thin film is near stoichiometric. The aluminum to nitrogen ratio varies from 1.06 to 0.94 for the films we studied. The ERD data indicates there is ~5% residual hydrogen incorporation into the film. The AlN films were ~0.2 μm thick for the 12 minute runs and ~0.4 μm for the 24 minute runs. The nearly linear change in film thickness indicates a prompt AlN nucleation.

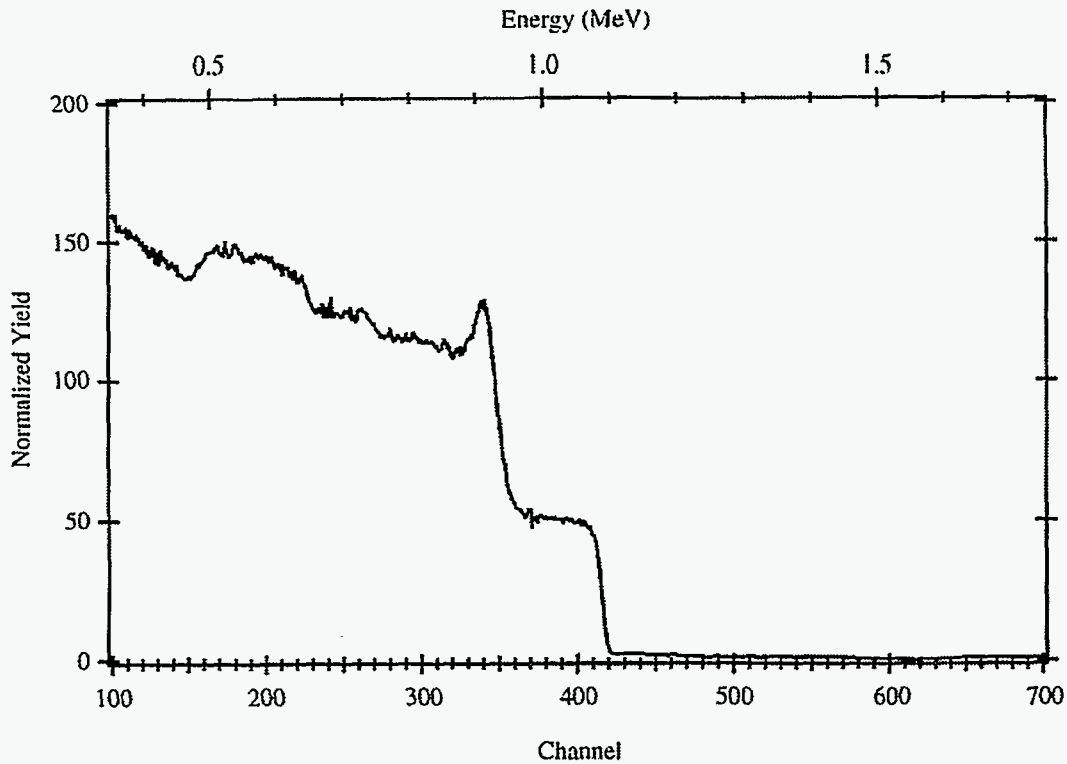

Figure 1: The RBS spectra for AlN sample AlN2. The film is nearly stoichiometric with little hydrogen incorporation.

Boron carbide film compositions were determined with RBS. Ion beam analysis of coatings showed that the composition was dependent on the gas composition. The boron to carbon ratio varied from 2.7 to 2.2. The hydrogen atomic content of the films also varied from 18% to 40%. Nanoindentation of coatings showed a hardness of 12-13 GPa and a Young's modulus of 115-140 GPa. The mechanical properties did not vary significantly with film composition. However, the tribological behavior of the coatings was observed to depend greatly on coating composition. It was observed that the coating

with the greatest carbon content also had the greatest wear resistance and lowest coefficient of friction.

MILESTONES

Initial thin-film coatings were deposited on silicon and steel substrates. The materials were characterized for thickness, composition, mechanical and tribological properties.

PUBLICATIONS

None.

PRESENTATIONS

None.

INDUSTRIAL INPUT AND TECHNOLOGY TRANSFER

Many companies have expressed an interest in this technology. These include General Motors, Chrysler, Empire Hard Chrome, Alcoa, and Renolys. We have kept them abreast of these developments.

COST SHARING

None.

ESTIMATED ENERGY SAVINGS

We have studied material lifetime and its effect on aluminum die casting in the automotive industry. Estimates indicate that dye life extension for this industry alone can result in energy savings of 3.3×10^{12} to 3.3×10^{13} BTU/year.

ADVANCED ORDERED INTERMETALLIC ALLOY DEVELOPMENT

C. T. Liu and P. J. Maziasz

Metals and Ceramics Division
Oak Ridge National Laboratory
Post Office Box 2008, Oak Ridge, Tennessee 37831-6115

INTRODUCTION

The need for high-strength, high-temperature, and light-weight materials for structural applications drives the development of ordered intermetallics, particularly γ-based titanium aluminides. The γ-based TiAl alloys have an attractive mixture of low density ($\sim 4 g/cm^3$), low thermal expansion and good thermal conductivity, good creep resistance, and high-temperature strength and oxidation resistance. Low density is particularly important for rotating or high-speed components, and TiAl also has a high damping coefficient which further minimizes vibrations and noise. These particular γ-TiAl alloys with 46 to 48 at. % aluminum contain two phases, α_2 ($D0_{19}$ structure) and $\gamma(L1_0)$, at temperatures below 1120°C, the eutectoid temperature. The mechanical properties of such alloys are very sensitive to both alloy compositions and microstructure. Depending on heat treatment and thermomechanical processing, microstructures with near-equiaxed γ, a duplex structure (a mix of the γ and α_2 phases) or a lamellar structure (mixtures of alternating plates of the γ and α_2 phases) can be developed in TiAl alloys containing 45 to 50 at. % Al. The major concern for structural use of TiAl alloys is their low ductility and poor fracture resistance at ambient temperatures. The purpose of this project is to improve the fracture toughness of TiAl-based alloys by controlling alloy composition, microstructure and thermomechanical treatment. This work is expected to lead to the development of γ-TiAl alloys with significantly improved fracture toughness and tensile ductility for structural use.

TECHNICAL PROGRESS - FY 1997

Summary

1. Alloy Preparation and Microstructural Features

This year we have completed the study of TiAl alloys in both hot extrusion and cast conditions. Table 1 lists the alloy compositions of cast and hot extruded TiAl alloys used in this study. The base composition of Ti-47Al-2Cr-2Nb (at. %) was modified with additions of 0.15B, 0.2Mo, and 0.2W. Boron, molybdenum and tungsten were added for refining the colony size, lamellar structure (or both), and improving their stability. Tungsten also has the beneficial effect of enhancing high-temperature properties. The five alloys (TIA-20 to 25) containing 46 to 48 at. % Al were prepared by arc melting and

drop casting into a copper mold, using high-purity charge materials. These alloy ingots were then canned in Mo billets and hot extruded at 1350°C and 1400°C ($T_\alpha \approx 1320$°C for Ti-47Al-2Cr-2Nb alloy).

Table 1. Nominal Compositions of Cast Alloys and Hot Extruded TiAl Alloys.

Alloy number	Alloy composition (at. %)	Alloy condition*
TIA-20	Ti-47Al-2Cr-2Nb-0.15B	HE at 1350°C
TIA-21	Ti-47Al-2Cr-1.8Nb-0.2W-0.15B	HE at 1350 and 1400°C
TIA-23	Ti-46Al-2Cr-2Nb-0.15B	HE at 1400°C
TIA-24	Ti-48Al-2Cr-2Nb-0.15B	HE at 1400°C
TIA-25	Ti-46Al-2Cr-1.8Nb-0.2W-0.15B	HE at 1400°C
TIA-27	Ti-46Al-2Cr-1.8Nb-0.2Mo-0.2W-0.15B	Cast
TIA-29	Ti-46Al-2Cr-1.5Nb-0.2Mo-0.5W-0.15B	Cast

*HE = hot extrusion.

All five alloys were successfully hot extruded above T_α without difficulty. The hot extrusion above T_α resulted in lamellar structures with extremely fine colony sizes (22-33 μm). The hot extrusion at 1350°C produced near fully lamellar structures, with some equiaxed and elongated γ grains existing along colony boundaries. On the other hand, the hot extrusion at 1400°C resulted in lower amounts of γ grains at those boundaries. In order to vary both grain size and lamellar spacing, the hot-extruded alloys were heat treated at 900°C to 1350°C. Metallographic examination indicates that the heat treatment at temperatures $\leq$ 1320°C caused no significant change in grain size, while heat treatment at 1350°C sharply increased grain size. The variation in grain size by heat treatment of hot extruded TIA-20 to 25 is given in Table 2.

Microstructural features of the lamellar structures within the grains in TIA-20 and -21 extruded at 1350°C, and in TIA-21-2, and TIA-25 extruded at 1400°C were examined by transmission electron microscopy (TEM) after stress relieved for 2 h at 900°C. The lamellar spacings were carefully measured and their results are summarized in Table 2. The average interlamellar spacing, measured to include both γ and α_2 platelets, varies from 105 to 440 nm, with the finest spacing for TIA-25 hot extruded at 1400°C. Because

of the fine interlamellar spacing in the as-extruded materials, the ratio of γ to α_2 platelets is close to 1:1, indicating only a few γ/γ boundaries. Figure 1 compares the lamellar structures in TIA-21 hot extruded at 1350°Cand 1400°C. The extrusion at 1350°C resulted in about 10% to 20% volume fraction of equiaxed and elongated γ in intercolony grain regions, whereas the extrusion at 1400°C resulted in less than 10% intercolony γ structures. This comparison suggests that, during the hot extrusion, the temperature of the extrusion billets (which were preheated to 1350°C) may have dropped to below T_α (($\approx$ 1320°C), resulting in the formation of γ along the α grain boundaries.

Table 2. Quantitative Lamellar Microstructural Data on Hot-Extruded and Heat-Treated TiAl Alloys.

Alloy/HT	Compositions (at. %)	Interlamellar Spacing (nm)	γ-Platelet width (nm)	Grain size (μm)
	Hot-Extruded at T_1			
TIA-20	47Al-2Cr-2Nb-0.15B			
2h/900°C		225	95-870	
2h/1320°C		440	160-1250	33
2h/1350°C				182
TIA-21	47Al-2Cr-1.8Nb-0.2W-0.15B			
2h/900°C		160	74-635	
2h/1320°C		300	290-1100	31
2h/1350°C				150
	Hot-Extruded at T_2			
TIA-21-2	47Al-2Cr-1.8Nb-0.2W-0.15B			
2h/900°C		141	40-750	25
2h/1320°C				35
2h/1350°C				99
TIA-25	46Al-2Cr-1.8Nb-0.2W-0.15B			
2h/900°C		105	21-520	26
2h/1320°C				135
2h/1350°C				148

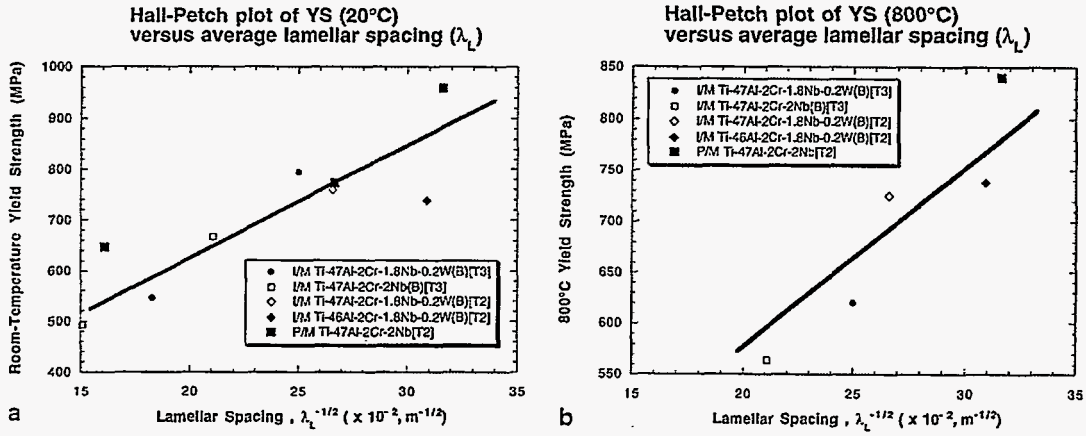

(a) extruded at 1400°C (b) extruded at 1350°C

Figure 1. Effect of hot extrusion temperature on intercolony structure in TIA-21.

2. Tensile Properties of Hot-Extruded Alloys

The tensile properties of hot-extruded TIA alloys were determined at room temperature, 300°C, 600°C, 800°C, and 1000°C in air. Figure 2 compares the tensile properties of TIA-25 (developed at ORNL) with an advanced two-phase TiAl alloy, K-5 (Ti-46.5Al-2.1Cr-3Nb-0.2W, at. %), developed recently. The comparison indicates that TIA-25 with an ultra-fine lamellar structure is much stronger and more ductile than K5. The superior tensile properties of TIA-25 are due to a combination of the fine colony size and fine interlamellar spacing produced by hot extrusion. Alloy TIA-25 is also stronger than TIA-21, with slightly finer and more uniform lamellar spacing within the colonies, and slightly different intercolony boundary region structure.

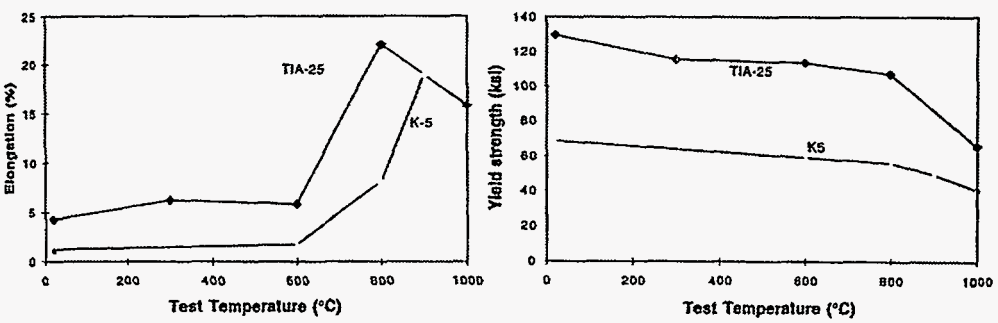

Fig. 2. Comparison of tensile properties of TIA-25 developed at ORNL with the advanced alloy K5 (Ti-46.5Al-2.1Cr-3Nb-0.2W, at. %).

3. Structure/Property Correlation

In order to identify a key parameter, the tensile elongation at various temperatures are plotted against grain size (d). Figures 3(a) and (b) show the plot of the room-temperature tensile elongation as functions of d and $d^{-1/2}$, respectively. As indicated in Figure 3(b), a linear relationship holds reasonably well between tensile ductility and $d^{-1/2}$. This relationship had been observed for quasi-brittle materials, based on a consideration of the propagation of cracks with an average length that is the same as the grain size. Note that such a relationship does not hold for the ductility at elevated temperatures, such as 800°C.

The yield strength of TIA alloys at room and elevated temperatures are analyzed by the Hall-Petch equation based on both the grain size and on the interlamellar spacing as strength-determining parameters. No linear relationships exist for the grain size plot, but an excellent relationship is found for the Hall-Petch plot of interlamellar spacings, as showing in Figure 4 for the yield strength at room temperature and at 800°C. These plots clearly indicate that the interlamellar spacing is the key parameter controlling the yield strength of these two-phase TiAl alloys. Hall-Petch relationships were observed for two-phase TiAl alloys where the yield strength at room temperature was plotted against grain size instead of interlamellar spacing. A more detailed comparison of the values of the Hall-Petch slope obtained in this work with those slopes obtained by others will be reported later.

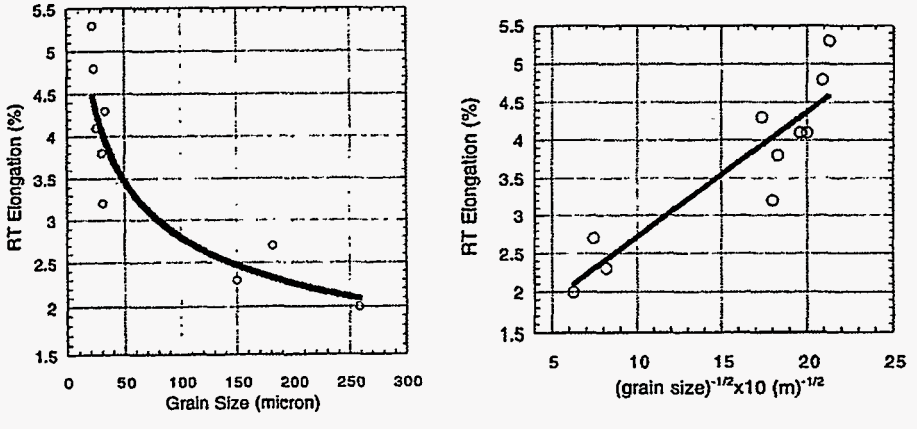

Figure 3. Plot of room-temperature tensile elongation as a function of (a) grain size (d) and (b) $d^{-1/2}$.

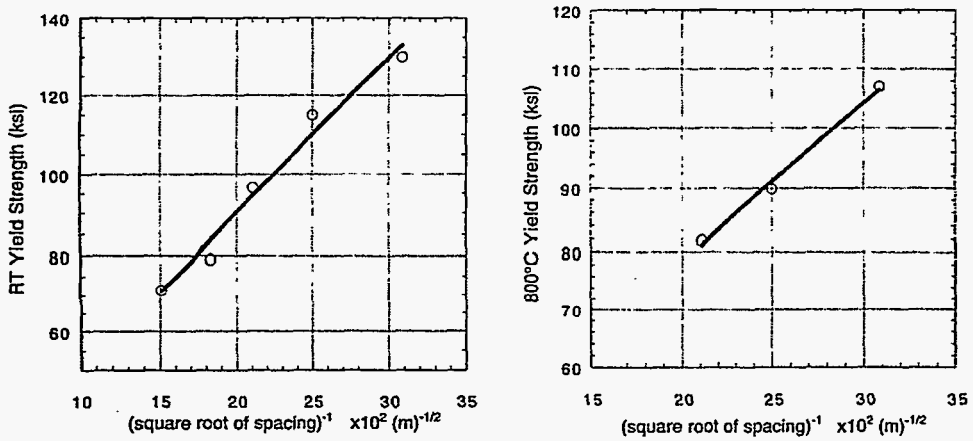

Figure 4. Hall-Petch plot of the room temperature and 800°C yield strength data for TIA alloys versus interlamellar spacing.

The study of microstructures and tensile properties of two-phase TiAl with lamellar structures based on Ti-47Al-2Cr-2Nb leads to the following important conclusions:

- The interlamellar spacing and grain size in the TiAl alloys with lamellar structures can be controlled by hot extrusion at temperature above T_α and subsequent heat treatment around T_α.

- The tensile ductility around 5% and strength close to 900 MPa at room temperature are obtained for the TiAl alloys with ultra-fine lamellar structures (grain size < 35 μm, and interlamellar spacing 0.1 μm).

- A Hall-Petch relationship exists between room-temperature tensile elongation and grain size, indicating that the grain size is the key parameter in controlling the ductility at room temperature. Such a relationship, however, does not hold for the elongation at elevated temperatures, such as 800°C.

4. Tensile Properties of Cast Alloys

Many industries are interested in using TiAl alloys in cast conditions because of the relatively lower cost for cast materials as compared with wrought materials. During this year, efforts have been focused on the study of the microstructure and mechanical properties of cast material without hot extrusion. Two alloys TIA-27 and -29, with their compositions listed in Table 1, were prepared by arc melting and drop casting, followed by various heat treatment to control cast microstructures.

The α transus temperature of TIA-27 is estimated to be around 1320°C. In order to control the grain size, as-cast samples were heat treated at 1320 ± 20°C for up to 60 min.

Figure 5 shows the microstructure of the as-cast sample together with ones heat treated at 1300°C, 1320°C and 1340°C for 20 min. The as-cast material [Fig. 5(a)] basically has a lamellar structure; however, the grain-boundary region in the etched sample showed a wide band of the dark contrast, possibly because of solute segregation and formation of second-phase particles (coarse α_2 or possibly β particles). The samples heat treated at and above 1300°C showed a more "regular" lamellar structure, with lamellar platelets clearly visible. A small amount of equiaxed γ grains is visible at grain boundaries in Fig. 5(b), indicating that the heat treatment temperature of 1300°C is slightly below the α-transus temperature. Such equiaxed γ grains are essentially not observed for samples heat treated at 1320°C and 1340°C [Figs. 5(c) and (d)]. The grain size for the as-cast and heat-treated samples is about the same (~66 μm), as measured by a linear intercept method. The alloy also showed no significant increase in grain size when the heat-treatment temperature was increased from 20 to 60 min at 1300°C to 1340°C.

The mechanical properties of TIA-27 in the as-cast and heat-treated conditions were determined by tensile testing at temperatures to 1000°C in air (stress relieved for 2 hr at 900°C does not change the microstructure). Table 3 shows the effect of heat treatment on tensile properties of cast TIA-27. Among all samples, the one heat treated for 20 min at 1320°C shows the best yield strength (98.1 ksi) and tensile ductility (0.5%) at room temperature. Since all the samples have a reasonably small grain size (~66 μm), the low tensile ductility may be caused by a combination of casting defects (such as porosities) and microscopic second-phase particles (β-phase particles).

The tensile data in Table 3 also show a general trend of decreasing strength and increasing tensile ductility as their test temperature increases. Among the samples, those annealed for 20 min at 1300°C and 1320°C showed the best tensile ductilities but lowest yield strength at elevated temperatures. Another heat of TIA-27 (designated as TIA-27-2) and a new heat of TIA-29 were similarly cast and heat-treated for 2 hrs at 900°C and tested at room temperature. Their tensile data is included in Table 3. Both showed fracture strengths of 80 to 90 ksi with only 0.3% total elongation. Both alloys were also aged for 72 hrs at 1000°C, which resulted in lower strength.

(a)

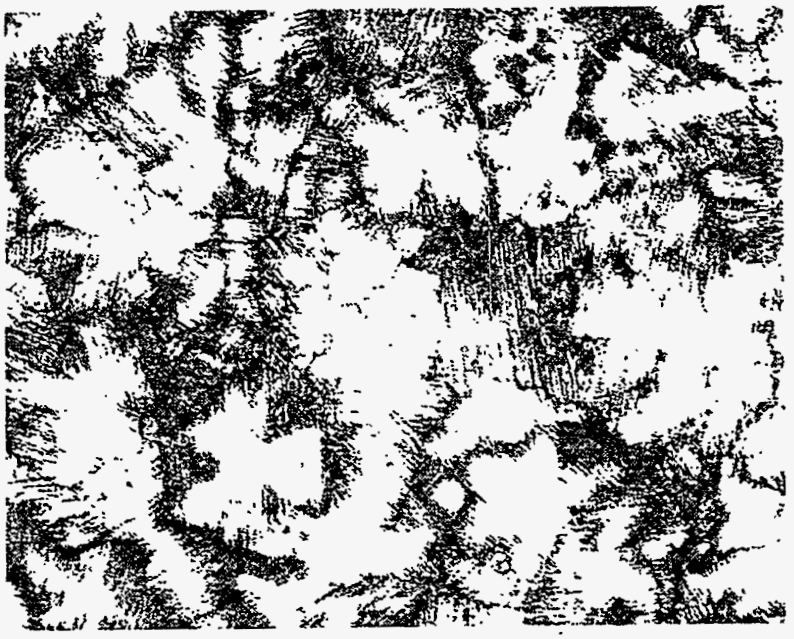

(b)

Figure 5. Effect of heat treatment on optical microstructures of cast TIA-27 alloy (a) as-cast, (b) heat treated 20 min/1300°C, (c) 20 min/1320°C, and (d) 20 min/1340°C. 200×.

(c)

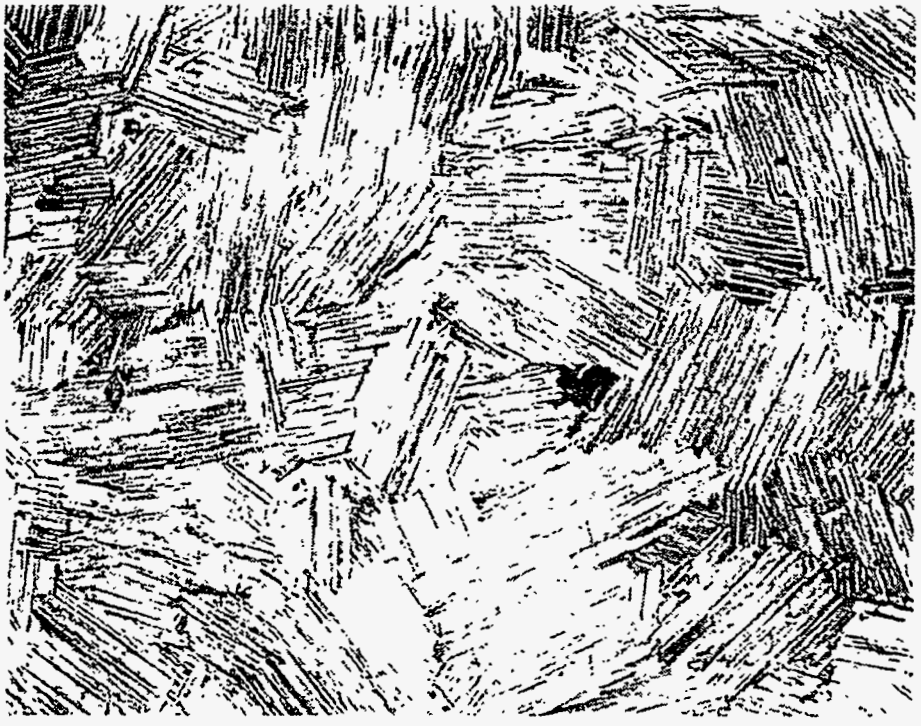

(d)

Figure 5 (continued). Effect of heat treatment on optical microstructures of cast TIA-27 alloy (a) as-cast, (b) heat treated 20 min/1300°C, (c) 20 min/1320°C, and (d) 20 min/1340°C. 200×.

Table 3. Effect of Heat Treatment on Tensile Properties of Cast TiAl Alloys.

Alloy	Heat treatment (°C)	Test temperature (C)	Yield strength MPa (ksi)	Fracture strength MPa (ksi)	Total elongation (%)
TIA-27-1[a]	2 h/900	20	617 (89.5)	617 (89.5)	0.5
TIA-27-1[a]	2 h/900	1000	431 (62.5)	442 (64.2)	1.3
TIA-27-2[a]	2 h/900	20	--	571 (82.6)	0.3
TIA-27-2[a]	2 h/900 + 3 d/1000	20	--	324 (46.9)	0.2
TIA-27-1[b]	2 h/900	20	--	634 (91.8)	0.3
TIA-27-1[b]	2 h/900 + 3 d/1000	20	--	500 (72.4)	0.3
TIA-27-1[a]	20 min/ 1300	20	--	497 (71.8)	0.3
TIA-27-1[a]	20 min/ 1300	600	487 (70.7)	524 (76.0)	3.3
TIA-27-1[a]	20 min/ 1300	1000	377 (54.7)	423 (61.4)	4.7
TIA-27-1[a]	20 min/ 1320	20	676 (98.1)	676 (98.1)	0.5
TIA-27-1[a]	20 min/ 1320	600	460 (66.7)	526 (76.3)	2.3
TIA-27-1[a]	20 min/ 1320	1000	360 (52.2)	395 (57.3)	4.7
TIA-27-1[a]	20 min/ 1340	20	--	444 (64.5)	0.2
TIA-27-1[a]	20 min/ 1340	600	548 (79.5)	548 (79.5)	0.7
TIA-27-1[a]	20 min/ 1340	1000	405 (58.8)	457 (66.4)	1.4

[a]TIA-27 (Ti-46Al-2Cr-1.8Nb-0.2Mo-0.2W-0.15B at. %).
[b]TIA-29 (Ti-46Al-2Cr-1.5Nb-0.2Mo-0.5W-0.15B at. %).

PUBLICATIONS

Journals

P. J. Maziasz and C. T. Liu, "Development of Ultrafine, Lamellar Structures in Two-Phase γ-TiAl Alloys," accepted by *Metallurgical and Materials Transactions A* for publication in January 1998.

P. J. Maziasz, R. V. Ramanujan, C. T. Liu, and J. L. Wright, "Effect of B and W Alloying Additions on the Formation and Stability of Lamellar Structures in Two-Phase γ-TiAl," *Intermetallics* **5** (1997) 83-96.

C. T. Liu, J. Stringer, J. N. Mundy, L. L. Horton, and P. Angelini, "Ordered Intermetallic Alloys: An Assessment" *J. Intermetallics* **5** (1997) 579-96.

C. T. Liu, J. H. Schneibel, P. J. Maziasz, J. L. Wright, and D. S. Easton, "Tensile Properties and Fracture Toughness of TiAl Alloys with Controlled Microstructures," *Intermetallics* **4**, 429-40 (1996).

R. V. Ramanujan, P. J. Maziasz, and C. T. Liu, "The Thermal Stability of the Microstructure of γ-Based Titanium Aluminides," *Acta Metall.* **44**, 2611-42 (1996).

C. G. McKamey, S. H. Whang, and C. T. Liu,"Microstructural Characterization of a γ-TiAl-Ni Alloy Produced by Rapid Solidification Techniques," *Scr. Metall.* **32**,383 (1995).

C. T. Liu and J. A. Horton, "Effect of Refractory Alloying Additions on Mechanical Properties of Near-Stoichiometric NiAl," *J. Mat. Sci. and Eng.* **A192/93**, 170-78 (1995).

J. A. Horton, C. T. Liu, and E. P. George, "Shape Memory Properties of a Two-Phase NiAl Plus Fe Alloy," *J. Mat. Sci. and Eng.* **A192-93**, 873-80 (1995).

Other Publications

P. J. Maziasz, C. T. Liu, and J. L Wright, "Stability of Ultrafine Lamellar Structures During Aging in Two-Phase γ-TiAl Alloys," to be published in Proc. International Symposium on Structural Intermetallics (ISSI-2), TMS, Warrendale, Pennsylvania (1997).

C. T. Liu, P. J. Maziasz, and J. L. Wright, "Key Microstructures Controlling the Mechanical Properties of Two-Phase TiAl Alloys with Lamellar Structures," pp. 83-90 in High-Temperature Intermetallic Alloys VII, eds. C. C. Koch, C. T. Liu, N. S. Stoloff, and A. Wanner, MRS Symp. Proc. Vol. 460, Materials Research Society, Pittsburgh, PA (1997).

P. J. Maziasz and C. T. Liu, "Ultrafine Fully-Lamellar Structures in Two-Phase γ-TiAl Alloys," pp. 219-223 in High-Temperature Intermetallic Alloys VII, eds. C. C. Koch, C. T. Liu, N. S. Stoloff, and A. Wanner, MRS Symp. Proc. Vol. 460, Materials Research Society, Pittsburgh, Pennsylvania (1997).

C. T. Liu and J. O. Stiegler, "Aluminides-Nickel," pp. 1752-60 *in Encyclopedia of Advanced Materials*, ed. M. C. Flemings, Pergamon Press, 1994.

HONORS AND AWARDS

C. T. Liu was appointed to NRC Panel on AFOSR Materials Science Proposal Reviews, National Research Council (NRC), 1996.

C. T. Liu and P. J. Maziasz received an ORNL R&D Accomplishment Award for a breakthrough in alloy design of TiAl alloys, May 1996.

C. T. Liu was promoted to Senior Corporate Fellow at ORNL, 1997.

PATENTS/DISCLOSURES

None.

LICENSES

No license agreements have been developed with industries. Pratt and Whitney, General Electric, Howmet, and Rolls-Royce of America are already interested in the ORNL work on alloy development of NiAl. We also have several contacts with these companies for possible joint work on the development of TiAl alloys, and have talked with Cummins Engine Company and Philip Morris as well.

INDUSTRIAL INPUT and TECHNOLOGY TRANSFER

Based on our initial contacts with Howmet, Pratt & Whitney, Rolls-Royce of America and other companies, one of the major technical concerns for structural uses of TiAl alloys is its poor tensile ductility and fracture toughness at ambient temperatures. Another concern are properties degradation after extensive service at elevated temperatures. Our program has been formulated based on such industrial input. P. Angelini and C. T. Liu visited Howmet Corporation to discuss technical corporation and technology transfer with Dr. Neil Paton, Vice President, and his research staff on November 9, 1995. C. T. Liu gave a seminar on "Development of NiAl and TiAl Alloys for Structural Applications" during their visit.

C. T. Liu and P. J. Maziasz discussed technology transfer with a representative from Cummings Engine Company in 1996. This work has also been discussed with Westinghouse Advanced Turbine Division in 1996. There may be some potential for TiAl to be considered in different stages of several different size gas-turbine designs in the ATS Program. Philip Morris is very interested in the TiAl alloy development sponsored by AIM, and the company will provide a new funding for ORNL in 1998 for further developing TiAl alloys for industrial applications.

ESTIMATED ENERGY SAVINGS

The development of high-temperature, light-weight intermetallic alloys based on γ TiAl will lead to improvement in performance (in terms of thermal efficiency, durability, etc.) of heat engines and energy conversion systems, resulting in substantial energy savings.

DEVELOPMENT OF WELDABLE, CORROSION-RESISTANT IRON-ALUMINIDE (FeAl) ALLOYS

P.J. Maziasz, G.M. Goodwin, X.L. Wang, R.W. Swindeman,
D.J. Alexander, and V.K. Sikka

Metals and Ceramics Division
Oak Ridge National Laboratory
Post Office Box 2008, Oak Ridge, Tennessee 37831

INTRODUCTION

A boron-microalloyed FeAl alloy [Fe-(36-38)Al-0.2Mo-0.05Zr-0.13C at.%, with 100-400 appm B] with improved weldability and mechanical properties was developed in FY 1994. A new scale-up and industry technology development phase for this work began in FY 1995, pursuing two parallel paths. One path is developing monolithic FeAl component and application technology, while the other is developing coating/cladding technology for alloy steels, stainless steels and other Fe-Cr-Ni alloys. In FY 1995, it was found that cast FeAl alloys had good strength at 700°C-750°C, and some (2%-5%) ductility in air at room temperature. Hot-extrusion of FeAl refined the grain size, and produced much more ductility and also dramatically improved the Charpy impact-toughness at room temperature. Powder-metallurgy (P/M) FeAl alloys, consolidated by direct hot-extrusion at 950°C-1000°C, were discovered to have an ultra-fine-grained microstructure, which produced the highest ductility, strength and impact-toughness that have even been seen in such intermetallic alloys.

TECHNICAL PROGRESS - FY 1997

1. Industry Testing and Corrosion Resistance

In FY 1996, testing by INCO (G. Smith) showed that bare and preoxidized as-cast FeAl specimens were very resistant to carburization at 1000°C and 1100°C. The INCO carburizing gaseous environments simulated industrial steam/methane reformer and ethylene pyrolysis environments. This year, INCO expand its testing matrix to include measuring oxidation and sulfidation resistance of several heats of cast FeAl alloys. New data (B. Baker and G. Smith) showed outstanding oxidation resistance of FeAl in air + 5% water vapor at 1100°C out to 1000 hr (Figure 1). More new data showing carburization resistance at 1100°C in both oxidizing (H_2-5.5% CH_4 - 4.5% CO_2) and reducing (H_2 - 1% CH_4) atmospheres (Figure 2), and sulfidation resistance at 816°C (Figure 3) were also obtained.

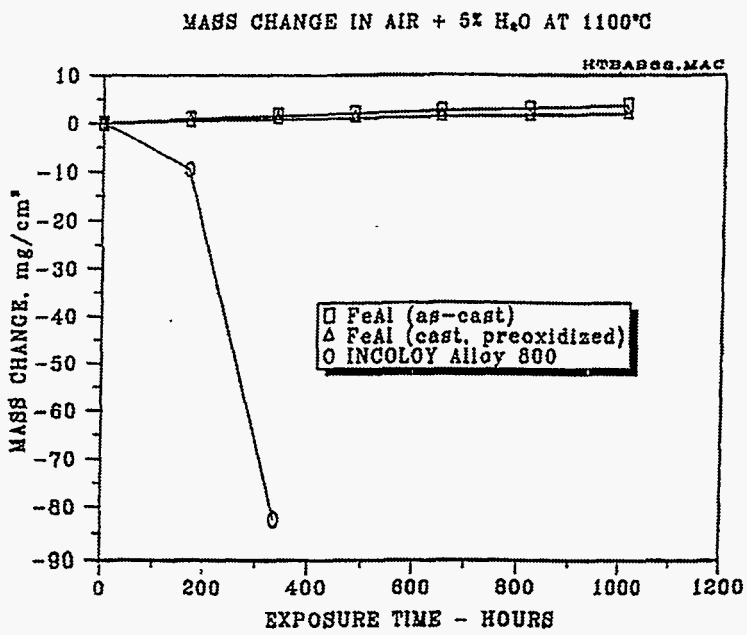

Figure 1. Oxidation testing of cast FeAl (FA-385M21 and FA-386M2) alloys, with and without preoxidation, at 1100°C (B.A. Baker and G. Smith, INCO).

Larger-diameter FeAl billets were hot-extruded for further testing of fine-grained effects on properties, including Charpy impact, tensile and welding, as well as on further hot fabrication.

Large-scale casting of FeAl have been made and successfully tested for skirt materials in aluminum refining applications. The result has been a license of ORNL's FeAl alloys for such applications by Anaconda Foundary and Fabrication Company (Anaconda, Montana).

Cast FeAl grate bars and pallet tips for conveyors used in calcination of phosphate ores have been produced and are in test by FMC, Inc. in San Jose, California (with V.K. Sikka). This application involves both strength and oxidation/sulfidation resistance at close to 1000°C, and FeAl components have been in test now for 5-6 months (Figure 4). The grate-bars at 1000°C show little or no signs of attack or sagging.

Interest in FeAl by M-C Power Corporation for corrosion resistance in molten carbonate salts for a benign molten carbonate fuel cell (MCFC) application, and cast plates were sent for testing.

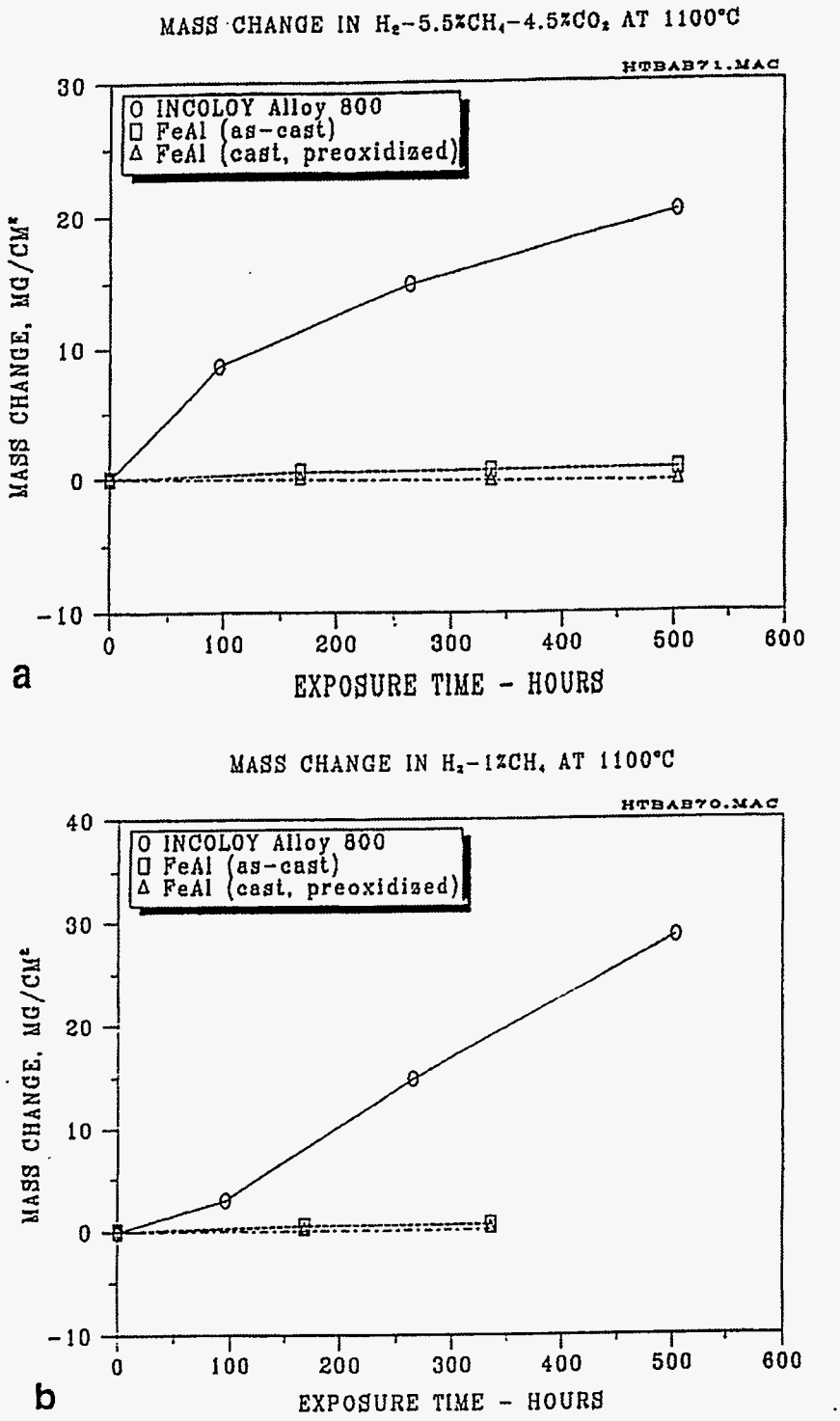

Figure 2. Carburization testing of cast FeAl (FA-385M21 and FA-385M2) alloys, with and without preoxidation, in: (a) oxidizing atmosphere, and (b) reducing atmosphere at 1100°C, together with alloy 800 (B.A. Baker and G. Smith, INCO).

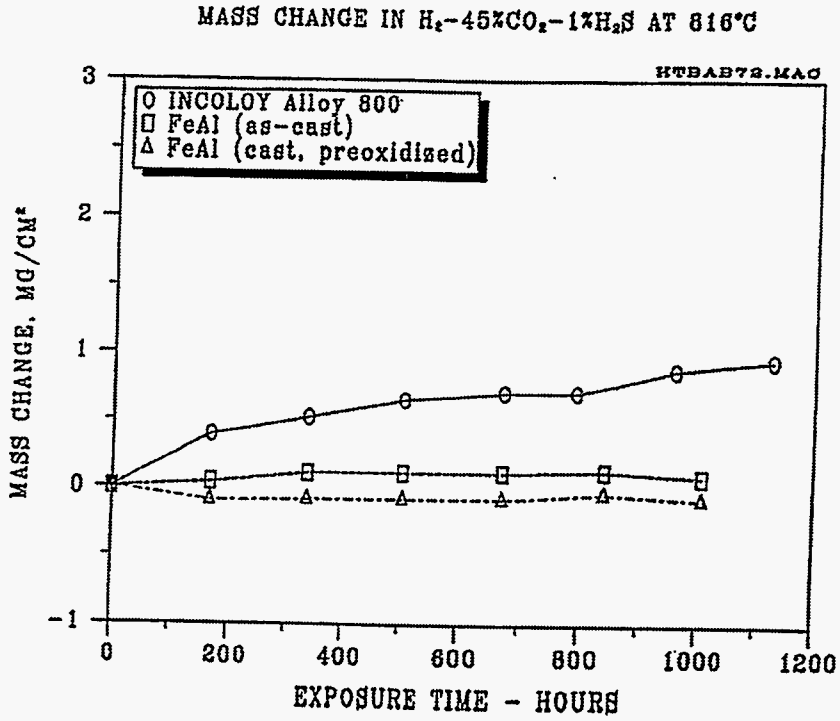

Figure 3. Sulfidation testing of cast FeAl (FA-385M21 and FA-386M2) alloys, with and without preoxidation, at 816°C, together with alloy 800 (B.A. Baker and G. Smith, INCO).

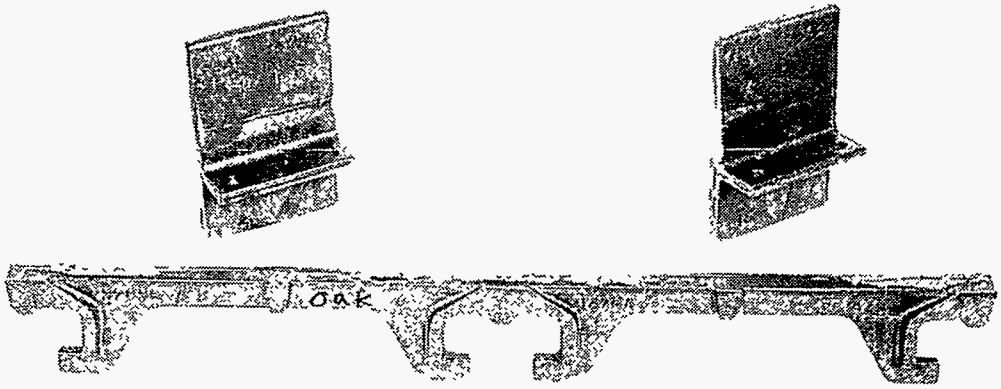

Figure 4. Cast FeAl grate-bar and pallet tip components, produced by FMC, Inc., for calcination of phosphate ores.

2. FeAl Fabrication Technology

Previous FeAl weld-overlay tests involved aspiration-cast wires for shielded-metal-arc (SMA) and gas-tungsten-arc (GTA) welding processes produced by Haynes International and others. Automated GTA and gas-metal-arc (GMA) commercial weld-overlay processing requires continuously coiled, small diameter weld wire. Stoody Company was able to produce 1.6-mm-dia. solid- and powder-cored Fe-Al weld wire with compositions formulated to produce FeAl weld deposits with near-optimum Fe - 36-39 at.% Al compositions, with (Stoody I) and without (Stoody II) Cr. Crack-free FeAl weld-overlay test pads have been produced on 2¼ Cr-1Mo and type 310 steels using the standard 350°C preheat and 750°C post-weld heat-treatment. Lower Al wires (Stoody III and IV) were also obtained.

Welding studies on monolithic FeAl components and thicker material began in FY 1996 and continued this year to solve the problem of cold-cracking. Initial efforts to weld FeAl centifugally-cast (FA-385M2) tubes using filler wire last year were unsuccessful due to cold-cracking without preheat and post-weld heat treatment. Subsequent microstructural examination also revealed significant micro-cracks in the as-cast materials. To test the hypothesis that cold-cracking and welding difficulties are related to the ductility in ambient air (which necessarily involves resistance to moisture-induced cracking), autogenuous automated GTA welds were made on hot-extruded P/M FeAl materials with much higher ductility and significantly refined grain sizes. Good crack-free welds were made on the P/M FeAl material with no preheat or post-weld heat-treatment. This was a major breakthrough for welding/weldability of FeAl alloys. Previously, hot-extruded I/M FeAl alloys with 30-50-μm grain size and 8%-10 % ductility in air at room temperature were also found to be weldable with no preheat or postweld heat treatment. As-cast materials FeAl with only 3%-4 % ductility were still found to cold-crack when similarly welded. However, there does appear to be a threshold ductility and strength level above which FeAl can be succesfully welded, because last quarter, one of the heats (FA-386M2) was found not to cold-crack after a heat treatment of 1hr at 1200°C. Systematic studies of the weldability as a function of minor alloy composition, processing-induced microstructures and ductility in air are on-going.

3. Mechanical Properties of I/M and P/M FeAl

Mechanical properties of monolithic FeAl alloys have been examined as functions of alloy composition and processing-induced microstructures. Emphasis has been on the as-cast and on the hot-extruded I/M materials, with some prior work on P/M FeAl alloys consolidated by direct hot-extrusion. Alloy compositional effects have focussed only on minor variations and combinations of B, C, and Zr added to the FA-385/FA-385M2 base alloys from previous work, as shown in Table 1.

Table 1. Compositions of new cast FeAl alloys.

Alloy	Composition (wt.%) Al	Cr	Nb	Ti	Mo	Zr	C	B	Heats
FA-385M2	21.1				0.42	0.1	0.03	0.005	16238
FA-385M21	21.1				0.42	0.1	0.03	0.010	16239
									16400
									16402
									16346
FA-386M1	21.1				0.42	0.15	0.07	0.005	16240
FA-386M2	22.1				0.42	0.15	0.07	0.005	16241
									16399
									16401
									16345

Previous work on as-cast FeAl alloys with B micro-alloying additions showed that they had about 400 MPa yield strength (YS) up to about 700°C-750°C due to fine dispersions of ZrC precipitates. Heat treatments of 1hr at 1200°C can increase room temperature ductility in air to 3%-4% and boost the YS to 500-550 MPa in new FeAl alloys with more added C and Zr, without sacrificing high temperature strength and creep-resistance at 700°C-800°C. Previously, such cast FeAl specimens heat-treated at 750°C or at 1200°C were also found to also have Charpy impact energies of 11-14 J (Table 2), which considering their coarse grain size (200μm-400 μm) and lower relative ductility, is quite good. Previous Charpy impact testing of similar FA-350 alloys hot-extruded to have more ductility and refined grain size (about 100 μm) only showed 3-5 J impact energy. TEM examination showed that there new FeAl heats also have more abundant dispersions of fine ZrC precipitates. High-temperature tensile testing also shows that these newer cast alloys have much better strength up to 800°C, and have strength comparable to cast HU alloys at 900°C and 1000°C (Figure 5).

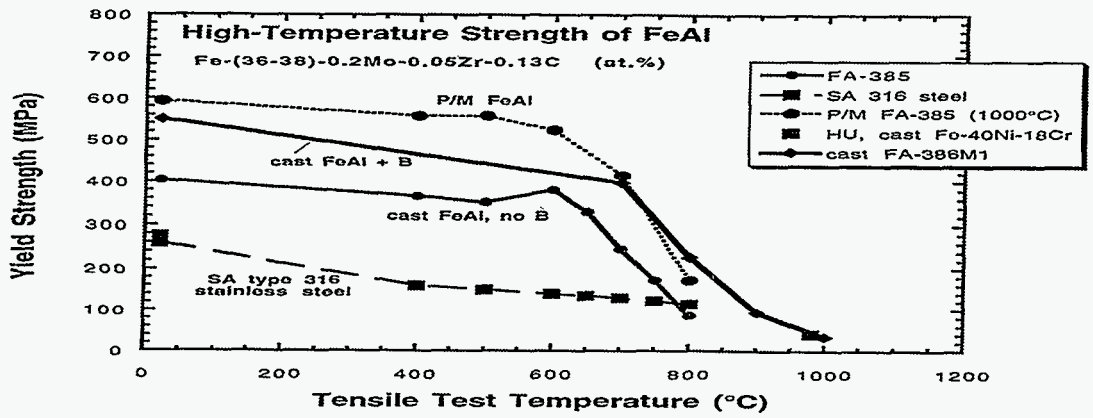

Figure 5. Plot of yield strength (YS) versus tensile test temperature for cast FeAl alloys with and without boron doping. Data for type 316 stainless steel and for cast HU stainless alloy are included for comparison.

Table 2. Charpy impact energy of cast and heat-treated FeAl alloys.

Alloy	Heat Treatment	Temperature (°C)	Charpy Impact Energy (J)
FA386M1	1h at 750°C	25	14.24
	1h at 1200°C	25	13.56
FA386M2	1h at 750°C	25	10.85
	1h at 1200°C	25	13.56

Elevated temperature strength and creep-rupture resistance were also examined in hot-extruded P/M, mechanically-alloyed (M/A) or oxide(yttria)-dispersion-strengthened (ODS) FeAl alloys to complete studies looking at wide-ranging effects of different kinds of processing and processing-induced microstructures on properties. Previous studies had shown that ultrafine grained P/M FeAl had outstanding room-temperature ductility, strength and impact-toughness, but less high-temperature strength and creep-resistance than cast FeAl alloys. Heat treatments of material extruded at 950°C-1000°C slightly coarsen the grain-size (10μm-12 μm) but also produced copious fine ZrC precipitation. These concurrent microstructural changes lower the room-temperature ductility and strength somewhat, but clearly enhance the high-temperature strength and creep-resistance. M/A FeAl shows the highest YS ever seen in FeAl at room-temperature, and retains significant strength even at 1000°C. The ODS FeAl does not behave much differently than P/M FeAl.

At the end of this year, new heats of cast FeAl alloys with minor additions intended to produce similar, more robust ZrC or MC carbide precipitate microstructures in as-cast and/or heat-treated FeAl alloys were produced. In addition, modified alloys with more Zr and C were also hot-extruded to determine the effects of such processing on grain size and precipitation behavior.

4. Residual Stress Measurements in FeAl Weld-Overlays

ORNL has unique neutron diffraction capabilities and methods at the High Flux Isotope Reactor (HFIR), and that facility is being used to measure residual strain/stress distributions in FeAl weld-overlays on 2¼ Cr-1Mo steel. This work, together with finite-element modeling (FEM) of elastic-plastic response of the FeAl weld-overlay and post-weld heat-treatment processes has been done to support optimizing those weld-overlay processing parameters which are required in order to eliminate cold-cracking. Previous studies have shown compressive stresses in the steel substrate underneath the FeAl weld-overlay, and high tensile residual stresses in the FeAl weld-deposit itself, close in value to the YS. The post-weld heat-treatment of 1h at 750°C relieves some of the stresses developed after welding, and indeed, specimens without the post-weld heat-treatment showed 300-750 MPa tensile stresses in the FeAl weld-overlay deposit. Such data

suggests that the FeAl alloy composition and microstructure in the weld-deposit must enable that material to be strong, ductile and resistant to moisture-induced embrittlement for such weld overlays to resist cold-cracking.

PUBLICATIONS

Journals

P. J. Maziasz, D. J. Alexander, and J. L. Wright, "High Strength, Ductility and Impact-Toughness at Room Temperature in Hot-Extruded FeAl Alloys," *Intermetallics* **5** (1997) 547-562.

Other Publications

P. J. Maziasz, G. M. Goodwin, D. J. Alexander, and S. Viswanathan, "Alloy Development and Processing of FeA: An Overview," in the Conf. Proc. Nickel and Iron Aluminides: Processing, Properties and Applications, eds. S.C. Deevi, P.J. Maziasz, V.K. Sikka and R.W. Cahn, ASM-International, Materials Park, Ohio (1997) pp. 157-176.

PRESENTATIONS

Oral Presentations

P. J. Maziasz, "Using Extreme Processing-Induced Microstructures to Radically Improve the Mechanical Properties of Advanced Intermetallic Alloys (B2-FeAl and □-TiAl)" Invited Graduate Seminar presented at the Department of Materials Science and Engineering, University of Tennessee - Knoxville, Tennessee, October 1, 1996.

P. J. Maziasz, G. M. Goodwin, D. J. Alexander, and S. Viswanathan, "Alloy Development and Processing of FeA: An Overview," invited talk given at the The International Conference on Nickel and Iron Aluminides: Processing, Properties and Applications, held during Materials Week '96 in Cincinnati, Ohio, October. 7-9, 1996 and sponsored by ASM-International.

P. J. Maziasz, D. J. Alexander and J. L. Wright, "Processing and Microstructure Control for Improved Impact Toughness of FeAl Alloys," talk given at the 4th International Conference on High Temperature Intermetallics, held April 27 - May 1, 1997, in San Diego, California, and sponsored by ASM-International.

HONORS AND AWARDS

Lockheed Martin Energy Research Corporation chose to submit this work for a R&D 100 Award in March 1996.

A poster, "Processing/Microstructure for High Ductility, Strength and Toughness in P/M FeAl Intermetallic Alloys," was awarded First Place in Electron Microscopy and the overall Grand Prize for the Metallography Contest at PM^{2}TEC'96 World Congress, held June 16-21, 1996 in Washington D.C., sponsored by APMI-International.

PATENTS/DISCLOSURES

C. T. Liu, C. G. McKamey, P. F. Tortorelli and S. A. David, "Corrosion Resistance Iron Aluminides Exhibiting Improved Mechanical Properties and Corrosion Resistance," U.S. Patent No. 5,320,802, granted June 14, 1994.

P. J. Maziasz, G. M. Goodwin and C. T. Liu, "High-Temperature Corrosion-Resistant Iron-Aluminide (FeAl) Alloys Exhibitin Improved Weldability," U.S. Patent No. 5,545,373, granted August 13, 1996.

LICENSES

A preliminary license on FeAl has been obtained by Anaconda Foundry and Fabrication Company (Anaconda, Montana) for use as a skirt material for an aluminum manufacturing process by Columbia Falls Aluminum Company. FeAl is in-test for calcination of phosphate ores by FMC, Inc. (San Jose, California).

Discussions have also begun with United Defense, M-C Power, Inc., Duralloy and other companies who have expressed interest in FeAl this year.

INDUSTRIAL INPUT and TECHNOLOGY TRANSFER

In 1995-96, a new series of industry tests began that was expanded in 1997. Thixomat Inc. (Ann Arbor, Michigan) has evaluated FeAl for wear-erosion in molten aluminum, and completed testing this quarter. Babcock & Wilcox (S. Cung) tested FeAl for resistance to coal-ash corrosion, and does not plan further tests. INCO Alloys International (G. Smith B.A. Baker) tested FeAl last year and discovered outstanding resistance to carburization at 1000°C and 1100°C. Carburization testing at 1000°C was extended to 1000 h, and testing was then expanded to include sulfidation and oxidation testing. INCO has expressed interest in FeAl for weld-overlay technology. Finkl & Sons (C. Manthe) is testing FeAl for resistance to corrosion molten neutral-salts used for heat-treating steels, and is interested in the oxidation resistance at very high temperatures.

Vinod Sikka initiated FeAl replacement of cast-iron for skirts around reduction cells that produce aluminum for Columbia Falls Aluminum Company this year. FeAl has also been cast as grid bars and pallet tips for application in calcination of phosphate ores by FMC, Inc., and have been in-test for 5-6 months at about 1000°C in a highly oxidizing and sulfidizing environment.

Cast plates of FeAl have been sent to M-C Power Corporation for corrosion resistance in molten carbonate salts for a benign molten carbonate fuel cell (MCFC) application.

ESTIMATED ENERGY SAVINGS

Energy savings of fifty percent accrue from using the Exo-Melt™ processing of FeAl compared to conventional metals melting processes, and enables even larger savings in energy and in materials wastage when FeAl replaces steels, stainless steels, or Fe-Cr-Ni alloys as a longer-lasting, corrosion-resistant and heat-resistant alloy. Benefits for reduced metal wear of FeAl may also be realized. FeAl is also a Cr- and Ni-free substitute for heat/corrosion resistant steels and alloys for applications with such environmental and toxicity requirements.

MATERIALS FOR THE PULP AND PAPER INDUSTRY

Section 1. Development of Materials for Black Liquor Recovery Boilers

J. R. Keiser, C. R. Hubbard, P. J. Maziasz, R. W. Swindeman,
B. Taljat, X. L. Wang, and L. E. Meyers

Metals and Ceramics Division
Oak Ridge National Laboratory
Post Office Box 2008, Oak Ridge, Tennessee 37831

D. L. Singbeil and R. Prescott

Pulp and Paper Research Institute of Canada
3800 Wesbrook Mall, Vancouver, BC, Canada V6S 2L9

INTRODUCTION

Black liquor recovery boilers are essential components of kraft pulp and paper mills because they are a crucial part of the system used to recover the pulping chemicals required in the kraft pulping process. In addition, the steam produced by these boilers is used to generate a significant portion of the electrical power used in the mill. Recovery boilers require the largest capital investment of any individual component of a paper mill, and these boilers are a major source of material problems in a mill. The walls and floors of these boilers are constructed of tube panels that circulate high-pressure water. Molten salts (smelt) are present on the floor of recovery boilers, and leakage of water into the boiler can result in a violent explosion if leaked water instantly vaporizes upon contacting the molten smelt. Tube leaks, sometimes leading to such explosions, have occurred with some regularity in the paper industry.

Because corrosion of the conventionally used carbon steel tubing was found to be excessive in the lower section of recovery boilers, use of stainless steel/carbon steel co-extruded tubing was adopted for boiler walls to lessen corrosion and reduce the likelihood of smelt/water explosions. Eventually, this co-extruded (or composite as it is known in the industry) tubing was selected for use as a portion or all of the floor of recovery boilers, particularly those operating at pressures greater than 6.2 MPa (900 psi), because of the corrosion problems encountered in carbon steel floor tubes.

However, cracking into, or through, the stainless steel outer layer of this composite tubing was subsequently encountered. Almost without exception, in sloped-floor boilers, cracks have first been seen in wall tubes that form the openings for removal of the molten salts (smelt spout openings). Subsequently, cracks have been found in floor tube membranes and eventually in floor tubes themselves in both sloped- and flat-floor types of boilers.

Since neither the cause of the cracking nor an effective solution has been identified, this program was established to develop a thorough understanding of the degradation that occurs in the composite tubing used for walls and floors. This is being accomplished through a program that includes the collection and review of technical reports, examination of unexposed and cracked tubes from boiler floors, collection and analysis of smelt samples, collection and tabulation of temperature data, measurement of residual stresses in as-produced, as-formed, and exposed composite tubing, computer modeling to predict residual stresses under operating conditions, and operation of laboratory tests to study corrosion, stress corrosion cracking, and thermal fatigue. From this work it is anticipated that alternate materials or operating procedures will be identified, and these will be tested in recovery boilers.

TECHNICAL PROGRESS - FY 1997

1. Examination of Unexposed and Exposed Recovery Boiler Floor Tube Components

A significant number of cracked composite tubes from boiler manufacturers, inspection companies, and paper mills have been carefully examined in order to define the characteristics of the cracking. In some cases, large panels have been provided when all or significant portions of a floor have been replaced, while others have come from floors in which single tubes, or no more than a pair of adjacent tubes, have been removed. Of special interest are samples of cracked membranes and a panel that was removed from a boiler floor after two years of operation.

1.1 Characterization of cracked composite membrane

Several mills have provided membrane samples from composite tube floor panels in which the membrane cracks proceed into the carbon steel. Examples from two different mills are shown in Figure 1. These samples show cracking in the stainless steel outer layer that is similar to cracking seen in co-extruded tubing. However, in some cases, the cracks in the membrane continue into the carbon steel rather than stopping at the interface as seen in composite floor tubes. In many cases, the cracks in the carbon steel are considerably wider than in the stainless steel, suggesting that corrosion probably contributes to a widening of the cracks in the carbon steel. Additional residual stress measurements and finite element modeling are being used to gain a better understanding

of the stresses in the carbon steel of the bimetallic membrane material. Initial results of the modeling indicate that tensile axial stresses are present in the carbon steel portion of bimetallic membranes.

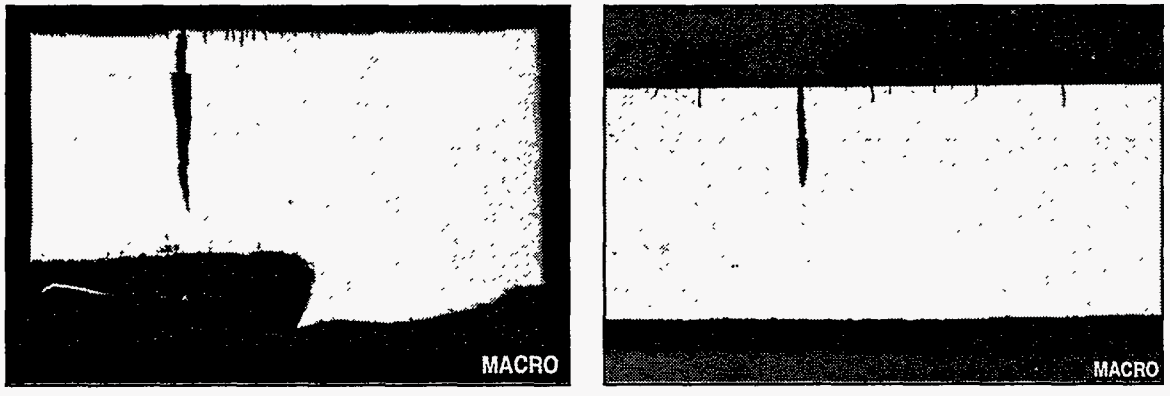

Figure 1. Examples of cracking in membranes from composite recovery boiler floors.

1.2 Characterization of weld overlay and coextruded boiler floor tubes

During the spring of 1995, a mill in the South Central U.S. installed five panels constructed of materials that are options for floor tubes. These materials include co-extruded 304L/carbon steel, 309L weld overlay on carbon steel, co-extruded Sanicro 38 (modified alloy 825)/carbon steel, weld overlay 625 on carbon steel, and coextruded alloy 625/carbon steel. The panels all contain three tubes which are each 6 ft (1.83 m) long, and they were installed in the floor directly in front of smelt spout openings. After the first year of operation, no cracks were found in any of the panels, but, after the second year, cracking was found in the 304L/carbon steel and the 309L weld overlay. The panel containing these six cracked tubes was removed from the floor and sent to ORNL for examination. Following careful surface cleaning, a dye penetrant examination was used to reveal extensive cracking in all six tubes. An example of the surface appearance of cracked weld overlay tubing is shown in Figure 2. Photomicrographs taken of cross sections of co-extruded and weld overlay tubes (see Figure 3) show that the cracking has many common characteristics in the two materials. The cracks in both materials originate at the outer surface, are transgranular, have little or no branching, do not extend into the carbon steel, and sometimes form corrosion pits in the carbon steel at their termination point. These results provide strong evidence that the cracking is more dependent on the composition of the stainless steel layer (300 series) than on the method used to apply the layer.

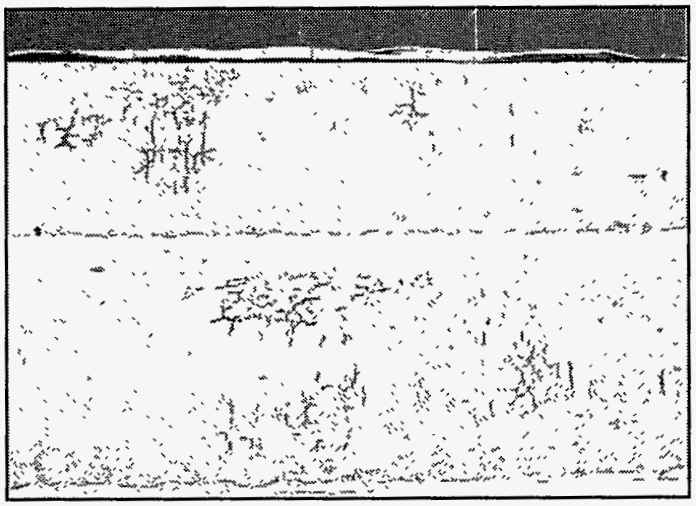

Figure 2. Photograph of the surface of 309L stainless steel weld overlay tube where cracks have been highlighted by dye penetrant inspection.

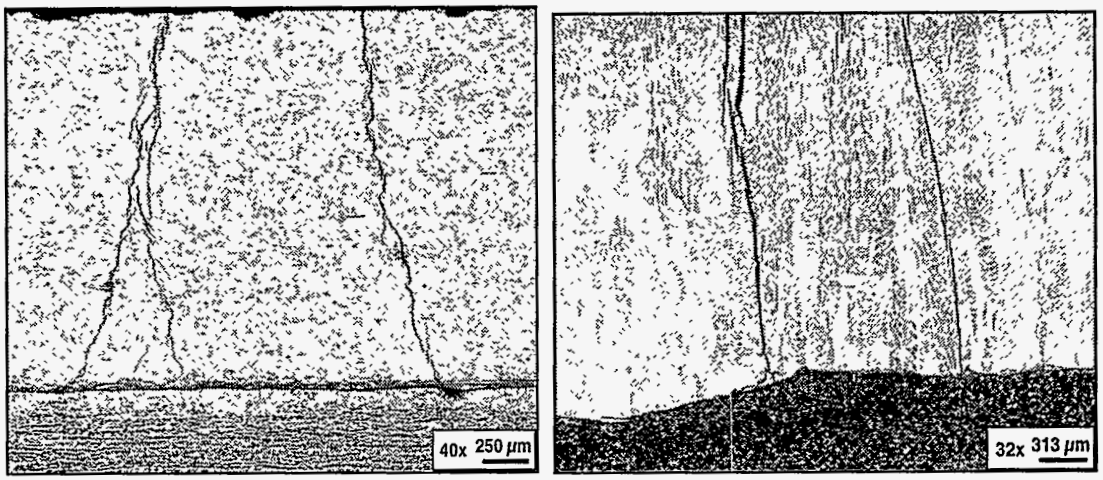

Figure 3. Photomicrographs showing cross sections of cracked coextruded 304L/CS and 309L weld overlay tubes after two years exposure in a recovery boiler floor.

2. Transmission Electron Microscopy Examination of Samples

The dislocation substructure that develops in a metal is influenced by the cyclic loading history experienced by the metal, and transmission electron microscopy (TEM) can be used to observe this dislocation structure. Information on the dislocation substructure of 304 and 304L stainless steels is widely available in the literature [1-4]. At high temperatures (above 600°C) and large strain ranges (above 1% strain range), it has been established that dislocation cells or subgrains form whose dimensions can be correlated with the cyclic stress range [1]. At lower temperatures and small strain ranges, however, the dislocation substructures developed in fatigue are quite sensitive to testing conditions.

Planar arrays of dislocations, tangles, cells, and labyrinth structures have been reported under thermal/mechanical loading conditions [17,19].

Previous studies examined the substructure in a fine-grained 304L specimen isothermally fatigued at 300°C and compared this substructure to that observed in 304L cladding from three composite tubes that cracked in service [5]. Two of the tubes were in service over ten years, and the third tube was removed after 18 months. The isothermally cycled test specimen revealed a substructure with a low concentration of network dislocations and some fine loops and stacking faults. In contrast, the substructure near the surface of the 304L stainless steel cladding from the long-term service tubes consisted of very dense dislocation networks similar to cold-worked (>20% strain) stainless steel [6]. The substructure in the composite tube was not judged to be comparable to the substructure in the isothermally fatigued specimen.

To provide another sample for comparison, a thermal/mechanical fatigue experiment was performed on a fine-grained 304L specimen to examine this phenomenon. The specimen was thermally cycled under full restraint (0.5% strain range) between 300°C and 600°C with a 0.1 h hold time at 600°C. The cycle-to-cycle hardening was more rapid than in isothermal tests performed at higher strain ranges (approximately 0.7%) at both 300°C and 600°C. The TEM investigation of the thermal/mechanical fatigue specimen tested for 200 cycles revealed a very dense tangle of dislocation networks and loops. For the sample in this laboratory test, these features were uniformly distributed throughout the matrix and cellular arrays were absent. Another important detail was the high concentration of kinks and jogs along individual dislocation segments. The substructure differed from the fatigue structure that was produced by isothermal cycling at 300°C.

Examination of cracked cladding from additional long-time-exposed tubes revealed little or no gradients in substructure from the near-surface to the mid-clad section. Both the near-surface and mid-clad substructures were qualitatively similar to the substructure observed in the thermal/mechanical test specimen in the sense that loops and kinked dislocation segments were present in both types of specimens. Overall, the dislocation density was lower in the exposed cladding than in the thermally cycled specimen. Specimens were examined from cracked and uncracked regions of the exposed cladding and the substructures were found to be similar.

Clearly, the microstructure and mechanical properties of the 304L cladding changed significantly during service relative to the as-manufactured cladding. Further, there is some evidence that thermal/mechanical cycling is a major factor in causing these changes. However, the concentration of the substructural features characteristic of thermal cycling is considerable less in the exposed samples than in the thermally cycled laboratory specimen.

3. Measurement of Residual Stresses in Unexposed and Exposed Tubing

One of the purposes of residual stress studies is to provide information to identify the cracking mechanism operative in composite tubes subjected to kraft recovery boiler service conditions. Both stress corrosion cracking and thermal fatigue have been suggested as likely explanations for the observed cracking. In either case, the residual stress state in the clad layer plays an important role in that tensile residual stresses at the surface could facilitate crack initiation, and tensile residual stresses below the surface layers assist the propagation of cracks. If, however, the surface is under a compressive residual stress, stress corrosion cracking is considered unlikely. During this period, the residual stresses in chromized carbon steel tubes and panels have been characterized, measurements of residual stessses in welded composite tube panels have been initiated, and surface residual stresses have been measured in cracked and uncracked panels removed from operating mills.

3.1 Residual stresses in chromized tubes and panels

Chromized tubes are being considered as an alternative to the composite tubes currently in use in kraft recovery boilers. According to the manufacturer, the chromized tubes were fabricated by diffusing chromium from a gas phase into carbon steel tubes a a temperature in excess of 2000°F (1093°C). Microanalysis revealed that the chromized layer extends about 0.45 mm into the carbon steel.

On cooling from the chromizing temperature, residual stresses were generated due to mismatch in (1) thermal expansion, and (2) lattice parameters (growth stress from diffusion of Cr) between the carbon and chromized steels. Typically, the chromized layer has a smaller coefficient of thermal expansion, and, as a consequence, the chromized layer is in compression after cooling. The lattice parameter of Fe-Cr increases with increasing chromium composition [7]. Such a mismatch in lattice parameters also generates compressive residual stresses in the chromized layer, followed by tensile residual stresses at larger depths within the carbon steel tube.

The X-ray measurements were made using Cr K_a radiation and the *bcc* (211) reflection, following the standard d-sin$^{2\psi}$ method. An electropolishing technique was used to permit measurement by the X-ray method of stresses below the surface ($\leq$ 0.5 mm). The (211) reflection was used for strain determination in the neutron diffraction experiment which permits through thickness stress measurements (up to 6 mm). Configurations of the neutron diffraction experiment are similar to those used in previous studies [8] of co-extruded composite tubes and weld overlay tubes [9]. The neutron diffraction data were analyzed based on the bi-axial stress assumption, which does not require the knowledge of stress-free lattice parameters which as described earlier, varies with depth in the chromized layer. Judging from previous works by Pintschvius et al. [10] and Wang et al.

[9], where a very small radial stress was measured throughout the wall thickness in tubes of similar dimensions, the bi-axial stress assumption is considered appropriate.

Figure 4 shows the through-thickness residual stress profile measured with neutron diffraction. A defining feature of Figure 4 are the large compressive residual stresses in the chromized layer, followed by small tensile stresses at larger depths, as might be expected from the mismatch in thermal expansion and lattice parameters between the chromized layer and steel substrate.

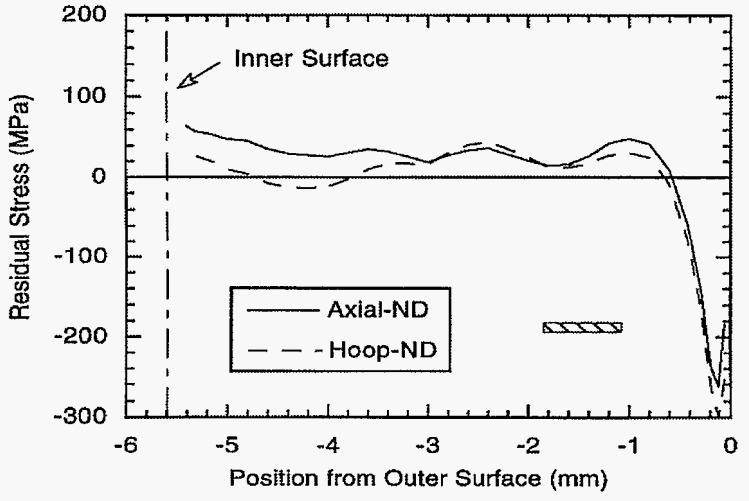

Figure 4. Through-thickness residual stress profile in a chromized tube as determined with neutron diffraction. The shaded bar indicates the approximate slit width used in the neutron diffraction measurements.

Figure 5 compares residual stress values near the outer surface obtained from neutron and X-ray experiments, respectively. While scattered, it appears that the average residual stress values measured by X-ray are somewhat less compressive than those measured by neutron diffraction. While the exact cause for this difference is unclear, a small tensile radial stress would certainly contribute to this difference, as the neutron data were analyzed based on the bi-axial stress assumption (zero radial stress).

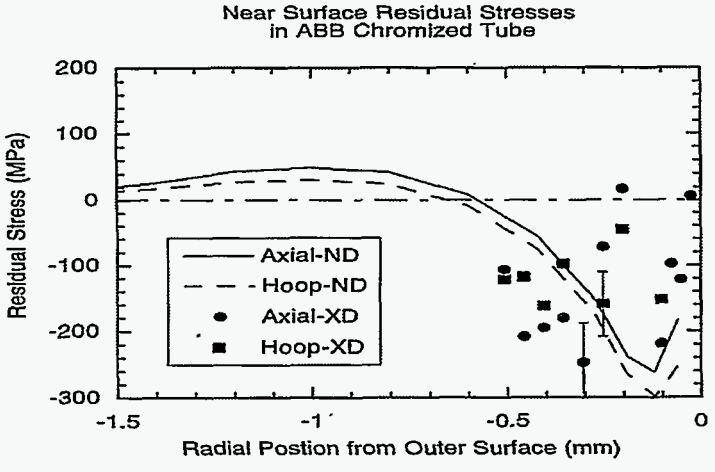

Figure 5. Comparison of the residual stresses obtained by X-ray diffraction and neutron diffraction near the outer surface of a chromized tube.

3.2 Residual stresses in welded composite tube panels

Following this study, a 5-tube chromized panel was investigated. The panel was fabricated by welding the carbon steel tubes together and then applying the chromized process. Because of the rather high chromizing temperature (>2000°F), the welding residual stresses are expected to be fully annealed and thus the residual stresses in chromized panels were expected to look similar to those in single tubes.

Figure 6 shows the through-thickness residual strain profiles measured at the crown by neutron diffraction. As can be seen, the residual stresses in the crown of the chromized tube panel are small (<±40 MPa). In comparison with the residual stresses measured in as-manufactured clad tube panels [11], it appears that the chromizing process has removed nearly all residual stresses produced during welding of the tubes to form the panel. Because 2-mm slits were used for these measurements, residual stresses in the chromized layer were not determined. However, based on measurements of single chromized tubes (discussed above) compressive stresses are expected in the chromized layers of the welded panel. In general, compressive residual stresses in the surface layers are beneficial for applications in kraft recovery boilers because they inhibit stress corrosion cracking and resist thermal fatigue induced cracking. However, before a recommendation can be made, the effect of thermal cycling and other properties will have to be investigated.

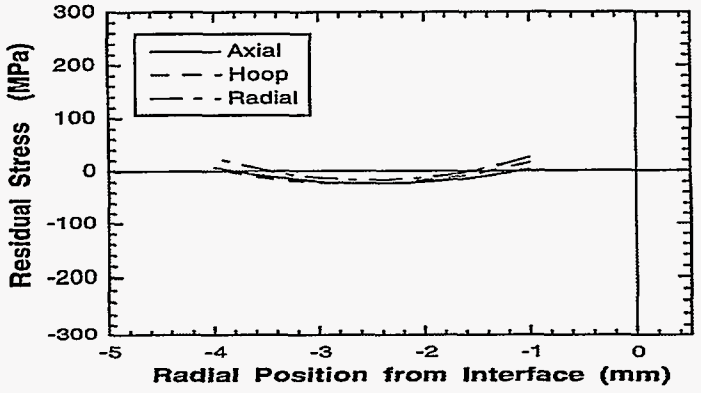

Figure 6. Residual stresses in a chromized tube panel. The measurements were made at the crown of the middle three tubes.

To validate the finite element model for composite tube floors developed at ORNL over the past two years, a composite tube panel was also investigated. The specimen chosen is a 5-tube panel made of Sumitomo coextruded 304L/SA210 2½ diameter tubing. This panel was specially fabricated by ABB CE for this study. The through-thickness measurements at the crown are now complete, and the results are shown in Figure 7. In contrast to the chromized tube panel, substantial residual stresses were observed at the crown of the composite tube panel. Specifically, the measured residual stresses are tensile in the clad layer and compressive in the carbon steel core. The spatial dependence and magnitudes of measured residual stresses support the predictions of ORNL's composite tube model.

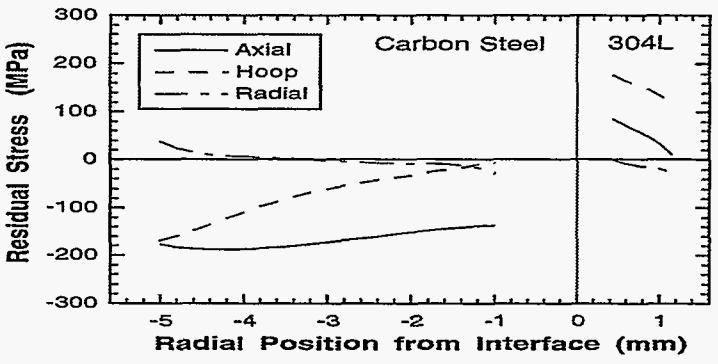

Figure 7. Residual stresses in a composite tube panel. The measurements were made at the crown of the middle three tubes.

Significant experimental difficulties were encountered while attempting to measure residual stresses in the membrane. An unidentified peak appeared adjacent to the fcc (311) peak from 304L, normally used for measurements in fcc metals. The intensity of this peak arises at the expense of the (311) peak, which indicates a phase change at the center of the web. Measurements at different orientations show that this unidentified peak is strongly textured, with the highest intensity observed when the scattering vector is perpendicular to the panel. X-ray and neutron diffraction experiments will be used to identify this peak and the associated phase which is essential in assessing the impact on properties used in the finite element model. Using a reference specimen made from the composite tube, normal strains were derived as a function of the position along the web, as shown in Figure 7. Qualitatively, the spatial dependence of the normal strain data are consistent with calculations by finite element analysis. However, until a stress-free reference specimen is prepared from the web material, a quantitative comparison cannot be made with finite element calculations.

3.3 Residual stresses in cracked and uncracked previously exposed tube panels

In support of failure analysis, several X-ray experiments were undertaken to determine surface residual stresses in exposed panels removed from operating mills. The measurement technique used here was developed in the early stage of this project with the use of Cr K_β radiation, which has allowed making precise measurements in the textured clad layer. First, a cracked panel from a mill in the South Central U.S. was examined. Figure 8 shows the measurement results along with a photograph of the analyzed panel. The measured residual stresses are large and compressive (~ -400 MPa). This is likely due to bending of the tube panel. A plastically bent tube should exhibit a compressive stress at one surface balanced by a tensile stress at the other surface. In the uncracked region, axial and hoop stresses are of the same magnitudes. In the cracked region,

however, the axial stress is considerably less compressive than the hoop stress. These data are being analyzed in conjunction with microstructural and failure analyses.

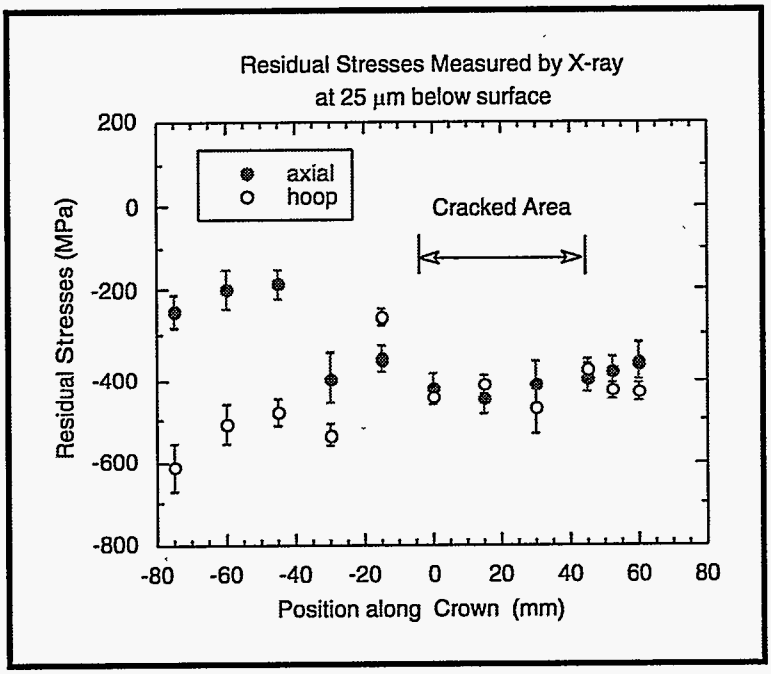

Figure 8. Residual stresses on the surface of a cracked 304L/CS tube panel from a mill in the South Central U.S.

Two panels from the Weyerhaeuser mill at Columbus, Mississippi, were examined. These two specimens were located on the same floor, but on opposite corners. Extensive cracking was found in panel 2L, while panel 1R showed no sign of cracking. X-ray measurements on polished surfaces show that residual stresses in the uncracked panel (1R) are tensile and equal in both axial and hoop directions, consistent with earlier X-ray data on straight tube panels and finite element calculations. In the cracked panel (2L), the axial stress becomes compressive, while the hoop stress remains roughly the same, as illustrated in Figure 9. This result is consistent with microstructural studies where cracks were found to penetrate radially into the clad layer.

It should be realized that the data shown in Figure 9, while useful, provide no information of residual stress in 2L before cracking.

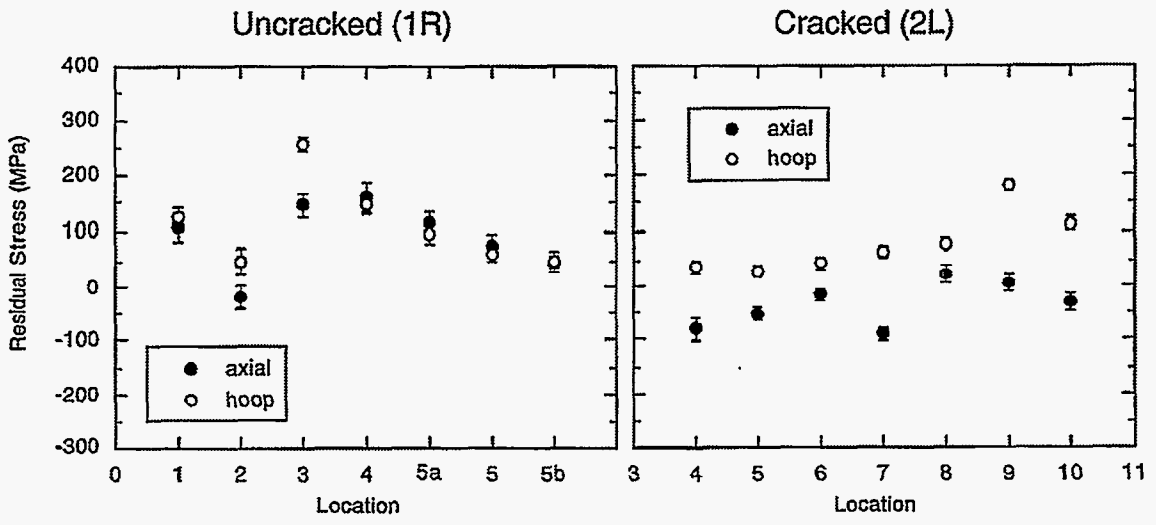

Figure 9. Residual stresses on the surface of cracked and uncracked panels removed from the smelt runs of a boiler in the southeastern United States.

Fortunately, one of the tubes in 2L appeared to be uncracked and X-ray measurements were made at the crown of this tube. Figure 10 compares residual stresses in panel 1R, where no cracking was observed, and in the uncracked region of panel 2L. From Figure 10, it can be concluded that, to within the experimental precision, panel 1R and 2L experience almost identical residual stresses before cracking occurs. This shows that residual stresses are only one of the factors causing cracking to occur. This shows that residual stresses are only one of the factors causing cracking in 2L; other factors (e.g., environment) must also play a role.

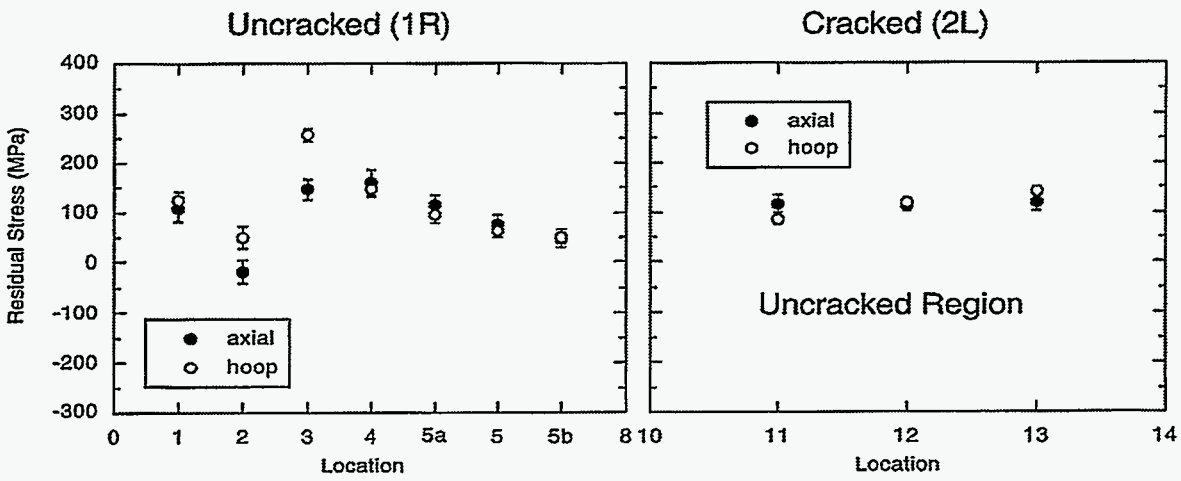

Figure 10. Comparison of surface residual stresses in cracked and uncracked panels removed from the same boiler.

Future studies will include completing measurements in the composite tube panel. To study the effect of exposure, an as-manufactured composite tube will be subjected to thermal conditions similar to that in an operating mill and the residual stresses determined at the end of selected cycles using X-ray and neutron diffraction. The experimental data will also serve to validate the finite element model currently being developed and provide guidance to improve the model. In addition, on-site X-ray measurements will be demonstrated at a selected mill.

4. Modeling of Residual Stresses

In this time period the modeling work on SS304L/SA210 tubes has continued. Several different situations that are likely to occur were studied: stresses that develop at service conditions as a result of temperature excursions of different magnitudes, transient stresses at shut-down event, stresses at operation after the shut-down and restart of the boiler, and the effect of local heating during panel straightening. The performance of the A625/SA210 weld overlay tubes were studied at various in-service conditions, including temperature excursions. Also, an analysis of chromized tubes was performed at different in-service conditions. Thé analysis was based on the calculated residual stresses from the panel assembly welding and the chromizing processes. Furthermore, a response surface study was performed providing a generalized solution of stresses in the floor of co-extruded composite tubes over an array of material properties (yield stress and coefficient of thermal expansion) of the overlay material. All of the above mentioned work is based on the thermal analyses performed during the last year and using the developed two- and three-dimensional finite element models. In this report only the results and phenomena learned that are of certain importance are briefly presented and discussed.

4.1. Coextruded SS304L/SA210 tubes

During the last year several finite element models were developed and a detailed thermal analysis of the composite SS304L/SA210 floor was performed. The stress-strain behavior of the composite tubes at normal operating conditions and at some temperature excursion scenarios was analyzed. These same models have been used to model additional situations that a composite SS304L/SA210 tube may experience.

4.1.1 Stresses at the floor fireside surface after temperature excursions of different magnitudes

Temperature excursions of different magnitudes were simulated to determine the stresses that remain at operating conditions at the hot spot location. In the previous reports it was shown that the stresses in the SS304L overlay are compressive and of the yield-stress magnitude at service conditions. It was shown that a 450°C hot spot causes additional yielding and then stresses are reversed to tensile when the tube returns to normal operating temperature. Some additional analyses were performed considering the minimum magnitude of temperature excursion that causes the stress reversal. The results show that any temperature excursion higher than about 40C° (fireside tube temperature of 355°C) causes tensile stresses at operating conditions (see Figure 11).

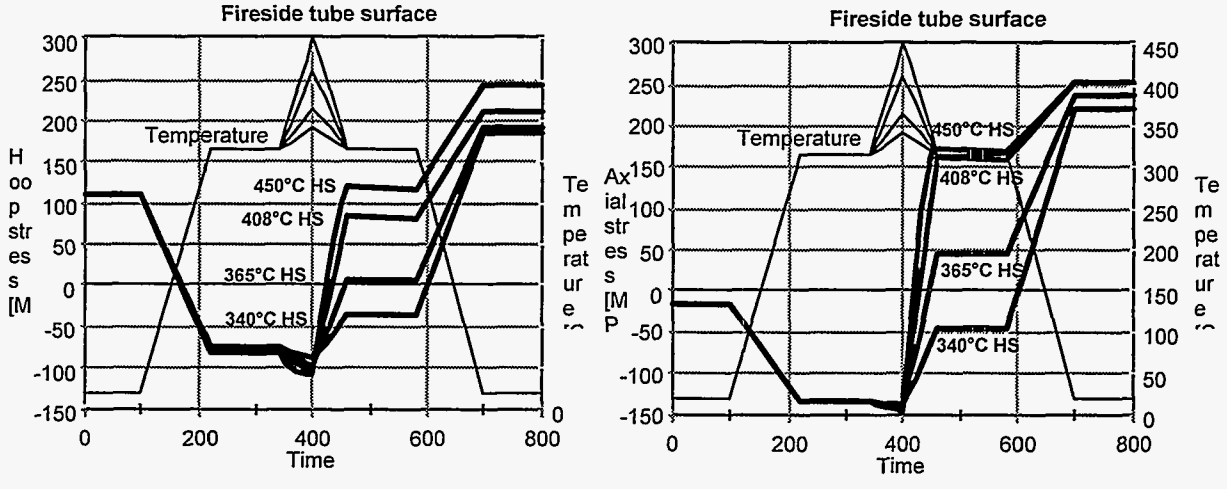

Figure 11. Tangential and axial stresses at the fireside surface of the tube crown for a normal operating cycle that includes temperature excursions to 340°C, 365°C, 408°C, and 450°C.

4.1.2. Transient analysis of the boiler shut-down event

Thermo-mechanical transient analysis of the boiler floor during the shut-down event was performed. A linear temperature variation from the operating temperature to room temperature was considered to occur in 300 min.Figure 12 shows the stress at the fireside surface of the tube crown and at the fireside surface of the membrane throughout the transient. Stresses at the side surface of tube crown become tensile at about 275°C and they reach the yield stress at about 225°C. Stresses at the fireside surface of the membrane become tensile at about 270°C and they each the yield stress at about 220°C. The effect of internal pressure variation during the shut-down transient on stresses in the tubes was also evaluated. It was determined that the stresses developed from the internal pressurization either at service or at room temperature are not significant.

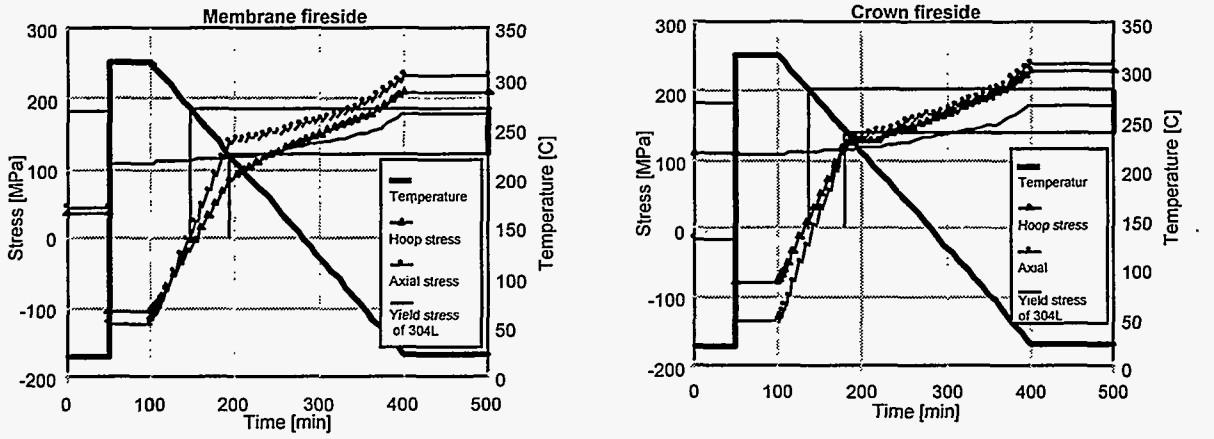

Figure 12. Stresses at the fireside surface of the tube and the membrane during the shut-down transient.

4.1.3. Stresses at service conditions after shut-down and restart of the boiler

The objective of this analysis was to explore the stress behavior of regions affected by temperature excursions after the boiler is shut-down and brought back to operation. Stresses were computed at the fireside surface of the tube crown and the membrane for a scenario that included a 65°C temperature excursion (380°C peak temperature) during normal operation, the boiler shut-down to room temperature and restart to operating conditions.

Figure 13 shows the stresses at the fireside surface of the tube crown and the membrane throughout the cycle. The results show that the tensile stresses that develop due to temperature excursions remain at that location throughout that service period but become compressive again when the boiler shuts-down and returns to operating conditions. The reason is yielding of the overlay material during the boiler shut-down. A conclusion that the stresses at the fireside surface of the SS304L/SA210 floor are compressive after each restart of the boiler can be accepted.

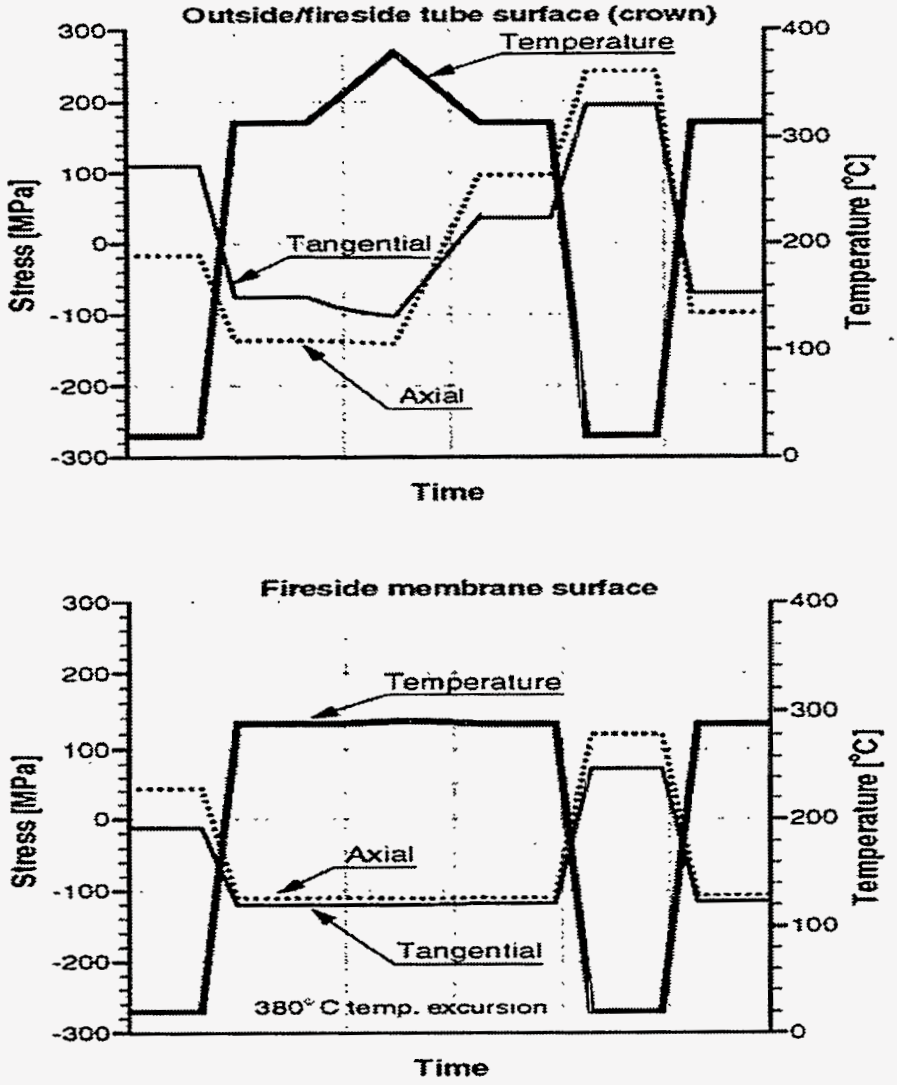

Figure 13. Stresses at the fireside crown of the tube and at the fireside of the membrane during the indicated temperature cycle.

4.1.4. Effect of local heating during panel straightening on stresses at service conditions

To determine the effect of local heating during straightening process on the in-service stresses the following analysis was performed. It was assumed that a tube was locally heated to 500°C and then cooled to room temperature. Then the operating conditions were simulated including a temperature excursion to 380°C. The panel was again cooled to room temperature.

The results presented in Figure 14 show that the stresses at the tube crown at service conditions, either before or after the temperature excursion, are not significantly affected by the local heating during straightening. Stresses at the fireside surface of the membrane are of small magnitude, but are brought toward tension (stresses are less compressive) by about 100 MPa. Therefore, one may conclude that local heating during straightening does not critically affect the stresses in the panel.

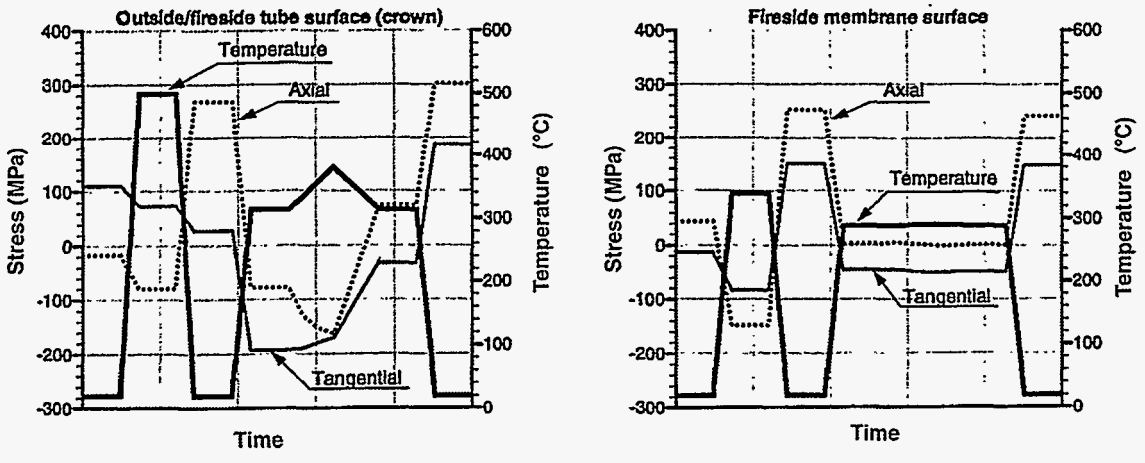

Figure 14. Stresses at the fireside crown of the tube and at the fireside of the membrane during the indicated temperature cycle.

4.2 Weld overlay A625/SA210 tubes

A finite element model was developed to analyze the residual stresses from the assembly welding for the alloy 625 weld overlay tubes. Several analyses were performed considering a stress-free tube (annealed tube condition) or tube with residual stresses from the weld overlay process. Annealing after the weld overlay process reduces the high residual stresses that often cause difficulties at the assembly welding. Here, only the stresses calculated for the annealed tube are reported. Stresses were calculated for normal operating conditions and a temperature excursion scenario with a peak temperature of 550°C.

Figure 15 shows the axial and tangential stresses at the fireside crown of the tube. The residual axial and tangential stresses from the assembly welding are compressive (around -100 MPa) and tensile (around 200 MPa), respectively, and are slightly reduced when the tube reaches operating conditions (see Figure 15). Stresses return to initial residual stress values when the boiler is cooled to room temperature, which means that the stresses are within the elastic region throughout the cycle. The stresses are compressive during the hot-spot occurrence and then tensile after returning to operating conditions.

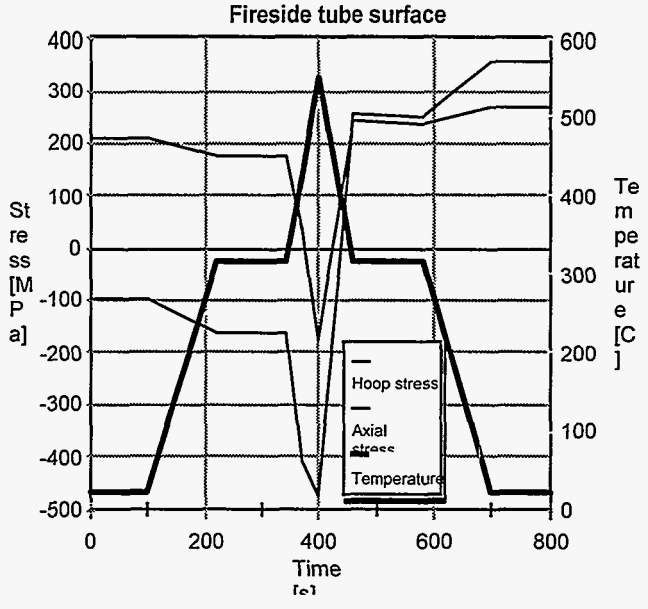

Figure 15. Tangential and axial stresses at the fireside crown of the weld overlay tube (annealed before the assembly welding).

4.3 Chromized tubes

A FE model was developed for stress analysis of the chromized tubes. First, the residual stresses from the assembly welding were computed. A plain carbon steel tube without the layer of chromium at the surface was considered in the assembly welding simulation. The calculated residual stresses were used as a basis in the simulation of the chromizing process. The panel was heated to 1100°C, and the chromium layer was applied (two cases were considered: a 0.45 mm and a 0.25-mm-thick layer), and then the panel was cooled to room temperature. The thermo-physical properties of SS445 (23%-27wt% Cr) were used for the chromized surface layer. The calculated stresses were used as initial conditions in the subsequent analyses of operating conditions. Three cases were studied: (a) normal service conditions, (b) service conditions with a temperature excursion reaching 380°C, and (c) temperature excursion with the peak of 550°C during operation. Figures 16-18 show the stress results for the tube crown and the membrane fireside for the three cases. The results presented are for the 0.45-mm-thick chromium layer.

Note that there is no significant difference in stresses between the tubes with 0.45-mm or 0.25-mm-thick chromium layer (the results are within 5% to 10%).

Based on the results the following observations can be made. Heating to service conditions tends to create tensile stresses in the chromized surface layer. The reason is lower coefficient of thermal expansion of Cr compared to SA210. The chromizing process creates high enough compressive stresses in the surface layer to keep the stresses from becoming tensile when the floor is brought to operating conditions (see Figure 16). Therefore, the chromizing process can be considered beneficial by creating high compressive stresses at the outside surface of the tubes. However, the axial stresses at the membrane surface are tensile during operation.

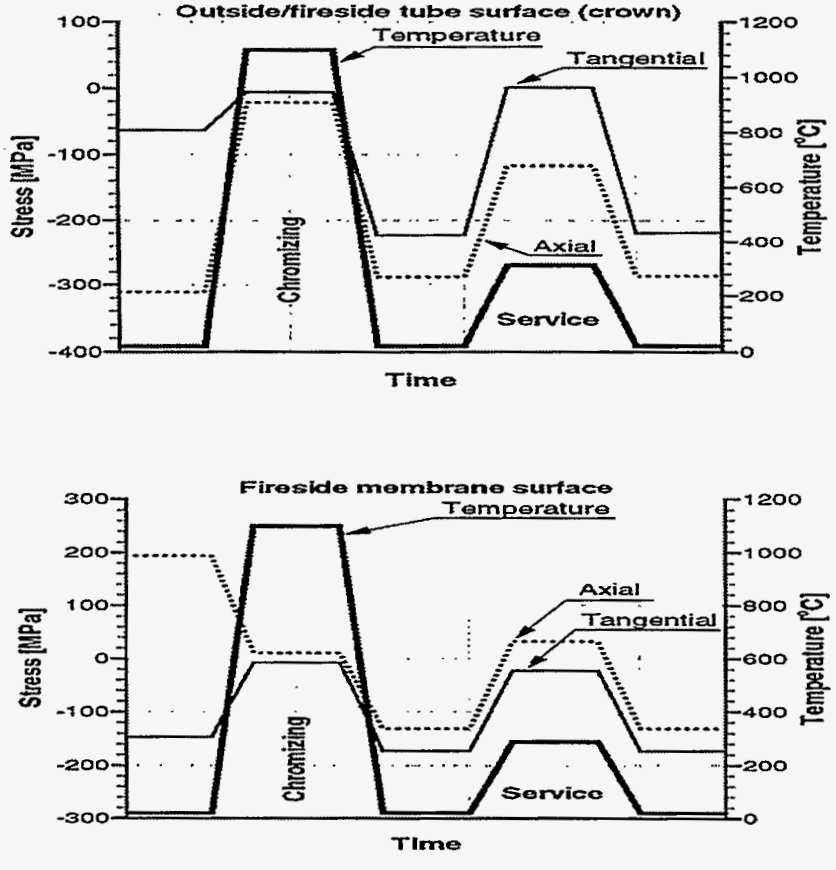

Figure 16. Axial and tangential stresses at the fireside surface of the tube crown and the membrane for a normal operating cycle.

The tangential stresses at the fireside crown of the tube become tensile after the 65°C temperature excursion, but the magnitude is not significant. The stresses at the membrane fireside surface remain unchanged. The stresses in the chromized layer are well below the yield stress throughout the assumed temperature cycle. One may conclude that a temperature excursion with the peak of 380°C does not critically affect the stresses at the fireside surface of the tube or the membrane (see Figure 17).

The chromized tube surface within the 550°C hot-spot region yields and the stresses at service conditions after the temperature excursion become tensile. The plastic deformation occurs due to a high-temperature gradient through the tube thickness. The magnitude of these stresses is not significant. The tensile axial stresses at the membrane fireside surface are reduced by the temperature excursion (see Figure 18).

The coefficient of thermal expansion (CTE) of the chromized layer is smaller than CTE of the carbon-steel base causing a tendency towards tensile (less compressive) stresses in the chromized layer during heating to operating temperature. An interesting phenomenon occurs during a temperature excursion. Because of the explained difference in CTE one would expect the stresses at the surface to grow higher in tension at a temperature excursion. For a temperature excursion that imposes high temperature gradient to the tube, this does not happen (see Figure 18). Contrary, the stresses grow towards compression, because of the temperature gradient in the tube, which is the reason that the surface layer tends to expand more than the base tube even though the CTE of the chromized surface layer is smaller than the CTE of the base tube.

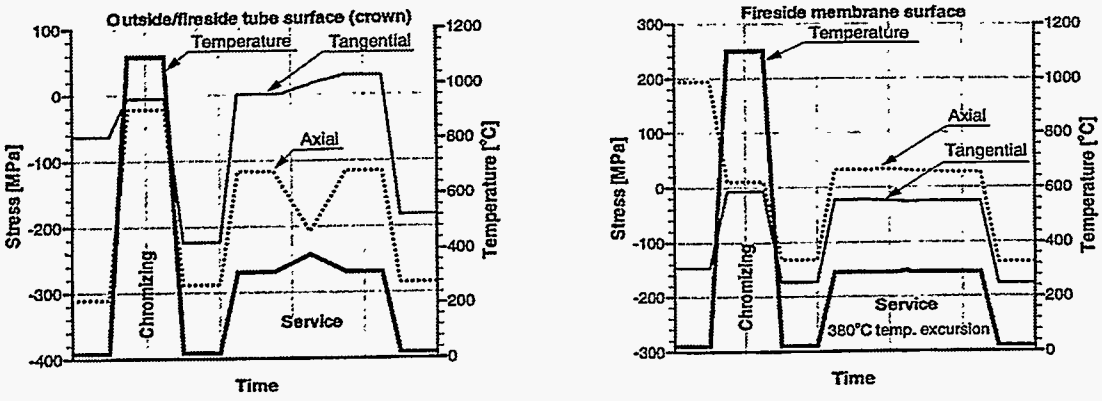

Figure 17. Axial and tangential stresses at the fireside surface of the tube crown and the membrane for a normal operating cycle with a 65°C temperature excursion.

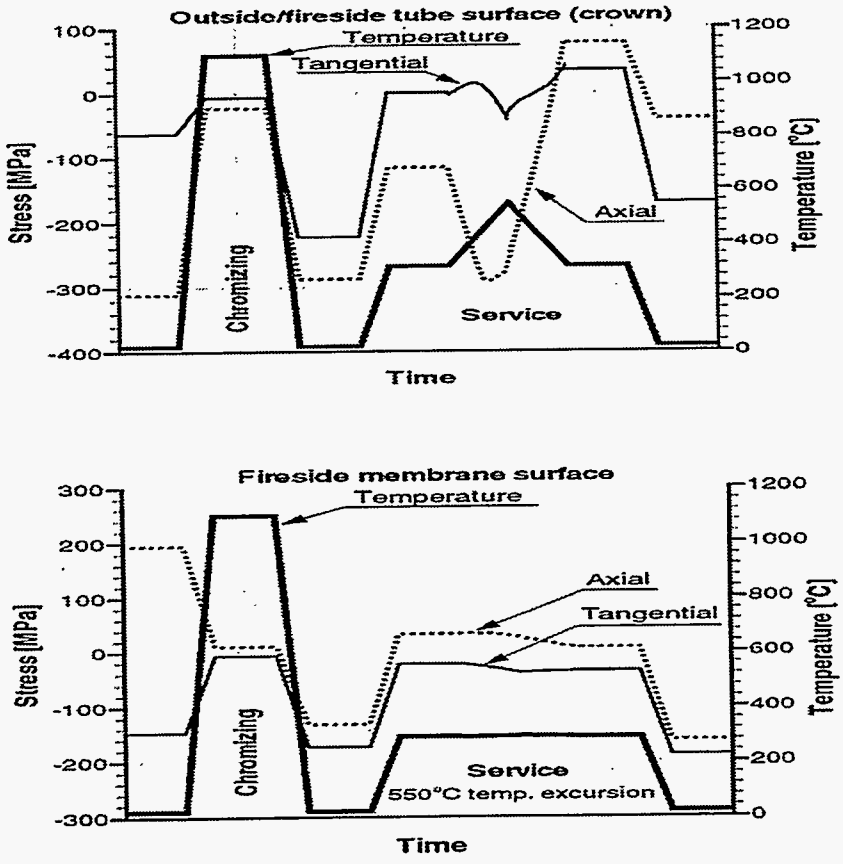

Figure 18. Axial and tangential stresses at the fireside surface of the tube crown and the membrane for a normal operating cycle with a 235°C temperature excursion.

4.4 Response surface study

Response surface study gives a generalized solution of the values of dependent variables over the selected array of independent variables by performing finite element computations according to an appropriate response surface design. Initially, two independent variables and two dependent variables were selected. The independent variables are the yield stress and CTE of the overlay material, and the dependent variables are the axial stress and the tangential stress at some particular locations in the tube and the membrane. Note that only the properties of the overlay material were assumed as the independent variables and that SA210 was assumed as the base tube material. The selected range for the yield stress is between 100 MPa and 700 MPa, and the range from 0.9×10^{-5} /°C to 2.1×10^{-5} /°C was selected for CTE. This is the range that covers most of the applicable materials. The materials already used in recovery boilers are also within the specified range. The dependent parameters were evaluated at the fireside and the cold side surface of the tube crown and the membrane. The normal boiler operation was considered (see Figure 19, transient A), and two temperature excursion scenarios with peak temperatures of 380°C (see Figure 19, transient C) and 550°C (see Figure 19, transient B).

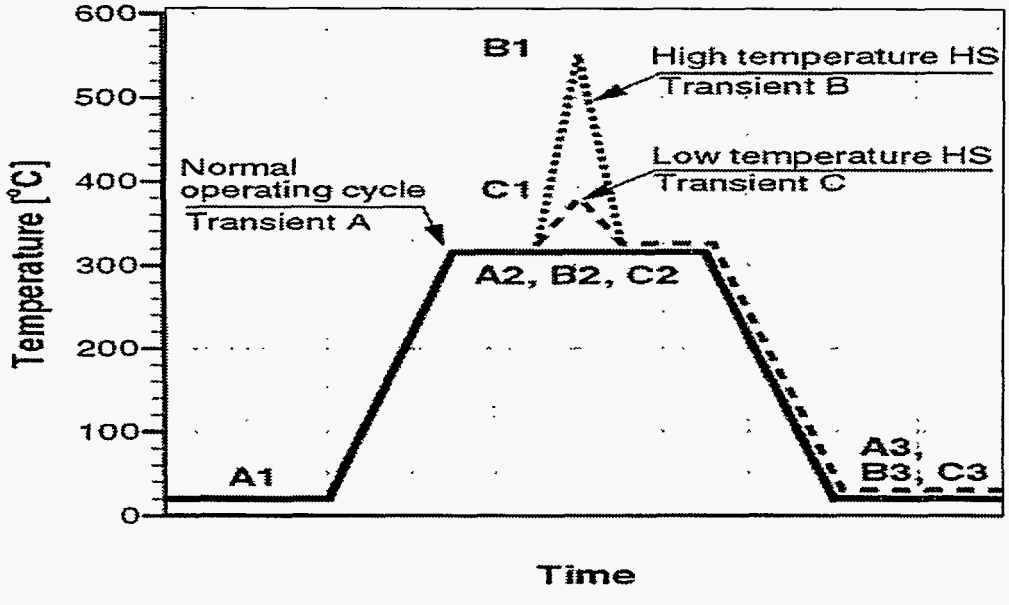

Figure 19. Temperature scenarios considered in response surface analysis.

The following assumptions were considered in the study:

- SA210 carbon steel material was considered as a base tube material in all calculations.

- The thermo-physical properties of SA210 carbon steel were considered for the base material and for the overlay material for all thermal analyses (assembly welding and in-service heating).

- The residual stresses from the tube manufacturing measured on a SS304L/SA210 tube by neutron diffraction were used in the analyses.

- The yield stress of the overlay materials was assumed to decrease linearly to 10 MPa at 1200°C.

- A linear work hardening was considered for overlay materials.

- The thermo-physical and mechanical properties of the weld material correspond to those of the overlay material.

Evaluation of the results was made according to the following criteria: stresses should not be tensile and stresses should be smaller than the yield stress. The evaluation was based on the axial and tangential stress components calculated at the fireside surface of the tube crown and at the fireside surface of the membrane for the three temperature scenarios. Figure 20 shows regions of the overlay material properties where the above criteria is (partially) met. The final results of the response surface study confirm that the SS304L overlay is not a suitable overlay material from the mechanical standpoint. A material that would satisfy the mechanical (stress-strain) requirements at normal operation and at temperature excursions of moderate magnitude (up to about 100°C) has the CTE of about 1.2×10^{-5} and the yield stress higher than about 300 MPa. Alloy 625 best suits these requirements. No material within the selected range of properties would meet the criteria if subjected to a temperature excursion of about 235°C (peak temperature of 550°C).

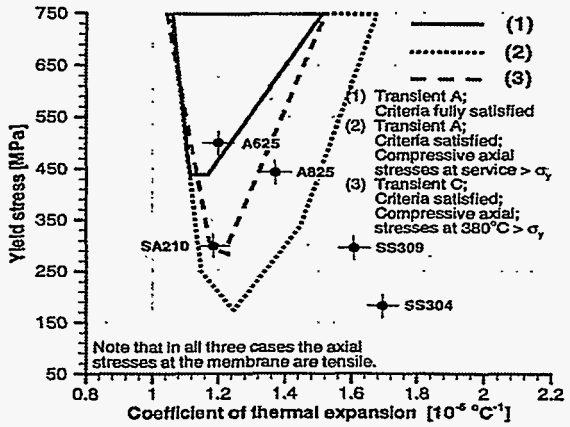

Figure 20. Regions of recommended overlay materials in terms of CTE and the yield stress.

4.5 Conclusions

Any temperature excursion higher than about 40C° (fireside tube temperature of 355°C) causes tensile stresses at the fireside crown of the SS304L/SA210 tubes at operating conditions.

On cooling to room temperature, stresses at the fireside crown of the SS304L/SA210 tubes become tensile at about 275°C and they reach the yield stress at about 225°C. Stresses at the fireside surface of the membrane become tensile at about 270°C and they reach the yield stress at about 220°C.

The stresses at the fireside surface of the SS304L/SA210 floor are compressive after each restart of the boiler.

Local heating during straightening does not critically affect the stresses in the tube panel.

Stresses in the A625/SA210 weld overlay tubes are within the elastic region throughout the normal operating cycle.

The chromizing process can be considered beneficial because it causes high compressive stresses at the outside surface of the tubes. The resulting residual stresses are high enough in compression to keep the stresses from becoming tensile when the floor is brought to operating conditions. A temperature excursion with the peak of 380°C does not critically affect the stresses at the fireside surface of the chromized tube or the membrane. The chromized tube surface within the 550°C hot spot region yields and the stresses at service conditions after the temperature excursion become tensile. The magnitude of these stresses is not significant.

A recommended overlay has the CTE around 1.2×10^{-5} /°C and the yield stress higher than 300 MPa, in the case where SA210 carbon steel is used as the base material. The material that satisfies the criteria established in this work is alloy 625.

The finite element analysis of the SS304L/SA210 composite tube floor reveals that SS304L is not a suitable clad material from the mechanical standpoint. The established facts supporting such conclusion show that compressive stresses in the SS304L overlay:

- exceed the yield stress at operating conditions,
- are reversed to tensile stress at operating conditions by a temperature excursion of 40C° or higher, and
- are reversed to tensile stress on cooling at about 270°C and exceed the yield stress at about 220°C.

5. Stress Corrosion Testing

Studies of stress corrosion cracking (SCC) in the molten hydrate of sodium sulfide ($Na_2S \bullet 9H_20$) and mixtures of sodium sulfide and other salts have continued. A constant load tensile test apparatus was built and is now being used to investigate the influence of test temperature, alloy composition, salt composition, and applied load on stress corrosion cracking. The results obtained from these studies permit a number of conclusions to be drawn.

5.1 Effect of test temperature on cracking

Laboratory tests to investigate the influence of temperature on stress corrosion cracking of 304L stainless steel U-bend test specimens by $Na_2S \bullet 9H_20$ have led to the following conclusions:

1.) SCC occurs at temperatures approaching the boiling point of the hydrated salt, that is about 170°C,

2.) In tests at temperatures significantly below the boiling point of the salt (i.e.,150°C) SCC has not been noted,

3.) At temperatures above the boiling point (e.g., 200°C), the liquid salt dries out and SCC has not been observed, and

4.) SCC can be promoted by repeatedly heating the hydrated salt above its boiling point, then cooling and rehydrating the salt by adding a small volume of water.

5.2 Observations on crack progression

Based on observations of cracking of C-rings made from a 304L/SA210 composite tubes, several conclusions can be drawn:

1.) Rates of crack progression are relatively rapid. Cracks have been found at the interface in composite tubes after tests lasting 48 hrs.

2.) Rates of crack progression are affected by the applied stress. In highly stressed C-rings, cracks reach the interface more rapidly than they do in moderately stressed C-rings. In lightly stressed C-rings, cracking does not occur, i.e. there appears to be a threshold stress level for SCC.

3.) In the tests conducted thus far, there has not been a single case where a crack has proceeded across the interface between the stainless steel outer layer and the carbon-steel core.

5.3 Resistance of potential boiler floor materials to SCC

C-rings with outer layers of 304L, 309L, and 310 stainless steels have been exposed in SCC tests. Nickel-based alloys 825 (Sanicro 38) and 625 have also been included. The 304L and Sanicro 38 C-rings were prepared from co-extruded tubes. The 309L and Alloy 625 C-rings were made from weld overlaid tubes and the 310 stainless steel coupon was machined from a centrifugally cast tube with a Cr-Mo alloy steel core. Resistance to SCC has been assessed simply by comparing the lengths of the cracks produced. The 304L and 309L showed poor resistance and the cracks progressed all the way to the interface (1.6-1.8 mm). There was a greater number of cracks in the 304L stainless. In the 310, the longest crack was approximately 500 μm. In the Sanicro 38, cracks were plentiful, but mostly less than 50 μm in depth. No cracks were found in Alloy 625. From these findings, it might be concluded that resistance to SCC in $Na_2S \bullet 9H_20$ increases with nickel content. In one test to date, carbon steel also appeared resistant to SCC.

6. Thermal Fatigue Studies of Composite Tubes

The activity on thermal fatigue of composite tubes involves a review of thermal/mechanical fatigue in composite tube materials, a compilation and production of the physical and mechanical properties needed for the modeling, the isothermal and thermal/mechanical fatigue of tubes, and determination of cracking patterns for various thermal/mechanical loadings. Materials of concern include carbon steel (equivalent to SA-210, Gr A-1), 304L stainless steel, Fe-Cr-Ni alloy 825, nickel-base alloy 625, 309L stainless steel filler metal, 312 stainless steel filler metal, and chromized carbon steel.

6.1 Review of thermal/mechanical fatigue in composite tube materials

The review, completed during 1995 [12], reached nine conclusions that bear on the experimental and analytical work: (1) the physical and mechanical properties of 309L and 312 stainless steel filler metals were needed; (2) tensile properties of very-fine-grained 304L stainless steel were required; (3) exploratory fatigue data to 600°C were needed for very-fine-grained 304L stainless steel, 309L deposited filler metal, 312 stainless steel deposited filler metal, and alloy 825; (4) the isothermal fatigue curves were required; (5) exploratory thermal-mechanical fatigue data were needed for alloy 825, alloy 625, 312 stainless steel and 309L stainless steel; (6) procedures for the fatigue damage under multiaxial strains recommended in the ASME Code Section III were applicable; (7) fatigue crack growth testing was not required; (8) the constitutive equations recommended in DOE RDT F9-5T [13] were suitable for use in elastic plastic analysis of composite tubes; and (9) transient stress fatigue testing of tubing was needed to confirm the validity of the analysis methods.

6.2 Collection of physical and mechanical properties

With the exception of chromized carbon steel, all physical properties measurements were obtained for the materials used in the composite tubing. Efforts were begun in this reporting period to gather data applicable to the chromized carbon steel at two chromium levels, namely 27% and 40% chromium. For 27% chromium, the literature data for 446 stainless steel was used. For the 40% chromium steel, a special material was produced that contained 40% Cr, 0.5% Mn, and 0.25% Si. This steel was argon-induction melted, hot-extruded to 19-mm bar, and annealed. Specimens for thermal expansion, thermal diffusivity, and specific heat were produced.

Tensile yield curves for alloy 825 were produced for the temperature range of room to 600°C. These curves to 1% strain are in Figure 21. Important to the analysis of inelastic behavior are the observations that the yield strength of the annealed material is very well defined, the yield decreases monotonically with increasing temperature, and the rate of work-hardening is independent of temperature. These observations confirm the behavioral trends specified for stainless steels and embodied in the constitutive equations recommended in DOE RDT F9-5T. Tensile yield curves for the 40% Cr steel were produced for the temperature range of room to 550°C. These curves are shown in Figure 22. The 40CrMnSi steel was found to be much stronger than 304L stainless steel and alloy 825. The 40CrMnSi was also stronger than type 446 stainless steel and possessed a hardness (HVN 230) comparable to that observed in the chromized tube for a similar chromium level.

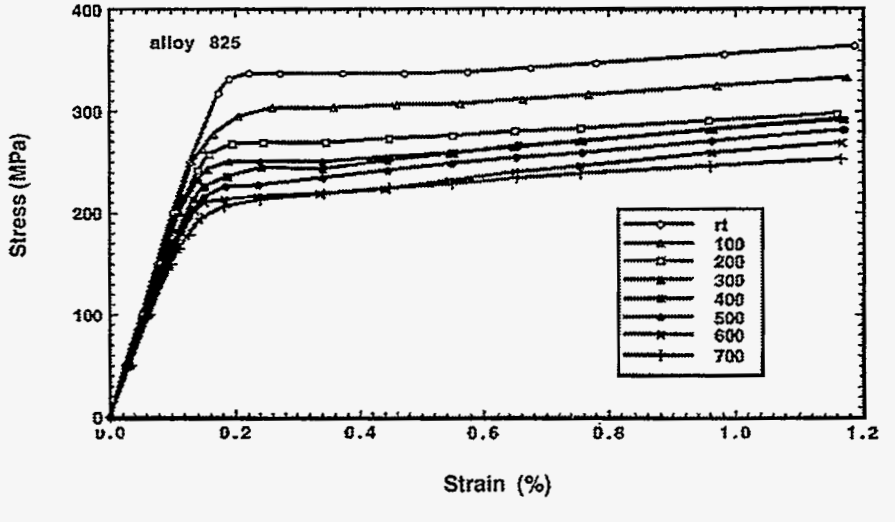

Figure 21. Stress versus strain curves for alloy 825°C to 700°C.

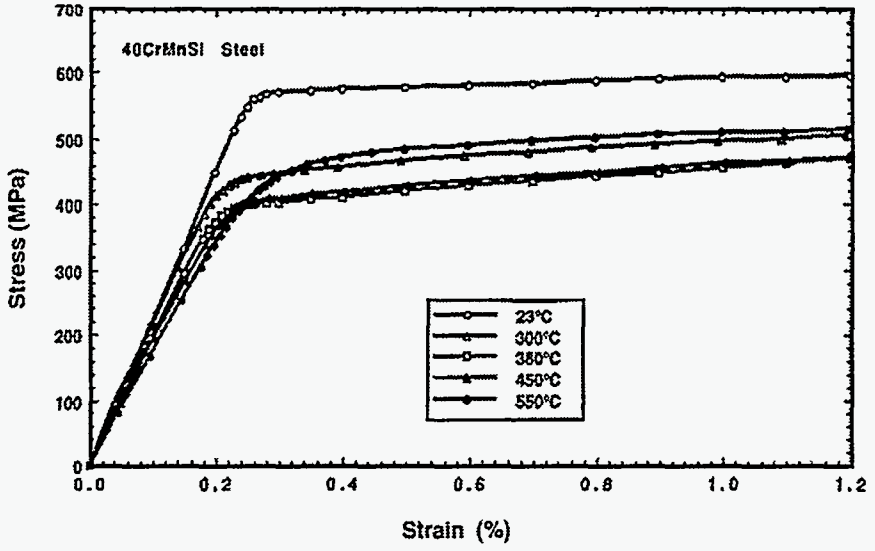

Figure 22. Stress versus strain curves for 40CrMnSi steel to 550°C.

Isothermal strain cycling tests were begun on alloy 825 to examine its hardening characteristics relative to 304L stainless steel. It was found that the material was stronger than 304L stainless steel at 300°C and 600°C. Further, the alloy exhibited hardening from one cycle to the next. The strain fatigue life was similar to that for 300-series stainless steels, so the fatigue design curves given in ASME Sect VIII, Div. 2 were judged to be applicable to alloy 825. The cracking mode for alloy 825 was examined and found to be similar to the cracking for type 304L stainless steel. A typical secondary fatigue crack produced in a test at 300°C (13,900 cycles at 0.9% strain range) is shown in Figure 23. Here, the crack started at the surface and progressed inward in a transgranular mode. Crack branching was present, but this branching was limited to spurs originating from the "main" crack.

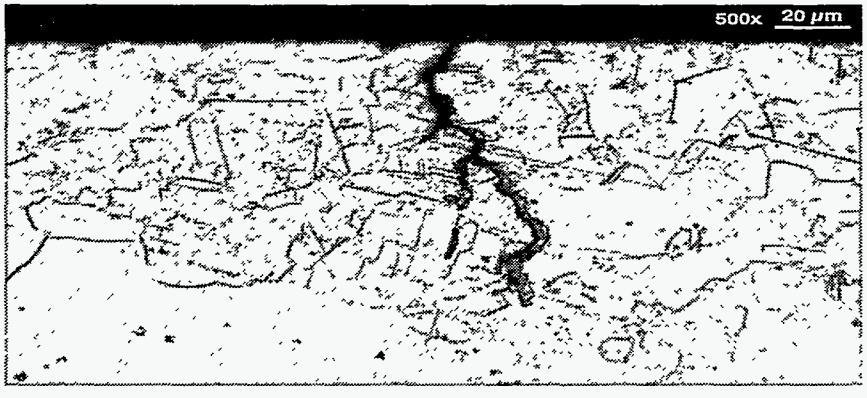

Figure 23. Secondary fatigue crack in alloy 825 produced in 13,900 cycles at 0.9% Δe at 300°C.

Thermal cycling of 304L-clad carbon steel tubes was begun. In one experiment, a tube was uniformly surface-heated between 215°C and 610°C in 2 minutes by means of a 14 KW radiant lamp furnace. The inside of the tube was cooled by air, and this produced a 30EC thermal gradient through the wall. The tube was cooled over a period of 13 minutes to produce a 15-min cycle, as shown in Figure 24. Stresses in the tube were self-induced and developed from the thermal gradient in the wall and the differential thermal expansion of the 304L stainless steel cladding and the carbon steel tube. After several hundred cycles the tube was examined for cracks but none were found. In a second experiment, a tube was heated on one side only between the temperature limits of 250°C and 450°C. Again, air cooling of the inside of the tube was introduced. The unheated side of the tube experienced some thermal cycling due to thermal conduction from the heated side. Temperature varied from 220°C to 320°C. The thermal gradient from the cold side to the hot side at the peak temperature was 130°C. After 1000 cycles, the tube was inspected. No cracks were found.

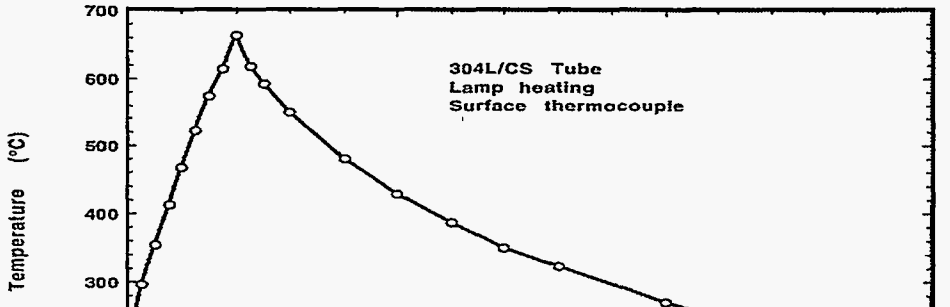

Figure 24. Thermal cycle for 304L-clad carbon steel tube.

Efforts were begun to prepare a panel for thermal cycling. A five-tube panel was selected, and instrumentation of the tubes was begun. A 7.5-KW bank furnace was obtained to heat the crown of the center tube in the panel. The cold side of the tubes will be instrumented for strain gauges, A second panel will be prepared. In this case, residual stresses will be measured by neutron diffraction methods before and after thermal cycling.

REFERENCES

1. D. Challanger and J. Moteff, "Correlation of Substructure with the Elevated Temperature Low-Cycle Fatigue of AISI 304 and 316 Stainless Steels," *Fatigue at Elevated Temperatures, STP 520*, American Society for Testing and Materials, Philadelphia, 1973, p. 68.

2. S.-H. Doong, D. F. Socie, and I. M. Robinson, "Dislocation Substructure and Non-proportional Hardening," *Journal of Engineering Materials and Technology*, **112**: 456 (1990).

3. R. Zauter, J. -J. Christ, and H. Mughrabi, *Metallurgical and Materials Transactions A*, "Some Aspects of Thermo-mechanical Fatigue of 304L Stainless Steel: Part II. Dislocation Arrangements," **25A**: 407 (1994).

4. M. Mäkipää, J. Salonen, P. Nenonen, and T. Hakkarainen, "Studies with TEM, SEM, and Optical Microscope on the Cracking of BLRB Composite Floor Tubes," *Proceedings of the 8th International Symposium on Corrosion in the Pulp & Paper Industry*, Swedish Corrosion Institute, Stockholm, 1995, p. 189.

5. J. R. Keiser, B.Taljat, X. -L. Wang, P. J. Maziasz, C. R. Hubbard, R. W. Swindeman, D. L. Singbeil, and R. Prescott, *Proceedings of 1996 TAPPI Engineering Conference*, "Analysis of Composite Tube Cracking in Recovery Boiler Floors," 693 (1996).

6. P. J. Maziasz and T. K. Roche, *Journal of Nuclear Materials*, "Preirradiation Microstructural Development Design to Minimize Properties Degradation During Irradiation in Austenitic Stainless Steel," **104,** 797 (1981).

7. G. D. Preston, *Phil. Mag.*, **13**, 419 (1932).

8. J. R. Keiser et al., "Development of Materials for Black Liquor Recovery Boilers," USDOE 1996 AIM Annual Progress Report (April 1997).

9. X. -L. Wang, E. A. Payzant, B. Taljat, C. R. Hubbard, J. R. Keiser, M. J. Jirinec, "Experimental Determination of the Residual stresses in a Spiral Weld Overlay Tube," *Mat. Sci. Eng.*, **A232**, 31-38 (1977).

10. L. Pintschovius, E. Macherauch and B. Scholtes, *Mat. Sci. Eng.*, **84**, 163-170 (1986).

11. X. -L. Wang, S. Spooner, C. R. Hubbard, B. Taljat, and J. R. Keiser, to be published in the Proceedings of *5th International Conference on Residual Stresses*.

12. R. W. Swindeman, A Review of Thermal/Mechanical Fatigue in Composite Tube Materials, Oak Ridge National Laboratory, Draft TM-13474 (to be published).

13. RDT Standard F9-5T, *Guidelines and Procedures for Design of Nuclear System Components at Elevated Temperature* (September 1974).

MATERIALS FOR THE PULP AND PAPER INDUSTRY

Section 2. Corrosion and Failure Analysis Studies in Support of the Pulp and Paper Industry

J. R. Keiser, S. J. Pawel, R. W. Swindeman, and H. F. Longmire

Metals and Ceramics Division
Oak Ridge National Laboratory
Post Office Box 2008, Oak Ridge, Tennessee 37831

INTRODUCTION

Technical support is being provided to various pulp and paper companies and related industries to help determine the cause of material degradation problems and identify alternate materials to prevent such degradation. During the past year, activities have included examinations of superheater tubes, economizer tubes, sootblower components, and tubes from the lower section of recovery boilers and inspection of continuous digesters. The results of the analyses and inspections were communicated to the plant operators and, in some cases, recommendations were made.

TECHNICAL PROGRESS - FY 1997

Examination of Failed Co-extruded tube

A failed co-extruded floor tube from a decanting type boiler in the South-Central U.S. was examined to determine the cause of the leak. The tube had been located at the edge of the floor so that heat flux to the tube was less than for tubes away from a side wall. The tube as-received at ORNL had a band along the top of the tube that contained a series of parallel, circumferentially oriented cracks. A tube butt weld was located a few inches downstream of the cracked area, and there had been enough push through of the weld metal that the diameter of the tube is reduced at the position of the weld. Examination of cross sections of the tube revealed several important pieces of information. First, there are many cracks, in a well defined region, that often originate at pits on the inside surface of the pipe. The crack that led to failure of the tube originated on the ID. Microstructural evidence indicated that the region of the tube containing the cracks had been subjected to appreciable overheating while adjacent areas of the tube had not seen excessive heating.

It was concluded that local overheating occurred as a result of irregular water flow with the subsequent development of a steam blanket. The weld metal push-through acted like a dam that trapped steam to form a gas pocket in the top of the tube. Pits developed on the tube ID beneath scale which was present because of, at least, periodically poor water

treatment. Cracks initiated at the stress concentrators (pits) in response to stresses from local overheating. Subsequent temperature and water quality cycles resulted in growth of scale in cracks generating a wedging action. Cracks propagated from the ID until the wall thickness at some point could not contain the load on the wall at which point tube failure occurred.

PUBLICATIONS

X. -L. Wang, E. A. Payzant, B. Taljat, C. R. Hubbard, J. R. Keiser, and M. J. Jirinec, "Experimental Determination of the Residual Stresses in a Spiral Weld Overlay Tube," Mat. Sci. Eng., A232, 31-38 (1997).

B. Taljat, T. Zacharia, X. -L. Wang, J. R. Keiser, Z. Feng, and M. J. Jirinec, "Residual Stresses in Weld Overlay Tubes: A Finite Element Study," PVP-Vol. 347, 83-89, Approximate Methods in the Design and Analysis of Pressure Vessels and Piping Components, ASME 1997.

J. R. Keiser, B. Taljat, X. -L. Wang, R. W. Swindeman, P. J. Maziasz, D. L. Singbeil, and R. Prescott, "Analysis of Cracking of Co-extruded Recovery Boiler Floor Tubes," Proceedings of the TAPPI 1997 Engineering Conference, Nashville, Tennessee (October. 6-9, 1997).

D. L. Singbeil, R. Prescott, J. R. Keiser, and R. W. Swindeman, "Composite Tube Cracking in Kraft Recovery Boilers: A State-of-the-Art Review," Proceedings of the TAPPI 1997 Engineering Conference, Nashville, Tennessee, (October 6-9, 1997). This paper was also published as ORNL/TM-13442 in July 1997.

PRESENTATIONS

All researchers make oral presentations on their work at the triannual program reviews.

Invited presentations reviewing the program's progress have been made at two AF&PA and one BLRBAC meetings, at NACE International's T-5H-1 committee meeting, at TAPPI's Steam and Power Committee meeting, and at meetings of recovery superintendents for Mead Corporation, Weyerhaeuser Company, and Georgia-Pacific Corporation.

INDUSTRIAL INPUT and TECHNOLOGY TRANSFER

An advisory committee composed of representatives of paper companies, boiler manufacturers, tube fabricators, and consulting companies meet three times a year to review the progress on the program. In addition, frequent contacts are made with representatives of several paper companies in order to discuss program activities with them.

ESTIMATED ENERGY SAVINGS

Recovery boilers provide sixty percent of the power for kraft mills, so continued operation is critical. Reductions in the downtime will provide an energy savings that is proportional to the number of operating days gained.

Ni_3Al and FeAl TECHNOLOGY TRANSFER

V. K. Sikka, G. Aramayo, M. L. Santella, R. W. Swindeman, and S. Viswanathan

Metals and Ceramics Division
Oak Ridge National Laboratory
Post Office Box 2008, Oak Ridge, Tennessee 37831

INTRODUCTION

Ductile Ni_3Al and Ni_3Al-based alloys have been identified for a range of applications. These applications require the use of material in a variety of product forms such as sheet, plate, bar, wire, tubing, piping, and castings. Although significant progress has been made in the melting, casting, and near-net-shape forming of nickel aluminides, some issues still remain. These include the need for: (1) high-strength/high room-temperature hardness; (2) castability (mold type, fluidity, hot-shortness, porosity, etc.; (3) welding and weld reparability of castings; (4) workability of cast or powder metallurgy product to sheet, bar, and wire; and, (5) technology transfer.

All of the issues listed above can be "show stoppers" for the commercial applications of nickel aluminides.

In addition to Ni_3Al-based alloys, FeAl-based alloys have progressed to a stage for commercial applications. For successful applications of FeAl-based alloys, some issues still remain. These include the need for: (1) identification of castable compositions, (2) development of melting practice to minimize/eliminate the furnace build-up issue, (3) properties of castings, and (4) technology transfer.

This report describes the work completed and to address some of these issues during FY 1997.

TECHNICAL PROGRESS - FY 1997

Summary

Major accomplishments have occurred during this year and are briefly summarized below.

1. The cast compositions have been licensed to Sandusky International (Sandusky, Ohio) and Alloy Engineering & Casting Company (Champaign, Illinois). These additions make a total of three licensees for castings of nickel aluminide compositions.

2. Castings of the cast alloy IC-221M were installed or continued to operate under commercial conditions at Delphi Saginaw (Saginaw, Michigan); Bethlehem Steel Corporation-Burns Harbor Plant (Chesterton, Indiana); United Defense LP (Anniston, Alabama); The Timken Company (Canton, Ohio); Chevron (Richmond, California); FMC Corporation (Pocotalo, Idaho); Wyman Gordon (Houston, Texas); and American Axle and Manufacturing (Detroit, Michigan). The alloy is also in test for chemical industry applications at E. I. DuPont de Nemours & Company (Wilmington, Delaware); FMC Corporation, and The Dow Chemical Company (Freeport, Texas).

3. Ten additional rolls were cast at Sandusky International and installed at Bethlehem Steel Corporation-Burns Harbor Plant.

4. A new weld wire composition was developed for the root pass. A patent application for this composition has been prepared.

5. The weld wire compositions were licensed to Polymet Corporation (Cincinnati, Ohio) for commercial manufacturing.

6. Test material was supplied to many new potential users for evaluation under their operating conditions.

7. The cast grate bars and pallet tips of FeAl-based alloy were installed at the phosphate calcination plant of FMC Corporation.

Task 1. High-Strength Castable Compositions (Start 10/96, End 9/97)

The IC-221M [8.0 Al-7.7 Cr-1.43 Mo-1.7 Zr-0.008 B (weight percent)] is the base castable composition of Ni_3Al-based alloy. This composition has been cast extensively into a wide range of cast components. Although it has excellent castability and weldability, its high-temperature applications are limited to ≤1150°C because of eutectic formation at 1174°C. Strong demand from the potential users to push the use temperature to above 1150°C, it was necessary to eliminate the eutectic formation at 1174°C. This has been accomplished by modifying the composition of IC-221M, which is free of the eutectic formation.

Two eutectic-free compositions have been identified: IC-396LZr and IC-438. The tensile properties of the compositions with the eutectic (IC-396M) and without the eutectic (IC-396LZr and IC-438) are compared at temperatures of 1150°C, 1175°C, and 1200°C in Figures 1 through 3. The three test temperatures chosen are below, at, and above the eutectic temperature. It is clear from Figures 1 through 3 that the IC-396M composition, which has 0.85 wt % Zr, still contains the eutectic. The indication of the eutectic is

reflected by its sharp drop in yield strength from 1150°C to 1175°C. Note, however, that the two new compositions (IC-396LZr and IC-438) with < 0.2 wt % Zr

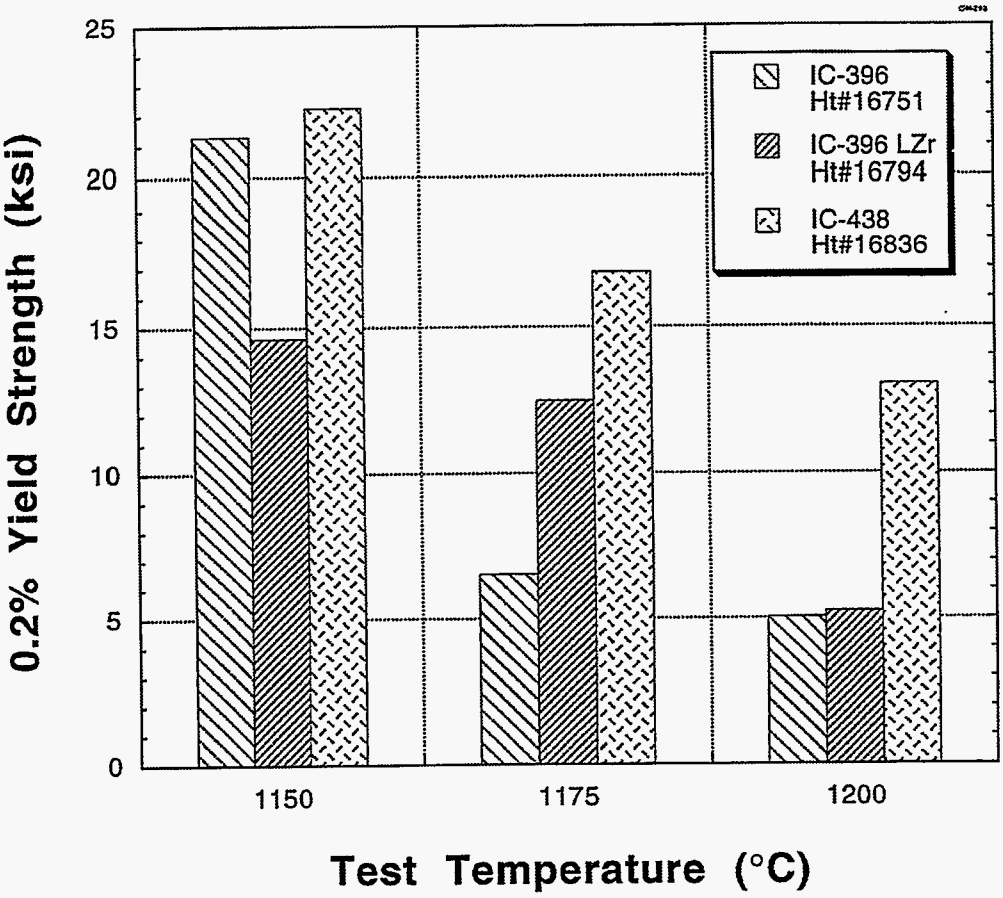

Figure 1. Yield strength of IC-396M, IC-396LZr, and IC-438 at temperatures of 1150, 1175, and 1200°C.

only show a gradual drop in yield strength at 1175°C and 1200°C. Between the two compositions, the IC-438 is superior in strength at 1200°C as opposed to IC-396LZr. However, the IC-396LZr is superior to the IC-438 interns of its ductility. Thus, the use of eutectic-free alloys at 1175°C to 1200°C will depend on the application requirements. A patent applications was filed for IC-438. The IC-396LZr is considered to be in the composition range of the currently patented IC-221M alloy.

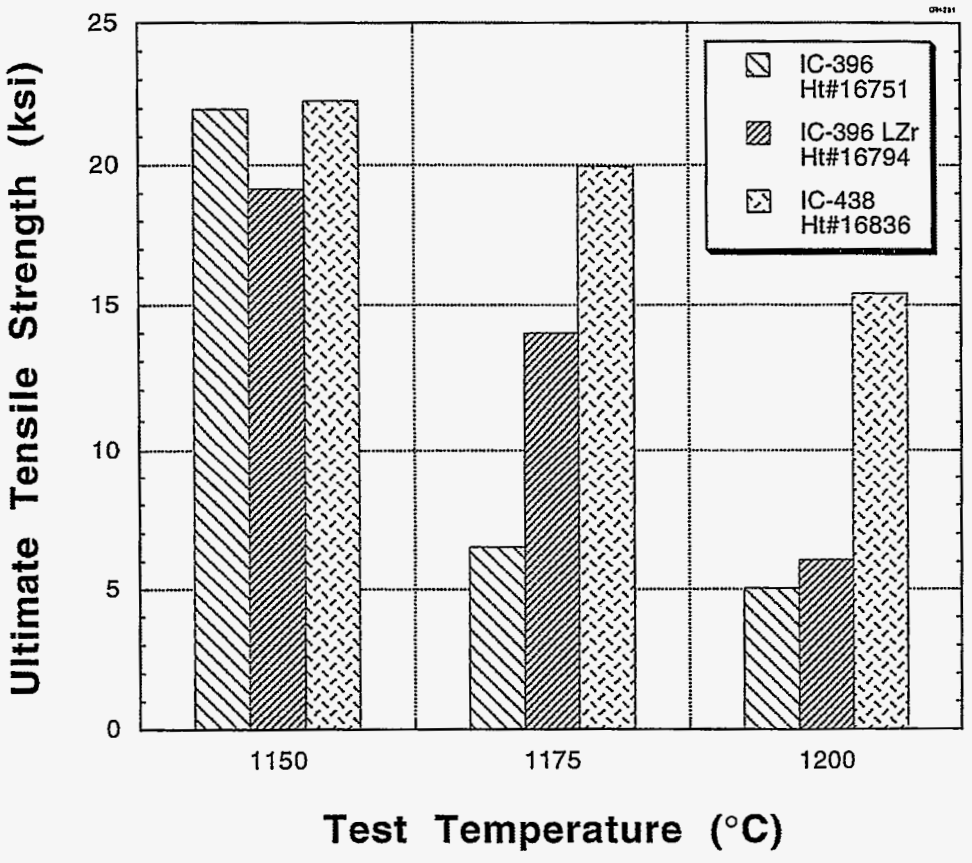

Figure 2. Ultimate tensile strength of IC-396M, IC-396LZr, and IC-438 at temperatures of 1150°C, 1175°C, and 1200°C.

Another composition, designated as B-13, has also been developed to provide two additional properties to IC-221M. The first additional property is the improvement in room-temperature hardness from R_C 30 for IC-221M to R_C 40 for B-13. The second improvement is the significant enhancement in acid solutions. Figures 4 through 6 show the improved corrosion resistance of B-13 as opposed to IC-221M and even a Ni_3Si-based alloy. A patent disclosure has been filed on the B-13 type composition, and sample material has been provided to testing to various potential users.

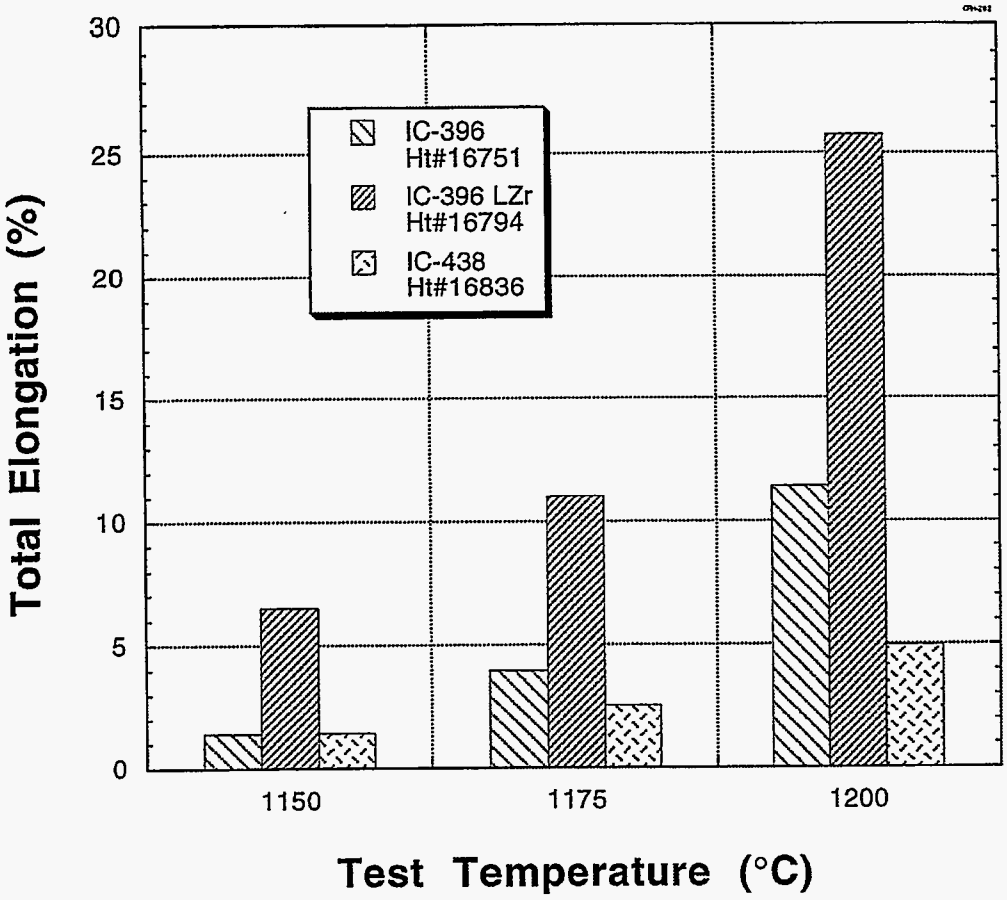

Figure 3. Total elongation of IC-396M, IC-396LZr, and IC-438 at temperatures of 1150°C, 1175°C, and 1200°C.

Creep and Fatigue Analysis of Joints in Ni_3Al Rolls
(R. W. Swindeman and M. L. Santella)

Tensile, creep, and fatigue testing of materials used in transmission rolls is under way to provide data needed for fatigue analysis of the roll-to-trunnion joint. Materials include cast alloy HU from exposed rolls, sand cast HU test bars, cast IC-221M, and dissimilar metal welds in which IC-221LA was used as a filler metal. In Figure 7, the tensile data for HU, exposed HU, and HU/LA/IC-221M joints are compared to the ultimate strength versus temperature curve for cast HT. It can be seen that the strengths for the exposed materials are equal to or better than the strength of unexposed cast HT. In Figure 8, creep curves for exposed HU are shown for a temperature of 871°C (1600°F). The steel maintains good creep ductility, and strength is comparable to its original strength. An HU/LA/IC-221M weldment exhibited the same creep behavior as the exposed HU. Creep testing of the IC-221LA weldments has continued, with testing temperatures as high as

1050°C (1922°F), and times as long as 6900 h. Fatigue testing to develop the modified Goodman diagram for the IC-221M/LA weldment continued with the most testing at 871°C (1600°F). Testing was designed to include the evaluation of the stress ratio and cyclic frequency on the stress-controlled fatigue life.

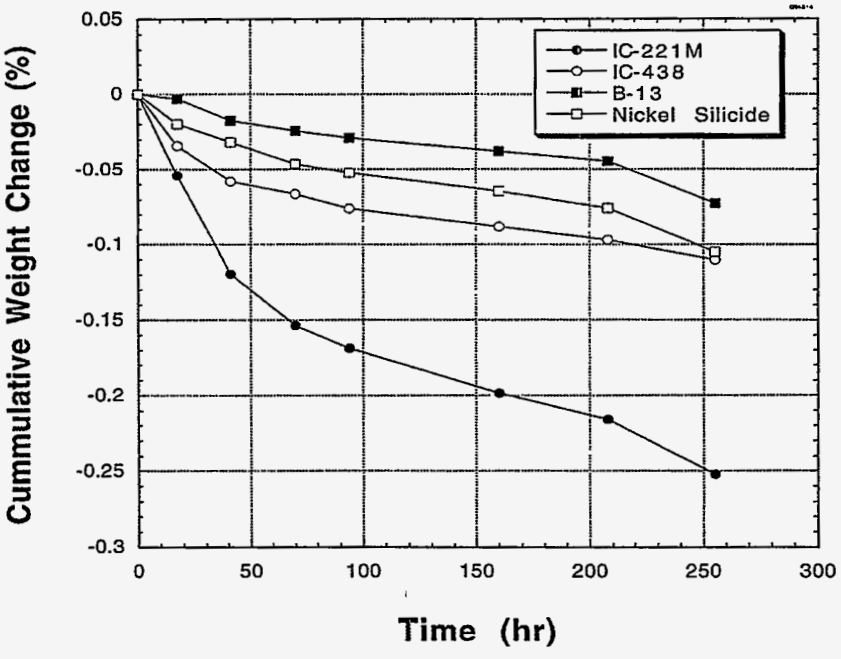

Figure 4. Corrosion resistance of B-13 in hydrofluoric acid (48% to 51%) at room temperature as compared to IC-221M, IC-438, and a Ni_3Si-based alloy.

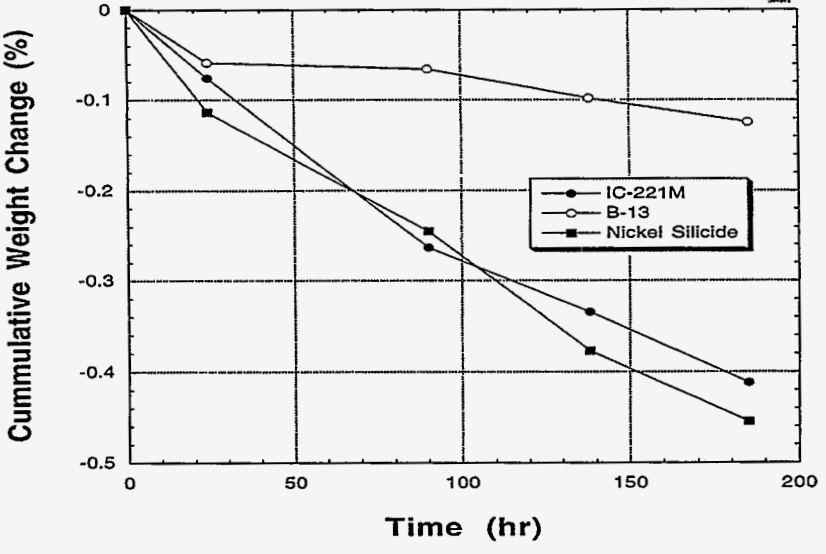

Figure 5. Corrosion resistance of B-13 in 15% solution of hydrofluoric acid (36.5% to 38.0%) at room temperature as compared to IC-221M and a Ni_3Si-based alloy.

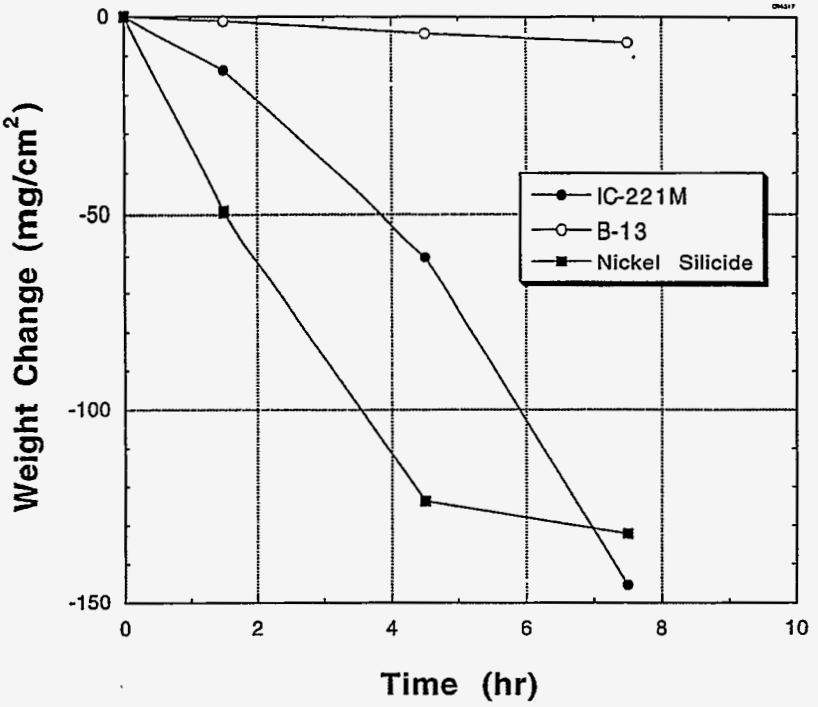

Figure 6. Corrosion resistance of B-13 in 15% hydrochloric acid (36.5% to 38%) at room temperature as compared to IC-332M and a Ni_3Si-based alloy.

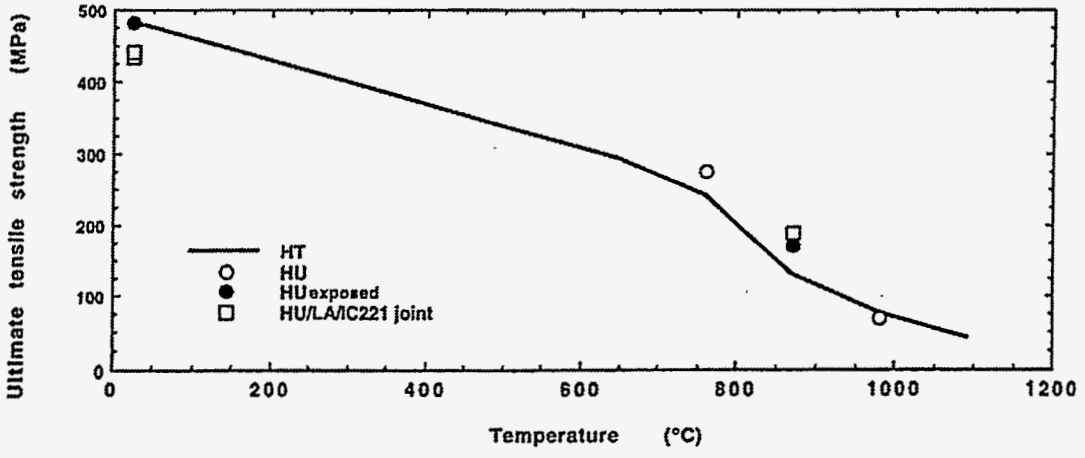

Figure 7. Ultimate tensile strength versus temperature for high alloy castings.

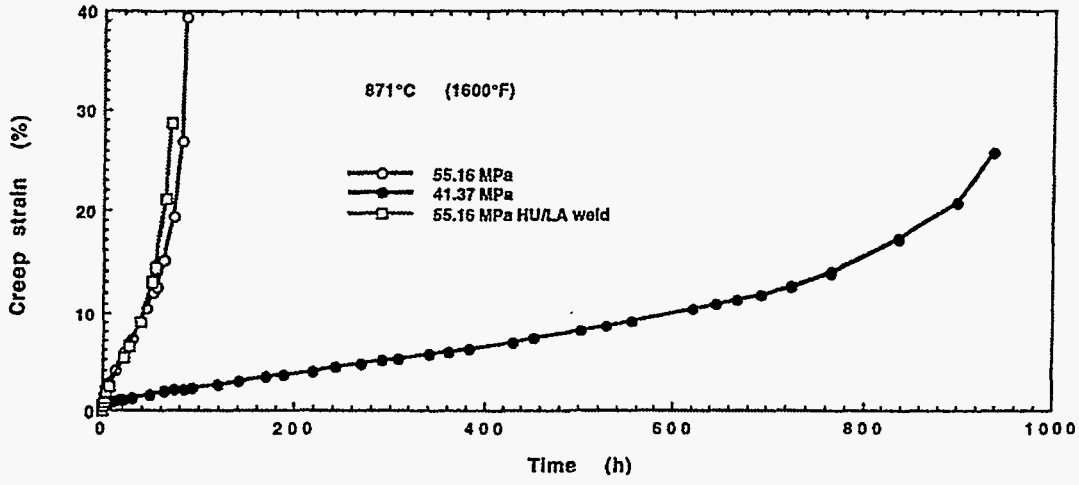

Figure 8. Creep curves for exposed cast HU alloys.

Task 2. Castability of Nickel Aluminides (Start 10/96, End 9/97)

This task examined the castability of nickel aluminide compositions for sand castings, investment castings, and centrifugal castings. Related to castability, the composition control was considered as the major issue. A total of 94 heats were poured at Alloy Engineering & Casting Company. Twenty-six of the heats were from virgin stock, and 68 heats were from a 50:50 mix of virgin and revert stock. The detailed chemical analysis of the 94 heats are given in Table 1. From this table the achievable range of various elements in both the virgin and revert heats are derived and shown in Table 2.

It is to be noted that silicon and iron are the two elements that continue to increase in the heats melted from the revert stock. The silicon comes from its entrapment in the runners and risers and onto the surface of pigs (the extra metal cast into molds). It also comes from the erosion of the crucible by the molten metal in which the SiO_2 reduced by aluminum in the alloy to silicon.

The alloy silicon content can be kept low by controlling the foundry practice. In the first case, the runners and risers can be sand blasted to minimize the entrapped SiO_2 on the surface. The SiO_2 from the pigs can be eliminated by using cast iron pigs or by using a ZrO_2 mold wash of the pig molds to minimize the interaction of the molten metal with SiO_2 in the uncoated sand molds.

The pickup of silicon from the furnace lining erosion can also be minimized by using Al_2O_3 or ZrO_2 as the furnace lining. The final control of silicon in the alloy will depend on the extent to which the proposed solutions to silicon reduction are practiced in the foundry production conditions. We have worked very closely with Alloy Engineering &

Casting Company, Sandusky International, and United Defense LP in minimizing the silicon content of the castings.

The pickup of iron in the revert heats primarily comes from the cross-contamination of melting nickel-based alloys in a iron-based alloy foundry. The only way to minimize the cross-contamination is to use nickel wash heats prior to melting nickel aluminides and to minimize any mixing of steel scrap with nickel aluminide melt stock.

Task 3. Welding and Weld Repairability of Castings (Start 10/96, End 9/97)

The major efforts during this reporting period were in: (a) continued development of the procedures for welding IC-221M castings in our licensees facilities, (b) technical support for fabrication (mainly transfer rolls at Sandusky International), (c) technical support for welding wire production, and (d) testing the mechanical properties of weldment.

Table 1. Chemical analysis of 94 heats of IC-221M melted to date at Alloy Engineering & Casting Company

Date of melt	Heat No.	Alloy								
		C	Si	Ni	Cr	Mo	Al	Zr	B	Fe
		26 virgin heats								
10/28/96	F2169	0.018	0.055	80.28	7.77	1.46	7.86	1.87	0.005	0.06
	F2170	0.017	0.034	80.24	7.89	1.50	8.19	1.90	0.008	0.03
	F2171	0.019	0.038	81.40	7.81	1.46	8.20	1.79	0.006	0.73
10/29/96	F2172	0.020	0.039	79.90	7.71	1.46	8.16	1.96	0.006	0.06
	F2173	0.023	0.021	80.20	7.93	1.43	8.20	1.96	0.005	0.08
	F2174	0.021	0.050	81.00	7.83	1.46	7.67	1.94	0.005	0.08
	F2175	0.023	0.030	81.10	8.11	1.43	7.50	1.96	0.006	0.041
10/30/96	F2176	0.012	0.043	80.68	7.81	1.45	7.91	2.02	0.005	0.077
	F2177	0.013	0.031	81.20	7.80	1.46	7.70	1.96	0.005	0.15
	F2178	0.014	0.035	80.85	7.76	1.47	7.79	1.98	0.006	0.12
	F2179	0.022	0.031	80.70	7.83	1.44	7.75	1.97	0.006	0.11
10/31/96	F2180	0.016	0.031	80.50	7.89	1.49	7.80	2.02	0.005	0.08
	E2559	0.013	0.032	80.67	7.86	1.43	7.98	1.93	0.004	0.063
11/04/96	F2182	0.021	0.038	80.30	7.63	1.44	7.71	1.93	0.005	0.10
	F2183	0.022	0.026	80.60	7.78	1.38	7.63	1.93	0.005	0.09
	F2184	0.023	0.031	80.70	7.70	1.41	7.72	1.88	0.006	0.52
11/05/96	F2185	0.021	0.032	80.00	7.68	1.42	8.12	1.93	0.005	0.06
	F2186	0.029	0.031	80.60	7.70	1.42	7.95	1.97	0.005	0.07
	F2187	0.030	0.034	80.30	7.68	1.41	8.03	1.96	0.005	0.181

Table 1. Chemical analysis of 94 heats of IC-221M melted to date at Alloy Engineering & Casting Company (Continued)

Date of melt	Heat No.	Alloy								
		C	Si	Ni	Cr	Mo	Al	Zr	B	Fe
11/08/96	F2188	0.026	0.042	81.10	7.90	1.42	7.70	1.81	0.005	0.15
	F2189	0.023	0.040	81.10	7.73	1.48	7.60	1.73	0.007	0.08
	F2190	0.024	0.032	80.95	7.85	1.46	8.10	1.93	0.005	0.056
	F2191	0.031	0.037	80.05	8.00	1.44	7.90	1.92	0.005	0.034
11/11/96	F2192	0.029	0.049	80.10	7.85	1.47	7.75	1.98	0.005	0.11
	F2193	0.031	0.046	80.05	7.85	1.47	7.75	1.97	0.006	0.067
	F2194	0.032	0.040	80.90	7.81	1.45	7.80	1.93	0.005	0.066
				50% revert heats						
11/18/96	F2195	0.021	0.051	80.40	7.82	1.41	8.08	1.96	0.006	0.05
	F2196	0.025	0.045	80.20	7.71	1.43	8.10	1.96	0.005	0.045
11/19/96	F2197	0.031	0.053	80.90	7.68	1.43	7.60	1.94	0.006	0.06
	F2198	0.021	0.052	80.60	7.90	1.50	7.63	1.77	0.007	0.05
11/20/96	F2199	0.020	0.046	81.10	7.80	1.46	8.01	1.80	0.006	0.11
	F2200	0.031	0.056	80.27	7.78	1.51	7.90	1.91	0.007	0.16
11/22/96	K1241	0.016	0.050	80.50	7.70	1.49	7.30	1.90	0.008	0.11
	K1242	0.018	0.055	81.00	7.76	1.46	7.80	1.83	0.006	0.13
11/26/96	F2202	0.020	0.063	81.05	7.76	1.40	7.68	1.85	0.005	0.07
	F2204	0.031	0.063	80.87	7.90	1.41	7.60	1.93	0.006	0.086

Table 1. Chemical analysis of 94 heats of IC-221M melted to date at Alloy Engineering & Casting Company (Continued)

Date of melt	Heat No.	Alloy								
		C	Si	Ni	Cr	Mo	Al	Zr	B	Fe
11/27/96	F2205	0.021	0.068	80.25	7.75	1.43	7.80	1.96	0.006	0.081
	F2206	0.024	0.051	80.04	8.01	1.42	7.71	1.94	0.006	0.056
	F2207	0.023	0.051	80.50	7.91	1.44	7.71	1.85	0.006	0.12
12/02/96	F2208	0.023	0.046	80.76	7.93	1.43	7.81	1.73	0.005	0.04
	F2209	0.024	0.051	80.50	7.88	1.44	7.79	1.85	0.006	0.05
12/03/96	F2211	0.031	0.029	79.91	8.30	1.45	7.30	1.70	0.003	0.03
	F2212	0.025	0.026	80.17	8.50	1.42	7.50	1.90	0.003	0.04
	F2213	0.031	0.045	79.69	8.10	1.56	7.88	1.85	0.004	0.04
12/04/96	F2214	0.041	0.091	78.97	7.66	1.43	7.91	1.98	0.006	0.55
	F2215	0.036	0.128	79.26	7.67	1.41	7.80	1.89	0.006	0.80
	F2216	0.050	0.119	79.57	7.82	1.34	7.30	1.93	0.007	0.70
	F2217	0.045	0.155	78.64	7.61	1.45	8.30	2.03	0.006	0.39
12/10/96	K1243	0.016	0.069	81.00	7.80	1.40	7.81	1.90	0.005	0.47
	K1244	0.020	0.058	80.72	7.65	1.45	7.60	1.93	0.006	0.36
	K1245	0.018	0.046	80.90	7.90	1.43	7.71	1.85	0.005	0.91
12/11/96	F2218	0.025	0.060	80.40	7.75	1.45	7.75	1.89	0.006	0.82
	F2219	0.023	0.070	80.50	7.93	1.41	7.93	1.95	0.006	0.52
	F2220	0.022	0.063	80.30	7.89	1.45	7.89	1.90	0.005	0.80
12/12/96	F2221	0.016	0.060	80.76	7.95	1.43	7.60	1.75	0.006	0.61
	F2222	0.020	0.058	80.05	7.65	1.40	7.75	1.81	0.006	0.11
	F2223	0.021	0.050	80.60	7.85	1.45	7.80	1.90	0.005	0.13
	F2224	0.026	0.061	80.50	7.81	1.41	7.68	1.73	0.005	0.25

Table 1. Chemical analysis of 94 heats of IC-221M melted to date at Alloy Engineering & Casting Company (Continued)

Date of melt	Heat No.	Alloy								
		C	Si	Ni	Cr	Mo	Al	Zr	B	Fe
12/18/96	F2226	0.025	0.060	80.10	7.68	1.39	7.70	1.78	0.005	0.19
	F2227	0.026	0.057	80.80	7.71	1.41	7.81	1.80	0.006	0.21
12/19/96	F2228	0.026	0.041	81.00	7.87	1.36	7.50	1.75	0.005	0.07
	F2229	0.025	0.045	80.50	7.90	1.43	7.40	1.80	0.004	0.09
	F2230	0.030	0.036	10.80	7.76	1.42	7.70	1.85	0.005	0.11
	F2231	0.029	0.041	80.80	7.99	1.41	7.60	1.83	0.005	0.22
	F2232	0.023	0.041	80.80	7.75	1.39	7.71	1.80	0.005	0.15
12/20/96	F2233	0.025	0.058	80.80	7.98	1.40	7.63	1.88	0.006	0.07
	F2234	0.023	0.053	80.20	7.85	1.38	7.76	1.90	0.005	0.08
	F2235	0.024	0.056	80.80	7.98	1.41	7.60	1.84	0.006	0.069
	F2236	0.027	0.057	81.30	8.20	1.46	7.89	1.86	0.005	0.055
	F2237	0.030	0.048	80.50	7.96	1.45	7.81	1.92	0.005	0.044
	F2238	0.031	0.059	80.20	7.90	1.49	7.91	2.00	0.006	0.11
12/23/96	F2239	0.010	0.078	80.80	8.09	1.46	7.85	1.98	0.004	0.09
	F2240	0.010	0.077	79.84	8.06	1.43	7.76	1.82	0.004	0.06
	F2241	0.010	0.065	80.58	8.16	1.46	7.66	2.00	0.005	0.11
	F2242	0.010	0.72	80.71	8.02	1.43	7.83	1.80	0.005	0.11
	F2243	0.010	0.066	80.13	8.26	1.47	7.63	1.80	0.004	0.13
12/24/96	F2244	0.010	0.070	80.26	8.15	1.43	8.00	1.77	0.005	0.09
	F2245	0.010	0.091	79.55	7.56	1.45	7.41	1.90	0.006	0.066
	F2246	0.010	0.082	80.54	8.08	1.50	8.05	1.62	0.005	0.13
	F2247	0.010	0.050	79.40	7.83	1.50	7.69	1.97	0.005	0.05

Table 1. Chemical analysis of 94 heats of IC-221M melted to date at Alloy Engineering & Casting Company (Continued)

Date of melt	Heat No.	Alloy								
		C	Si	Ni	Cr	Mo	Al	Zr	B	Fe
01/06/97	F2249	0.025	0.053	79.95	7.85	1.41	7.75	1.99	0.006	0.088
	F2250	0.031	0.060	80.50	7.76	1.44	7.65	1.92	0.005	0.09
	F2251	0.026	0.056	80.48	7.79	1.41	7.77	1.91	0.006	0.45
01/07/97	F2252	0.030	0.056	80.20	7.81	1.42	7.60	1.86	0.005	0.2
	F2253	0.025	0.061	80.40	7.96	1.36	7.70	1.75	0.005	0.15
	F2254	0.031	0.060	80.70	7.79	1.38	7.65	1.73	0.005	0.07
	F2255	0.029	0.056	80.20	7.80	1.41	7.71	1.93	0.005	0.06
	F2256	0.030	0.051	80.40	8.01	1.42	7.80	1.96	0.006	0.11
01/08/97	F2257	0.025	0.061	80.40	7.89	1.38	7.65	2.05	0.005	0.08
	F2258	0.021	0.060	80.60	7.70	1.40	8.10	1.78	0.006	0.06
01/20/97	F2259	0.025	0.061	80.10	7.95	1.35	8.01	1.75	0.005	0.04
	F2260	0.021	0.065	80.12	8.00	1.34	7.68	1.73	0.005	0.03
	F2261	0.025	0.060	80.10	7.90	1.40	7.90	1.80	0.006	0.6
01/22/97	F2262	0.030	0.090	80.10	7.93	1.35	7.60	1.71	0.005	0.12

Table 2. Comparison of nominal chemical analysis of IC-221M with the range observed for heats made using virgin and revert stock in a pilot commercial melt run of 94 heats carried out at Alloy Engineering & Casting Company

Element	Nominal (wt %)	Virgin heats (wt %)		Revert heats (wt %)[a]	
		Range	Average	Range	Average
Al	8.0	7.5 □ 8.2	7.86	7.3 □ 8.3	7.74
Cr	7.7	7.63 □ 8.11	7.81	7.56 □ 8.5	7.88
Mo	1.43	1.38 □ 1.50	1.45	1.34 □ 1.56	1.43
Zr	1.70	1.73 □ 2.02	1.93	1.62 □ 2.05	1.86
B	0.0080	0.004 □ 0.008	0.0054	0.003 □ 0.008	0.0054
C	--	0.012 □ 0.032	0.022	0.01 □ 0.05	0.024
Si	--	0.021 □ 0.055	0.036	0.026 □ 0.155	0.061
Fe	--	0.03 □ 0.15	0.077	0.03 □ 0.91	0.194
Ni	81.1	b	80.81	b	80.81

[a]50% virgin and 50% revert.

[b]Balance.

Weld Procedure Development

The weld joint design originally specified for attaching trunnions to roll shells for transfer roll fabrication was a single U-groove geometry that included a type 304 stainless-steel backing ring. Several roll assemblies were made using this configuration. Another feature incorporated into this design was an extension of the trunnion under the weld joint area that was referred to as a "catcher." The purpose of the catcher was to provide some insurance from having a roll shell drop to the furnace floor in the event of a weld failure. One result of the weld joint design and the catcher was that machining of the trunnion was relatively difficult. This caused undesirable delays in trunnion manufacturing and contributed to high trunnion costs.

Meetings with our licensees (United Defense LP and Sandusky International) led to a major modification of the weld joint design. The revised design included a single v-groove, eliminated the stainless steel backing ring, and eliminated any machining requirements for the catcher detail. Mock assemblies of the revised design were machined and welded at ORNL to establish a welding procedure.

The stainless steel backing ring was used in our original design to gain some mechanical compliance in depositing the root pass of the weld. The sensitivity to the effects of mechanical restraint is highest for the root pass meaning it is the most likely to experience cracking problems during welding. A byproduct of eliminating the backing ring was that depositing crack-free root passes with IC-221LA filler metal became much more difficult. A wide variety of commercial weld filler metals was evaluated as alternatives to IC-221LA, but none was capable of producing high-quality weld beads on the IC-221M castings. Analysis of weld wire chemistries and weldment specimens suggested that chemical elements (e.g., niobium and titanium) added to the commercial weld filler metals were creating cracking problems when they were deposited on IC-221M. Efforts were then renewed to develop additional weld filler metal alloys for welding IC-221M castings under conditions of high mechanical restraint. Two alloys were identified as acceptable candidates and were fabricated into wire at ORNL. The metallurgical compatibility of these wires with IC-221M was demonstrated and several small lots were produced at ORNL for supply to our licensees. An invention disclosure was prepared for these alloys and patent application is under consideration. Also, negotiations to establish a commercial supply through a welding wire manufacturing company were initiated.

Technical Support for Fabrication

In January, two IC-221M rolls were fabricated at Sandusky International. ORNL staff supervised in the entire activity and participated in the welding. Training was also provided to Sandusky International employees. Both of these roll assemblies used the original u-groove joint design incorporating the stainless steel backing ring.

In May, ORNL participated in the fabrication of another roll assembly using the revised joint design.

In June, ORNL participated in the fabrication of another roll assembly, but this time the trunnions were made of HK and HP stainless steel. The trunnions were obtained from Bethlehem Steel's Burns Harbor Plant and had previously been in service in their heat-treating furnace. The use of the stainless steel trunnions was viewed as a significant opportunity to reduce the overall cost of roll assemblies, thereby making them more attractive to potential customers including Bethlehem Steel. The ability to weld this assembly was a direct result of the new weld filler metal discussed above, and of our continued efforts to develop welding procedures.

Technical Support for Welding Wire Production

Efforts at Stoody Company (Bowling Green, Kentucky) to perfect production procedures for the IC-221LA weld filler metal were supported by coordinating the establishment of chemical analysis standards and composition ranges for the IC-221LA wire, and by confirming that Stoody's approach for making the wire produced weld deposits with acceptable tensile properties. The chemical analysis work involved making weld deposits at ORNL and at Stoody Company with identical procedures and the same weld filler metal wire. The chemical compositions of specimens from these deposits were then determined at Stoody Company and at the Metallurgical Services Laboratory of ABB Combustion Engineering (ABB-CE, Chattanooga, Tennessee). ABB-CE has a long history of analyzing nickel aluminide alloys, and comparison of their techniques and results with those of Stoody Company enabled Stoody to establish the chemical analysis procedures required for composition control in their weld wire manufacturing facilities. Part of this effort also involved working with Stoody to establish chemical element ranges that are consistent with established commercial practice.

Much of our early work to develop welding procedures and determine weldment properties was done using weld filler metal supplied by Ametek. The Ametek wire was produced as metal-powder-cored product by Cor-Met, Inc. (Brighton, Michigan) using standard commercial processing. The unique feature of this product was that the welding wire was fabricated from a nickel sheath containing prealloyed powder. The prealloyed powder was melted and atomized by Ametek. The chemical composition of the powder was formulated so that when it was combined with the nickel sheath and melted during

welding, it produced a weld deposit of the desired IC-221LA composition. Stoody Company viewed the process of prealloying the powder as an unnecessary complication and expense. They desired to make IC-221LA from unalloyed, elemental powders. It was decided to duplicate a weldment made with the Ametek wire to help establish whether the elemental powder approach would yield acceptable operating characteristics during welding and comparable tensile properties. To accomplish this, a weld was made with Stoody wire in 95-mm-OD centrifugally cast tube made by Alloy Engineering & Casting Company. The weld was made using gas-tungsten-arc (GTA) welding with 0.062-in.-diam wire as was previously done. The operating characteristics of the Stoody wire were acceptable and no unusual problems were encountered during the welding. The appearance of the finished weld was good. For comparison, a series of cross-weld tensile specimens were made from the tube and tested up to 1100°C. A plot of yield strength for the IC-221M base metal, the weld made with Ametek/Cor-Met wire, and the weld made with the Stoody wire is given in Figure 9. The yield strength values for specimens from the Stoody weld are within the expected scatter band for tensile tests of similar materials. This data led to the conclusion that Stoody's approach of using unalloyed powder to fabricate IC-221LA weld filler metal was acceptable.

Testing the Mechanical Properties of Weldments

Tensile testing was done on two weldments, centrifugally cast IC-221M welded to itself, and centrifugally cast IC-221M welded to Alloy 800. The IC-221M pieces were rings about 14.375-in-dia. by 4-in. length that were cut from a centrifugal casting produced by Sandusky International (Heat 184876). The Alloy 800 piece was fabricated from a 0.5-in.-thick plate that was rolled and welded into a ring to match the dimensions of the IC-221M. Both welds were made by GTA welding with 0.062-in.-diam wire produced by Ametek/Cor-Met. A schematic drawing showing the joint design and bead placement for the IC-221M/IC-221M weld is shown in Figure 10. Identical joint design and similar bead placement were used for the IC-221M-alloy 800 weld. Alloy 800 was chosen for this test because it is a relatively common alloy used for elevated temperature service, and because it was readily available. It was believed that the success of this weld would indicate that welding of IC-221M to other alloys would be feasible. A photograph of the finished weld of IC-221M-to-Alloy 800 is shown in Figure 11.

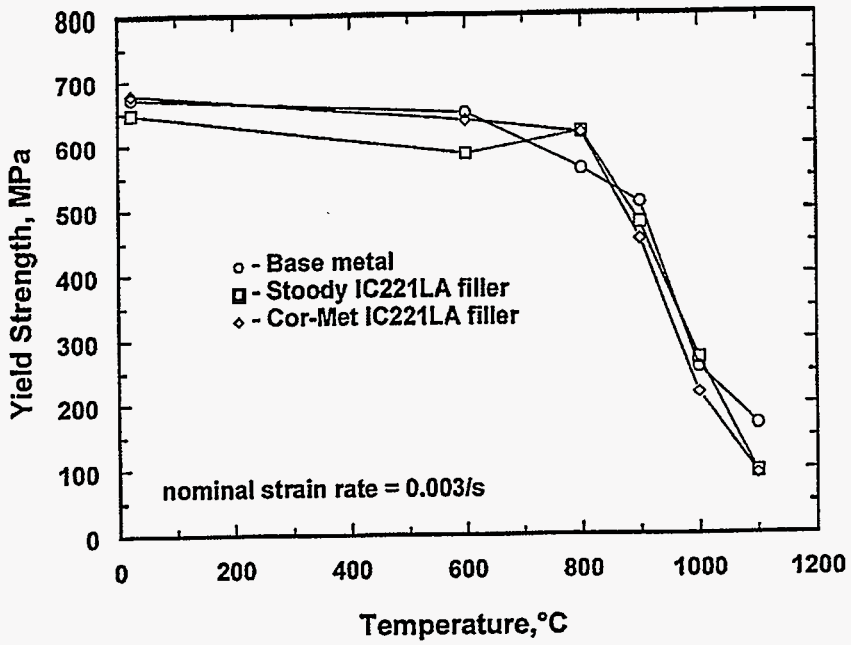

Figure 9. Variation of yield strength with temperature for 95-mm-OD centrifugally cast pipe and pipe weldments made with IC-221LA filler metal made by Ametek/Cor-Met and Stoody Company.

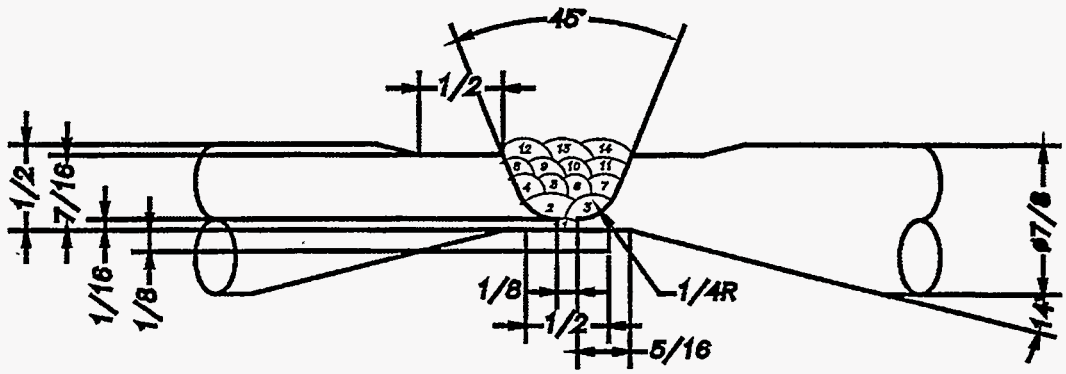

Figure 10. Joint design and schematic representation of bead placement for weld of 14.375-in. rings of centrifugally cast IC-221M.

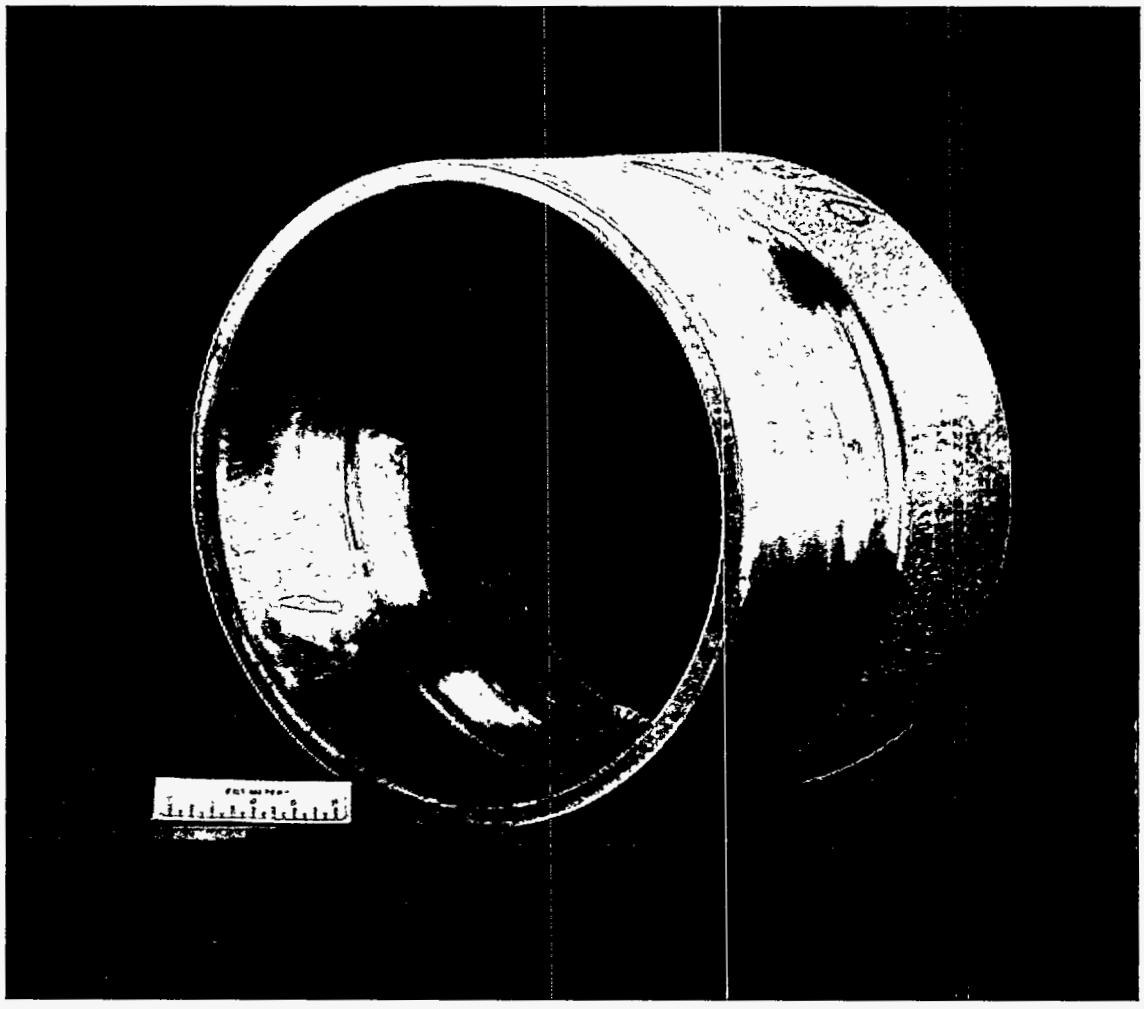

Figure 11. Photograph of centrifugally cast IC-221M ring welded to Alloy 800 ring with IC-221LA filler metal.

The yield strength results from cross-weld specimens from the IC-221M/IC-221M weld are given in Figure 12. The strengths of the weldment specimens were comparable to those of the base metal specimens at test temperatures up to 800°C. Above 800°C, the yield strengths of the weldment specimens were slightly lower than those of the IC-221M base metal, as might be expected. All of the weldment specimens broke with the weld metal which is consistent with the weld metal having a lower strength than the base metal and with stress concentration effects in cross-weld test conditions.

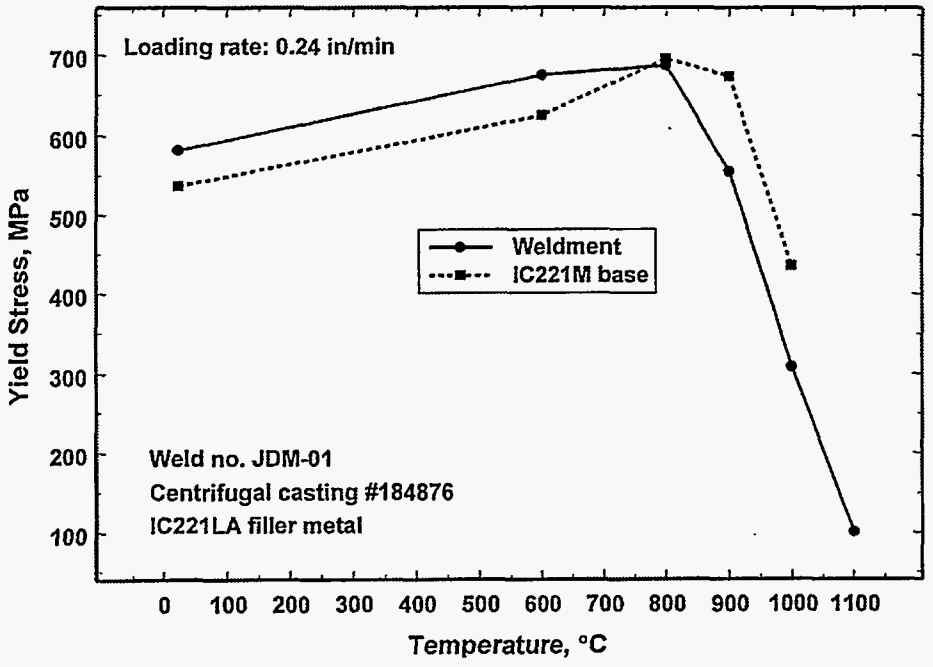

Figure 12. Variation of yield strength with temperature for centrifugally cast IC-221M base metal and weldment.

The yield strength results from testing of the IC-221M/Alloy 800 weld are given in Figure 13. The strengths values of these specimens was controlled by the strength of Alloy 800, which is much lower than those of IC-221M or IC-221LA at all test temperatures. All of the IC-221M/Alloy 800 specimens broke within the Alloy 800 base metal.

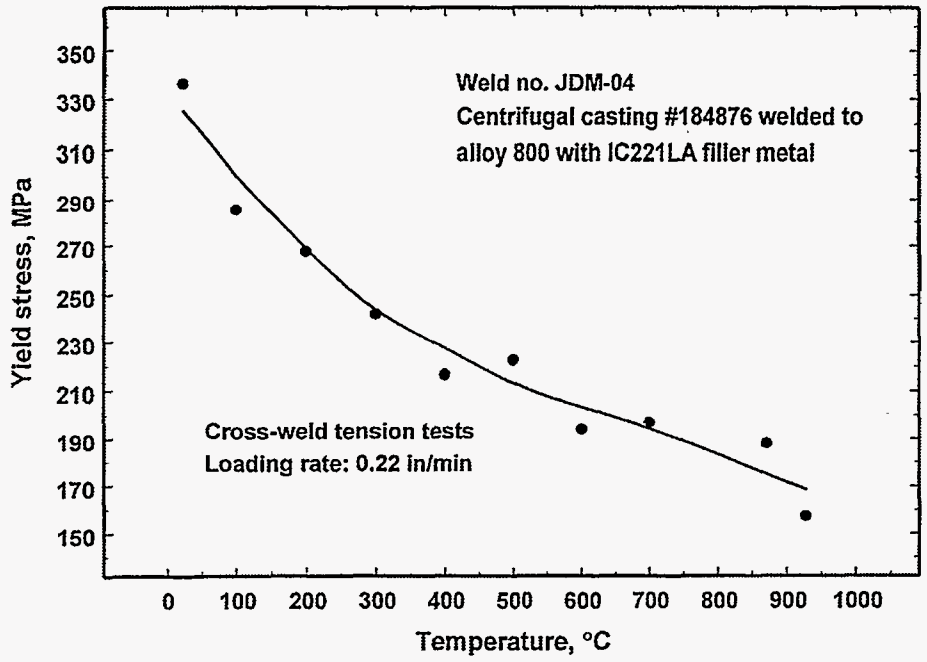

Figure 13. Variation of yield strength with temperature for centrifugally cast IC-221M welded to Alloy 800 with IC-221LA filler metal.

Task 4. Workability of Cast or Powder Metallurgy Product to Sheet, Bar, and Wire (Start 10/96, End 9/97)

Workability of nickel aluminides using conventional processing techniques such as forging, rolling, and extrusion are essential in developing a wide spread use of these materials. In order to be successful in processing aluminides, we need a comprehensive knowledge of flow stress data at a wide range of temperatures and strain rates approaching those used in commercial techniques. A test program to develop such data was set up with Prof. Y.V.R.K. Prasad at the Indian Institute of Science (IIS), Bangalore, Karnataka State, India. The program is best on the unique capability of equipment and expertise of IIS in developing such data and its analysis into deformation maps. The test program exchanges no funds and is based on ORNL supplying the specimens and some metallurgical characterization of tested specimens, and IIS to carry out the data development. The program has been in place since September 1997, and specimen preparation is currently under way.

The end product of this program is expected to be the window of temperature and strain rate that will result in hot workability of nickel aluminides. The first set of results are expected during the first quarter of FY 1998.

Task 5. Technology Transfer Activities (Start 10/96, End 9/97)

Strong technology transfer activities continued with the current and potential users and producers. Specific examples of interactions are listed below.

Bethlehem Steel/Sandusky Interactions

ORNL continued to play a very active role in the successful manufacturing and installation of rolls in the austenitizing furnace at Bethlehem Steel. Specific contributions included: (1) visits to Burns Harbor Plant for examination of rolls in service; and, (2) visits to Sandusky International to assist in welding issues and welder training, conducting stress analysis for various combinations of roll and trunnion combinations and examination of weld versus pinned roll design. A lot of additional mechanical property data were developed along with the production of a lot of scale weld wire for welding at Sandusky International. This has been the most demanding interaction with significant benefits to the steel industry, once the nickel aluminide technology is fully implemented.

United Defense LP

In this interaction, ORNL assisted with the computer modeling of the castings, weld repair of the castings, and training the welders. Technology transfer efforts also included assistance with machining of trunnions and other castings, chemical analysis standards, and obtaining centrifugal cast tubes for the radiant burner tube applications.

Alloy Engineering & Casting Company

A major activity of the technology transfer effort was a three-hour workshop session on the nickel aluminide development with the sales staff at Alloy Engineering & Casting. We also provided assistance in the preparation of a data sheet for cast nickel aluminide for heat-resistant component applications. Other technology transfer activities included extensive support with the preparation of chemical analysis standards, weld repair of castings, and training of the welders.

Chemical Industry Interactions

Strong interactions occurred with the three major players (E. I. DuPont, Dow Chemical, and FMC Corporation) in the chemical industry. In each case, visits were made, data exchanged, and test coupons provided. Results of the test coupons are expected during the second quarter of FY 1998.

Coronado Steel

Coronado Steel Company (Youngstown, Ohio) is a small foundry that can produce small production orders on a very rapid basis. ORNL personnel have trained several of Coronado's personnel on the Exo-Melt[a] process and property data on nickel aluminides. They have demonstrated skills in the production of small pilot heats of specialty shapes and are currently looking at a potential license. They are developing applications in the area of cast heating elements, dies for intricate extrusion processed shapes, and permanent molds for copper alloy casting and burners for gas-fired furnaces. Coronado Steel is a very progressive company, and a strong interaction with them has a strong potential for many new applications of nickel aluminides.

Multi-Metals and Truecast

Our interactions with Multi-Metals (Louisville, Kentucky) indicated that they have potential applications for nickel aluminide components for their heat-treating baths. We worked with Multi-Metals and Truecast (Louisville, Kentucky) in identifying the melt and cast parameters to investment-cast the initial set of components. These components are currently in test at Multi-Metals. This interaction has resulted in a potential investment casting foundry, which did not exist to date.

Other Interactions

Many other companies were sent the data packages and test coupons of nickel aluminide for new potential applications.

FeAl

The technology transfer activities resulted in the production of sand-cast shapes at Anaconda Foundry Fabrication Company, Inc. (AFFCO, Anaconda, Montana) for aluminum industry applications and sand-cast shapes (grate bars and pellet tips) for the phosphate calcination process. The shapes were cast at United Defense LP. The grate bars and pellet tips have been in service for almost one year. The centrifugal-cast FeAl tubes were cast at Alloy Engineering & Casting Company. These tubes were cast to demonstrate the commercial melting and casting process and for potential applications in molten salt baths and specialty applications in the steel industry.

Test coupons of iron aluminides were supplied to potential users for heat treating and sulfidation-related applications.

PUBLICATIONS

V. K. Sikka, M. L. Santella, and J. E. Orth, "Processing and Operating Experience of Ni_3Al-Based Intermetallic Alloy," Mater. Sci. Eng. A239-240 (1997), pp. 564-569.

S. C. Deevi, V. K. Sikka, and C. T. Liu, "Processing, Properties, and Applications of Nickel and Iron Aluminides," Progress in Materials Science 42 (1997), pp. 177-192.

V. K. Sikka, "Commercialization of Nickel and Iron Aluminides," pp. 361-375 in *Proceedings of the International Symposium on Nickel and Iron Aluminides: Processing, Properties, and Applications,* ed. S. C. Deevi, V. K. Sikka, P. J. Maziasz, R. W. Cahn, ASM International, Materials Park, Ohio (1997).

S. C. Deevi and V. K. Sikka, "Reaction Synthesis and Processing of Nickel and Iron Aluminides," pp. 283-299 in *Proceedings of the International Symposium on Nickel and Iron Aluminides: Processing, Properties, and Applications,* ed. S. C. Deevi, V. K. Sikka, P. J. Maziasz, R. W. Cahn, ASM International, Materials Park, Ohio (1997).

M. L. Santell, "An Overview of the Welding of Ni_3Al and Fe_3Al Alloys," pp. 321-327 in *Proceedings of the International Symposium on Nickel and Iron Aluminides: Processing, Properties, and Applications*, ed. S. C. Deevi, V. K. Sikka, P. J. Maziasz, R. W. Cahn ASM International, Materials Park, Ohio (1997).

PRESENTATIONS

S. C. Deevi and V. K. Sikka, "Reaction Synthesis and Processing of Nickel and Iron Aluminides," Proceedings of the International Symposium on Nickel and Iron Aluminides: Processing, Properties, and Applications, ASM-TMS Materials Week '96, Cincinnati, Ohio (October 8, 1996).

V. K. Sikka, "Commercialization Status of Ni_3Al-Based Alloys," Materials Research Society 1996 Fall Meeting, Boston, Massachusetts, December 2, 1996, to be published in Materials Research Society.

V. K. Sikka, "Development and Commercialization of Intermetallics," Resource Group Meeting, Clearwater Beach, Florida (February 24, 1997).

V. K. Sikka, M. L. Santella, and C. T. Liu, "Processing, Properties, and Applications of Ni_3Al-Based Alloys," Golden Jubilee Celebrations, International Conference on Recent Advances in Metallurgical Processes (ICRAMP '97), Indian Institute of Science, Bangalore, India (July 16-19, 1997).

V. K. Sikka, S. Viswanathan, and J. E. Orth, "Net Shape Fabrication of Aluminides," Near Net Shape Manufacturing Conference, Session 4: Net Shaping of Advanced Materials, Indianapolis, Indiana, September 17-18, 1997, to be published in ASM International.

V. K. Sikka, "Intermetallics," CANMET-IRAP Forum on Latest Developments and Applications of Emerging Technologies in Metallic Materials, Humber College, Toronto, Ontario, Canada (September 30, 1997).

HONORS & AWARDS

Lockheed Martin NOVA Award for Teamwork, Oak Ridge National Laboratory, Oak Ridge, Tennessee, presented June 27, 1997 at Third Annual NOVA Awards Ceremony, National Air and space Museum, Washington, DC.

PATENTS/DISCLOSURES

"High-Strength, Thermally Stable, and Oxidation Resistant Alloy for Die and Cutting Tool Application," V. K. Sikka, S. C. Deevi, J. D. Vought, and C. R. Howell, Lockheed Martin Energy Research Corporation, Invention Disclosure No. ESID 1877-X, S-85,549.

"Ductile Filler Metal Alloys for Welding Nickel Aluminide Alloys," M. L. Santella, J. D. McNabb, and V. K. Sikka, Lockheed Martin Energy Research Corporation, Invention Disclosure No. ERID 0410, S-88,672.

LICENSES

Three new licenses were signed: Alloy Engineering & Casting Company, Sandusky International, and Polymet Corporation. Two other licensing agreements are currently under negotiation.

INDUSTRIAL INPUT AND TECHNOLOGY TRANSFER

Delphi Saginaw

Two pusher furnace fixtures have been in operation for two years at Delphi Saginaw. Sixty-three pusher furnace fixtures have completed nine months in commercial operating furnaces. Six batch furnace trays have been operating for almost ten months at Delphi Saginaw.

Bethlehem Steel Corporation

A total of 14 rolls were installed in Bethlehem Steel Corporation's furnace. Two of these rolls have been operating for 42 months. The others have seen different operating periods. Four of the rolls had to be taken out of service for weld repairs.

FMC

Nickel aluminide pellet tips have been operating for nearly two years. The FeAl grate bars have completed ten months.

Ford Motor Company

Ford Motor Company (Dearborn, Michigan) has ordered fifty trays for their carburizing heat-treating furnaces.

The Timken Company

The Timken Company (Canton, Ohio) has completed the first round of use of nickel aluminide with twice the use of the currently used forty trays. They are currently waiting on a supply of new sets of fixtures to go into their furnaces.

Chevron

Chevron (Richmond, California) has completed the use of the first set of tube hangers and is awaiting the supply of a larger batch.

COST INFORMATION

None.

COST SHARING

A significant amount of industrial cost sharing occurred through the testing of nickel aluminide under commercial production conditions.

Research performed at the Oak Ridge National Laboratory, sponsored by the U.S. Department of Energy, Assistant Secretary for Energy Efficiency and Renewable Energy, Office of Industrial Technologies, Advanced Industrial Materials Program, and the Steel Industry Team under contract DE-AC05-96OR22464 with Lockheed Martin Energy Research Corporation.

PARALLEL IMPLEMENTATION OF CASTING MODELING PROGRAM

T. Zacharia, S. Simunovic, S. Viswanathan, and P. F. Locascio

Metals and Ceramics Division
Oak Ridge National Laboratory
Post Office Box 2008, Oak Ridge, Tennessee 37831

INTRODUCTION

Casting modeling is important to the design and optimization of casting processes for the production of ordered intermetallic alloy components. Due to the large size of some components such as heat treating trays and centrifugally cast rolls, and complex coupled physical phenomena involved, simulation time on even high-end workstations, can range from a few days to a week or more. The objective of this project is to develop a massively parallel processing capability for modeling of casting processes. Parallel implementation of the simulation program will allow for rapid analysis and will enhance projects on improved castability on metallic and intermetallic alloys.

The commercial casting code ProCAST, from UES, Inc., has been chosen to be implemented on massively parallel computers at ORNL. ProCAST is a finite element code that can be used for the analysis of complex casting shapes by modeling coupled effects of heat flow, fluid flow, solidification, and stress. The program also has very good capabilities for simulating radiation that is important for investment casting.

The first step in project was to parallelize the heat conduction module in ProCAST. This task was done using Parallel Virtual Machine (PVM) approach. The next step was to port this implementation onto ORNL massively parallel computers. Consequently, the assessment of this implementation is to be performed by analyzing the performance on the parallel computers and identifying the areas that need to be improved. A detailed parallelization strategy, data structures, and function design have to be developed next in collaboration with UES so that the developments in the serial and parallel versions of the code be compatible and complement the overall objective of improvement of casting simulation capabilities. Successive parallelization of ProCAST modules (heat flow, fluid flow, and stress analysis) is to be done next following the developed strategy.

TECHNICAL PROGRESS - FY 1997

A parallel version of a heat flow conduction module in ProCAST has been ported on ORNL's parallel computers SGI Onyx and Intel Paragon. The performance of the implementation is currently being assessed. The function call trees and program profiling

were performed to identify the main program functions for each of the modules and determine a proper sequence and subsets of functions that need to be parallelized. The meeting with industrial collaborators has been scheduled in order to coordinate the efforts and develop a strategy for development of parallel implementation of fluid flow module of ProCAST.

SYNTHESIS AND DESIGN OF SILICIDE INTERMETALLIC MATERIALS

J. J. Petrovic, R. G. Castro, D. P. Butt, Y. Park,
K. J. Hollis, and H. H. Kung

Los Alamos National Laboratory
Los Alamos, New Mexico 87545

INTRODUCTION

The overall objective of this program is to develop structural silicide-based materials with optimum combinations of elevated temperature strength/creep resistance, low-temperature fracture toughness, and high-temperature oxidation and corrosion resistance for applications of importance to the U.S. processing industry. A further objective is to develop silicide-based prototype industrial components. The ultimate aim of the program is to work with industry to transfer the structural silicide materials technology to the private sector in order to promote international competitiveness in the area of advanced high temperature materials and important applications in major energy-intensive U.S. processing industries.

The program presently has a number of developing industrial connections, including a CRADA with Johns Manville Corporation targeted at the area of $MoSi_2$-based high-temperature materials and components for fiberglass melting and processing applications. We are also developing an interaction with the Institute of Gas Technology (IGT) to develop silicides for high temperature radiant gas burner applications, for the glass and other industries. With Combustion Technology, we are developing silicide-based periscope sight tubes for the direct observation of glass melts.

TECHNICAL PROGRESS - FY 1997

CRADA with Johns Manville Corporation

Corrosion Behavior of $MoSi_2$ in Molten Glass

We have been examining the corrosion behavior of $MoSi_2$ in molten glass. This has involved both static and dynamic corrosion experiments in fiberglass composition glass, at temperatures in the range of 1050°C -1550°C. Corrosion rates of $MoSi_2$ are comparable to those of AZS refractory. Dynamic corrosion is similar to static corrosion, indicating no corrosion rate effects. Maximum corrosion rates for $MoSi_2$ occur at the glass-air line. Above the glass line, the formation of a protective SiO_2 layer occurs, while below the glass line, a protective Mo-rich layer is formed. At the glass line, no protective

layers are formed in pure $MoSi_2$. Efforts are now concentrating at optimizing the corrosion behavior at the glass line, through composite, alloying, and anodic protection approaches.

$MoSi_2$ Coating of Refractory Bricks

Silica refractory bricks were coated with $MoSi_2$ and tested in a Johns Manville oxy-fuel-fired glass melting furnace. Coated and uncoated bricks were exposed in the furnace at a temperature of 1554°C for a period of eight weeks. After this exposure, the $MoSi_2$ coating was still present, although some of the coating spalled off of the brick upon removal from the furnace. Analysis showed the formation of an amorphous silica layer between the $MoSi_2$ and the silica refractory brick.

Interaction with Institute of Gas Technology

We have been interacting with the Institute of Gas Technology (IGT) to test $MoSi_2$ and $MoSi_2$ composite materials in a gas radiant tube environment, to initially assess these materials for potential melting, heat treating and drying applications which employ gas radiant tubes. Planning was initiated to conduct a 500-hr test at 1800°F of bend test specimens of the following materials: (1) Pure $MoSi_2$; (2) 30 vol.% SiC-$MoSi_2$ matrix composite; (3) 30 vol.% Si_3N_4-$MoSi_2$ matrix composite; (4) Reaction bonded SiC; 5) Plasma sprayed $MoSi_2$ and Mo_5Si_3. Specimens of aluminide materials from ORNL will also be included in this test.

Mechanical Properties of $MoSi_2$ Materials

Impression creep tests were performed on $MoSi_2$ materials, in the temperature range of 1000°C-1200°C, and impression creep stresses of 260-370 MPa. The impression creep behavior of air plasma sprayed (APS) and hot pressed (HP) $MoSi_2$ was compared. In general, the creep rates of APS materials were higher than the creep rates of HP materials, by roughly one order of magnitude. Impression creep rates at 1200°C were in the range of 10^{-6}-10^{-8} s^{-1}. Creep activitation energies were in the vicinity of 350 kJ/mole, and creep stress exponents were in the range of 1.4-2.0. The higher creep rates observed for APS material as compared to HP material were probably related to the somewhat smaller grain size and greater porosity in the APS material.

Joining of $MoSi_2$ Materials

Our efforts on the joining of $MoSi_2$ to important engineering metals were scaled back somewhat due to funding constraints. However, somewhat limited efforts continued on the joining of $MoSi_2$ to 316L stainless steel. Finite element analyses and neutron diffraction experiments were employed to obtain estimates of the residual stresses in the $MoSi_2$-stainless steel joints, using Nb, Ni, and Ni-Fe interlayer materials. An Ni-Fe

interlayer material with a coefficient of thermal expansion intermediate between the $MoSi_2$ and the stainless steel provided the most favorable residual stress states in the joints.

CRADA with Johns Manville Corporation

Corrosion of $MoSi_2$ in Molten Glass

The primary task this quarter was to evaluate and compare the corrosion resistance of $MoSi_2$-based composite materials in the molten glass. Yittria alumina garnet (YAG)-reinforced and yittria-partially- or fully-stabilized ZrO_2-$MoSi_2$ composites were fabricated by hot pressing. The compositions of the composites and their basic properties are listed in Table 1. Tests were performed under static conditions at 1300°C for 3 or 12 hours at 1300°C in molten alkali borosilicate glass.

Figure 1 summarizes the results of the static tests and compares the rates of corrosion to those of other refractory materials above, below, and at the glass line. Although other physical properties may be improved, the addition of the aforementioned oxides do not significantly improve the corrosion resistance over that of pure $MoSi_2$. Figure 2 illustrates the relative effect of YAG concentration in the YAG-$MoSi_2$ composites on corrosion. It is apparent that the corrosion rate of the composite is inversely proportional to the concentration of YAG. The effect of various types of Y_2O_3-ZrO_2 additions on the corrosion of $MoSi_2$ is illustrated in Figure 3. In this case, the corrosion rate of the composite was inversely proportional to the concentration of yittria.

Research next quarter will continue to focus on the corrosion testing of plasma sprayed $MoSi_2$ and Mo_5Si_3 at longer exposure times. In addition, we will investigate Mo_5Si_3 and FeCrSi coated alumina and will continue with electrochemical measurements of corrosion. We are also designing an apparatus for studies of the sulfidation resistance of $MoSi_2$. It is anticipated that we will begin constructing the apparatus near the end of the first quarter of FY 1998.

Table 1. Test matrix of $MoSi_2$ composites.

Reinforced Elements of $MoSi_2$	$MoSi_2$ Composites	Theoretical density (%)
YAG -$MoSi_2$	20% YAG -$MoSi_2$	96.65
	40% YAG -$MoSi_2$	92.72
	60% YAG -$MoSi_2$	86.33
	80% YAG -$MoSi_2$	80.86
	100% YAG	75.91
(Y_2O_3-ZrO_2)+$MoSi_2$	20% (ZrO_2)-$MoSi_2$	91.2
	20% (2.5 Y_2O_3-ZrO_2)-$MoSi_2$	94.2
	20% (8.0 Y_2O_3-ZrO_2)-$MoSi_2$	94.1

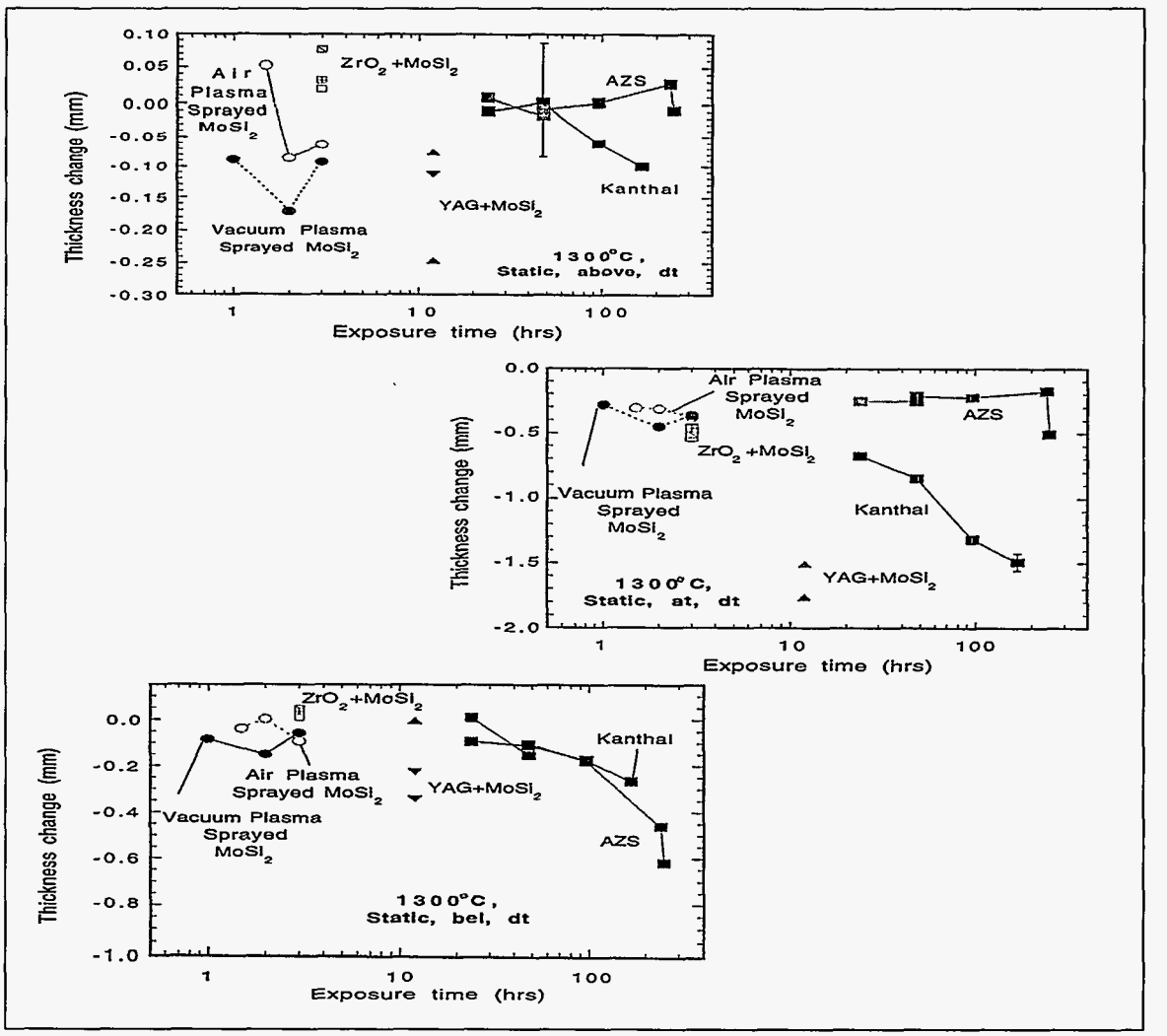

Figure 1. Material loss (thickness change) of composite materials exposed to molten alkali borosilicate glass under static corrosion conditions at 1300°C, showing mass loss above (top), at (middle), and below the glass line (bottom).

$MoSi_2$ Coatings

Powders and coatings of Ti_3SiC_2 and FeCrSi are being evaluated for potential applications for glass refractory coatings. Both powders have been produced by a combustion synthesis process and have been manufactured by Exotherm Corporation. Initial results have shown that the SHS Ti_3SiC_2 powders are single phase and fairly uniform in composition as determined by backscattered electron imaging (BEI) and X-ray diffraction. The FeCrSi SHS powders, however, were very non-uniform with a number of unidentifiable phases present in the X-ray diffraction pattern. Plasma sprayed coatings of the FeCrSi were produced and are currently being tested for their glass compatibility. We were unsuccessfully in producing plasma sprayed coatings of the Ti_3SiC_2 powders.

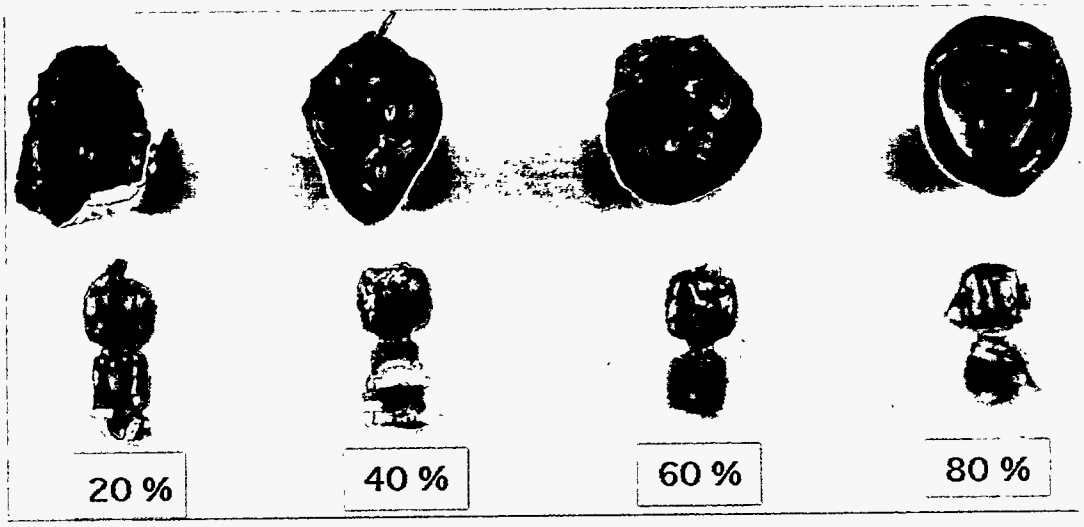

(a)

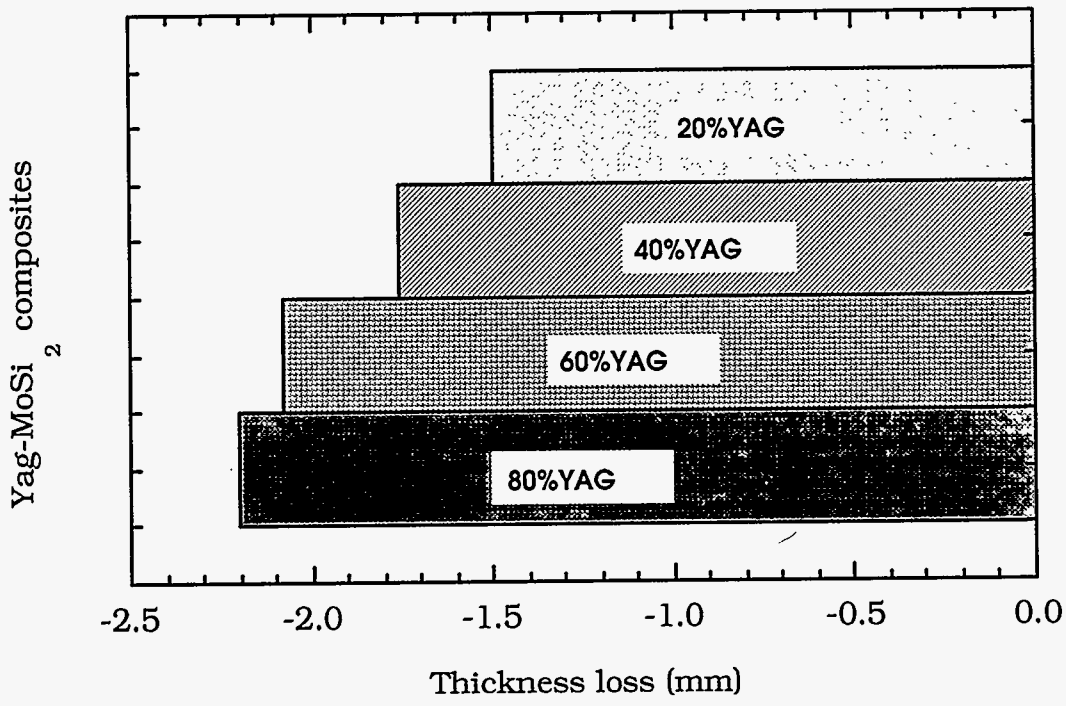

(b)

Figure 2. Effect of YAG reinforcement on the corrosion of YAG -$MoSi_2$ composites exposed at 1300°C for 12 hrs showing (a) postmortem composites and (b) comparative mass losses after exposure.

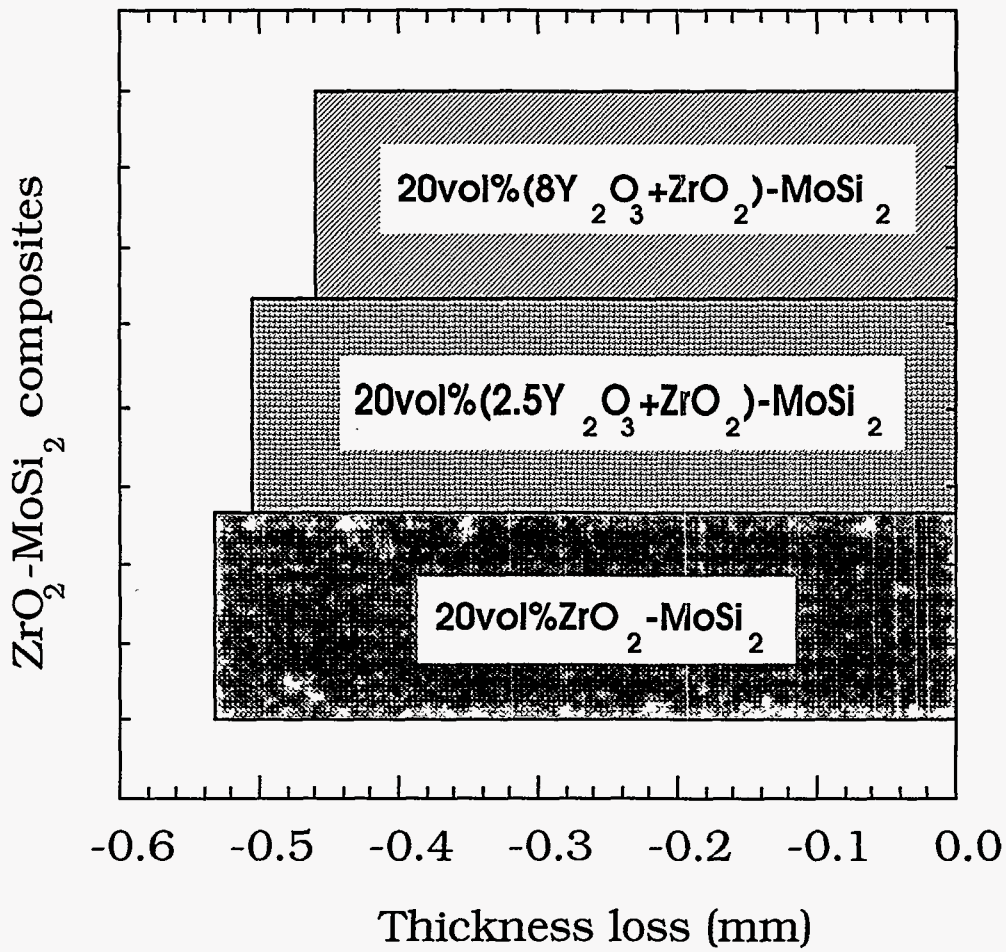

Figure 3. Effect of Y_2O_3 concentration on the corrosion resistance of 20% (Y_2O_3+ZrO_2)-$MoSi_2$ composites in molten alkali borosilicate glass at 1300°C for 3 hrs.

IGT Interaction

Ordered and received radiant U-tube for high-temperature testing of silicide and aluminide-based materials at IGT. Designed and fabricated six holding fixtures for the four-point bend test samples which will be evaluated in a combustion and endothermic environment at IGT. Plasma sprayed three $MoSi_2$ spray formed tubes and three Mo_5Si_3 tubes as machining stock for the bend test samples. A total of 365 samples will be machined from the following materials for testing at IGT:

- Plasma sprayed-formed $MoSi_2$ tubes on graphite rods
- Plasma sprayed-formed Mo_5Si_3 tubes on graphite rods
- SCRB210 SiC plate
- $MoSi_2$ "C" hot-pressed discs
- $MoSi_2$ - A10/SiC hot-pressed discs

- $MoSi_2$ - E10/Si_3N_4 hot-pressed discs

ORNL will provide two types of aluminide materials (approx. 60 samples) for testing at IGT. Testing of the samples is expected in December 1997.

Combustion Tec Interaction

Started investigating the plasma spray-forming of a periscope sight tube for observing glass processes. CTI specializes in monitoring systems of glass furnaces, and heat flux and gas sampling probes for glass processing operations. CTI closed circuit television furnace monitoring system is one of the most advanced systems for observing flame characteristics and batch distribution inside glass melting furnaces. They currently have a need to use advanced silicide-based materials to enhance the performance of a periscope site tube which is used for directly viewing the glass during processing. $MoSi_2$ powder produced by Exotherm Corporation has been purchased and used on the initial spray trials.

Oxford University Interaction

Hosted Dr. Patrick Grant and Adam Baker of the Materials Department at Oxford University. Dr. Grant is currently interested in developing continuous reinforced composites of $MoSi_2$/SiC using monotape technology. Monotapes of $MoSi_2$/SiC are produced by filament winding continuous fibers of SiC on a mandrel followed by plasma spray deposition of $MoSi_2$ on the fibers. This process technology has been used to produce continuous reinforced composites of Ti-based material. Mr. Adam Baker was sponsored by R. Castro of MST-6 for a two-month period to characterize monotape composite which were successfully produced at LANL by atmospheric plasma spraying. A collaborative research program is being established with the Materials Department at Oxford University to investigate spray/wind techniques for produced continuous reinforced composites of $MoSi_2$/SiC. An abstract of this work will be submitted to the International Conference on High Temperature Structural Silicides. R. Castro visited Oxford University in September 1997 and presented a seminar on "$MoSi_2$ Composites Produced by Plasma Spraying.".

Joining of $MoSi_2$ to Common Metals:

Work this past quarter has focussed on making residual stress measurements on joints and on using new interlayer materials, in particular, amorphous alloy foils. The new experimental work has just begun and will be reported in future reports. Much of the residual stress data has been reported in previous reports and has been summarized in detail in a recent paper which was submitted and accepted for publication in *Acta Mater. et Metall.*

PUBLICATIONS

Journals

M. Sandlin, D. P. Butt, T. N. Taylor, and J. J. Petrovic, "Aqueous Zeta Potential of Molybdenum Disilicide," *J. Mater. Sci. Lett.*, **16**, 1336-1338 (1997).

S. D. Conzone, D. P. Butt, and A. H. Bartlett, "Joining $MoSi_2$ to 316L Stainless Steel," *J. Mater. Sci.*, **32**, 3369-3374 (1997).

T. N. Taylor, D. P. Butt, and C. G. Pantano, "Auger Parameter Determination of Bonding States on Thinly Oxidized Silicon Nitride," accepted for publication in *Surface and Interface Analysis* (1997).

R. U. Vaidya, P. Rangaswamy, M. A. M. Bourke, and D. P. Butt, "Measurement of Bulk Residual Stresses in Molybdenum Disilicide/Stainless Steel Joints Using Neutron Scattering," accepted for publication in *Acta Mater. et Metall.*, (1997).

J. J. Petrovic, M. I. Pena, I. E. Reimanis, M. S. Sandlin, S. Conzone, H. H. Kung, and D. P. Butt, "Mechanical Behavior of $MoSi_2$ Reinforced-Si_3N_4 Matrix Composites," *J. Am. Ceram. Soc.* (December 1997).

R. U. Vaidya, A. H. Bartlett, H. H. Kung, and D. P. Butt, "Joining of $MoSi_2$ to Itself and Reactions with Aluminum Interlayers," accepted for publication in *J. Mater. Sci. Lett.* (1997).

D. P. Butt, D. Albert, and T. N. Taylor, "Kinetics of Thermal Oxidation of Silicon Nitride Powders," *J. Am. Ceram. Soc.*, **79** [11] 2809-2814 (1996).

H. Kung, Y. C. Lu, A. H. Bartlett, R. G. Castro, J. J. Petrovic, and E. Shtessel, "Structural Characterization of Combustion Synthesized $MoSi_2$-Si_3N_4 Composite Powders and Plasma Sprayed $MoSi_2$-Si_3N_4 Composites," J. Mater. Res., in press.

A.H. Bartlett and R.G. Castro, "Elevated Temperature Mechanical Properties of Molybdenum Disilicide/Silicon Nitride Molybdenum Disilicide/Silicon Carbide Composites Produced by Self-Propagating High Temperature Synthesis," accepted for publication in the Journal of Material Science (1996).

A. H. Bartlett and R. G. Castro, "High Temperature Deformation and Damage for Plasma-Sprayed Layered Molybdenum Disilicide/Aluminum Oxide Beams," accepted for publication in the J. of Acta Materiali (1997).

A. H. Bartlett and R. G. Castro, "Residual Stress in Net-Shape Plasma Sprayed Tubes" submitted for publication in the J. of American Ceramics Society (1997).

J. J. Petrovic, M. I. Pena, and H. H. Kung, "Fabrication and Microstructures of $MoSi_2$ Reinforced-Si_3N_4 Matrix Composites", J. Am. Ceram. Soc., 80, 1111-1116 (1997).

Other Publications

K. J. Hollis, D. P. Butt, and R. G. Castro, "Impression Creep Behavior of Atmospheric Plasma Sprayed and Hot Pressed $MoSi_2/Si_3N_4$," in *Proceedings of the 1997 United Thermal Spray Conference*, Indianapolis, Indiana (1997).

A.H. Barlett and R.G. Castro, "Measurement and Modeling of Residual Stress in Net-Shape Plasma Sprayed Tubes," 9th National Thermal Spray Conference Proceedings, ASM International, Materials Park, Ohio, (October 1996), 841-845.

K.J. Hollis, R.G. Castro, A.H. Bartlett and R. Neiser, "Investigation of the Silicon Loss in APS $MoSi_2$ Under Typical Spray Conditions," 9th National Thermal Spray Conference Proceedings, ASM International, Materials Park, Ohio (October 1996) 429-437.

PRESENTATIONS

Invited Presentations

D. P. Butt, S. L. Conzone, A. H. Bartlett, "Partial Transient Liquid Phase Joining of $MoSi_2$ to Commercial Alloys," presented at the *98th Annual Meeting of the American Ceramic Society*, Indianapolis, Indiana (1996).

R.G. Castro and J.J. Petrovic, "$MoSi_2$ Based Composites," DOE Workshop on Intermetallic Alloys, Atlanta, Georgia (June 3-4, 1996) (Invited).

Other Presentations

T. N. Taylor, D. P. Butt, and C. G. Pantano, "Charge Independent Surface Analysis of Chemical States on Thinly Oxidized Silicon Nitride," to be presented at the 100th Annual Meeting of the American Ceramic Society, Cincinnati, Ohio (1998).

Y. S. Park, K. J. Hollis, R. G. Castro, and D. P. Butt, "Corrosion Behavior of $MoSi_2$ in Molten Glass Environments," presented the *99th Annual Meeting of the American Ceramic Society*, Cincinnati, Ohio (May 1997).

R. U. Vaidya, A. H. Bartlett, D. P. Butt, M. A. M. Bourke, and P. Rangaswamy, "Measurement of Residual Stresses in $MoSi_2$/Stainless Steel Joints Using Neutron

Diffraction," presented the *99th Annual Meeting of the American Ceramic Society*, Cincinnati, Ohio (May 1997).

A. H. Bartlett, D. P. Butt, and R. U. Vaidya, "Mechanical and Chemical Issues in Joining $MoSi_2$," presented the *99th Annual Meeting of the American Ceramic Society*, Cincinnati, Ohio (May 1997).

T. N. Taylor, D. P. Butt, and C. G. Pantano, "Auger Parameter Determination of Bonding States on Thinly Oxidized Silicon Nitride," presented at the *33rd Annual Symposium of the New Mexico Chapter of the American Vacuum Society*, Albuquerque, New Mexico (May 1997).

K. J. Hollis, D. P. Butt, and R. G. Castro, "Impression Creep Behavior of Atmospheric Plasma Sprayed and Hot Pressed $MoSi_2/Si_3N_4$," presented at the *1997 United Thermal Spray Conference*, Indianapolis, Indiana (September 1997).

S. Park, D. P. Butt, K. J. Hollis, R. G. Castro, and J. J. Petrovic, "Viability and Degradation of Molybdenum Disilicide Materials in Molten Glass Environments," to be presented at the 22nd Cocoa Beach Conference on Composites, Advanced Ceramics, Materials and Structures, American Ceramic Society Engineering Division, Cocoa Beach, Florida (1998).

R.G. Castro and J.J. Petrovic, "Development of Molybdenum Discilicide," Advanced Industrial Materials Program Annual Review (June 1997).

K.H. Hollis, A.H. Bartlett and R.G. Castro, "Investigation of the Silicon Loss in Plasma Sprayed $MoSi_2$ Under Typical Spray Conditions," 9^{th} National Thermal Spray Conference, Cincinnati, Ohio (October 7-11, 1996)

A.H. Bartlett and R.G. Castro, "esidual Stress in Net-Sprayed Plasma Sprayed Tubes: Measurement, Modeling and Modification,"9th National Thermal Spray Conference, Cincinnati, Ohio (October 7-11, 1996).

R.G. Castro and J.J. Petrovic, "$MoSi_2$-Based Composites for the Glass Industry," 2nd Industrial Energy Efficiency Symposium & Exposition, Arlington, Virginia (February 24-27, 1997).

R.G. Castro, "$MoSi_2$-Based Composites by Plasma Spraying," Oxford University (September 1997).

HONORS AND AWARDS

James I Mueller Memorial Award, presented to John J. Petrovic, American Ceramic Society Engineering Ceramics Division Cocoa Beach Meeting, Cocoa Beach, Florida (January 1997).

Robert L. Coble Award for Young Scholars, presented to Darryl Butt at the 99th Annual Meeting of the American Ceramic Society, Cincinnati, Ohio (May 1997).

PATENTS/DISCLOSURES

None.

LICENSES

None.

INDUSTRIAL INPUT and TECHNOLOGY TRANSFER

Johns Manville Corporation

We have a CRADA with Johns Manville Corporation to develop $MoSi_2$-based materials for fiberglass processing.

Institute of Gas Technology (IGT)

We are interacting with IGT to perform tests on $MoSi_2$-based materials in radiant gas combustion tube environments.

Exotherm Corporation

We have been investigating the plasma spraying of advanced $MoSi_2$, Mo_5Si_3, and composite powders from the Exotherm Corporation.

Combustion Tec, Inc.

We are interacting with Combustion Tec to develop a $MoSi_2$ sight tube for a glass furnace monitoring system, that can withstand 3000°F at the glass furnace wall.

LightPath Inc.

We are working with LightPath Inc., to help solve problems with Pt crucible cracking in the fabrication of their Gradium optical glasses.

Mississippi State University

We are exploring the possibility of using $MoSi_2$ materials as part of a system for measuring the viscosity of molten glasses with personnel at the Diagnostic Instrumentation and Analysis Laboratory.

Oxford University

We are interacting with Oxford University to examine the plasma spray fabrication of continuous SiC fiber-$MoSi_2$ matrix composites.

Research performed at the Los Alamos National Laboratory, sponsored by the U.S. Department of Energy, Assistant Secretary for Energy Efficiency and Renewable Energy, Office of Industrial Technologies, Advanced Industrial Materials Program, and the Glass Industry Team under contract to the Los Alamos National Laboratory.

UNIFORM-DROPLET PROCESS

C. A. Blue and V. K. Sikka
Metals and Ceramics Division
Oak Ridge National Laboratory
Post Office Box 2008, Oak Ridge, Tennessee 37831

J.-H. Chun
Massachusetts Institute of Technology
Laboratory of Manufacturing and Productivity
77 Massachusetts Avenue
Cambridge, Massachusetts 02139

T. Ando
Department of Mechanical Engineering
Northeastern University, 334SN
Boston, Massachusetts 02115

INTRODUCTION

This report summarizes the joint study titled, Uniform-Droplet Spray (UDS) Process sponsored by the U.S. Department of Energy, Assistant Secretary for Energy Efficiency and Renewable Energy, Office of Industrial Technologies, Advanced Industrial Materials (AIM) Program, under contract DE-AC05-96OR22464 with Lockheed Martin Energy Research Corp. and conducted jointly at the Oak Ridge National Laboratory (ORNL), Massachusetts Institute of Technology (MIT), and Northeastern University with the objective of studying the uniform-droplet spray (UDS) process for advanced industrial materials processing. The UDS process is a nongas atomization process developed in the Laboratory for Manufacturing and Productivity at MIT and uses the concept of controlled break-up of a laminar jet to produce uniform alloy droplets having identical thermal histories [1-5]. Unlike other methods for producing thermal sprays [6-14], the spray parameters in the UDS process are fully decoupled and, therefore, permit materials processing under conditions inaccessible by conventional thermal spray processes. Systematic studies are conducted to optimize the process parameters, understand the solidification of droplets and spray deposits and develop UDS apparatuses appropriate for processing engineering alloys. The study was initiated in March 1995.

TECHNICAL PROGRESS - FY 1997

Oak Ridge National Laboratory

Summary

The main focus of the work at ORNL has been in the area of extending the UDS process to high-temperature engineering alloys. This development started with the construction of a low-temperature apparatus (300°C) which was utilized to gain the appropriate base technology and verify results previously produced by Massachusetts Institute of Technology (MIT). Upon completion of this phase, a medium-temperature apparatus was developed and constructed which is capable of spraying up to temperatures of approximately 1200°C. This work is included in the 1997 calendar year. With this system, aluminum-based alloys and copper-based alloys have been successfully sprayed: 6061 Al, Cu-8% P, Cu-10% Sn, and Cu (all in the 150- to 300-mm powder size range).

This previous calendar year consisted of finishing the work with the medium-temperature system while developing the high-temperature system. Challenges with the high-temperature systems include materials compatibility, temperature gradients through high-temperature crucibles, orifice clogging, and orifice placement. When spraying higher melting alloys, reaction kinetics have to be looked into extensively for each material to be sprayed. This must be accomplished for both the crucible and the orifice material. In an effort to spray as many materials as possible with the same crucible, alumina was chosen for preliminary high-temperature spraying. This is the same material utilized for the nozzle. Preliminary calculations revealed that temperature gradients as large as 300°C could be observed from the inside of the crucible to the outside of the crucible. This caused freezing in the nozzle. External insulation on the bottom of the ceramic crucible was incorporated to minimize these temperature gradients. The other area of critical importance is orifice placement in the bottom of the crucible. A series of high-temperature adhesives and a orifice housing design have been implemented to eliminate orifice blowout. Work with Hoeganaes and Jim Ingram was accomplished in order to extract industrial spraying experience. Presently, ORNL has UDS spray capabilities up to 1500°C. Because ORNL has the highest temperature spray capabilities, two separate companies, Uniform Metals Technologies, Inc. (Watertown, Massachusetts) and Micro Engineering (Cinnaminson, New Jersey) spent a total of three weeks at ORNL to better understand the UDS process and systems. Uniform Metals Technologies, Inc.'s president, Chris Brown, and MIT's UDS masters-level. graduate worked with ORNL on the spraying of copper-based alloys for filtration applications potentially in the petroleum industry. Uniform Metals Technologies, Inc., is presently finalizing exclusive licensing of the UDS process for porous products and free-form fabrication.

This year, the primary focus will be in the area of multinozzle spraying and high-temperature spraying. The multinozzle work will be accomplished in conjunction with

the splat and spreading work accomplished at MIT in order to develop the necessary parameters for spraying aluminum sheet. The basic work here will be able to be translated to other materials.

The initial high-temperature spraying will be in the area of low-temperature intermetallics. Upon successful completion of this work and gaining further high-temperature knowledge, work with high-temperature intermetallics, and stainless steels will commence. A list of industrial interactions and collaboration is shown in the back section.

TECHNICAL PROGRESS - FY 1997

Northeastern University

Summary

Scope of the Joint Project

Understanding the in-flight thermal state of traveling uniform droplets is a critical issue for the commercial application of uniform-droplet spray for advanced materials processing and, thus, is a primary task in our joint effort. A major emphasis has been on studying droplet enthalpy and droplet solidification. One of our goals was to extend the previous model developed at MIT in which a simple solidification model based on local equilibrium and the Scheil equation was used to provide crude estimations of the solid fraction in the droplets. To achieve this, we needed to develop a more sophisticated solidification model, which accounted for the prior droplet undercooling and deviations from local equilibrium conditions [15,16] to better describe the thermal state of the traveling uniform droplets. This capability, together with the understanding of the micro-impact behavior of the droplets upon deposition onto a substrate, was essential for the prediction of resultant microstructures from the process conditions applied.

The application of the UDS process to engineering alloys requires further optimization of melt delivery and jet break-up together with a higher temperature processing capability. In this area, efforts were made, primarily at MIT, to study the uniform break-up of a molten jet for the steady production of aluminum alloy droplets, while apparatus construction for higher temperature capability was achieved at ORNL.

Unique opportunities exist in the area of producing uniform powders with controlled size and microstructure. Potential applications of such uniform powders include micro-solder balls, shots, and rapidly solidified high-performance powders. One of the areas that was targeted in the joint study was the application of the UDS process to the mass production of micro-solder balls for ball-grid array IC packaging. Our work at Tufts University and Northeastern University in the area of uniform powder processing was aimed at characterizing and controlling the thermal state and solidification of uniform droplets by the aforementioned rigorous modeling and experimental verification to allow for precise control of the microstructure evolution in the powders produced by the UDS process.

With uniform-droplet sprays, controlled spray forming with completely decoupled spray and substrate parameters is possible at ultimate levels of microstructural control. Novel microstructures that can result include equiaxed microstructures with controlled uniform grain size, rapidly solidified single or polycrystalline microstructures with controlled texture and a bulk amorphous material. Also, the capability of controlling droplet trajectory permits spray forming of near-net-shape products at an essentially 100% spray yield. Thus, an important goal of the joint project was to develop a controlled spray forming process suitable for the production of high-performance materials having desired microstructure and geometry directly from the molten state.

Objectives

The objective of the work at Tufts University and Northeastern University was to characterize the solidification and microstructural evolution in the UDS process through experimentation and modeling, with the eventual goal of developing novel microstructures by the UDS process in a controlled manner. The specific tasks of our work were: (1) construction of experimental apparatuses suitable for studying the in-flight solidification of traveling uniform droplets and controlled spray forming, (2) characterization and modeling of the solidification of traveling droplets, (3) characterization and development of uniform powders, and (4) controlled spray forming for advanced materials processing.

Thermal State and Solidification of Traveling Droplets

The in-flight thermal state of traveling uniform droplets is the most important parameter that affects the microstructure of the material produced by the UDS process, whether it is a powder or a spray deposit. All droplets in a uniform droplet spray have identical thermal histories, which depend only on the distance traveled [1-4]. It is for this capability that the UDS process is very uniquely different from other existing rapid solidification powder production and spray-forming processes.

Apparatus Construction

We constructed a UDS apparatus that could process low-melting-point alloys for the study of droplet in-flight solidification. Figure 1 shows the apparatus. The main features of the apparatus include a Pyrex glass chamber 9-in.-dia. x 1-m in height, a melting crucible with band heaters, a melt vibrating system, a gas supply system, a droplet charging system, a jet break-up monitor system, a melt temperature control system, and a data acquisition system consisting of a personal computer, a Keithly Metrabyte DAS-TC-DAQ board and Labtech Notebook software. The droplet monitoring system consists of a CCD video camera, a VCR monitor, and a stroboscope, which is synchronized with the piezoelectric transducer through a function generator. The melting furnace is made of AISI 304 stainless steel and can accommodate approximately 0.5 kg of low-melting temperature alloys up to a maximum temperature of about 600°C. This low-temperature apparatus was also used to test/produce uniform powders and balls of tin and tin-based alloys.

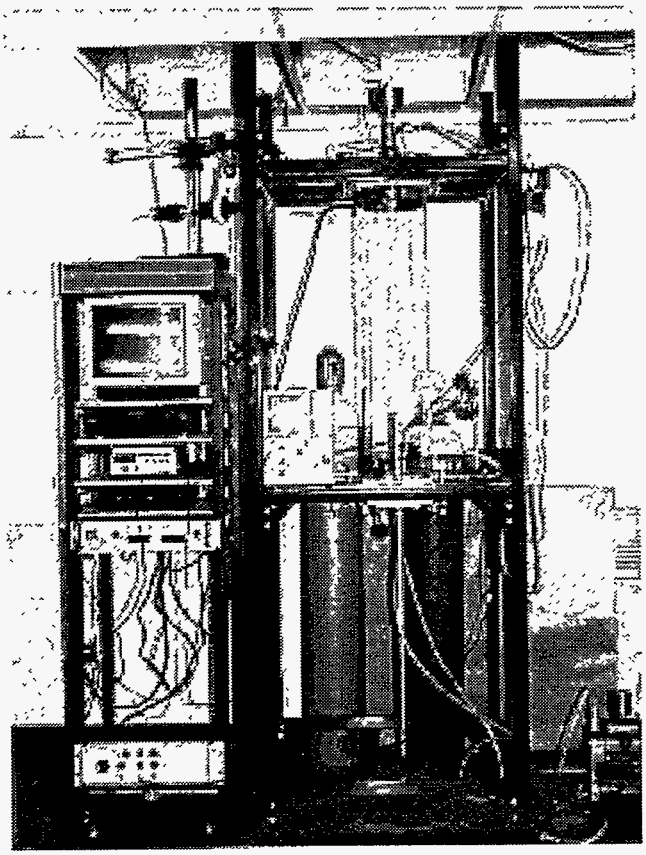

Figure 1. Uniform droplet spray apparatus constructed at Northeastern University.

Modeling of the In-Flight Solidification

We developed a new model for the free dendritic solidification in a binary system that accounts for nonlinear phase boundaries. Assuming linear liquidus and solidus lines (as done in existing models), can lead to significant errors particularly at high undercoolings where the metastable extensions of the phase boundaries are typically nonlinear. The new solidification model, which consists of four implicit equations, were numerically solved for the case of Sn-Pb alloys. The model applies readily to other binary systems and can be extended for ternary and multicomponent systems for which thermodynamic data are available. The types of information that this model generates include the dendrite tip velocity, radius, solute partitioning, and the values of the four components of the undercooling (i.e., the curvature, constitutional, kinetic, and thermal). The latter capabilities are very essential in predicting the resultant microstructures in the UDS process. Figures 2 and 3 show the tip velocity and solute partitioning in Sn-Pb alloys computed as a function of total undercooling.

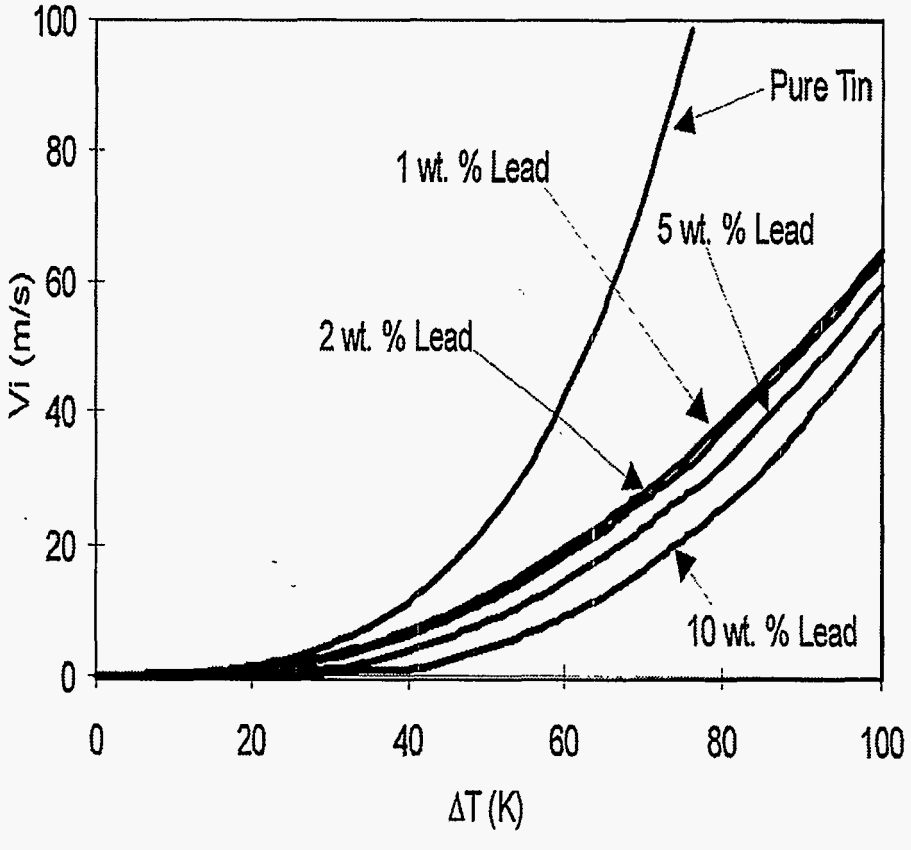

Figure 2. Predicted dendrite tip velocity versus undercooling for various tin-lead alloys.

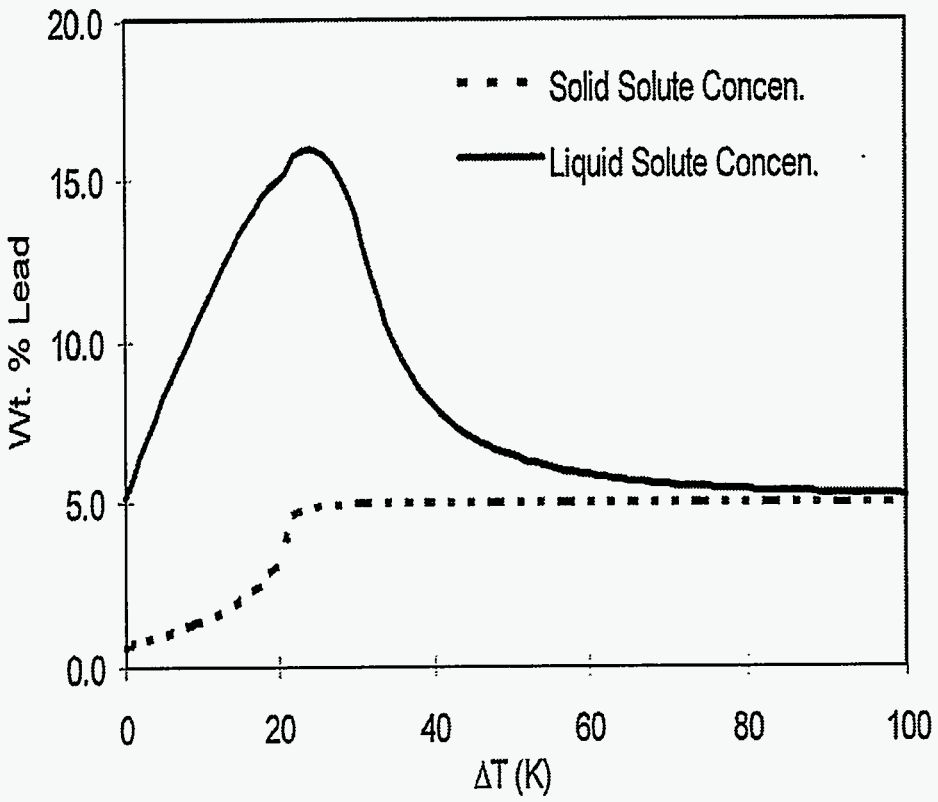

Figure 3. Predicted solute partitioning versus undercooling for Sn-5 wt % Pb alloy.

The developed solidification model is readily applicable to simulating the solidification of traveling uniform droplets. We adopted the schemes developed earlier at MIT, which were used to simulate droplet solidification with no undercooling. In our modification, both the prior undercooling and recalescence are taken into account using the developed solidification model. The recalescence stage is computed separately so that the rapid change in temperature can be simulated with accuracy. Also, the use of the Scheil equation is abandoned as it requires complete solute homogenization in the remaining liquid, which is unrealistic in rapid solidification. The new simulation model predicts the droplet temperature, fraction solid, enthalpy, and solute partitioning as a function of the flight distance. Figures 4 and 5 show simulated enthalpy loss and fraction solid for 100-, 200-, and 300-mm uniform droplets of a Sn-5 wt % Pb alloy.

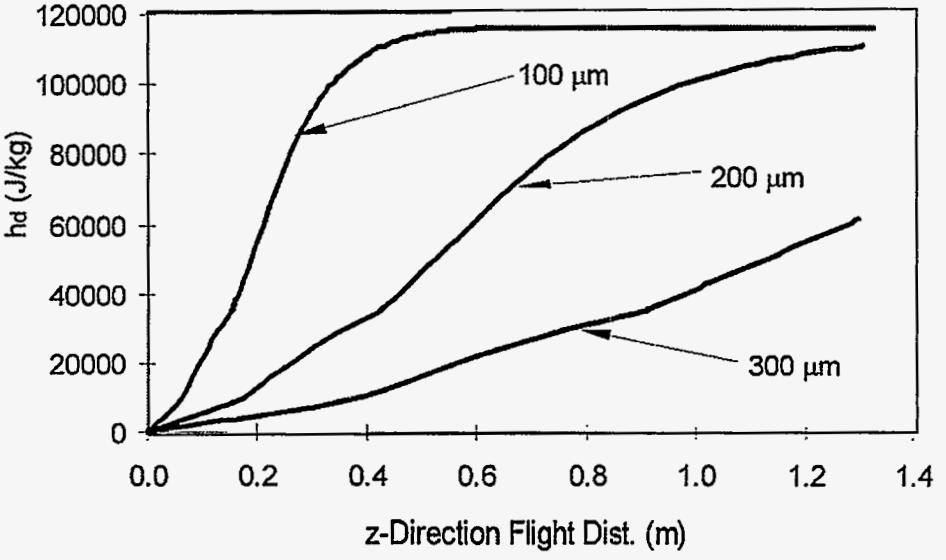

Figure 4. Enthalpy loss per unit mass of uniform droplets calculated as a function of flight distance for 100-, 200-, and 300-μm Sn-5 wt % Pb alloy droplets.

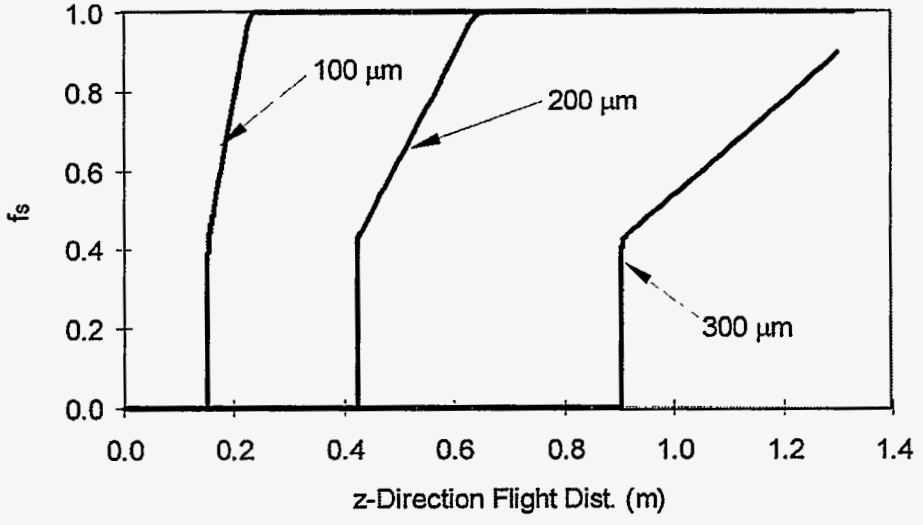

Figure 5. Fraction solid calculated as a function of flight distance for 100-, 200-, and 300-μm Sn-5 wt % Pb alloy droplets.

Droplet Enthalpy Measurement

The enthalpy of droplets produced in the UDS process must be determined as a function of flight distance in order to accurately predict the thermal state of a spray deposit and, consequently, the droplet microstructure. Also, critical information is required for controlled spray forming with uniform droplet sprays. We have developed a nonadiabatic calorimetric method that can consistently determine droplet enthalpy values over a range of flight distance. Figure 6 shows a schematic of the calorimetric apparatus. The need

for collecting droplets in the calorimeter requires a calorimeter design with a large top opening. This inevitably causes significant heat loss from the calorimeter. Such nonadiabatic calorimetry can be carried out only if the heat loss during droplet collection is accounted for. In our method, this is achieved by a calibration technique as described in our publications that resulted from this work [18-20].

Figure 7 shows the values of enthalpy released from 185-mm Sn-5 wt % Pb uniform droplets for a series of runs performed in a N_2 atmosphere containing 35 ppm oxygen together with simulated values of droplet enthalpy. The simulation was done using our droplet solidification simulation model [17]. The simulated droplet enthalpy exhibits moderate cooling rates of about 1.5 10^{-4} J/droplet(cm at flight distances up to about 13 cm and increased cooling rates of about 3.0 10^{-4} J/droplet (cm at greater distances up to about 25 cm. The initial moderate cooling rate result from the aerodynamic shielding effects due to droplet alignment in the travel direction, which decreases the convective heat transfer coefficient. As the droplets scatter due to the repulsive Coulombic forces between them, convective heat transfer increases resulting in the increased cooling rates about 13 cm.

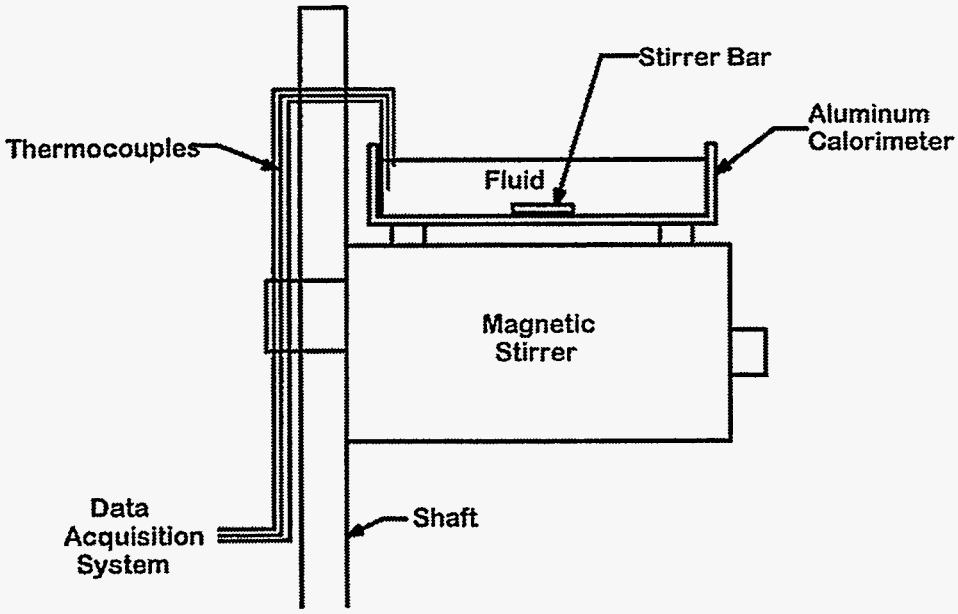

Figure 6. Nonadiabatic calorimetric apparatus.

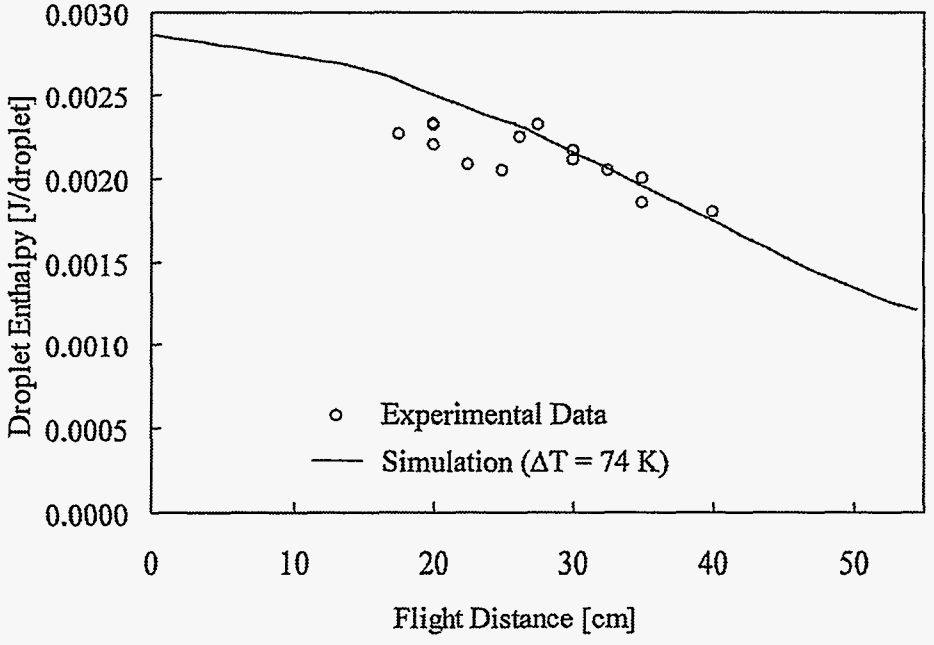

Figure 7. Measured and simulated droplet enthalpy as a function of flight distance. Chamber atmosphere: nitrogen (35 ppm oxygen).

The measured values of released enthalpy decrease at the same rate as simulated droplet enthalpy values but are consistently lower than the simulation by about 3.0 10^{-4} J/droplet up to the flight distance of 25 cm. The sudden increase in measured values of released enthalpy at about 25 cm corresponds to nucleation and subsequent recalescence, which occurred rapidly over a very short flight distance. Above 25 cm, the measured values agree with the simulation. The discrepancy between model and experiment below 25 cm reflects retention of enthalpy in the droplet, which solidified into a metastable microstructure. The prior undercooling at 25 cm was calculated to be 74 K. The simulation shows a further increase in cooling rate above 25 cm, which reflects increased droplet temperatures after recalescence. The measured values closely follow the simulation and decrease at faster rates than those at shorter distances, indicating that the droplets indeed recalesced at 25 cm.

Figure 8 shows the released enthalpy and simulated droplet enthalpy for a series of runs performed in a $CaSO_4$-desiccated N_2 - 2% H_2 atmosphere containing 9 ppm oxygen. Nucleation occurred at a much larger flight distance of about 43 cm, which corresponded to a droplet undercooling of 146 K. Thus, the use of the $CaSO_4$-desiccated N_2 -2% H_2 atmosphere increased the prior undercooling by suppressing the formation of oxides on the droplet surface.

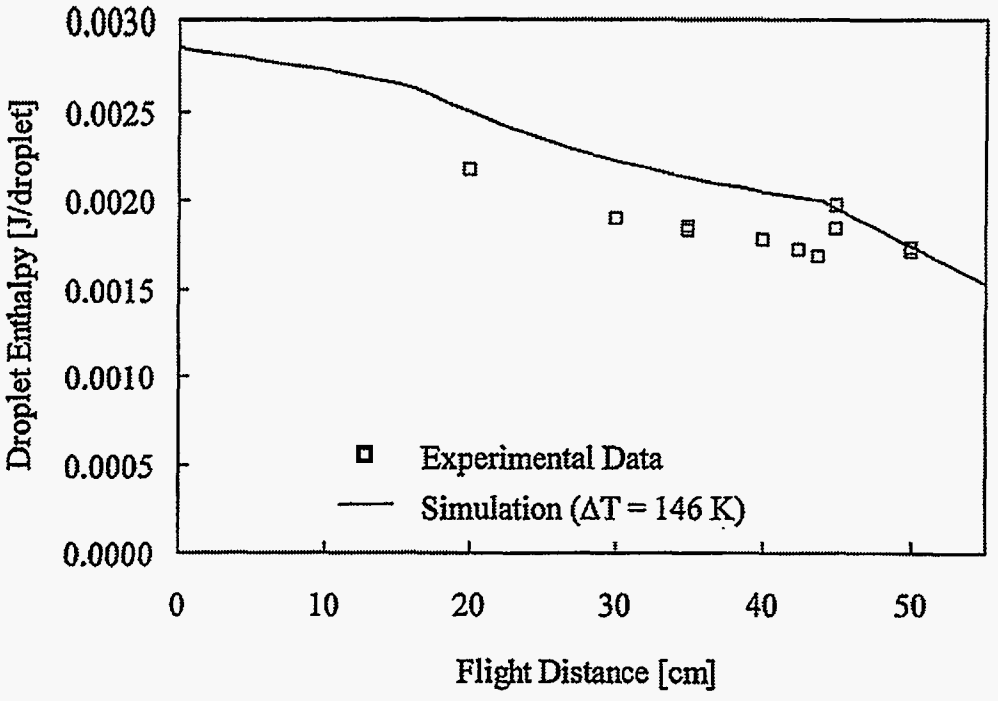

Figure 8. Measured and simulated droplet enthalpy as a function of flight distance. Chamber atmosphere: nitrogen - 2% H_2 (9 ppm oxygen).

Microstructure Evolution

The close agreement between the simulated droplet and experimentally determined enthalpy values after nucleation and recalescence suggests that the solidified droplets collected after recalescence have lost most of the structural metastability, regardless of the degree of prior undercooling. This means that droplets in a thermal spray, whether it is produced by gas atomization or the UDS process, do not solidify into rapidly solidified powders unless they are subjected to secondary quenching while they are still molten. (This argument does not necessarily apply to glass-forming alloys nor to very fine droplets that undergo hypercooling prior to solidification.) In the UDS process, however, controlled droplet quenching in the molten state, or in any stage of droplet solidification, is possible. This secondary quenching may be achieved by quenching into a fluid medium or onto a solid substrate.

Figures 9 and 10 compare the microstructures of 185-mm Sn-5 wt % Pb alloy droplets quenched under different conditions. Clearly, the most uniform rapid solidification microstructures resulted in droplets that were quenched while they are molten [Figures 9(a) and 10(a)]. Segregation and structural coarsening are much more apparent in droplets that were quenched after recalescence whether in oil or on a substrate [Figures. 9(b), 10(b), and 10(c)]. Thus, secondary quenching of uniform droplets combines the

effects of controlled large undercooling and rapid heat removal, a concept which has not been realized in most existing rapid solidification processes. This ultimate level of rapid solidification effects, together with the assurance of structural uniformity, has profound implications in industrial applications.

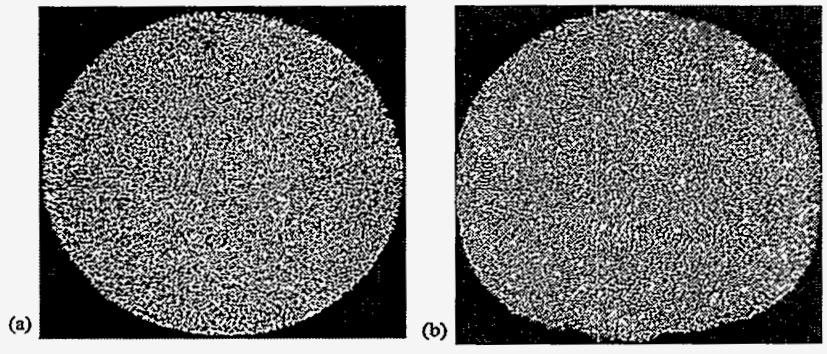

Figure 9. The 185 μm Sn-5 wt % Pb alloy droplets quenched in (a) oil before nucleation and (b) after nucleation and recalescence.

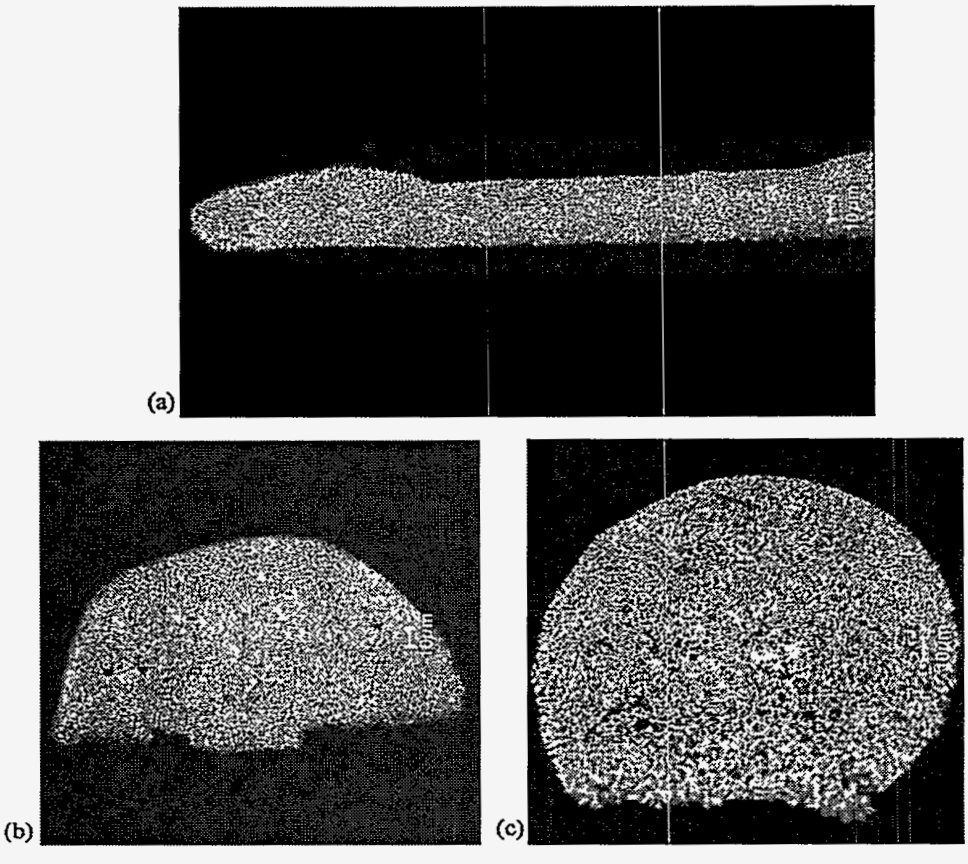

Figure 10. The 185-μm Sn-5 wt % Pb alloy droplets quenched on a metallic substrate (a) before nucleation at a flight distance of 35 cm, (b) after nucleation and recalescence at a flight distance of 45 cm, and (c) after nucleation and recalescence at a flight distance of 50 cm.

Industrial Applications

Uniform Powders

Using the low-temperature UDS apparatus that we constructed (Figure 1), we processed tin and tin alloys to produce uniform powders in diameters range from 50 to 1000 mm. Among them, uniform powders 750-mm-dia. are of particular industrial importance due to their potential use as micro-solder balls for ball-grid array IC packaging. Uniform tin-lead alloy solder balls, 750-mm-dia. for the ball-grid array application have been successfully produced by the UDS process and compared with commercial balls produced by the less efficient, cut-wire remelting technique employed in current ball-grid array solder ball production. Our results have been published jointly with MIT and ORNL [21,22]. Use of UDS solder balls in ball-grid array packaging is expected to increase in future, particularly in conjunction with the development of lead-free and/or higher melting-point solder alloys. Thus, further process optimization is necessary and are continued in our study with the particular goals of improving the sphericity, surface quality, and size distribution in mass production.

We have also improved our apparatus to enable the stable production of <100 mm powders. Fine uniform powders have many potential applications such as metal injection molding. However, producing fine uniform powders by the UDS process is difficult due to orifice clogging and vibration damping effects at high frequencies. We are modifying the crucible bottom design to allow for stable uniform breakup. Figure 11 shows a 78-mm uniform powder of a Sn-5 wt % Pb alloy produced using a modified crucible bottom. Work is under way to further optimize conditions and design for the mass production of finer uniform powders.

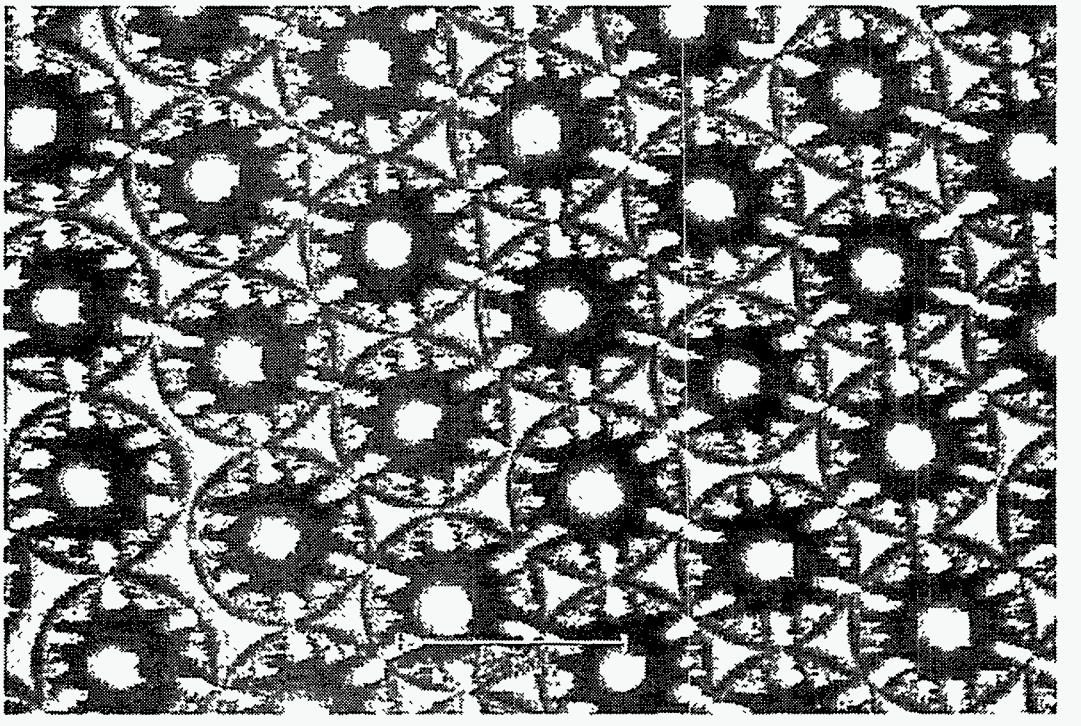

Figure 11. The 78 -μm uniform powder of a Sn-5 wt % Pb alloy.

Controlled Spray Deposition

In order to extend our capabilities of the UDS process for controlled spray deposition of engineering alloys, a high-temperature UDS apparatus has been designed and constructed (Figure 12). The spray deposition system consists of a deposition chamber, a motion-controlled substrate system, and a high-temperature droplet generator. The deposition chamber measures 40-in-dia. x 26-in.-high with a top-mounted furnace section that houses a high-temperature melting furnace. The chamber is rated as a high vacuum chamber and permits complete preevacuation prior to backfilling with an inert gas. It also permits controlled spray deposition in vacuum. The substrate motion is computer-controlled in the X- and Y-directions using two linear motion control tables powered by dc stepper motors. Another table is to be added to control the motion in the Z-direction. Optical encoders determine motor velocity and position and control is implemented using a MC Basic motion control package and cascaded single axis servo controllers. Substrate temperature can be controlled via water circulation or arrays of thermoelectric cooling modules.

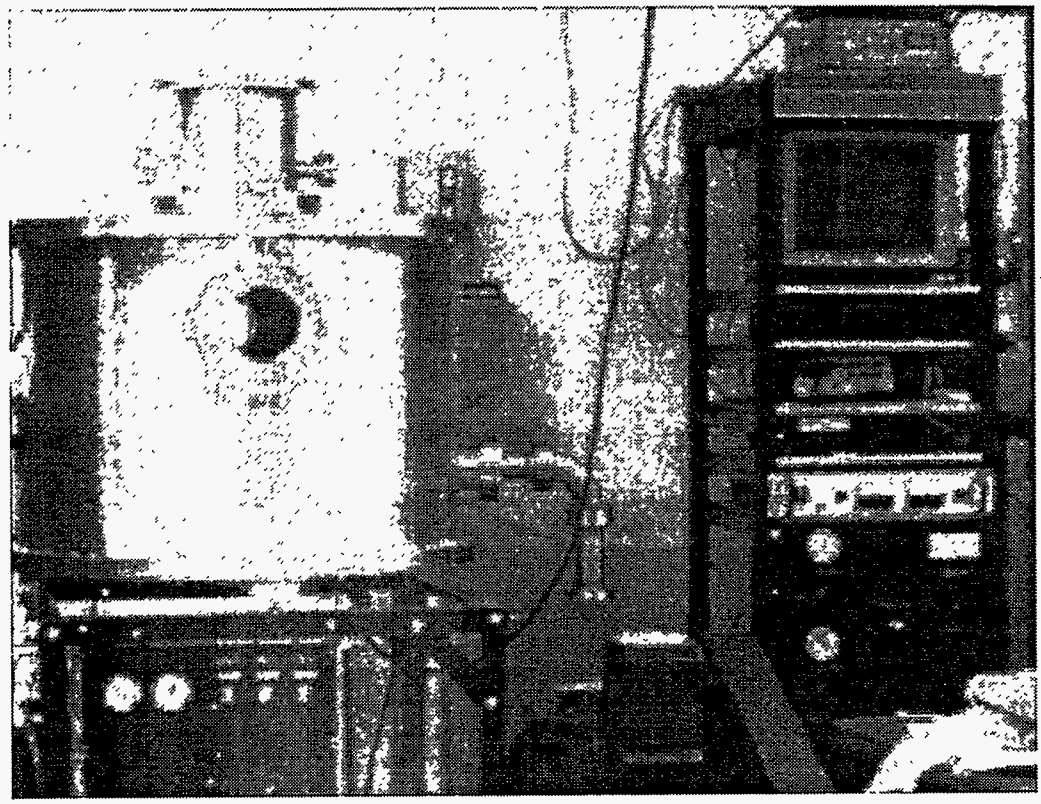

Figure 12. Controlled spray deposition system built at Northeastern University.

Controlled spray deposition is the main focus in the final stretch of our work. The planned areas of our work in controlled spray deposition are: (1) production of novel deposit microstructures, (2) spray forming for aluminum sheet, and (3) processing of immiscible alloys.

List of Supported Graduate Students

The following graduate students obtained partial or full support from this grant from the Advanced Materials Program of the U.S. Department of Energy under contract DE-AC05-96OR22464 with Lockheed Martin Energy Research Corporation (subcontract 19X-ST367V) for their work towards their degrees. The graduate students are listed in Table 1.

Table 1. Graduate students.

Name	Institution	Degree	Graduation date
Rajesh Shingavi	Tufts University	M.S.	May 1995
Alfred G. DiVenuti	Tufts University	M.S.	May 1996
Charles D. Tuffile	Tufts University	M.S.	May 1996
	Northeastern University	Ph.D.	June 2000[a]
Younes Abesi	Northeastern University	M.S.	June 1998[a]
Walter Fortner	Northeastern University	M.S.	June 1998[a]
Xiaotao Dong	Northeastern University	M.S.	June 1999[a]

[a]Expected graduation date.

TECHNICAL PROGRESS - FY 1997

Massachusetts Institute of Technology (MIT)

Summary

Task 1. Study of the impact behavior of uniform droplets

One of the primary motivations to study droplet spreading behavior is to find the conditions which determine the impact types such as nicely spreading, splashing, etc. Impact types have direct influences on the porosity formation, packing (deposition) efficiency, oxygen incorporation, etc. In general, it is desirable to keep the spray conditions to achieve the impact behavior of nicely spreading for the best quality of sprayed deposits or coatings. Experimental efforts are being exerted to monitor the actual spreading behavior of droplets using microdroplet spreading sensors. At the same time, an analytical model is being developed to predict the impact types with given impact conditions.

A currently developed model predicts and quantifies the mechanism of splashing unstable wave propagation around a splat periphery. Figure 13 shows an example of a splashed droplet. As an origin of the splashing, it is proposed that the instability on a periphery of a droplet be induced by high-impact inertia and that the growth rate overcome the elastic limit of the liquid resulting in a splashed splat. Furthermore, the Rayleigh-Taylor instability theory suggests that the instability of a rapidly decelerating interface and the subsequent formation of surface tension-dominated waves be the basic mechanism of splashing.

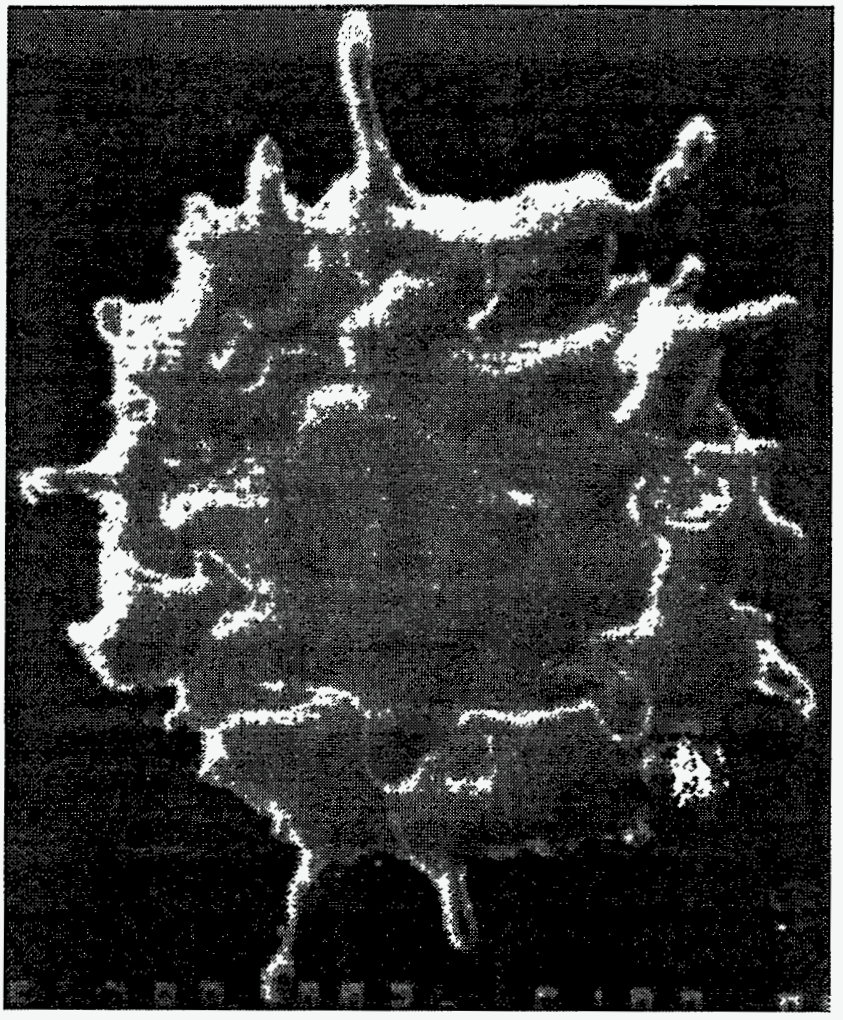

Figure 13. Splashed droplet.

When two fluids of different densities are accelerated towards each other, the instability occurs at the plane interface between the two fluids. The current model ignores the viscosity of both fluid and environment, and estimates the maximum deceleration of the spreading droplet using the characteristic spreading time and the initial rim-jet velocity (about three times higher than impact velocity). This order-of-magnitude model was used to predict the wavelength of the tin splat shown below, whose initial diameter was 321 mm and impact speed, 6.2 m/s. The calculated wavelength was 160 mm. The radius of the splat is 449 mm, the number of major fingers shown is approximately 17, and the corresponding actual wavelength is 166 mm, which is in good agreement with the model.

It has been shown that Rayleigh-Taylor instability can be a possible mechanism of the star-like finger formation in the droplet splashing. The model presented above has included an effect of surface tension, but a viscosity effect has been neglected. In addition, the deceleration rate assumes several uncertain quantities. Therefore, a more complicated model which accounts for viscosity needs to be employed, and an exact experimental value of liquid spreading speed is necessary.

According to the theory, although it assumes inviscid flow, instability always exists for sufficiently long wavelengths. For this theory to be useful in the determination of the splashing threshold, a further study on the disturbance stabilizing factors such as viscosity as well as surface tension should be conducted. The bifurcation behavior of liquid fingers emerging from the spreading droplets needs to be studied if the disintegration of the splashed droplets is to be understood.

Task 2. Applications to engineering alloys and processes

Optimization of closed-loop control of the UDS system apparatus for the production of uniform powders. Repeatability tests were performed after the ball-sized control was implemented to the UDS process. These tests showed that the control system can deliver a very high percentage of the solder ball production within specification limits. In every run, more that 99.9% of the total production was within specifications. However, the current control algorithm is consistently placing the mean ball diameter below the target diameter. This behavior is predictable from the dynamics of the process; the ball diameter is constantly decreasing as the hydrostatic pressure inside the crucible decreases with time. The control algorithm does not make a frequency correction until the ball diameter hits the lower control limit. Then, the ball diameter is brought back to the target diameter, and then it starts to decrease again. Thus, the final mean ball diameter is placed between the target diameter and the lower control limit. The evidence shows that the control system is biased towards the lower control limit.

Currently, new control algorithms are being tested. The first approach used to solve the biasing problem was to combine the current control algorithm with statistical process control (SPC). This way, the SPC part of the new control algorithm will be able to identify any trend and make the necessary corrections. Preliminary results have shown that, in fact, the mean ball diameter is no longer biased; but the variation of the ball size distribution increased considerably. The new SPC control algorithm offers a nonbiased, high-variation, ball size distribution. After the lack of success in implementing SPC into the control algorithm, a new control method is being developed. This new control method includes the dynamics of the UDS process in the computation of the control corrections. In other words, it uses the current control algorithm to maintain the ball diameter within the control limits, while constantly compensating for the change in hydrostatic pressure. This method was implemented and is being tested for mean ball bias and variation.

Spray forming of continuous aluminum strip

Previous studies have shown that the quality of spray-formed parts strongly depends on the heat and mass flux distribution of the spray as it impacts the deposit surface. In our efforts to apply the UDS process to the production of aluminum sheet material, we have modeled the thermal and dynamic states of the droplets during flight. Using a droplet quenching technique, the evolution of microstructure in traveling droplets of Al-4.5 wt % Cu and Al-4.3 wt % Fe was observed. However, due to the existence of a mushy zone in the Al-Cu droplets and undercooling of the Al-Fe droplets, it was not possible to measure the liquid fraction of the droplets to validate the droplet solidification model. Currently, our efforts have been focused on developing an alternative method to measure the thermal state of the traveling droplets.

Microelectronic temperature sensors based on the resistive temperature detection concept were designed and fabricated to measure the impact temperature of droplets at different flight distances. Using boron-doped silicon as the sensing material, the temperature sensors are expected to show a sensitivity of about 0.7%/K. Each chip device has three arrays of sensor pads, as shown in Figure 14, which can be used to detect droplet impact temperature as well as the temperature profile of the droplet during spreading. Due to the nonlinear behavior of the sensors resistance as a function of temperature and the contact resistance between the droplet and the sensor, each chip is currently being calibrated. After calibration, the goal is to place the sensors in the path of the droplet spray and acquire the droplet impact temperature with high-speed data acquisition hardware.

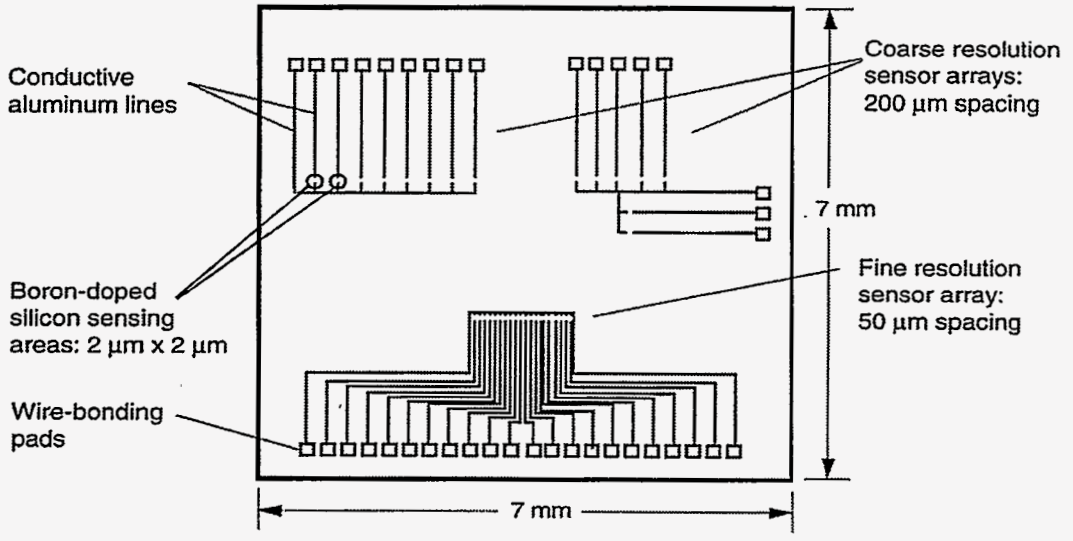

Figure 14. Schematic of microelectronic temperature sensor.

REFERENCES

1. C. H. Passow, M.S. thesis, Dept. of Mechanical Engineering, Massachusetts Institute of Technology (1990).

2. C. H. Passow, J.-H. Chun, and T. Ando, Metall. Trans. A, 24A, 1187 (1993).

3. T. Ando, J.-H. Chun, and S. Sahu, Proc. 93 PM World Congress, Part II., Kyoto, Japan: Jap. Soc. of Powder and Powder Metall., 971 (1993).

4. C.-A. Chen, S. Sahu, J.-H. Chun, and T. Ando, Science and Technology of Rapid Solidification and Processing, NATO ASI Series, Series E-Vol. 278, Kluwer Academic Publishers, Dordrecht, 123 (1994).

5. C.-A. Chen, J.-H. Chun, and T. Ando, Proc. 1994 Powder Metall., Toronto, 1994.

6. A.R.E. Singer, Met. Mater., 4, 246 (1970).

7. A.R.E. Singer and R. W. Evans, Met. Technol., 10, 61 (1983).

8. A. G. Leatham, R. G. Brooks, and M. Yaman, Modern Developments in Powder Metallurgy, 15, E.N. Aqua et al., eds., APMI: Princeton, New Jersey, 157 (1985).

9. E. J. Lavernia and N. J. Grant, Int. J. Powder Metall., 2(2), 93 (1986).

10. Y. Ikawa, K. Kumagai, H. Hamabe, Y. Ozaki, and S. Yamauchi, J. Jap. Inst. Met., 30(6), 548 (1991).

11. S. Matsuo, T. Ando, M. C. Zody, and N. J. Grant, Advances in Powder Metall., 5, L. F. Pease III et al., eds., APMI: Princeton, New Jersey, 161 (1991).

12. P. Mathur, D. Apelian, and A. Lawley, Acta Metall. Mater., 37(2), 429 (1989).

13. B. P. Bewlay and B. Cantor, Metall. Trans., 20B, 899 (1990).

14. X. Liang, J. C. Earthman, and E. J. Lavernia, Acta Metall. Mater., 40, 3003 (1992).

15. J. Lipton, M. E. Glicksman, and W. Kurz, Metall. Trans. A, 18A, 341 (1987).

16. W. Boettinger, S. R. Coriell, and R. Trevedi, Rapid Solidification Processing - Principles and Technologies, IV, R. Mehrabian and P. A. Parrish, eds. Claitors Publishing Division, (1988).

17. A. G. DiVenuti, M.S. thesis, Tufts University (1996).

18. C. D. Tuffile, M.S. thesis, Tufts University (1996).

19. C. D. Tuffile, A. G. DiVenuti, T. Ando, and J.-H. Chun, J. Materials Synthesis and Processing, 5(1), 31-37 (1997).

20. C. D. Tuffile, T. Ando, and J.-H. Chun, submitted to the Proc. TMS Annual Meeting (1998).

21. P. W. Yim, J.-H. Chun, T. Ando, and V. K. Sikka, Int. J. Powder Metall., 32(2), 155-64 (1996).

22. P. W. Yim, J.-H. Chun, T. Ando, and V. K. Sikka, Proc. Int. Conf. on Powder Metallurgy and Particulate Materials, Seattle, Washington (May 14-17, 1995).

PUBLICATIONS

P. W. Yim, J.-H. Chun, T. Ando, and V. K. Sikka, Production and Characterization of Mono-Sized Sn-38 wt % Pb Alloy Balls, Int. J. Powder Metall., 32(2), 115-64 (1996).

C. D. Tuffile, A. G. DiVenuti, T. Ando, and J.-H. Chun, Calorimetric Enthalpy Measurement of Traveling Uniform Droplets, J. Mater. Synthesis and Processing, 5(1), 31-37 (1997).

C. D. Tuffile, T. Ando, and J.-H. Chun, Characterization of the In-Flight Solidification of Sn-Pb Uniform Droplets, submitted to the Proc. 1998 TMS Annual Meeting.

PRESENTATIONS/THESES

C. A. Blue, V. K. Sikka, J.-H. Chun, and T. Ando, Uniform-Droplet Process, poster, ASM Educational Symposium, Oak Ridge, Tennessee (April 7, 1995).

P. W. Yim, J.-H. Chun, T. Ando, and V. K. Sikka, Production and Characterization of Mono-Sized Sn-38 wt % Pb Alloy Balls, Int. Conf. on Powder Metallurgy and Particulate Materials, Seattle, Washington (May 14-17, 1995).

J.-H. Chun, C. A. Blue, V. K. Sikka, and T. Ando, The Uniform-Droplet Spray Process, poster, Advanced Industrial Materials Program Annual Meeting, Washington, DC (June 14-16, 1995).

C. A. Blue, V. K. Sikka, J.-H. Chun, and T. Ando, Uniform-Droplet Spray Forming, poster, Advanced Industrial Materials Program Annual Meeting, Oak Ridge, Tennessee (June 24-26, 1996).

C. A. Blue, V. K. Sikka, J.-H. Chun, and T. Ando, Uniform-Droplet Spray Process, poster, Advanced Industrial Materials Program Annual Meeting, Albuquerque, New Mexico (June 16-18, 1997)

Rajesh Shingavi, Processing and Characterization of Uniform-Droplet Sprayed Sn and Sn-Pb Alloys, M.S. thesis, Tufts University (1995).

Charles D. Tuffile, Characterization of the Thermal State and Solidification in the Uniform-Droplet Process, M.S. thesis, Tufts University (1996).

Alfred G. DiVenuti, Modeling of the Solidification of the Solidification in the Uniform-Droplet Process, M.S. thesis, Tufts University (1996)

HONORS AND AWARDS

None.

PATENTS/DISCLOSURES

ERID No. 0263, S-87,628

LICENSES

Uniform Metals Technologies, Inc. (Watertown, Massachusetts)
Aeroquip Corporation (Ann Arbor, Michigan)

INDUSTRIAL INPUT AND TECHNOLOGY TRANSFER

Aeroquip Corporation (Ann Arbor, Michigan)
Alcoa Aluminum (Alcoa Center, Pennsylvania)
Hoeganaes (Riverton, New Jersey)
Micro Engineering (Cinnaminson, New Jersey)
Uniform Metals Technologies, Inc. (Watertown, Massachusetts)

Contacts who have an interest in the UDS process:

ACuPowder International, LLC (Union, New Jersey)
Allvac (Monroe, North Carolina)
Ametek Specialty Metal Products Division (Wallingford, Connecticut)

Eckart America L.P. (Louisville, Kentucky)
Ervin Industries, Inc. (Ann Arbor, Michigan)
Homogeneous Metals (Clayville, New York)
Los Alamos National Laboratory (Los Alamos, New Mexico)
Postle Industries Inc. (Cleveland, Ohio)
SCM Metal Products, Inc. (Research Triangle Park, North Carolina)
Wright-Patterson Air Force Base (Kettering, Ohio)

NEW MATERIALS AND PROCESSES

ADVANCED INDUSTRIAL MATERIALS (AIM) FELLOWSHIP PROGRAM

D. Duncan McCleary

Science/Engineering Education Division
Oak Ridge Institute for Science and Education
Oak Ridge, Tennessee 37830

P. S. Sklad

Metals and Ceramics Division
Oak Ridge National Laboratory
P. O. Box 2008, Oak Ridge, Tennessee 37831

INTRODUCTION

The Advanced Industrial Materials (AIM) Program administers a Graduate Fellowship Program focused toward helping students who are currently under represented in the nation's pool of scientists and engineers, enter and complete advanced degree programs.

The objectives of the program are to: 1) establish and maintain cooperative linkages between the Department of Energy (DOE) and professors at universities with graduate programs leading toward degrees or with degree options in Materials Science, Materials Engineering, Metallurgical Engineering, and Ceramic Engineering, the disciplines most closely related to the AIM Program at Oak Ridge National Laboratory (ORNL); 2) strengthen the capabilities and increase the level of participation of currently under represented groups in master's degree programs, and 3) offer graduate students an opportunity for practical research experience related to their thesis topic through the three-month research assignment or practicum at ORNL.

The program is administered by the Oak Ridge Institute for Science and Education (ORISE). The following abstracts summarize the activities of three of the participants.

SECTION 1.

OPTICALLY MONITORING CONDUCTIVE Bi_2O_3 CONTENT IN FERROELECTRIC CAPACITORS

B. D. Dickerson

Materials Science and Engineering Department
Virginia Polytechnic Institute and State University
Blacksburg, Virginia 24061-0237

E. A. Kenik and S. B. Desu*

Metals and Ceramics Division
Oak Ridge National Laboratory
P. O. Box 2008, Oak Ridge, Tennessee 37831

* author to whom correspondence should be addressed

INTRODUCTION

A systematic analysis method based on effective-media approximations (EMA) enabled variable angle spectroscopic ellipsometry (VASE) to accurately characterize second-phase Bi_2O_3 contamination in ferroelectric $SrBi_2Ta_2O_9$ (SBT) films. Excess Bi_2O_3 is often included in precursor solutions for metal-organic deposition (MOD) of SBT to promote grain growth at lower annealing temperatures. However, any second phase Bi_2O_3 which remains in the final crystallized film may significantly increase the leakage current through the SBT capacitor, which would degrade performance by increasing noise and power consumption in pyroelectric thermal imaging arrays and nonvolatile random-access memories. It will be shown that VASE analysis could estimate Bi_2O_3 concentrations in SBT films even when x-ray diffraction (XRD) could not.

TECHNICAL PROGRESS - FY 1997

Samples were optically characterized using a Woollam spectroscopic ellipsometer (Lincoln, NE) to measure the polarization angles, Δ and Ψ, as a function of wavelength, λ, and incident angle, θ. The D and Y spectra were also simulated using Bruggeman effective-media approximations (EMA)[10] to estimate the behavior of a homogeneous mixture of SBT and Bi_2O_3. These two materials were found to have distinct optical properties in the wavelength range from 300 nm to 500 nm, due to high absorption in

Bi_2O_3 near 4.0 +- 0.1 eV. Therefore the Bi_2O_3 contents of contaminated SBT films could be estimated using WVASE curve fitting software.

As expected from the presence of a more conductive second phase, the conductivity of contaminated films was generally several orders of magnitude higher than that of standard SBT. The standard SBT sample had a low-leakage current density of 10^{-8} A/cm^2 under an applied field of 100 kV/cm. For films with 5 % to 10 % Bi_2O_3, according to the EMA method, the leakage current flux was 0 to 3 orders of magnitude higher than in standard SBT, but SBT grains were sufficiently large (~150 nm) to produce acceptable remnant polarizations of 8×10^{-6} C/cm^2. Films that contained 15 ± 2 % Bi_2O_3 had leakage current densities that were 2 to 6 orders of magnitude higher than standard SBT, and the grains were 50 % smaller (~75 nm). For infrared detectors and ferroelectric memories, larger grains are desired to develop stronger reversible polarizations for higher signal to noise ratios. Ellipsometry was able to estimate second phase Bi_2O_3 contents that were consistent with measured electrical properties.

X-ray diffraction (XRD) is a traditional method of monitoring phase formation. However, in this case both normal and defective films produced nearly identical XRD patterns. Although trace amounts of Bi_2O_3 were detected, XRD could not detect any significance difference in Bi_2O_3 content. Two factors may explain the limitations of XRD in this materials system. SBT and Bi_2O_3 are crystallographically similar. The Bi_2O_3 particles may have been so small that many Bi_2O_3 diffraction peaks became wide and lost in background noise.

CONCLUSIONS

Using EMA principles, VASE measured the amount of second phase Bi_2O_3 in SBT films made by MOD. Optically detectable Bi_2O_3 in SBT films generally reduced grain size and increased leakage current. Ellipsometry was particularly useful in this system because XRD did not show any consistent trends in Bi_2O_3 peak heights, even between films with drastically different electrical properties. A more detailed description of these results has been submitted for publication.

ACKNOWLEDGMENTS

I would like to thank Tirumala Shridhar, Pooran C. Joshi, and Allen Matthys for making the samples used in this study.

This research was sponsored by the U.S. Department of Energy, Assistant Secretary for Energy Efficiency and Renewable Energy, Office of Industrial Technologies, Advanced Industrial Materials (AIM) Program; and Division of Materials Sciences, under contract DE-AC05-96OR22464 with Lockheed Martin Energy Research Corporation as an AIM Fellowship administered by the Oak Ridge Institute for Science and Education. Research utilized the Shared Research Equipment (SHaRE) User Facilities at Oak Ridge National Laboratory.

PUBLICATIONS

B. D. Dickerson, E. A. Kenik, and S. B. Desu, Characterization of Ferroelectric Films. by Spectroscopic Ellipsometry, Journal of Materials Research, submitted December 17, 1997.

SECTION 2.

1. PHASE TRANSFORMATION STUDIES IN MECHANICALLY ALLOYED Fe-Zn-Si INTERMETALLICS

2. EFFECTS OF MINOR ALLOYING ADDITIONS ON THE PHASE TRANSFORMATIONS AND KINETICS OF FeAl AND Ni_3Al BASED ALLOYS

A. Jordan and O. N. C. Uwakweh

Materials Science and Engineering Department
University of Cincinnati
498 Rhodes Hall, Cincinnati, Ohio 45221-0012

P. J. Maziasz

Metals and Ceramics Division
Oak Ridge National Laboratory
P.O. Box 2008, Oak Ridge, Tennessee 37831

INTRODUCTION

The first part of this study is a continuation of work done in FY 1996, which is a more detailed analysis characterizing the influence of Si in the Fe-Zn system and how it affects the overall properties of an Fe-Zn coating. The zinc coating of Si bearing steels (i.e., Si in the range of 0.12 wt. %) during galvanization processes, is generally plagued with an abnormal development of the coating thickness, otherwise known as the Sandelin effect. The microstructural changes cause problems such as, diminished corrosion resistance, poor coating adherence and uncontrollable coating thickness. To study this phenomenon, the effect of Si in the Fe-Zn system through a solid-state reaction process involving non-equilibrium means was used. This entails the use of a high-energy processing technique involving the ball-milling of elemental powders of appropriate compositions, which yield metastable materials, whose transformation to equilibrium following thermal anneals are evaluated.

The second part of this study is a joint project with Oak Ridge National Laboratory (ORNL) to evaluate the effects of minor elemental additions on the microstructure, and phase transformations of iron and nickel based aluminides. These materials have great potential for use in structural applications because they have an excellent combination of high strength, corrosion, and oxidation resistance properties. However, a major concern is that these materials possess low ductility and poor resistance to fracture in room temperature environments. In addition, these alloys are also susceptible to solidification

cracking, which in turn, affects their ability to be welded. While an extensive amount of work has been geared towards improving the ductility and resistance to brittle fracture in these materials, little information exists concerning their solidification behaviors and pertinent phase transformations due to the addition of minor elements. The phase transformation kinetics occurring during the heating and cooling of these materials (i.e., simulated welding process), is essential to tailoring a specific welding technique in order to create sound welds that are free from defects. The focus of this study is to evaluate the phase transformation sequence of the alloys in their pre-existing condition, for the purpose of understanding and predicting the behavior of these materials during certain process applications such as welding.

TECHNICAL PROGRESS - FY 1997

1. Alloy Processing

The alloy compositions used in this study are listed in Tables 1, 2 and 3. The Fe-Zn-Si alloys studied were prepared from high purity powders ($\geq$ 99.9 %). A total of 10 grams was ball milled continuously for 8 hours under a controlled argon atmosphere. The FeAl and Ni3Al based alloys, which are previously being studied, were provided by ORNL. The 1" x 0.5" x 0.5" ingots were prepared by arc melting under argon and drop casting into copper chilled molds.

Table 1. Fe-Zn-Si Compositions Ball-Milled.

Phase designation base on Fe to Zn ratio	*Composition in wt. %*		
	Fe	Zn	Si
$\Gamma(Fe_3Zn_{10}) + Si$	25.37	74.51	0.12
$(\Gamma + \Gamma_1) + Si$	22.14	77.74	0.12
$\Gamma_1\ (Fe_5Zn_{21}) + Si$	18.03	81.85	0.12
$\delta\ (FeZn_7) + Si$	9.10	90.78	0.12
$(\delta + \zeta) + Si$	6.47	93.41	0.12
$\zeta(FeZn_{13}) + Si$	5.60	94.28	0.12

Table 2. Compositions of FeAl based alloys provided by ORNL, composition in wt. %.

Alloy Identification	*Fe*	*Al*	*Mo*	*B*	*Zr*	*C*
Heat #564	77.48	22.10	0.42			
Heat #565	77.475	22.10	0.420	0.005		
Heat #567	76.630	22.10	0.420		0.150	0.700
Heat #568	76.625	22.10	0.420	0.005	0.150	0.700

Table 3. Compositions of Ni_3Al based Alloys provided by ORNL, composition in wt. %.

Alloy Identification	*Ni*	*Al*	*Cr*	*B*	*Zr*	*Mo*
Heat #560	84.295	8.000	7.700	0.005		
Heat #561	82.595	8.000	7.700	0.005	1.700	
Heat #562	81.295	8.000	7.700	0.005	3.000	
Heat #563	81.095	8.000	7.700	0.005	1.700	1.500

2. FeSi Phase Formation in Fe-Zn-Si Ternary Alloys

Based on DSC thermal analyses, and X-ray diffraction (XRD) measurements, an equilibrium isopleth of the Fe-Zn-Si system at a constant Si content of 0.12 wt. % was determined, and is shown in Figure 1. The figure depicts a plot of temperature versus Fe content identifying points obtained from XRD patterns. The hatched area shows where FeSi is expected to be an equilibrium phase in a two- or three-phase field. In essence, this figure shows that the FeSi phase forms in the Fe-Zn-Si system even when limited amounts of Si are present in the Fe-Zn binaries. This shows that the kinetic reaction, as opposed to the thermodynamic evolution, accounts for the Sandelin process. Thus, the suppression of the FeSi formation during coating processes lead to various microstructures associated with the Sandelin process.

Data on the isopleth at constant 0.12 wt% Si in the Fe-Zn-Si system is shown in Figure 1.

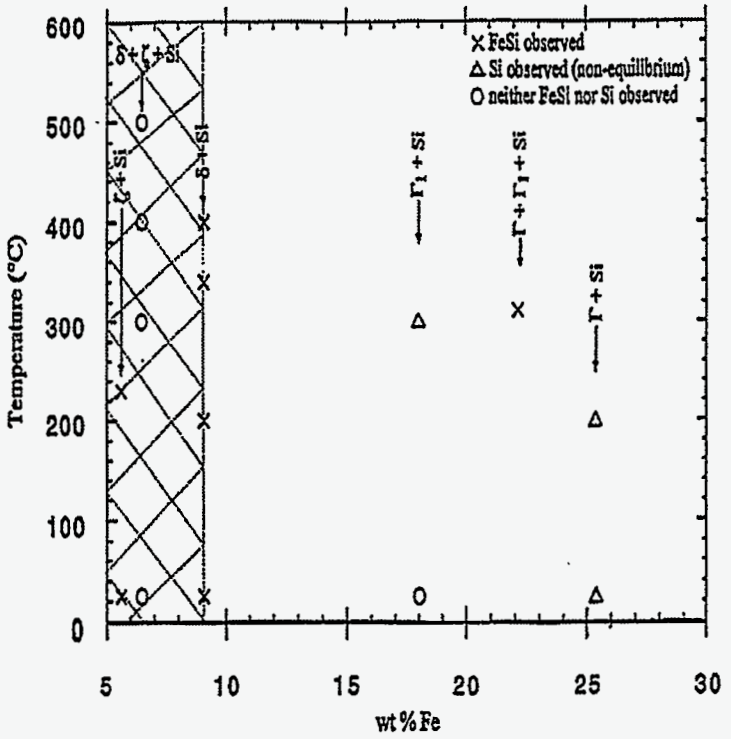

Figure 1. Isopleth at constant 0.12 wt.% Si in the Fe-Zn-Si system. The region of stability for FeSi is shown by the cross-hatched lines.

3. Microstructural Features and Thermal Analyses of FeAl Alloys (selective results)

Optical micrographs of the as-cast FeAl materials containing, (Fe-22.10Al-0.420Mo-0.005B, Heat #565), and (Fe-22.100Al-0.700C-0.420Mo-0.150Zr-0.005B, Heat #568), are shown in Figures 2 and 3, respectively. There is an obvious change in the microstructure with the addition of Zr and C. The Fe-Al-Mo-B material shows a structure with varying grain sizes, whereas, the Fe-Al-Mo-B-Zr-C alloy forms a dendritic structure. DSC results on heating and cooling of the Fe-Al-Mo-B alloy material are shown in Figures 4 and 5, respectively. The endothermic and exothermic reactions, along with the reaction temperatures, are indicated on the plots for the various heating rates selected.

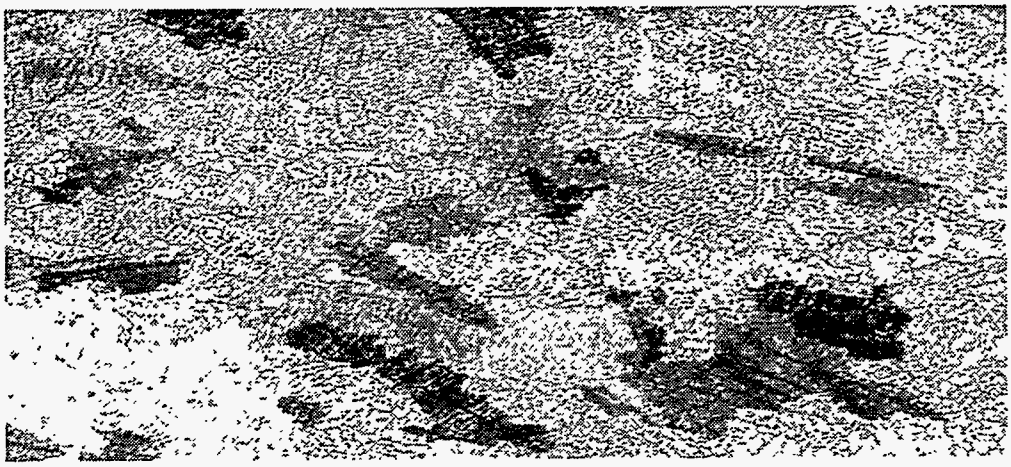

Figure 2. Optical micrograph of Fe-Al-Mo-B (heat #565) material. Magnification=50X.

The melting and solidification temperatures are listed in Table 4. The first endothermic process observed upon heating the Fe-Al-Mo-B material occurs between 741°-755°C. Although not confirmed, this peak is most likely a result of the materials transformation through the Fe_3Al phase field. This is based of the fact that some segregation may have occurred during material processing. Preliminary kinetics analysis of the endothermic reaction reveals that the process is diffusion controlled with an activation energy of 89 kJ/mole. The second endothermic reaction is only observed at a heating rate of 40°C/min and is associated with the order/disorder temperature (i.e., 1200°C), as shown in Figure 4. The last endothermic peak is associated with melting of the material. On cooling, two reactive processes are observed from Figure 5. The exothermic reaction between 1446°-1434°C is the solidification peak. The peak which occurs at 1162°C for a heating rate of 40°C/min is where the material re-orders.

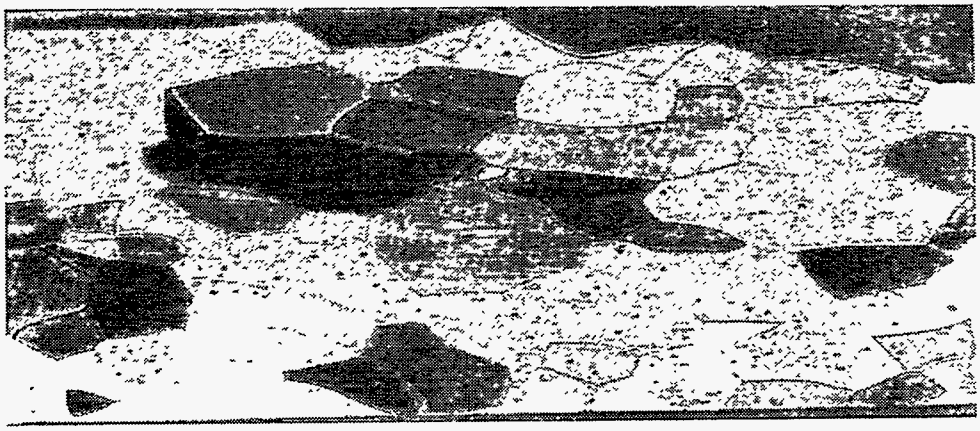

Figure 3. Optical micrograph of Fe-Al-Mo-Zr-C-B (heat #568) material. Magnification=50×.

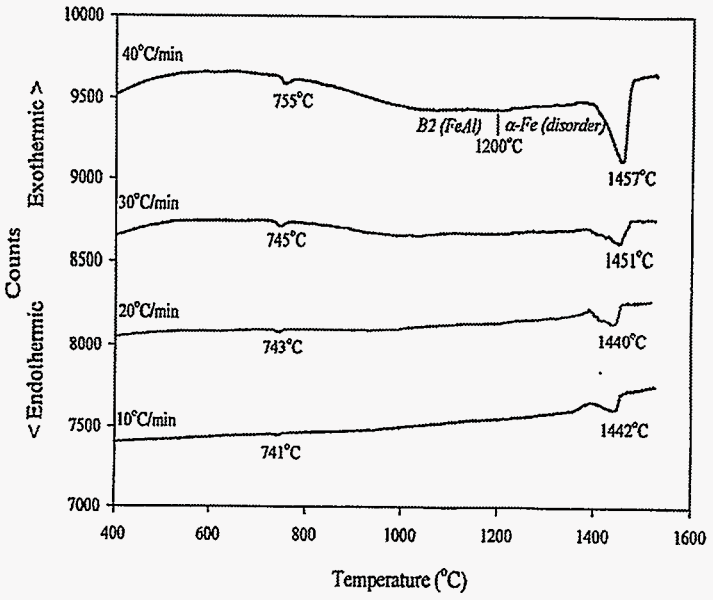

Figure 4. DSC heating curves for the FeAlMoB (heat #565) alloy at heating rates of 10, 20, 30 and 40°C/min.

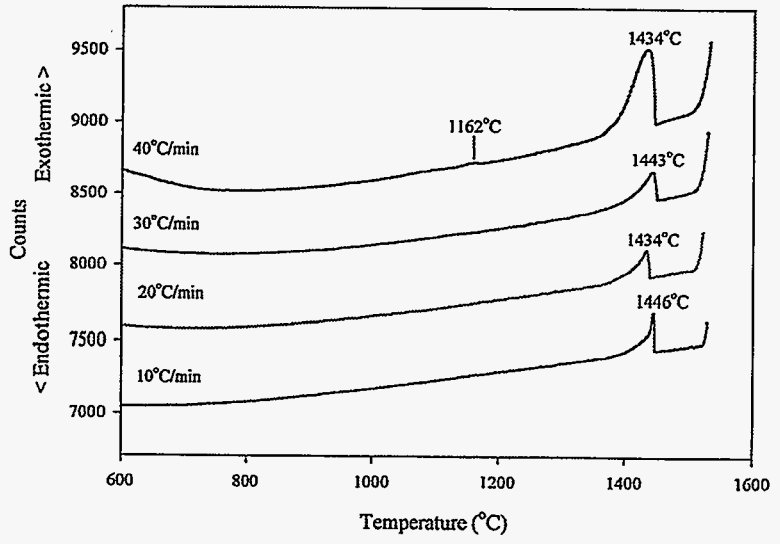

Figure 5. DSC cooling curves for the FeAlMoB (heat #565) alloy at cooling rates of 10, 20, 30 and 40°C/min.

Table 4. Melting and soldification temperatures for the Fe-Al-Mo-B (Heat #565) material.

Heating rate (°C/min)	*Onset Melting (°C)*	*Onset Solidification (°C)*
10	1393	1448
20	1398	1440
30	1405	1450
40	1394	1446

MILESTONES

Goals for the FY 1998 will be to complete the joint project with ORNL concerning the effects of minor alloying additions on the phase transformation and kinetics of FeAl and Ni3Al alloys received by ORNL while continuing to publish various articles related to the results obtained from this research. Kinetic analyses of the metastable or non-equilibrium material will be used in discussing/explaining the influence of the minor elements of addition.

ACKNOWLEDGMENTS

This research was sponsored by the U.S. Department of Energy, Assistant Secretary for Energy Efficiency and Renewable Energy, Office of Industrial Technologies, Advanced Industrial Materials (AIM) Program and Division of Materials Sciences, under contract DE-AC05-96OR22464 with Lockheed Martin Energy Research Corporation as an AIM Fellowship administered by the Oak Ridge Institute for Science and Education.

PUBLICATIONS

A. Jordan and O. N. C. Uwakweh, "The study of Mechanically Alloyed Fe-Zn-Si Intermetallic Phases" accepted for publication in the, *Journal of Materials Synthesis and Processing* (February 1997).

A. Jordan and O. N. C. Uwakweh "Verification of Sandelin Phenomenal in Mechanical Alloyed Fe-Zn and Fe-Zn-Si" accepted for publication in, *Materials Transactions, JIM* (November 1997), scheduled to appear in the Vol. 38, No. 12 issue.

O. Uwakweh and A. Jordan, "Application of Metastable Transformation of Mechanically Alloyed Fe-Zn-Si in Equilibrium Phase Studies," *Journal of Phase Equilibria*, Vol. 18, No. 5, pp. 448-457, (1997).

O. N. C. Uwakweh, Z. Liu, A. Jordan, B. Chakoumakos, S. Spooner, and P. Maziasz, "Neutron Diffraction and Phase Evolution of the Mechanically Alloyed Intermetallic Compound ζ-$FeZn_{13}$," accepted for publication in, *Metallurgical and Materials Transactions* (July 1997).

O. Uwakweh, A. Jordan and P. Maziasz, "Thermal Transformations in Mechanically Alloyed Fe-Zn-Si Materials," accepted for publication in, *Metallurgical and Materials Transactions* (May 1997).

A. Jordan and O. N. C. Uwakweh, "Structural Evolution and Kinetics Studies of Mixed Phases Terminal Solid Solutions of Fe-Zn and Fe-Zn-Si Alloys," submitted to the *Journal of Materials Research*, (October 1997).

A. Jordan, Z. Liu and O.N.C. Uwakweh, "Mechanical Alloying Studies in the $\Gamma(Fe_3Zn_{10})$ and $\Gamma_1(Fe_5Zn_{21})$ Single and Mixed Phase Compositions," submitted to the *Journal of Materials Research* (April 1997).

POSTER SESSIONS

A. Jordan, "Phase Evolution in Mechanically Alloyed Fe-Zn-Si Ternary Alloys," presented at the annual meeting of the AIM program, sponsored by the Advanced Industrial Materials program, held in Albuquerque, New Mexico, on June 16-18, 1977.

HONORS AND AWARDS

A. Jordan, Advanced Industrial Materials program Ph.D. Fellowship, administered by the Oak Ridge Institute for Science and Education (ORISE), 1996-present.

SECTION 3.

MECHANICAL BEHAVIOR OF EPOXY-BONDED JOINT FOR PIPE REPAIR

M. K. Lian and B. J. Love

Department of Materials Science and Engineering
Virginia Polytechnic Institute and State University
Blacksburg, Virginia 24061

J. R. Keiser and D. F. Wilson

Metals and Ceramics Division
Oak Ridge National Laboratory
P. O. Box 2008, Oak Ridge, Tennessee 37831

INTRODUCTION

There are instances where efficiency and safety may be compromised as a result of damaged pipes. Thus, it is worth investigating other methods that can repair the damage for a temporary period without shutting down the operation. The objective of this project is to evaluate the mechanical properties of the epoxy-bonded joint in aqueous environments that might be the conditions of such repair.

TECHNICAL PROGRESS – FY 1997

The epoxy adhesive studied consisted of EPON® resin 828, dicyandiamide, and 2-methylimidazole. Low-alloy carbon steel was chosen as the substrate. The epoxy bonded joints were exposed in either distilled water or 3.4% NaCl solution at 50°C for one or two weeks.

Three-point bend test was used to evaluate the mechanical properties of the bonded joints. The shear stress at the interface between the epoxy and the steel was calculated and the results are shown in Figure 1.

CONCLUSIONS

The average shear stress of the epoxy-bonded joints decayed with time for all three surface treatments in both aqueous environments. The environment might have penetrated and weakened the interface. Therefore, the bond strength decreased with increasing exposure time. The samples made with soap- and water-scrubbed steel had the

highest initial shear stress. After two weeks of exposure in distilled water, the shear stress differences between three surface treatments were not statistically significant. It was recommended that scrubbing the steel with soap and water was sufficient for applications in distilled water, since it is the easiest surface pretreatment method.

Surface 1 - soap and water scrubbed; Surface 2 - 220 grit sandpaper sanded; Surface 3 - sandblasted.

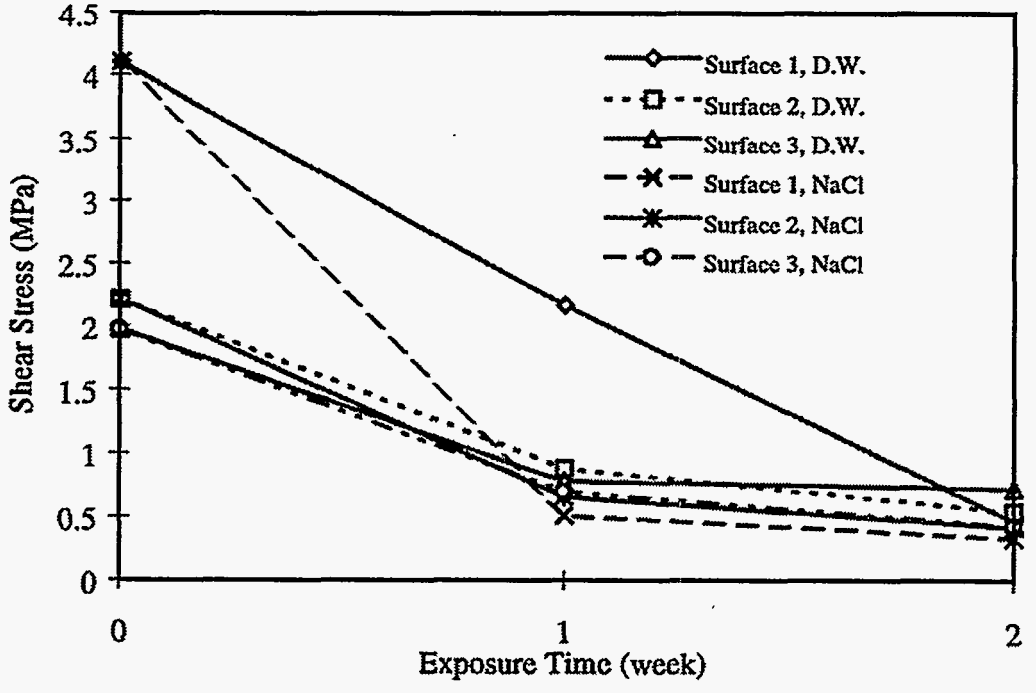

Surface 1 - soap- and water-scrubbed; Surface 2 - 220 grit sandpaper sanded; Surface 3 - sandblasted.

Figure 1. Shear stress for epoxy-bonded steel.

The samples made with sandblasted steel had the highest shear stress after two weeks of exposure in 3.4% NaCl solution. If longer lifetime of the bonded joint is needed, sandblasting is recommended for the surface pretreatment. If the simplicity of the surface pretreatment is preferred, scrubbing the surface with soap and water is adequate.

Future Work

This was a model study of sample fabrication and mechanical testing. Curing agent that is capable of curing the EPON® resin 828 underwater is being evaluated. The bonded joints will be fabricated their mechanical behavior will be studied using the same technique.

ACKNOWLEDGMENTS

This research was sponsored by the U.S. Department of Energy, Assistant Secretary for Energy Efficiency and Renewable Energy, Office of Industrial Technologies, Advanced Industrial Materials (AIM) Program; and Division of Materials Sciences, under contract DE-AC05-96OR22464 with Lockheed Martin Energy Research Corporation as an AIM Fellowship administered by the Oak Ridge Institute for Science and Education.

DEVELOPMENT OF IMPROVED REFRACTORIES

A. A. Wereszczak and K. C. Liu

Metals and Ceramics Division
Oak Ridge National Laboratory
P.O. Box 2008, Oak Ridge, Tennessee 37831

R. E. Moore
University of Missouri-Rolla
1870 Miner Circle, 222 McNutt Hall
Rolla, Missouri 65409-0330

INTRODUCTION

The goal of the project is to provide expertise and facilities for the high-temperature mechanical properties characterization of refractory materials which are of interest to the U.S. DOE's Office of Industrial Technologies' Advanced Industrial Materials Project. The project dedicates refractory testing facilities which are capable of generating representative engineering creep data to a temperature of 3300°F (1815°C) in ambient air. The generated engineering creep serves R&D requirements of refractories/manufacturers and its glass manufacturer end-users and designers. The relevance of this effort to the refractory and glass-making industries is ensured by coordinating our research activities (1) with Glass Industry Advisory Committee (GIAC), comprised of recognized technical representatives from refractory vendor and glass manufacturing companies, (2) receiving input from key representatives and furnace refractory specialists from the glass manufacturing community, and (3) through a subcontract with the University of Missouri-Rolla (UMR), whose reputation in refractory research is internationally recognized.

Valid engineering creep data currently do not exist for almost all commercial refractories. Refractory end-users such as glass-manufacturers require such data for (1) comparing competing brands, and (2) the efficient and economical design of their various glass-melting furnace superstructures. Refractories in glass production furnaces may be subjected to extreme temperatures as high as 3200°F (1760°C). With the simultaneous imposition of mechanical and thermal stresses, creep deformation of the refractory material occurs as a consequence. Designers must ensure that the structural integrity is maintained for optimal service, so these high-temperature deformations must be considered for successful glass furnace superstructure design. These criteria can only be satisfied with the utilization of representative engineering creep data for the refractory materials that are chosen for the design of the refractory superstructures.

The high-temperature refractory testing facilities are equipped with instrumentation to accurately control and monitor refractory creep tests. Two test frames are used for the project. Each testing station is comprised of a testing frame, a computer and appropriate software for test control and data acquisition, a furnace and load train capable of achieving and maintaining loads and temperatures to 3300°F, and a high-temperature extensometer to monitor strain as a function of time or stress. High-temperature test conditions will be selected that mimic those of refractory service (determined through consultation with the GIAC). Success of this subtask will be demonstrated when representative engineering creep data become available to those scientists, engineers, and technicians, and academicians requiring it for use in refractory materials development and furnace superstructural design.

TECHNICAL PROGRESS - FY 1997

Two test frames were constructed during FY 1997. The load cells and extensometers for both frames were conditioned and calibrated. The frames are capable of accurately measuring compressive creep strain in refractory specimens up to 1800°C. A glass industry advisory committee (GIAC), comprised of refractory vendors and glass manufacturing representatives, was formed so the present project would receive insight, advice, and input from them. Representatives from thirty-four domestic glass manufacturers were surveyed to determine which refractory materials their furnace designers desired engineering data for. Eight refractory materials were identified as the most popular: fused-cast alumina, andalusite, bonded AZS, fused-cast AZS, fused-grain mullite, conventional silica, fused silica, and bonded zircon. Conventional silica and fused-cast alumina were prioritized and will be tested first. Commercially available conventional silica brands were received (six in all) and speciments were core-drilled from the bricks. Density measurements were made on all six brands and metallographically prepared speciments from each of the six were prepared from grain size and grain-size-distribution measurements. Near the end of FY 1997, a subcontract was initiated at the UMR. Staff at UMR will characterize the refractory materials tested in the present project with the aid of their catholuminesce imaging.

MILESTONES

Completed initial compressive creep testing and modulus of elasticity testing of refractories (September 1997).

PUBLICATIONS

None.

PRESENTATIONS

Oral Presentations

"Characterization of Refractories for the Glass Manufacturing Industry," *1997 Glass Industry Project Review*, Washington, DC, September 25, 1997.

"Development of Improved Refractories," *2nd Annual OIT/AIM Program Review*, Albuquerque, NM, June 18, 1997.

"High Temperature Mechanical Properties and Corrosion Resistance of Refractories," *2nd Industrial Energy Efficiency Expo*, Arlington, VA, February 27, 1997.

"Compressive Creep Performance of Glass Furnace Crown Refractories," *University of Missouri-Rolla Ceramic Engineering Department Seminar Series*, Rolla, MO, October 10, 1996.

HONORS AND AWARDS

None.

PATENTS/DISCLOSURES

None.

LICENSES

None.

INDUSTRIAL INPUT and TECHNOLOGY TRANSFER

A survey was completed in which container-, fiber-, flat-, and special-glass manufacturing representatives identified which refractory materials the present project is to mechanically test. The results from this survey were significant because they were the first of their kind (i.e., glass manufacturing competitors willingly identified refractory materials of interest) used in a manner to identify refractory materials and mechanical test matrices for such an objective test program.

GELCASTING POLYCRYSTALLINE ALUMINA

M. A. Janney

Metals and Ceramics Division
Oak Ridge National Laboratory
P.O. Box 2008, Oak Ridge, Tennessee 37831

INTRODUCTION

This work is being performed as part of a CRADA with Osram-Sylvania, Inc. (OSI), a major U.S. manufacturer of high-intensity lighting. Among its products is the Lumalux® line of high-pressure sodium vapor arc lamps, which are used for industrial, highway, and street lighting. The key to the performance of these lamps is the polycrystalline alumina (PCA) tube that is used to contain the plasma that is formed in the electric arc. That plasma consists of ionized sodium, mercury, and xenon vapors. The key attributes of the PCA tubes are their transparency (95% total transmittance in the visible region), their refractoriness (inner wall temperature can reach 1400°C), and their chemical resistance (sodium and mercury vapor are extremely corrosive). The current efficiency of the lamps is very high, on the order of several hundred lumens/watt. (Compare incandescent lamps -13 lumens/watt; fluorescent lamps -30 lumens/waft.)

Osram-Sylvania, Inc., would like to explore using gelcasting to form PCA tubes for Lumalux® lamps, and eventually for metal halide lamps (known as quartz-halogen lamps). Currently, OSI manufactures PCA tubes by isostatic pressing. This process works well for the shapes that they presently use. However, there are several types of tubes that are either difficult or impossible to make by isostatic pressing. It is the desire to make these new shapes and sizes of tubes that has prompted OSI's interest in gelcasting.

The purpose of the CRADA is to determine the feasibility of making PCA items having sufficient optical quality that they are useful in lighting applications using gelcasting.

TECHNICAL PROGRESS - FY 1997

Introduction

Gelcasting is a process for forming ceramic and metal powders into complex shapes. It was originally developed for ceramic powders. It is a generic process that has been used to produce complex-shaped ceramic parts from over a dozen different ceramic compositions ranging from alumina-based refractories to high-performance silicon

nitride. The present application is to gelcast thin-walled tubes of polycrystalline alumina (PCA) having high enough quality that they are useful in high-pressure sodium vapor arc lamps. Background information on the gelcasting process is given in another section of this Annual Report, entitled Advanced Powder Processing.

Results and Discussion

During FY 1996, we successfully gelcast straight, thin-walled tubes (0.3-in. OD, 0.020-in. wall, 1-in. long) in molds supplied by OSI. The tubes were fired using a standard schedule and produced translucent material having total transmittance values that were equivalent to those obtained in commercial materials, Figure 1.

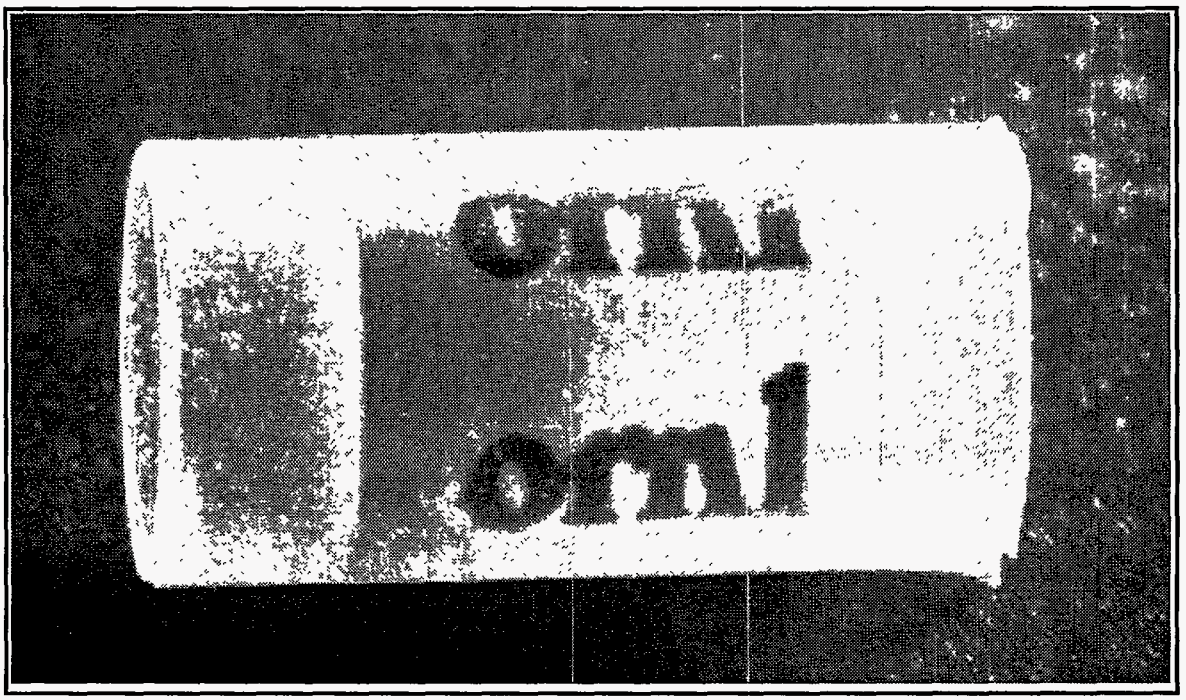

Figure 1. A thin-walled gelcast PCA tube (0.3-in. diam, 0.020-in. wall) with excellent transmission.

The goal for FY 1997 was to further demonstrate that we could gelcast complex-shaped tubes of a proprietary design while maintaining high transmittance. To accomplish this goal, we investigated several fugitive core strategies. A fugitive core is one that can be used during gelcasting and can then be removed without damaging the gelcast part, even if the part contains re-entrant angles or closed ends. Two of the approaches investigated used meltable cores made from pattern wax and a fusible alloy—Wood's metal. Both of these materials were used successfully as cores. The procedure involved in gelcasting using removable cores follows.

A standard gelcasting mix was used for making the complex-shaped tubes. The slurry consisted of 45 vol % high-purity alumina, 500 ppm MgO (as spinel) and 1 wt% Darvan 821A dispersant, with 15 wt % hydroxymethylacrylamide in water as the vehicle.

After filling, the molds were placed in a 50°C convection oven. Gelation was accomplished at 50°C to avoid melting the wax or metal cores. Typically, the molds were enclosed in a high-humidity box during gelation to prevent drying of the top of the molded part. We used a covered polyethylene box which had towels saturated with water covering the bottom of the box. About 45 min was allowed for gelation. This was not an optimized time; the parts may have gelled in much less time.

When the parts were gelled, the wax core was removed. The molds were disassembled under flowing deonized water. This served to cool the mold and the part, which helped prevent undesired drying. It also tended to eliminate meniscii, which could make opening the mold somewhat more difficult. After the part was removed from the mold, it was placed in hot deionized water (85°C). It took several minutes for the wax or metal in the part to melt and become fluid enough to flow from the interior of the part. The parts were rinsed repeatedly to make sure that all of the core material was removed from the interior of the part.

The parts were dried using conventional high-humidity drying. First, the part was rinsed in cold, deionized water to reduce its temperature to ambient. Then it was placed in a 95% RH chamber for 24 h followed by 24 h in a 75% RH chamber. Final drying was accomplished at ambient conditions on the lab bench.

Firing was done at OSI using standard binder burnout and high firing techniques such as are used for isopressed parts. Using meltable core materials such as wax or fusible alloy allowed us to produce thin-walled objects in large numbers (over 100 were cast and fired) with excellent quality and repeatability.

MILESTONES

Demonstrated the ability to gelcast complex-shaped tubes of optical quality.

PUBLICATIONS

None.

PRESENTATIONS

None.

HONORS AND AWARDS

None.

PATENTS/DISCLOSURES

One in preparation.

LICENSES

None.

INDUSTRIAL INPUT and TECHNOLOGY TRANSFER

OSI is actively pursuing applications of gelcast tubes to their product line.

MATERIALS R&D — STUDENT INTERNSHIPS

R. B. Thompson and S. Chumbley
Materials Science and Engineering Department
Ames Laboratory
Iowa State University
Ames, Iowa 50014

INTRODUCTION

This program's objective is to the conduct of programmatic research for the Advanced Industrial Concepts Materials Program while training minority students in the process.

Well-known demographics indicate that minorities will constitute an increasing fraction of our future work force. Consequently, efforts have been initiated to increase the fraction of minorities and women who choose and successfully follow technical career paths. Included are a wide ranging set of programs beginning with pre-school education, progressing through efforts to retain students in technical paths in grades K-12 and undergraduate education, and ending with encouraging graduate education. The Materials R&D — Student Internships is a unique approach in the latter category. Here, we have focused on a particular area of applied materials research, the Advanced Industrial Materials (AIM) Program. Our goal, then, is to educate minority graduate students in the context of this program. The Ames Laboratory was selected as a site for this pilot project since it is a DOE national laboratory, located on the campus of a major research university, which includes in its research interest programs with a strong technological flavor. Many of the Laboratory staff hold shared faculty appointments.

More specifically, the pattern through which a student will pass involves a sequence of steps progressing through recruitment, project selection, research, mentoring, and graduation. Recruiting is being accomplished by nationally advertising "Advanced Industrial Materials Program Technology Fellowships for Minorities." We feel that it would be desirable to offer at least one such fellowship each year to maintain continued visibility on minority campuses and to establish effective working relationships with appropriate personnel. Other factors which we believe to be essential to the success of the project include offering each student a variety of project opportunities—active choice in project selection will greatly increase the student's motivation and likelihood of success—and continued mentoring throughout the program. The projects offered to the students are consistent with the guidelines of the AIM program.

TECHNICAL PROGRESS — FY 1997

Summary

During FY 1997, our second student, Ms. LaVonne Carson, completed her Master's Degree in Materials Science. Her work concerns the preparation of nanocrystalline materials and deposition of Cr layers using an inductively-coupled RF plasma. She has now accepted employment with the American Competitiveness Institute in Indianapolis, IN. Technical progress on her project is summarized below.

The project which used the RF-ICP plasma torch to produce nanocrystalline material involved the construction of a system that allowed powder to be fed into the plasma stream. Early studies had shown that if Ti_5Si_3 and Cr_3Si were processed by plasma heating, nanocrystalline material resulted. However, if $MoSi_2$ were processed the resulting powder consisted of a mixture of Mo-rich phases as well as nanocrystalline Si. In this study a number of different intermetallic compounds, primarily silicides, were processed and the dissociation/recombination kinetics were studied to determine the relevant physical properties of the compounds that favored/hindered nanocrystalline formation. These compounds included $TiSi_2$, $CrSi_2$, Cr_5Si_3, Mo_5Si_3, Mo_3Al_8, and W_5Si_3. These compounds were chosen because they represented a range of possibilities that might affect the recombination kinetics. For example, the effect of compound stoichiometry could be studied by comparing the recombination of line compounds to those which exist over a compositional range. The effect of compound melting and vaporization temperature, and thermodynamic heats of formation could be examined as these compounds vary widely in this areas. Finally, the effect of compound and individual constituent density was considered.

No consistent trends were seen when thermodynamic factors of recombination were considered. Similarly, the composition range over which the compound existed seemed to only slightly affect the results. The ease with which some compounds formed nanocrystalline material as opposed to others seem to be most closely related to the differences in vapor pressure between the elemental constituents. If the difference in vapor pressure between the constituents was small, such as for the Cr-silicides, nanocrystalline material was readily produced. If the difference were large, (e.g., Mo and W silicides) a mixture of compounds was produced. If the difference was somewhat in between the two extremes, such as for the Ti-silicides, factors such as the compositional range then seem to play a role. For example, these compounds produced a range of results, the line compounds being less likely to form nanocrystalline material than those with a compositional range.

The second project used the RF-ICP torch to deposit Cr coatings and also met with mixed results. It was possible to deposit films of desirable thickness on metallic substrates

using two different feed materials: Cr metal powder and the compound chromium hexacarbonyl. However, the quality of the deposited films was poor. The adherence of the film was low and they could easily be scraped from the surface of the substrates. The presence of oxygen in the system is a major factor in the poor quality as all of the deposited films contained oxides of one form or the other. This was confirmed by Auger analysis and transmission electron microscopy studies. The source of the oxygen in the film is not known with certainty, although a number of possibilities exist. For example, although the surfaces of the substrates were cleaned it is almost certain that a small layer of oxide is still present on the surface. Similarly, the Cr powders used as feed material would contain a small oxide layer. The vaporization of the chromium hexacarbonyl as it passed through the torch would be a source of oxygen in these samples. The presence of small amounts of oxygen in the feed gas and chamber is also a possibility. Finally, oxidation of the substrate upon removal from the chamber can occur. All of these factors need to be considered.

If the oxygen can be removed from the system the possibility of producing adherent Cr coatings using a plasma torch presents several advantages over conventional electroplating in the area of waste reduction. Monitoring of the effluent gases from the plasma torch over the course of a deposition revealed no particulate present and no harmful gases. The only affect to the environment was a slight increase in the amount of CO_2. However, the amount present was still within the range of levels found in cities in the US. Thus, a clean method for producing a Cr plate might be developed if the adherence can be improved by maintaining a stricter control over the feed material and chamber atmosphere.

Both studies were completed in FY 1997. The results are given in detail in the Master's thesis of L. J. Carson, Iowa State University. Two papers on the separate studies were also prepared. The first paper, covering the Cr deposition study, has been published and the bibliographic information is given below. The second paper, covering nanocrystalline production, was returned for further work and information to be provided before publication. That work is still in progress.

MILESTONES

A new method of depositing a thin layer of hard Cr was investigated. The method allows the deposition of Cr without toxic chemicals or the generation of hazardous wastes. The drawback is that at this time the mechanical properties exhibited by the coatings are greatly inferior to those of electroplated Cr. More work needs to be done to see if these properties can be improved.

PUBLICATIONS

Journals

L. Carson and L. S. Chumbley, "The Deposition of Chromium by the Use of an Inductively-Coupled Radio-Frequency Plasma Torch," *Scripta Materialia*, Vol. 37, No. 10, pp. 1531-1538, (1997).

Other Publications

Plasma Processing of Materials, L. J. Carson, Master's Degree Thesis, Materials Science and Engineering Department, Iowa State University.

PRESENTATIONS

Oral Presentations

None.

HONORS AND AWARDS

None.

PATENTS/DISCLOSURES

None.

LICENSES

None.

INDUSTRIAL INPUT AND TECHNOLOGY TRANSFER

John Deere provided samples for the Cr coating portion of this study.

METALS PROCESSING LABORATORY USER CENTER (MPLUS)

G. Mackiewicz-Ludtka and H. W. Hayden

Metals and Ceramics Division
Oak Ridge National Laboratory
P. O. Box 2008, Oak Ridge, TN 37831

INTRODUCTION

The Metals Processing Laboratory Users (MPLUS) Center was officially designated as a DOE User Facility in February 1996. It's primary purpose is to assist researchers in key US industries, universities, and federal laboratories in improving energy efficiency and enhancing US competitiveness in the world market. The MPLUS Center provides users the unique opportunity to address technology-related issues to solve metals processing problems from a fully integrated approach. DOE facilitates the process and catalyzes industrial interactions that enables technical synergy and financial leveraging to take place between the industrial sector identifying and prioritizing their technological needs, and MPLUS, which provides access to the technical expertise and specialized facilities to address these needs.

MPLUS was designed to provide US industries with access to the specialized technical expertise and equipment needed to solve metals-processing issues that limit the development and implementation of emerging metals-processing technologies. As originated, MPLUS includes the following four primary user centers: Metals Processing, Metals Joining, Metals Characterization, and Metals Process Modeling. These centers are devoted to assisting US industries in adjusting to rapid changes in the marketplace and in improving products and processes. This approach optimizes the complementary strengths of industry and government. Tremendous industrial response, has resulted in MPLUS expanding to meet the ever-growing technical needs and requests initiated by US industry.

TECHNICAL PROGRESS - FY 1997

Summary

1. From the official inception of MPLUS as a DOE designated User Center on February 9, 1996, MPLUS has grown continuously, always initiated by industrial needs and requests, from representing only the Engineering and Materials Section within the Metals & Ceramics Division, to include other User Centers within ORNL (e.g., the High Temperature Materials Laboratory (HTML), and the Computational Center for Industrial Innovativeness (CCII)), and even beyond. MPLUS has provided industry (based upon its

need and request) with access to unique capabilities and technologies beyond those originally designated within ORNL as DOE User Centers,(e.g., the Microwave Facilities within the Fusion Energy Division). In fact, it is becoming quite clear, with the growing response and needs being identified via MPLUS, that MPLUS is a viable vehicle/mechanism to unite other National Laboratory User Facilities to provide industry with a mechanism to access these National Resources as *a Distributed Laboratory* .

2. As of September 30, 1997, a total of 76 MPLUS Proposals were received from 60 companies and universities representing 26 states (Figure 1). This represents approximately a 50% increase in proposals, and >50% increase in the number of states that have requested MPLUS facilities and expertise since FY96. The demand for and success of the MPLUS User Facilities are evidenced by a.) the sheer number of users (60 Companies); b.) the twelve (12) organizations who requested repeated assistance and submitted multiple (2 to 4) proposals for different MPLUS projects; and c.) the five (5) companies who chose to do Proprietary (P) MPLUS projects. In fact, two of these five P Users did multiple MPLUS projects.

3. Of the 76 proposals, 53 were reviewed, and 31 of *these 53 MPLUS User projects were initiated* (a 60% increase).

*4. Ten **(10)** MPLUS projects were **completed*** (~a 300% increase), and the other 23 proposals were either a.) accepted contingent on legal approval, b.) under development, or c.) being modified.

4. As of September 30, 1997, a total of 546 user days were logged during FY 1997, which is approximately a *100% increase since FY 1996.*

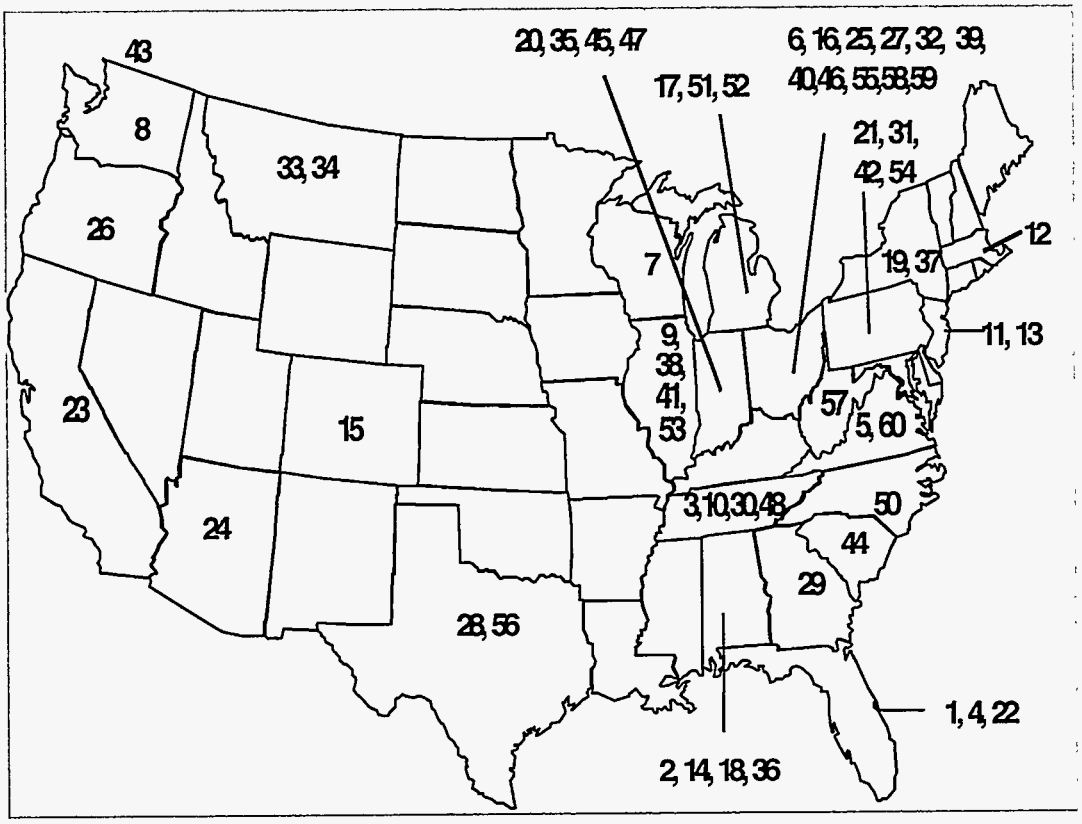

1. Westinghouse (2)
2. Reynolds(2)
3. ForMat Industries
4. Memtec
5. E.R. Johnson
6. Sandusky Int'l
7. Waukesha Electric
8. Weyerhauser(2)
9. A.Finkl(3)
10. Jeffrey Chain Corp
11. Materials Tech.
12. ABB C-E Serv.(3)
13. Union Camp Corp
14. United Defense(2)
15. CO School of Mines
16. Doehler-Jarvis
17. General Motors
18. Univ. of AL(2)
19. Cornell Univ.
20. Cummins Engine(3)
21. Bethlehem Steel(2)
22 Anchor Glass
23. FMC Corp.
24. Arizona State U
25. Ohio State Univ.
26. Goldendale Al
27. Lincoln Electric
28. CarboMedics
29. IPST
30. Univ. of TN
31. PPG industries (4)
32. Owens Corning(2)
33. Columbia Falls Al
34. AFFCO
35. Allison Engine
36. MacMillan-Bloedel
37. Gray-Syracuse
38. Wagner Castings
39. Rhenium Alloys
40. Uniform Metal Tech
41. Amoco
42. J&L Specialty Steel
43. Process Simulations (B.C.)
44. Milliken Res. Ctr.
45. Welding Services
46. General Electric
47. MicroPyretics
48. Pathway Bellows
49. Stoody
50. Torrington(2)
51. Ford Motor Co.
52. Eaton
53. Hoskins Mfg.(2)
54. AHT Inc.
55. Timken Co.
56. B.F.Goodrich
57. INCO Alloys Int'l
58. LTV Steel
59. Park OH Transp.
60. VA Poly.& St. U.

Figure 1. As of September 30, 1997, a total of 76 MPLUS Proposals were received from 60 companies and universities representing 26 states.

MILESTONES

FY 1997

Developed a 1-Page MPLUS Summary Sheet	May 1997
Developed an MPLUS Vision Industry Summary Notebook	June 1997
Investigate Partnering with additional Facilities *(Adv. Steel Processing Center)*	June 1997
Developed internet-downloadable version of MPLUS Proposal form *(http://www.ms.ornl.gov/emfacility/mplus/forms.htm_)*	September 1997
Initiated 53 MPLUS Proposals (48 NP and 5 Proprietary)	September 1997
Completed 10 MPLUS Projects (1 Proprietary)	September 1997

PUBLICATIONS

Metals Processing Laboratory Users Center Report, ORNL/M-4466.

ORNL Internal Report, "Metals Processing Laboratory User Facility - *Facilities Capabilities, Interactive Programs, and Recent Experience,"* March 1997.

One (1) -Page MPLUS DOE User Facilities Summary Sheet, May 1997

Summary Binder of MPLUS User Projects according to Vision Industry, June 1997.

MPLUS User Program Brochure (updated April 1997).

Internet Information/ Web Pages (updated: May 1997).
(URL: http://www.ms.ornl.gov/emfacility/mplus/mplus.htm)

PRESENTATIONS

Poster Sessions

"Metals Processing Laboratory User Center," Oak Ridge National Laboratory User Center, for Poster Session at 1997 Advanced Industrial Materials (AIM) Program Annual Meeting in Albuquerque, NM, June 16 -18, 1997.

"Metals Processing Laboratory User Center," Oak Ridge National Laboratory User Center, for Poster Session AIM booth at the OIT Exposition (1997).

"Metals Processing Laboratory User Center," Oak Ridge National Laboratory User Center, for Poster Session for the ASM Materials Exposition at the 1997 ASM/AIME Annual Technical Meeting (October 1997).

"Metals Processing Laboratory User Center," Oak Ridge National Laboratory User Center, for Poster Session at the Advanced Industrial Materials (AIM) Program Annual Meeting in Pollard Auditorium, Oak Ridge, TN, June 24 -26, 1996.

Informal Oral Presentations

"Metals Processing Laboratory Users Center (MPLUS)," for visit by Ford Motor Co. Rough Part Forming Forum, emphasis on Metal Casting & Forging (October 8, 1997).

"Metals Processing Laboratory Users Center (MPLUS)," for visit by Sara Dillich Program Mgr. Of the Aluminum Vision Industry Team for DOE/OIT, emphasis on Aluminum & Metal Casting (October 2, 1997).

"Metals Processing Laboratory Users Center (MPLUS) Update" for Program Managers (Tony Schaffhauser and Mike Karnitz) Meeting (July 25, 1996).

"Overview of the Metals Processing Laboratory Users Center (MPLUS)", for the Directors and staff members of 10 State Energy Offices, as well as representatives from the Southern States Energy Board, the Harmony Project from Charleston, SC, and the DOE Atlanta Regional Support Office (November 20, 1996).

"Metals Processing Laboratory Users Center (MPLUS)" for DOE/OIT: Bill Parks and Charlie Sorrell, (December 5, 1996).

HONORS AND AWARDS

November 1996: The President's Award for Continuous Improvement for the MPLUS Users Center Metals Processing Users Project

LICENSES

None.

INDUSTRIAL INPUT and TECHNOLOGY TRANSFER

As of September 30, 1997, a total of **76 MPLUS Proposals** were received from **60 companies and universities representing 26 states.** This represents almost a 50% increase in the number of proposals submitted, and greater than a 50% increase in the number of states that have requested MPLUS facilities and expertise since FY 1996. The demand for and success of the MPLUS User Facilities are evidenced by a.) the sheer number of users (60 Companies); b.) the twelve (12) organizations who requested repeated assistance and submitted multiple (2 to 4) proposals for different MPLUS projects; and c.) the five (5) companies who chose to do Proprietary (P) MPLUS projects. In fact, two (2) of these five (5) P Users did multiple P MPLUS projects.

Of the 76 proposals, 53 were reviewed, and 31 of these 53 MPLUS User projects were initiated (a 60% increase). Ten (10) MPLUS projects were completed (a 300% increase), and the other 23 proposals were either a.) accepted contingent on legal approval, b.) under development, or c.) being modified. A total of **546 user days** were logged during FY 1997, which is approximately a 100% increase since FY 1996.

ESTIMATED ENERGY SAVINGS

This amount is different for each individual MPLUS project.

MICROWAVE JOINING OF SiC

R. Silberglitt and G. A. Danko

FM Technologies, Inc.
10529-B Braddock Road
Fairfax, Virginia 22032

P. Colombo

University of Padua
via Marzolo 9
35131 Padua, Italy

INTRODUCTION

The purpose of this work is to optimize the properties of SiC-SiC joints made using microwave energy. The current focus is on identification of the most effective joining methods for scale-up to large tube assemblies, including joining using SiC produced in situ from chemical precursors.

During FY 1997, continuous fiber-reinforced SiC/SiC composite (CFCC) and sintered SiC specimens were joined with SiC formed in situ from pyrolysis of either polysiloxane (silicone resin) or allyhydridopolycarbosilane (AHPCS) precursors. This work used the microwave applicator that was designed, fabricated and tested during FY 1996, which provides the capability for vacuum baking of the specimens and insulation and for processing under inert environment.

Maximum values of average shear strengths of the microwave-processed CFCC joints were comparable to those of similar joints produced with conventional heating. The effect of processing conditions on mechanical strength of sintered SiC specimens was investigated, and processing conditions were selected for fabrication of 8" long, 1" outer diameter (OD) sintered SiC-joined specimens. These specimens were joined under the DOE HiPHES project and will be evaluated by high temperature tensile testing at Oak Ridge National Laboratory (ORNL).

TECHNICAL PROGRESS - FY 1997

Summary

Joining of Continuous Fiber-Reinforced SiC/SiC Composites

Joining experiments on continuous fiber-reinforced (CFCC) SiC/SiC composites were performed using a 16" x 16" multimode applicator, together with a 0-6 kW continuous wave (CW) microwave source operating at 2.45 GHz. The experiments were performed inside an insulated enclosure that was lined on the inside with a SiC microwave susceptor, thus providing hybrid (microwave plus radiant) heating. Specimens were 3 mm thick plates with a 5 mm x 8 mm cross-section. Two types of composites were used, both of which had been fabricated using chemical vapor infiltration (CVI) methods from either 2-dimensional (2D) or 3-dimensional (3D) woven preforms. The interlayer material, polysiloxane (silicone resin), was mixed with either metallic or SiC powder. The silicone resin is a preceramic polymer which upon pyrolysis yields silicon oxycarbide. Pairs of composite plates were assembled with the interlayer material and cross-linked by heating in a furnace at 200°C (located at the University of Padua) prior to the microwave processing, which was performed at FM Technologies.

Prior to inserting the specimens to be joined, the multimode applicator was pumped to a vacuum of 2 $x10^{-2}$ torr to remove water vapor and other impurities from the heating enclosure and supporting structures. The applicator was then back-filled with inert gas and opened for sample placement. The specimens were placed inside the hybrid heating enclosure, using a 2" high reaction bonded SiC tube as a setter platform so that the specimens were at the same height as a hole in the hybrid heating enclosure and the interface could be viewed directly through a vacuum window using a two-color optical pyrometer. After sample placement, the chamber was evacuated to 5 x 10^{-1} torr , back-filled with inert gas, evacuated again to 5 x 10^{-1} torr, and back-filled again with inert gas.

The variables that were investigated in this study were the processing environment (Ar, N_2, or air), the processing temperature (1200°C or 1380°C), and the filler material (metallic or SiC powders). Microwave input power for the 1200°C processing was approximately 1600 watts and for the 1380°C processing was approximately 2600 watts. Microwave input power was initially 600 watts and was increased gradually to 1200 watts within 30-40 minutes at which time the specimen temperature reached 800°C, as observed using the pyrometer. The input power was then adjusted to achieve a temperature ramp from 800°C to the processing temperature of approximately 10-20°C per minute. Soak time at the processing temperature was 1 hour. A total of 29 specimens were processed, as follows:

- 10 each, 3D composites with filler material consisting of the silicone resin and SiC powder, 5 of which were processed at 1200°C in Ar and 5 of which were processed at 1200°C in N_2;

- 11 each, 3D composites with filler material consisting of the silicone resin and metallic powder, 5 of which were processed at 1200°C in Ar, 2 of which were processed at 1200°C in N_2, 2 of which were processed at 1380°C in N_2, and 2 of which were processed at 1200°C in air;

- 8 each, 2D composites with filler material consisting of the silicone resin and metallic powder, 3 of which were processed at 1200°C in N_2, 3 of which were processed at 1380°C in N_2, and 2 of which were processed at 1200°C in air.

The mechanical strength of the joints was determined at the University of Padua by measurement of fracture shear stress according to ASTM D905-89, using a crosshead speed of 1 mm/min, and the values were compared to those for similar specimens that were processed at the University of Padua under the same temperatures and environmental conditions using a conventional furnace. As shown in Table 1, the results for the microwave-processed specimens are somewhat different than those for the conventionally processed specimens, but the maximum values of average shear strength for the two types of processing are quite similar. (Since there were not significant differences between the data for the specimens described above that were prepared with metallic filler and those with SiC filler, these data have been combined.)

Table 1. Average Shear Strengths (MPa) for Microwave and Conventionally Processed SiC/SiC Composite Joints.

Processing Conditions	*Microwave (2D)*	*Microwave (3D)*	*Conventional (2D)*	*Conventional (3D)*
1200°C, N_2	13.00	2.80	10.17	22.33*, 4.80**
1200°C, Ar	24.8***	6.67	4.23*, 7.59**	4.80
1200°C, air	7.19	1.59	---	---
1380°C, N_2(MW) 1400°C,N_2(Conv)	16.06	3.40	6.2	---
1350°C, Ar(MW) 1400°C,Ar(Conv)	12.8***	---	15.8	---

* Processed for 1 hour; ** Processed for 8 hours; *** Previous work, single specimen.

Joining of Sintered alpha-SiC

Microwave joining experiments were also performed during this period using monolithic sintered SiC. The specimens were 12-mm diam, 12-mm high cylinders of Hexoloy™ (St. Gobain, NY), that were surface ground to 400 grit and cleaned with acetone, but not etched. The joining material in this case was a slurry composed of alpha-SiC powder mixed with the polymer precursor allylhydridopolycarbosilane (AHPCS), which was supplied by Starfire Systems, Inc. of Watervliet, NY. AHPCS is a preceramic polymer which yields stoichiometric SiC upon pyrolysis, which then crystallizes upon further heating to beta-SiC. The joints were assembled by applying the slurry to the faces of the specimens and squeezing them together. The specimens were then inserted into the cavity inside the hybrid heating enclosure, without any loading or elevation. An additional 5-in. high SiC tube was placed inside the enclosure was used as a sighting target for temperature measurement.

In order to allow for temperature measurement below the 700°C-1700°C range of the optical pyrometer, the vacuum window was replaced with a vacuum fitting through which a type K thermocouple was inserted. The thermocouple extended slightly into the hybrid heating enclosure through the hole that also served as the pyrometer sighting port. The chamber was pumped to a vacuum of 6.2×10^{-2} torr before processing was begun. Using the thermocouple, it was then possible to process the AHPCS at a slow heating rate, similar to that used in conventional processing, in order to minimize the formation of bubbles that could produce voids in the interlayer. The heating rate was increased once the polymer had been successfully cross-linked (300°-400°C), and the temperature was then increased to the pyrolysis temperature (1000°C). The cavity was back-filled with Ar at approximately 600°C, and pyrolysis was performed in Ar. Following this pyrolysis step, the specimens were allowed to cool and removed from the cavity. A set of experiments was then performed to investigate the effect upon joint strength of an additional infiltration with neat AHPCS, followed by a second pyrolysis, as well as the effect of annealing the specimens at different temperatures (1200°C, 1300°C, 1400°C, 1450°C).

The relative strength of the 24 joined specimens processed as described above was determined by inserting them halfway into a vertical fixture with a machined hole that just fit the specimen diameter, and then loading with a downward force at the point of the specimen farthest from the fixture. Figures 1 and 2 are plots of the strength values obtained (load to failure) for the specimens processed under different conditions. From this study we concluded that there was benefit to the second infiltration and that an annealing temperature between 1300°C and 1400°C would provide the strongest joints. These conditions were then used to fabricate 8" long, 1" OD Hexoloy-joined specimens under the DOE HiPHES project. Eight of those joined tubes were delivered to ORNL for high-temperature tensile testing.

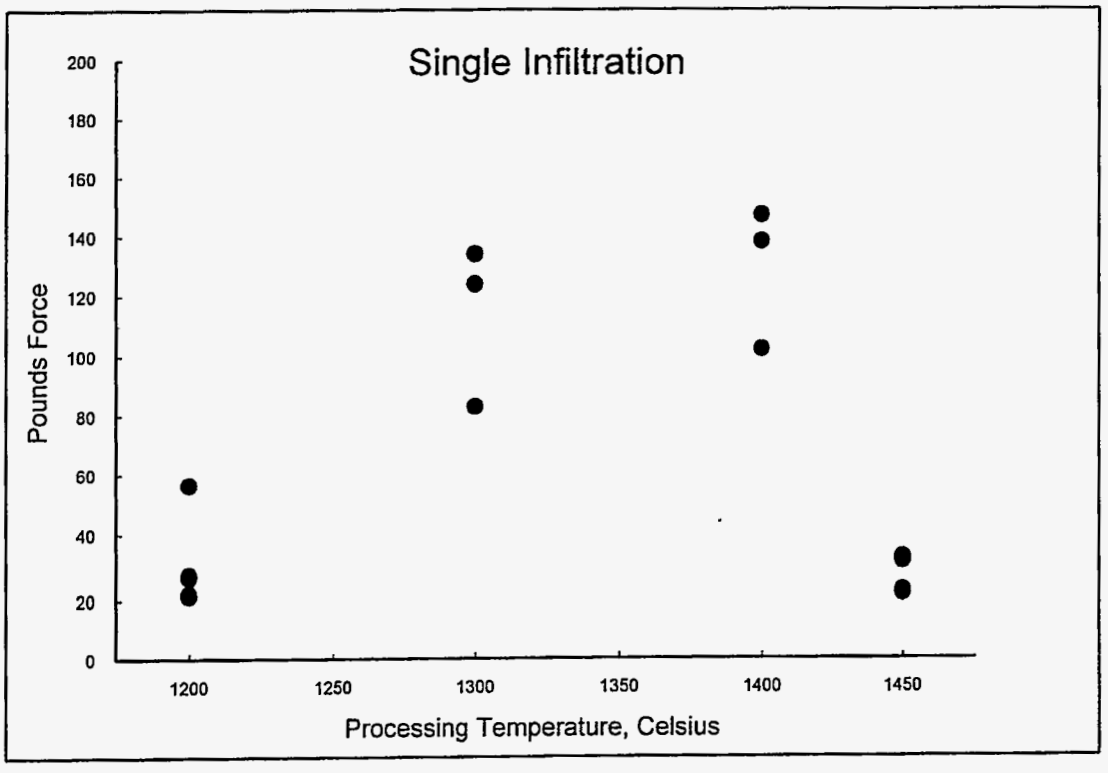

Figure 1. Strength vs. processing temperature for microwave joined sintered SiC (single infiltration).

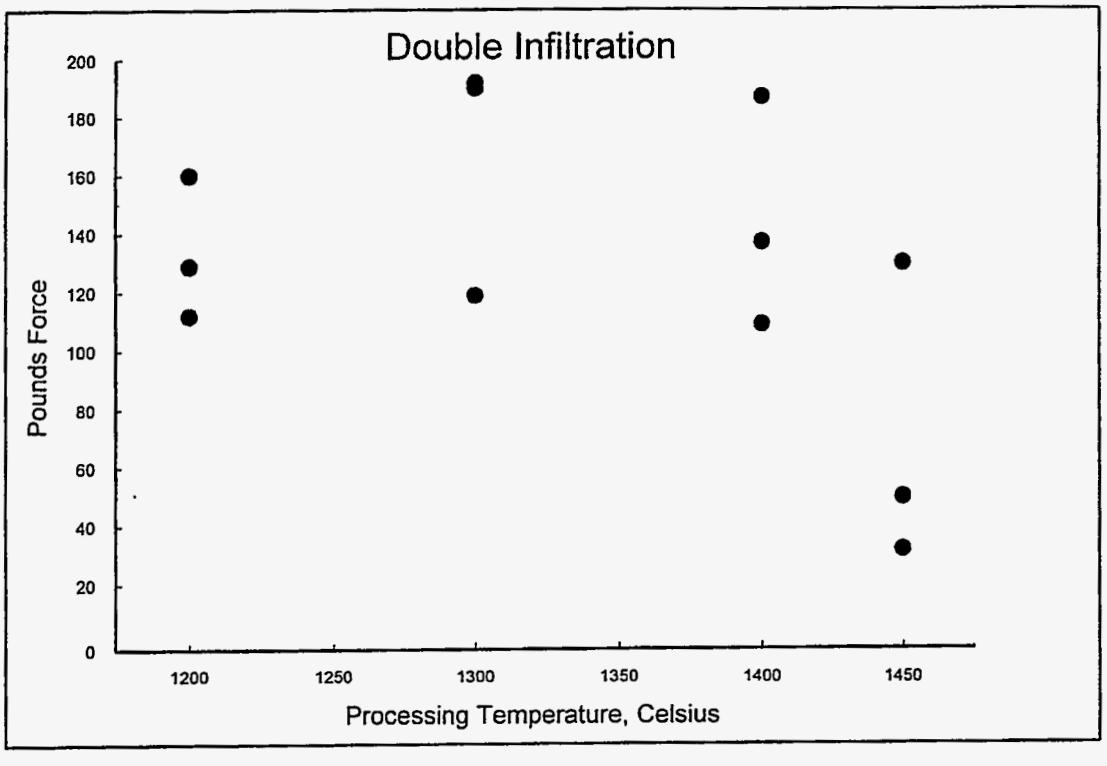

Figure 2. Strength vs. processing temperature for microwave joined sintered SiC (double infiltration).

MILESTONES

Investigation of the effect of joining parameters on the mechanical properties of both sintered SiC and CFCC SiC/SiC composite materials joined with a pure SiC interlayer formed in situ from pyrolysis of polymer precursors (September 1997).

PUBLICATIONS

I. Ahmad, R. Silberglitt, Y. L. Tian, and J. D. Katz, "Microwave Joining of SiC Ceramics and Composites," Ceramic Transactions, Vol. 80, American Ceramic Society, Westerville, OH (in press).

PRESENTATIONS

I. Ahmad, R. Silberglitt, Y. L. Tian, and J. D. Katz, "Microwave Joining of SiC Ceramics and Composites," poster presented at the First World Congress on Microwave Processing, Lake Buena Vista, FL (January 5-9, 1997).

R. Silberglitt, "Microwave Joining of SiC Tubes for High Temperature Materials Processing," presented at the Advanced Industrial Materials Annual Review Meeting, Albuquerque, NM (June 16-18, 1997).

HONORS AND AWARDS

None.

PATENTS/DISCLOSURES

None.

LICENSES

None.

INDUSTRIAL INPUT and TECHNOLOGY TRANSFER

Beginning with a meeting in September 1997 at the DuPont Lanxide Composites (DLC) facility in Newark, DE, planning is underway between FM Technologies, DLC and Foster Wheeler to use joining methods developed under this program for fabrication of CFCC components, with particular emphasis on field joining and repair. A presentation of the results of the microwave joining experiments on CFCC SiC/SiC composites was

also planned for the CFCC Review Meeting and BES/CFCC Workshop on Joining in Lake Tahoe, CA on October 6-8, 1997.

ESTIMATED ENERGY SAVINGS

Natural gas savings are estimated at $172,892 per year due to 4-7% higher efficiency of SiC radiant burner tubes. Use of a SiC tube heat exchanger in externally fired combined-cycle coal power plants is projected to produce a 20% increase in thermal efficiency, together with a 20% reduction in CO_2 emissions and a 90% reduction in SO_x emissions. Energy savings through the reduction of feedstock consumption and decoke fuel and steam requirements with an advanced ethylene production process using a SiC tube heat exchanger are projected at 63.9 trillion BTUs per year.

SELECTIVE INORGANIC THIN FILMS

T. M. Nenoff, P. I. Pohl, C. J. Brinker and A. Martino

Sandia National Laboratories
Albuquerque, New Mexico 87185

INTRODUCTION

Separating light gases using membranes is a technology area for which there exists opportunities for significant energy savings. Examples of industrial needs for gas separation include hydrogen recovery, natural gas purification, and dehydration. A membrane capable of separating H_2 from other gases at high temperatures could recover hydrogen from refinery waste streams, and facilitate catalytic dehydrogenation and the water gas shift ($CO + H_2O \rightarrow H_2 + CO_2$) reaction. Natural gas purification requires separating CH_4 from mixtures with CO_2, H_2S, H_2O, and higher alkanes. A dehydrating membrane would remove water vapor from gas streams in which water is a byproduct or a contaminant, such as refrigeration systems.

Molecular sieve films offer the possibility of performing separations involving hydrogen, natural gas constituents, and water vapor at elevated temperatures with very high separation factors. It is in applications such as these that we expect inorganic molecular sieve membranes to compete most effectively with current gas separation technologies. Cryogenic separations are very energy intensive. Polymer membranes do not have the thermal stability appropriate for high temperature hydrogen recovery, and tend to swell in the presence of hydrocarbon natural gas constituents. Our goal is to develop a family of microporous oxide films that offer permeability and selectivity exceeding those of polymer membranes, allowing gas membranes to compete with cryogenic and adsorption technologies for large-scale gas separation applications.

The microporous media in these films consist of zeolites and nonaluminosilicate open framework structures such as zinc phosphates. Zeolites are microporous aluminosilicates with pore diameters in the 3-7 Å range; they are already used in bulk form for gas separations and dehydration. We are using the very narrow pore size of aluminosilicate zeolites, in particular those found (through diffusion modeling studies) to be specifically sensitive to arene isomer separations, to synthesize inorganic thin films. Specifically, we have begun a CRADA with Amoco Chemical Company to determine the feasibility of using membranes containing shape-selective zeolites to enrich *p*-xylene from mixtures of xylene isomers. Other studies focus on zinc phosphates (ZnPOs) which have pore diameters that are generally smaller than those of zeolites; the range of sizes currently available is ideal for dehydration and hydrogen recovery. These phases are also stable at

higher temperatures (up to 700°C) than those generally tolerated by typical alkali zeolites. Many of the ZnPO phases and all of the ZnPO films described here were synthesized for the first time in the course of this project.

TECHNICAL PROGRESS - FY 1997

Summary

Selectivity is controlled in polymer membranes by differences in gas solubility and diffusivity. In contrast, zeolitic phases can separate gases via molecular sieving. Gas molecules smaller than the critical pore diameter are allowed to permeate; larger molecules are completely rejected. A zeolite film with a pore diameter of 4.1 Å (such as Linde Type A) would thus effectively separate methane (kinetic diameter = 3.8 Å) from propane (kinetic diameter = 4.3 Å) or higher alkanes (Figure 1).

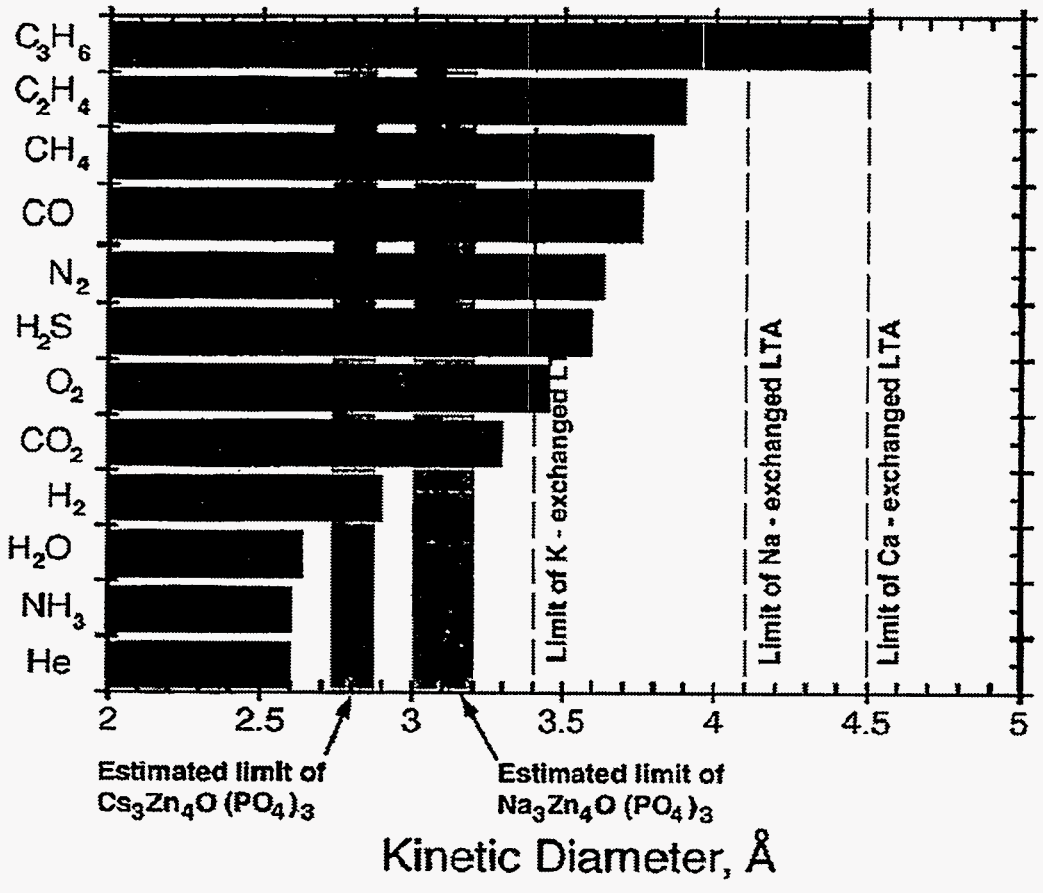

Figure 1. Molecular sieving ability of some zeolites.

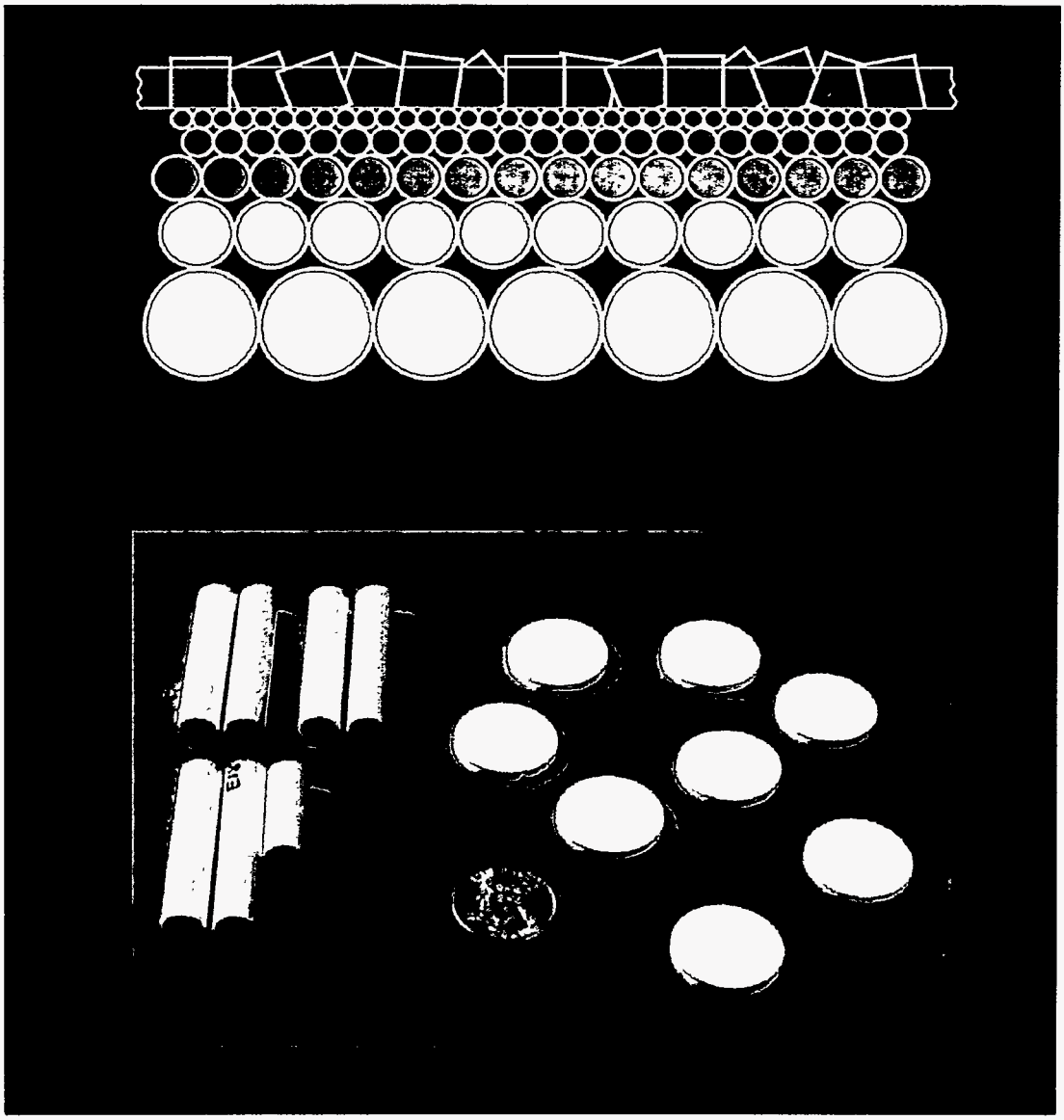

Figure 2. Membrane schematic (top) and Al_2O_3 substrates (bottom).

The molecular sieve membranes described in this report consist of films of microporous phases deposited on porous supports, such as α-Al_2O_3 or ZnO wafers, and Al_2O_3 tubes (Figure 2). The latter are one-directional gas filter membranes in which pore size becomes progressively smaller toward the tube interior, terminating with a layer of 40 Å γ-Al_2O_3 (Figure 2). The films must completely cover the substrate in order to demonstrate any selectivity based on molecular sieving, and the films must be thermally durable enough to withstand operating temperatures and/or calcination. In particular, the film must survive the thermal expansion mismatch between itself and the substrate without cracking or peeling. In our membranes this is accomplished by incorporating an amorphous phase that acts as a binder or "caulk". The limited porosity of the amorphous

phase reduces nonselective gas flow between zeolite crystals, while its flexibility mitigates the thermal expansion mismatch between the film and the substrate. We have used a number of different binders for this purpose, including sol-gel silicas (alone or combined with colloidal aluminas) organic-inorganic hybrid gels, and silicones.

In FY 1997, we investigated methods of film deposition and caulking with Linde Type A and MFI-type zeolites. We have studied permeation of light gases through the resulting membranes. In addition, we synthesized films of new and known zinc phosphates, and identified numerous new ZnPO phases. In the course of this work we prepared the first ZnPO films with molecular sieving behavior, and the first organic-templated ZnPO in which the template can be removed without altering the host framework.

1. Zeolite films

In FY 1995, we demonstrated the synthesis of supported membranes consisting of pure LTA from the action of aqueous NaOH on kaolinite films deposited on porous alumina discs. We also collected gas permeation data from both unconverted clay films and from zeolite films. Permeation results from kaolinite and metakaolinite films revealed gas separation that is characteristic of Knudsen diffusion and surface flow; this showed that these precursor films can be prepared without macroscopic cracks or holes. However, the films cracked upon conversion to LTA. In FY 1996, we studied the effects of precursor film thickness and substrate porosity on cracking susceptibility. We found that reducing the thickness of the kaolinite film can eliminate macroscopic cracking, but that leakage still occurs through microscopic intercrystalline gaps. We then studied the effects of "caulking" the LTA film surface to fill in the intercrystalline voids. Caulking materials tested included silicone polymers, nonporous silica sols, colloidal boehmite suspensions, organic-inorganic silica-based sols, kaolinite (with subsequent conversion to LTA), and LTA mother liquor.

The silica sol approach involves coating the films with silica sols (partially hydrolyzed solutions of tetraethyl orthosilicate [TEOS] in ethanol), then heat treating the membrane to render the films impermeable. We found that the intercrystalline gaps in the LTA films are too large (>0.1 μm) to be adequately caulked using these sols. We have since investigated regrowing the film crystallites in LTA mother liquor, and precaulking with boehmite (α-AlOOH) prior to SiO_2 film deposition to reduce intercrystalline voids prior to treatment with silica sol. In the mother-liquor approach, the LTA film is immersed in an aqueous solution of $(CH_3)_4NOH$, Al_2O_3, SiO_2, and NaOH that precipitates colloidal LTA upon heating. In the precaulking approach, a boehmite sol is deposited onto the LTA film to reduce the intercrystalline surface porosity to ≈ 40 Å, which is fine enough to be caulked by the silica sol.

Both the kaolinite retreatment and mother-liquor methods yielded growth of additional crystallites on the surfaces of the films, rather than expansion of the original crystallites. Therefore, these processes alone have not reduced intercrystalline gaps to sizes that TEOS silica sols can effectively caulk. We have synthesized LTA films sequentially caulked with colloidal boehmite and SiO_2 sol, and will continue the studies with MFI zeolite films.

It has been reported that the selectivities of silicone rubber films for light gases and water/alcohol mixtures can be altered by incorporating zeolite crystallites.[1] Previously, we performed a series of similar experiments to determine if a silicone rubber film can improve the selectivity of a pre-deposited LTA film via caulking. We found that the silicone inhibited viscous flow at coating concentrations in excess of 10%, but allowed some permeation of CO_2 and CH_4, probably due to solution/diffusion. With sufficiently thick application, the silicone rubber can indeed stop gas flow through the membrane, though the required thickness is ca. 20 times that of the LTA film. We have concluded that the permeability of RTV silicone adhesive is probably too great to be used as a caulk.

We further investigated deposition of thin LTA films from suspensions of colloidal LTA and metallic Al films as an alternative to kaolinite films in order to control intercrystalline porosity. Colloidal LTA was prepared according to [2], and centrifuged onto alumina wafers. This yielded continuous thin films similar in appearance to those made from kaolinite, with similar macroscopic porosity. To test the possibility of synthesizing LTA films from thin Al films, Al coupons were soaked in sodium silicate solutions with Na_2O/SiO_2 ratios of 1 and 2, and held at 100°C for several days. This process yielded spongy masses of boehmite at a Na_2O/SiO_2 ratio of 1, and a mixture of boehmite and faujasite in the more alkaline solution. No syntheses were made using Al thin films. We are continuing in this mode with current research involving the deposition of this ZSM-5 films onto α-Al_2O_3 disks and γ-Al_2O_3 tubes from suspensions of colloidal ZSM-5 (provided by Amoco). (See section 3: *Shape selective membranes - xylene separation.*) Results will be presented in the near future.

2. Zinc Phosphates

In recent years a number of phosphate-based molecular sieve phases have been identified. The most well-known of these are the $AlPO_4$ structures, which are neutral porous frameworks templated by organic bases. Anionic frameworks such as zinc phosphates and beryllophosphates (and arsenates) have been identified as well. These phases are not as thermally stable as the AlPOs, probably because of lower cation-oxygen bond order, and generally have not heretofore survived dehydration or template removal. Unlike the AlPOs, however, microporous zinc phosphates (ZnPOs) can be made using inorganic templates, which may not have to be removed in order for these phases to function as

molecular sieves. In addition, ZnPOs are much easier to synthesize as thin films than are the AlPOs.

2.1. Thin film synthesis

In FY 1994, we reported that certain ZnPOs thought to be microporous could be readily synthesized as films from metallic zinc-coated substrates. In FY 1996 we showed via computer modeling of gas permeation that the zinc oxide phosphates $M_3Zn_4P_3O_{13}$ and MZn_2OPO_4 (M = Na, Li) should admit He and H_2, but reject larger gas molecules.[4] In addition, these pores are interconnected in three dimensions, so that gas permeation through the lattice should be both rapid and independent of crystallographic orientation of the film. The phases containing smaller cations generally possess larger kinetic diameters. For example, $Na_3Zn_4O(PO_4)_3$ should accommodate H_2, but not CO_2; while $CsZn_2OPO_4$ should reject H_2, but still be permeable to He, H_2O and NH_3. This prediction is partially corroborated by the observation that these phases can reversibly absorb and desorb both NH_3 and H_2O (kinetic diameters $\approx$ 2.6 Å) without structural change. A $Na_3Zn_4O(PO_4)_3$ membrane could therefore be used for H_2 recovery, while a $CsZn_2OPO_4$ membrane could be used for gas dehydration.

In FY 1996, we devised routes to $K_3Zn_4O(PO_4)_3$ and $CsZn_2OPO_4$ films from ZnO wafers (prepared by cold pressing ZnO powder, then sintering) and Zn metal films (Figure 3). The K phase is particularly useful, since it is readily ion exchanged to yield the more permeable Na and Li phases. We have also found that the ZnO wafers are gas permeable, allowing viscous flow, and are thus useful as membrane substrates. Early results from gas-flow experiments with CsZn2OPO4 films made from ZnO wafers show significant permeabilities only to He, which is consistent with molecular sieving. While the films can be made leak-free, they are still fairly thick ($\approx$ 20 μm), and thus do not yield high gas flow rates. To render these process compatible with conventional tubular gas membranes, a method for depositing Zn metal or ZnO film on the inside of an alumina tube must eventually be found.

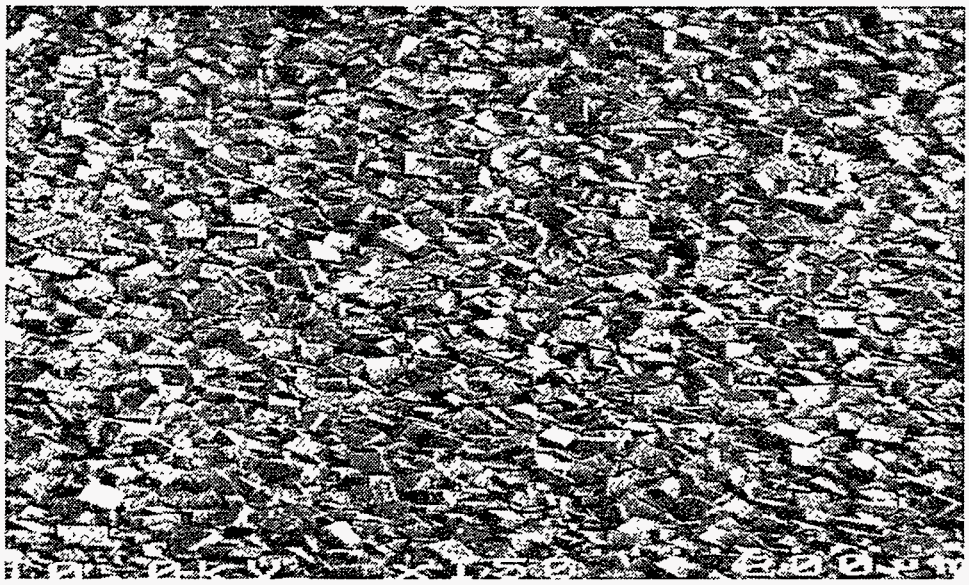

Figure 3. Inorganic thin film of $CsZn_2OPO_4$.

2.2. New zinc phosphate phases

In addition to the inorganic ZnPOs described above, we are investigating organic ZnPOs as molecular sieves. Because organic cations are larger than alkali metal cations, it is possible to produce larger-pore structures using organic templates. Given the relative facility of preparing ZnPO films, we view this approach as an alternative route to molecular sieve films with pores in the 3-5 Å range. However, all zinc phosphates stable with respect to dehydration or ion exchange have, to date, been inorganic zinc oxide phosphates. The goal of this project element is thus to identify large-pore ZnPOs that are stable enough to survive template removal without structural collapse.

It is possible that Zn-O-Zn bonds, such as those present in the Zn4O groups in the $M_3Zn_4O(PO_4)_3$ phases, may be responsible for their exceptional thermal stability. Extra ZnO units are generally absent from organic zinc phosphates, and these cannot be dehydrated or have template removed without structure collapse. However, all of the templates used in organic ZnPOs reported to date have been too weakly basic to stabilize the excess zinc oxide. Therefore, we have investigated ZnPO synthesis using template species that are basic enough to dissolve ZnO, and contain a high nitrogen/carbon ratio to facilitate post-synthesis template removal via calcination in oxygen.

In FY 1997, we continue our survey of the aqueous phase space of ZnO and P_2O_5 with guanidine, dimethylamine, DABCO (1,4-diazobicyclo[2.2.2]octane), ethylenediamine, and propylamine. New phases synthesized include a new "dimethylammine • ZnO • P_2O_5 • H_2O", its analog "dimethylammine • ZnO • As_2O_5 • H_2O" and a "DABCO • ZnO • P_2O_5 • H_2O". These phases have all been characterized by single crystal and powder X-ray

diffraction, elemental and thermal analyses. The dimethylamine phases appear to retain their pore structures upon detemplation. Currently, studies are ongoing to grow thin films of these phases and to study their gas separation abilities.

The "guanidine • ZnO • P_2O_5 • H_2O" phase space has yielded a new family of guanidine zinc phosphates, with six new phases discovered so far. Crystallographic structure solutions have been obtained for four of these phases by Prof. W. T. A. Harrison at the University of Western Australia, and were published in FY 1997. One phase in particular, "$(CN_3H_6)_3$ • $Zn_7(H_2O)_4(PO_4)_6$ • H_3O", contains the unusual structural feature of three guanidinium ions acting in concert to template an 18-membered ring. Rings of this size have never been identified in zeolites, and only recently in aluminophosphates [5], and this is the first example of cooperative templation in metal oxide frameworks (Figure 4).

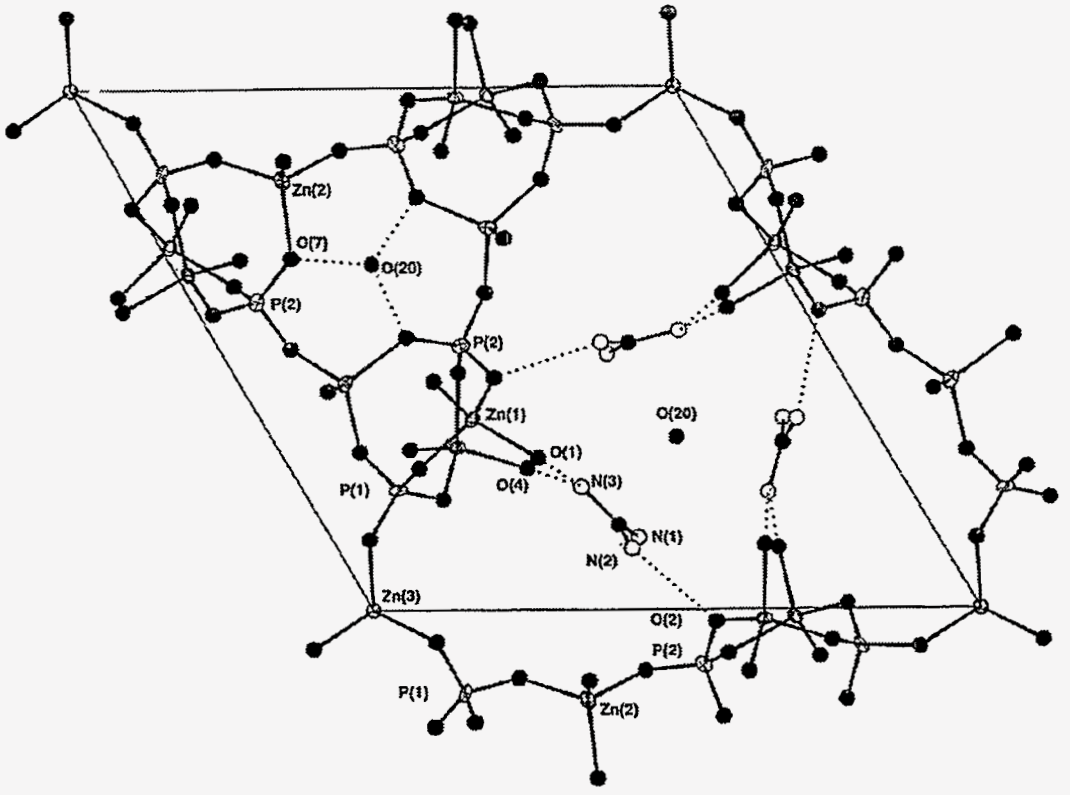

Figure 4. 18-membered ring, containing 3 guanidine cations, of the "guano-zinc phosphate."

Two of the other three structures that have been solved contain unusual structural features as well. The phase $(CN_3H6)_2$ • $Zn(HPO_4)_2$ has the lowest framework density (number of tetrahedral atoms per unit volume) of any crystalline microporous material identified to date. $(CN_3H_6)_6$ • $Zn_2(OH)(PO_4)_3$ • H_2O adopts a one-dimensional chain structure

involving three PO_4 groups triply-bridging pairs of distorted ZnO_4 tetrahedra. This feature has been seen in long-chain metal phosphonates, but this phase appears to be the first simple phosphate to adopt this polymeric configuration. We have not yet demonstrated template removal with retention of structure in the guanoZnPOs, but are currently attempting to stabilize the framework by including alkali metal cations to increase the Zn/P ratio.

Impact

The petroleum and natural gas refining industries would benefit significantly from high permeability molecular sieve films capable of separating light, fixed gases, particularly if the membranes can be used at high temperatures. The alkali metal zinc phosphates that we have synthesized as membranes are stable up to 700°C, which is compatible with hydrogen recovery. With sufficiently high permeability and low unit area cost, energy savings of several quad/yr could be achieved when all feasible applications of inorganic membranes are considered.[6]

3. Shape selective membranes - xylene separation

We are studying with Amoco Chemical Co. the use of microporous inorganic membranes to separate *p*-xylene from mixtures of the isomers. The *para* isomer is the precursor to terephthalic acid, which is principally used in poly (ethylene terephthalate) plastics. Because of this, *p*-xylene is a high-tonnage commodity, and a significant component of chemical industry production. Conventional technology for separating the isomers requires successive recrystallizations of the mixture at cryogenic temperatures, which is very energy intensive. The membranes will be used to enrich the mixture in *p*-xylene prior to crystallization, which will allow warmer temperatures and fewer crystallization steps to be used.

The composition of the "equilibrium mixture" of xylenes that results from toluene alkylation or disproportionation reactions is approximately 2 meta : 1 ortho : 1 para (i.e., 25% p-xylene). In *p*-xylene production, a feedstock containing an "equilibrium" mixture of xylenes is fed into a series of crystallizers operating at -90°C. The solid phase is enriched in the *para* isomer. The remainder is reisomerized (at ≈ 500°C) and returned to the first crystallizer unit. Our goal is to use shape-selective membranes to replace the first crystallizer, which is the most energy consumptive unit in the process.

It is known that the diffusivity of *p*-xylene through the zeolite phase ZSM-5 (MFI structure type) is 10,000 times that of ortho- or meta-xylene, due to smaller kinetic diameter of the para isomer.[7] This enhanced diffusivity favors synthesis of *p*-xylene in toluene alkylation and disproportionation reactions, and xylene isomerization, with the appropriately modified ZSM-5 catalysts. MFI/sol-gel films might thus be used to separate

p-xylene from a product stream consisting of a mixture of isomers; in addition, such a membrane could be packed with catalyst, separating *p*-xylene as it is formed. Our modeling efforts confirm this result. The ZSM-5 zeolite (MFI type framework) out perform a number of zeolites with similar pore sizes and structures for *p*-xylene separations. (The zeolites modeled include ZSM-5, Ferrierite, ZSM-22 and ZSM-23) (Figure 5).

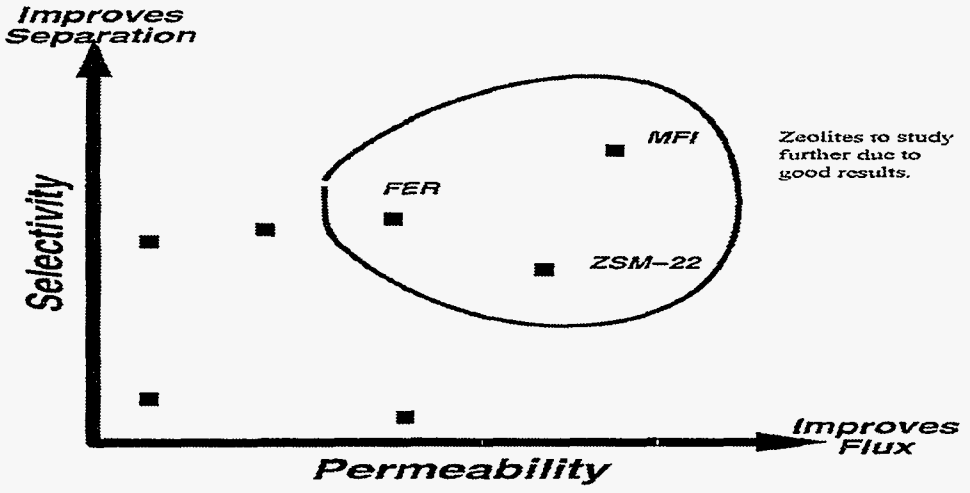

Figure 5. Results of Lennard-Jones interactions modeling (neglecting entrance and cation effects.

Three general methods for synthesizing MFI-type molecular sieve films have been explored. The first involves suspending the zeolite in a silica sol, then dip coating the substrate with the suspension. We used this method to make selective films with several zeolites, including ZSM-5, that have been used as discriminating elements in acoustic wave sensors.[8] An advantage of this "slurry" method is that it can be used with any desired molecular sieve that can be prepared with a sufficiently fine particle size (typically <1 μm). We have also demonstrated a second method in which a nonpermeable sol-gel film is added to a zeolite film that has been previously deposited on a porous support. The sol-gel phase acts to caulk intercrystalline gaps, and promote adhesion to the substrate. In a third method, the zeolitic phase is hydrothermally nucleated and crystallized from sol-gel derived nutrients pre-deposited on a substrate (Figure 6).[9] Initial experiments repeatedly produce ZSM-5 films of various Si/Al ratios and crystallite sizes (Figure 7). Each of these methods will be used to synthesize composite MFI/sol-gel membranes for testing in a bench-scale xylene separation module.

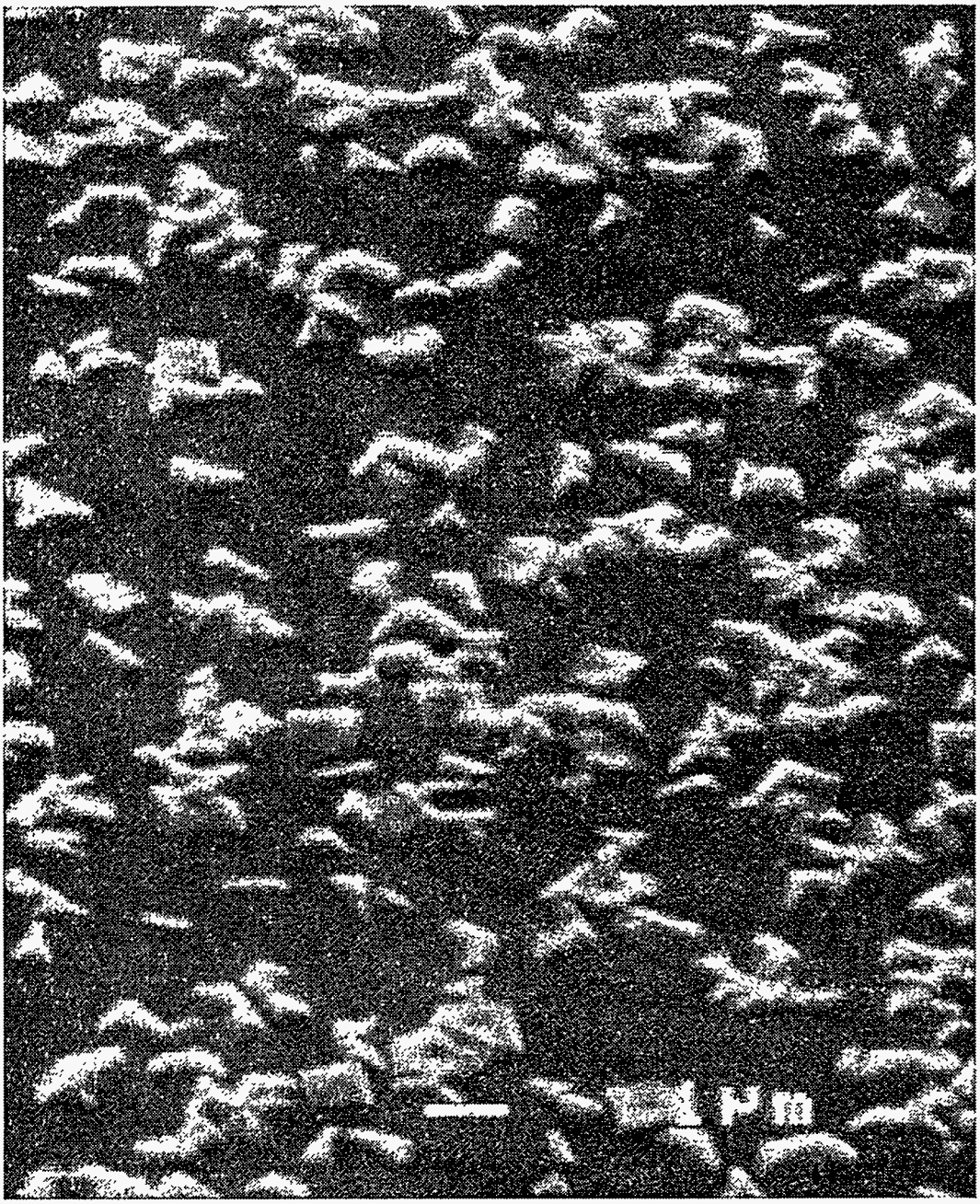

Figure 6. Inorganic thin film composite of Zeolite and Sol-gel.

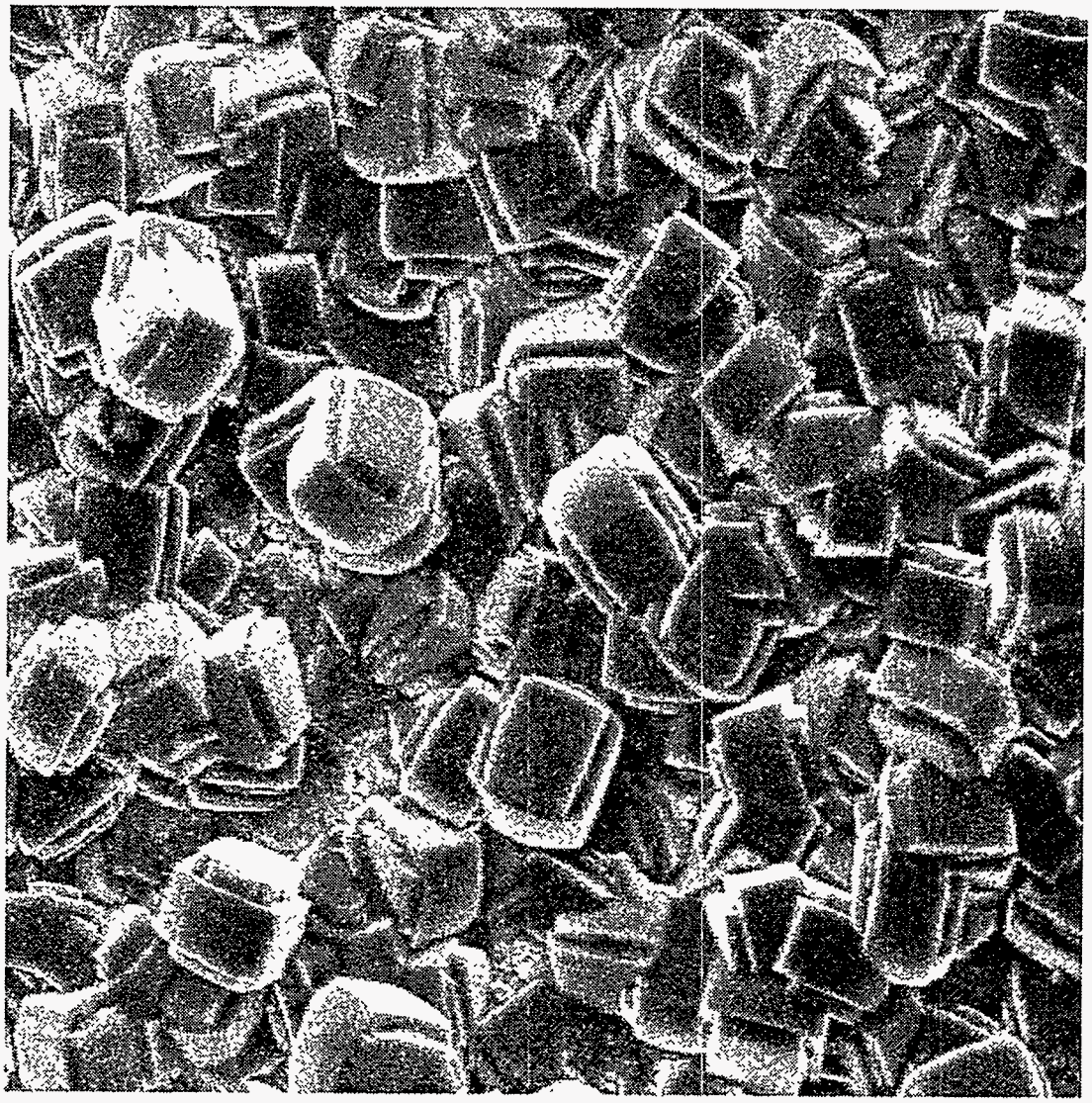

Figure 7. MFI crystals grown on α-Al_2O_3 surface (crystals approximately 200nm across), pre sol/gel "caulking."

Started in FY 1997 and continuing through June 1998, the following milestones will be met for the first full year of the CRADA:

A. Model the permeation of xylene mixtures through MFI structures in order to identify the zeolite phase that will maximize permeability of *p*-xylene in an equilibrium (2:1:1) vapor stream;
B. Synthesize leak-free MFI-type membranes by caulking MFI films with silica sols and hydrocarbon solutions, and by coating suspensions of MFI phases in silica sols onto membrane substrates; and
C. Employ different Si/Al ratios in the zeolite (in the MFI structure type, these range from unity to infinity) to obtain different acidities, and thereby affect the isomerization of the xylene.

Impact

If these membranes eliminate the first crystallization step in *p*-xylene production worldwide, approximately 0.070 quad/yr will be saved, principally in the form of decreased natural gas consumption.

4. Synthesis of Novel Encapsulated Gel Supported Nanocluster Catalysts

The synthesis of three new catalysts this quarter highlights the versatility of our methodology in catalyst synthesis. We are now capable of making highly dispersed noble and base metals, mixed metal systems, alloys, and layered particles on silica, alumina, and silica/alumina mixtures. The catalysts can be used as pseudo-homogeneous liquids and heterogeneous powders, monoliths, and thin films.

We have synthesized three new types of encapsulated gel supported nanocluster catalysts:
(1) A literature preparation for the synthesis of a silica monolith in ethanol is used. The procedure will be extended to alumina;
(2) Exploration in using these materials as thin films. Our cluster, gel monomer solution is incipient wet onto Al_2O_3 extrudate. The powdered is filtered, briefly rinsed in acetone, and then incipient wet in an acidic solution. The powder is once again filtered, rinsed, and finally dried. It is hoped the clusters and gel monomer are adsorbed onto the extrudate and then hydrolyze and condense to form a cluster embedded thin film in the presence of the acidic solution;
(3) A support of varying composition. We have synthesized a full range of Al_2O_3 / SiO_2 mixtures. As mentioned earlier, Al_2O_3 is generally more active than SiO_2 due to surface acidity. This increased activity can lead to a decrease in selectivity. For example, the dehydrogenation of propane gives only propylene with SiO_2 supports. With Al_2O_3, propane disappears much more quickly, but hydrogenolysis can lead to the formation of unwanted ethylene. By providing mixtures of SiO_2 and Al_2O_3, it may be possible to finely tune the activity and selectivity of our catalysts.

REFERENCES

1. *a.* te Hennepe, H. J. C.; Bargeman, D.; Mulder, M. H. V.; Smolders, C. A. *J. Membr. Sci.* **1987**, *35,* 39-55. *b.* Jia, M.; Peinemann, K.-V.; Behling, R.-D. *J. Membr. Sci.* **1991**, *57,* 289-296.

2. Schoeman, B. J.; Sterte, J.; Otterstedt, J.-E. *Zeolites* **1994**, *14,* 208-216.

3. Marquart, T. A. Ph.D. Dissertation, University of Illinois-Urbana, 1994.

4. The synthesis of bulk $M_3Zn_4(PO_4)_3$ phases was first reported in Harrison, W. T. A.; Broach, R. W.; Bedard, R. A.; Gier, T. E.; Bu, X.; Stucky, G. D. *Chem. Mater.* **1996**, *8*, 691-700. The MZn_2OPO_4 phases were first synthesized in FY94 as part of this project.

5. Freyhardt, C. C.; Tsapatsis, M.; Lobo, R. F.; Balkus, K. J.; Davis, M. E. *Nature* **1996**, *381*, 295-298.

6. Fain, D. E. *MRS Bulletin* April 1994, p. 40.

7. *a.* Chen, N. Y.; Kaeding, W. W.; Dwyer, F. G. *J. Amer. Chem. Soc.* **1979**, *101*, 6783. *b.* Young, L. B.; Butter, S. A.; Kaeding, W. W. *J. Catal.* **1982**, *70*, 418.

8. Bein, T; Brown, K.; Frye, G. C.; Brinker, C. J. *J. Am. Chem. Soc.* **1989**, *111*, 7640.

9. Dong, J.; Dou, T.; Zhao, X.; Gao, L. *J. Chem. Soc., Chem. Commun.* **1992**, 1056-8.

PUBLICATIONS

W. T. A. Harrison and M. L. F. Phillips, "Crystal Structures of Novel Guanidinium Zinc Phosphates", *Chem. Mater.* **1997**, *9*, 1837.

A. Martino, S. A. Yamanaka, J. S. Kawola, D. A. Loy, "Encapsulation of Gold Nanoclusters in Silica Materials via an Inverse Micelle / Sol-Gel Synthesis," *Chem. Mater.* **1997**, *9(2)*, 423.

B. G. Karle, C. J. Brinker, and M. L. F. Phillips, "Zeolite Membranes from Kaolin," Mat. Res. Soc. Symp. Proc. **1997**, *431*, in press.

W. T. A. Harrison and M. L. F. Phillips, "Template Cooperation Effect Leading to 18-Ring Cavities in the Open-Framework Guanidine Zincophosphate $(CN_3H_6)_3 \cdot Zn_7(H_2O)_4(PO_4)_6 \cdot H_3O$," *Chem. Comm.* **1996**, 2771-2772.

PRESENTATIONS

P. I. Pohl, D. Fisler, T. M. Nenoff, "Modeling of Gas Permeation in Zeolite Membranes," The Nineth Annual Joint Meeting of the New Mexico Secions of the Americal Ceramic Society and the Materials Research Society, Albuquerque, NM (November 1997).

T. M. Nenoff, E. D. Ozokwelu, "Selective Inorganic Thin Films," AIM Program Annual Review, Albuquerque, NM (June 16-18, 1997).

SYMPOSIUM ORGANIZED

A symposium entitled "Catalysis with Designed Materials" has been accepted by the Colloid and Surface Science Division of the American Chemical Society, and scheduled for the Fall 1998 Boston National ACS Meeting. Tina Nenoff is the organizer. The focus of the symposium will be the use of computer modeling, tied with materials synthesis, to efficiently predict and synthesize novel materials for catalysis and separations. The work from this program and, in particular from the CRADA, will be presented here.

PATENTS

None during this reporting period.

PATENT DISCLOSURES

M. Phillips, "A Thermally Stable Zinc Phosphate Molecular Sieve", SD-5962.

M. Phillips, "A New Method for Preparing Zinc Oxide Thin Films from Solution", SD-5963.

LICENSES

None during this reporting period.

INDUSTRIAL INPUT AND TECHNOLOGY TRANSFER

As part of the CRADA in negotiation, Amoco Chemical Company will provide crystallographic data for and samples of zeolites of interest for xylene separation. We will use the structure data to model relative permeation rates of xylene isomers in mixtures, and synthesize membranes from the zeolite samples. Amoco will then measure selectivity of composite zeolite-sol gel membranes invented at Sandia to determine feasibility of scale-up to a pilot plant.

COST SHARING

The 3-year, $2.769M CRADA has been signed and is in effect between Sandia National Laboratories and the Amoco Chemical Company. Amoco is to contribute in-kind funds in the following manner: $512K for year 1; $480 for year 2; $502 for year 3. The start date was June 16, 1997.

HIGHLIGHTS

We have fabricated molecular sieve membranes by depositing films of microporous cesium zinc phosphate onto porous zinc oxide wafers. These membranes are permeable to helium, but not to hydrogen or to the other light, fixed gases tested. We have also synthesized an organic zinc phosphate phase that survives removal of template and water without altering the structure of the ZnPO framework. This is the first ZnPO phase for which nondestructive template removal has been demonstrated. Films of this phase were successfully grown onto ZnO wafers.

We have negotiated and begun (6/16/97) a CRADA with Amoco Chemical Company to study the feasibility of using shape-selective molecular sieve membranes to enrich *p*-xylene from mixtures of the isomers. In FY 1997, we will write a computer code that will allow us to predict relative permeation rates of xylene isomers through several zeolitic phases with a variety of compositions. We will also synthesize shape-selective membranes using zeolitic phases identified by Amoco as having promise for arene separations. Amoco will measure xylene permeation through these Sandia-synthesized membranes.

PROJECT INVESTIGATORS

In FY 1997 this project involved the following participants from Sandia National Laboratories, Albuquerque, NM; University of New Mexico, Albuquerque, NM; and the University of Western Australia, Nedlands, WA.

NAME	PROJECT ROLE
Dr. Tina M. Nenoff, SNL	Principal investigator, film synthesis
Dr. Phillip I. Pohl, SNL	Permeation modeling
Dr. C. Jeffrey Brinker, SNL	Sol-gel film development
Dr. Anthony Martino, SNL	Nanocluster catalysts
Alejandra V. Chavez, SNL & UNM	Zinc phosphate synthesis
Steven G. Thoma, SNL	Membrane synthesis
Prof. William T. A. Harrison, UWA	Crystallography

POLYMERS

INDUSTRIAL APPLICATIONS OF CONDUCTING POLYMERS: POLYMER ELECTROLYTE ELECTROCHEMICAL REACTORS OF LOWERED ENERGY CONSUMPTION

S. Gottesfeld
Electronic and Electrochemical Materials and Devices, MST-11
Los Alamos National Laboratory
Los Alamos, New Mexico 87545

INTRODUCTION

The Conducting Polymer Project funded by the AIM Program has developed new methods for the synthesis of conducting polymers and evaluated new industrial applications for these materials which would result in significant reductions in energy usage or industrial waste. During FY 1997, we specifically addressed electrochemical reactors (ECRs) based on polymeric electrolytes. In the chlor-alkali industry, electrochemical reactors based on polymer electrolyte membranes consume around 2% of the total electric power generated in the United States. Our newest activity which started in FY 1996, is devoted to energy efficient ECRs for this industry. Energy savings as high as 50% could be achieved with the energy-saving ECR technology which is being developed by us and corresponding lowering in CO_2 emissions would result.

Background

During FY 1996, we explored a scheme for effectively reducing energy consumption in a chlor-alkali ECR, using an oxygen cathode and a cation conducting polymeric membrane (CCM) as basis for effective membrane/electrode assemblies (MEAs) for chlor-alkali ECRs. Figure 1 above shows the basic idea of the advanced, polymer membrane based ECR which we now develop. The conventional configuration of a chlor-alkali ECR which generates chlorine and caustic soda by electrolysis of sodium chloride brine is shown on the left hand side of Figure 1. The cell voltage required for significant electrolysis rates of , 300 A/ft^2, is 3.2-3.3 V. Energy consumption per-unit-weight of the products (chlorine and sodium hydroxide) is directly proportional to cell voltage. Lowering cell voltage at given current density (i.e., at given production rate) is therefore the key for achieving energy savings in this industrial process which consumes 2% of the electric energy produced in the United States.

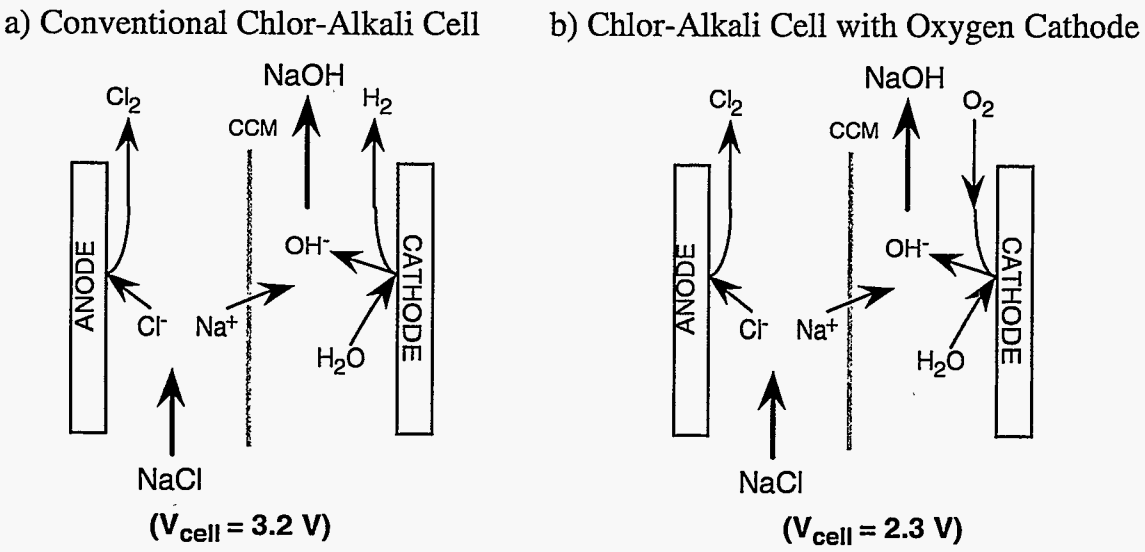

Figure 1. Scheme for reducing energy consumption in a chlor-alkali ECR using an effective oxygen cathode and a cation conducting polymeric membrane (CCM) as basis for an effective membrane/electrode assembly.

Some time ago it was recognized that if the hydrogen-evolving cathode were replaced by an oxygen-reducing cathode, the voltage of the cell could be reduced (in principle) by about 0.9V. The change of the cathodic process by introduction of oxygen as cathode reactant and the corresponding expected lowering in cell voltage are schematically depicted on the right-hand-side of Figure 1. To achieve the expected savings in cell voltage from introduction of oxygen as "cathode depolarizer," a very effective oxygen electrode is required. Furthermore, the cell configuration has to be such that a gas (oxygen supplied) cathode could operate side-by-side with a liquid (brine) filled adjacent cell compartment. Both of these targets have not been easy to achieve and the result has been that the concept of a chlor-alkali cell with an oxygen cathode has not yet been implemented commercially. This is in spite of the fact that efforts to prove feasibility of the concept continue to date, particularly in Japan where the availability and cost of electric power are more significant issues today than in the United States.

With stronger attention to the generation rate of CO_2 in the context of global warming concerns, possible cutting of 40% of the total volume of CO_2 generated by this major US industry may become a significant target.

In light of the energy savings incentives described above, in 1996 we adapted an advanced oxygen electrode technology (developed at LANL originally for application in polymer electrolyte fuel cells) for application in chlor-alkali ECRs. An important element

of the new project has been immediate industrial interest: Dow Chemical expressed interest in working with us on this project based on a CRADA.

TECHNICAL PROGRESS - FY 1997

(1) Experiments in small scale Fuel Cell Hardware

(a) Cell with single-layer ionomeric membrane

We started experimentation with small scale hardware employed at LANL for fuel cell work (5 cm^2 active area). The membrane employed was a fuel cell membrane, rather than chlor-alkali membrane, and, therefore, current efficiencies were limited. Furthermore, the graphite fuel cell hardware would not have sufficient long-term stability as chlor alkali ECR hardware. This fuel cell hardware was used first in spite of those shortcomings, to generate initial data.

Cell polarization curves obtained with this chlor-alkali ECR, using an ordinary fuel cell membrane (Figure 2) demonstrated that an advantage of about 1.0 V was gained when the chlor-alkali ECR was operated with an oxygen cathode (E_{cell} = 1.85 V at 0.4 A/cm^2, vs. the same ECR with a hydrogen-evolving cathode requiring E_{cell} = 2.82 V).

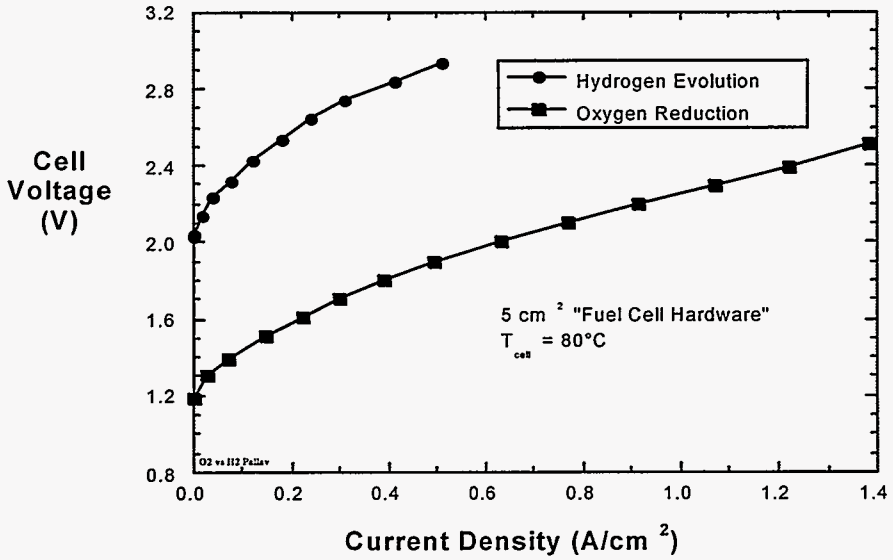

Figure 2. Small scale chlor-alkali cell based on fuel cell hardware and utilizing single layer ionomeric membrane: performance with hydrogen-evolving and oxygen-consuming cathodes

(b) Cell with bilayer ionomeric membrane of type used in chlor-alkali ECRs

Next we tested our oxygen cathode in the same 5 cm^2 cell employing a commercial chlor-alkali membrane which would be the membrane of choice in the chlor-alkali industry. This is a bilayer membrane which provides higher selectivity, hence higher current efficiency in the chlor alkali process, at some cost in cell voltage. A cell voltage of 2.0 V was now measured at 0.4 A/cm^2 in the 5 cm^2 cell hardware operated with an oxygen cathode (Figure 3). This is approximately 0.2V higher than obtained with a single-layer fuel cell membrane (Figure 2), fully explained by the higher resistance of the more selective, bilayer membrane. Current efficiencies were indeed substantially higher with the bilayer membrane in the oxygen cathode operation mode, an important requirement from any competitive chlor-alkali reactor. Cell voltage lowering remained substantial: cutting cell voltage from 3.2 V down to 2.0 V at constant commercial level throughput corresponds to savings of 38% in electric energy used per-unit-weight of product.

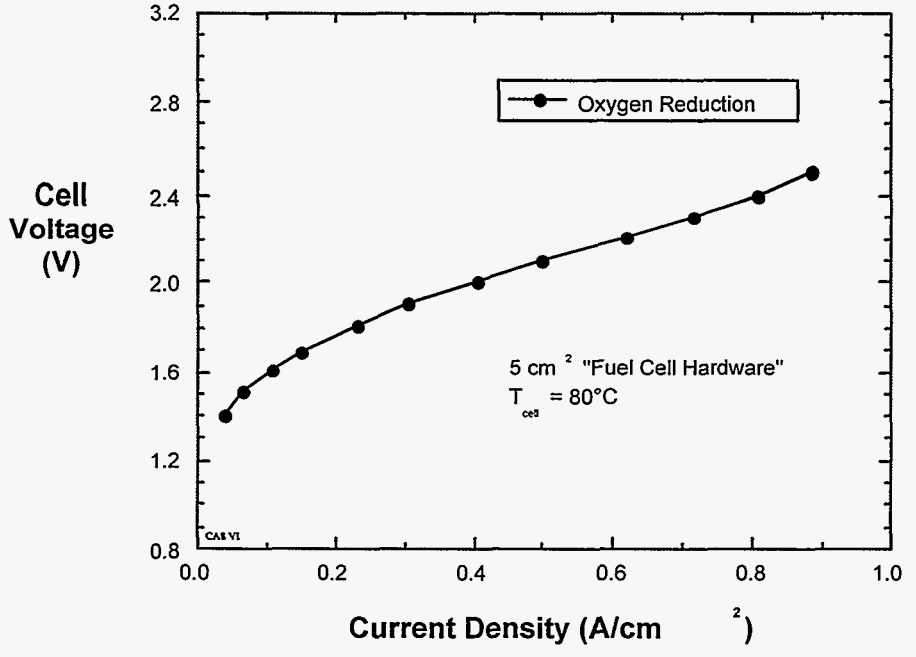

Figure 3. Polarization curve obtained using a 5 cm^2 chlor-alkali ECR with oxygen cathode and commercial chlor-alkali membrane.

(2a) Implementation of Dow test hardware and modification of oxygen cathode for use in it

Adaptation by LANL of a small scale reactor (58 cm^2), employed for testing and development in the Dow chlor-alkali laboratory at Freeport, TX, was subsequently implemented. Use of this cell type allows us to compare directly with the performance

obtained by Dow in an exact same cell configuration under ordinary mode of chlor-alkali ECR operation (with hydrogen evolving cathode), and thus conclude on the real voltage advantage obtained with our oxygen consuming cathode.

Making the change from operating 5 cm^2 chlor-alkali cells to Dow's 58 cm^2 test cells, necessitated also redesigning and rebuilding of a chlor-alkali ECR lab testing system at LANL. The new system has been designed and built to accommodate continuos operation of 3 test cells in parallel. Several engineering controls were designed and implemented such as water make-up to the brine and to the caustic to maintain desired solution concentrations, a chlorine scrubber system to safely convert chlorine gas to ordinary "bleach" for disposal, and a brine purification system. Brine purification, in particular, is critical to achieve optimum current efficiencies over sustained periods of operation. Our brine purification system went through some iterations to achieve eventually the level of purity required (20 ppb or less calcium ion).

A critical design issue for implementing the oxygen cathode in the Dow hardware has been efficient sodium hydroxide removal from the cathode and provision of adequate oxygen and water access to the cathode catalyst layer. We designed new cathode chambers to replace the ones typically used for caustic-submerged hydrogen evolution electrodes. The new cathode chambers facilitate collection of caustic and in-situ oxygen reactant humidification by deionized water. The water is separated from the caustic collection side and the former can also heated by a cartridge heater to maximize the water vapor pressure in the oxygen inlet gas stream.

We began testing LANL oxygen electrodes in the 58 cm^2, industrial-style cells, employed by Dow Chemical for lab-scale testing. The much lower pressure across the industrial cell components (about 1 psi) has important engineering advantages and should preferably be maintained in the context of any cell retrofitting plans. It requires, however, achievement of low contact resistances at very low applied force across the cell. We first attempted to attain better contact at 1 psi across the cell with our carbon based cathode material, followed by in-house fabrication of cathode gas diffusion structures with 60 mesh wire screens replacing the carbon cloth. By applying the carbon black/PTFE filler in an optimized way, enhanced contact with the current collector component could be ensured. After further replacement of the current collector material, quite good performances (i.e., cell voltage of 2.3 V at 350 mA/cm^2) was initially observed but subsequently degraded. A polarization curve for the 58 cm^2 cell with a metal screen cathode is shown in Figure 4. The cell resistance was as high as 3 Ω cm^2, the main reason for the high cell voltage (a typical value for this ECR at high mechanical pressure across the cell is 1.5 Ω cm^2) . Correcting the voltage-current curve for ohmic losses illustrates that the electrode processes themselves were very efficient. Were the cell resistance to remain at 1.5 Ω cm^2, the voltage at 350 mA/cm^2 would have been below the 2.2 V target.

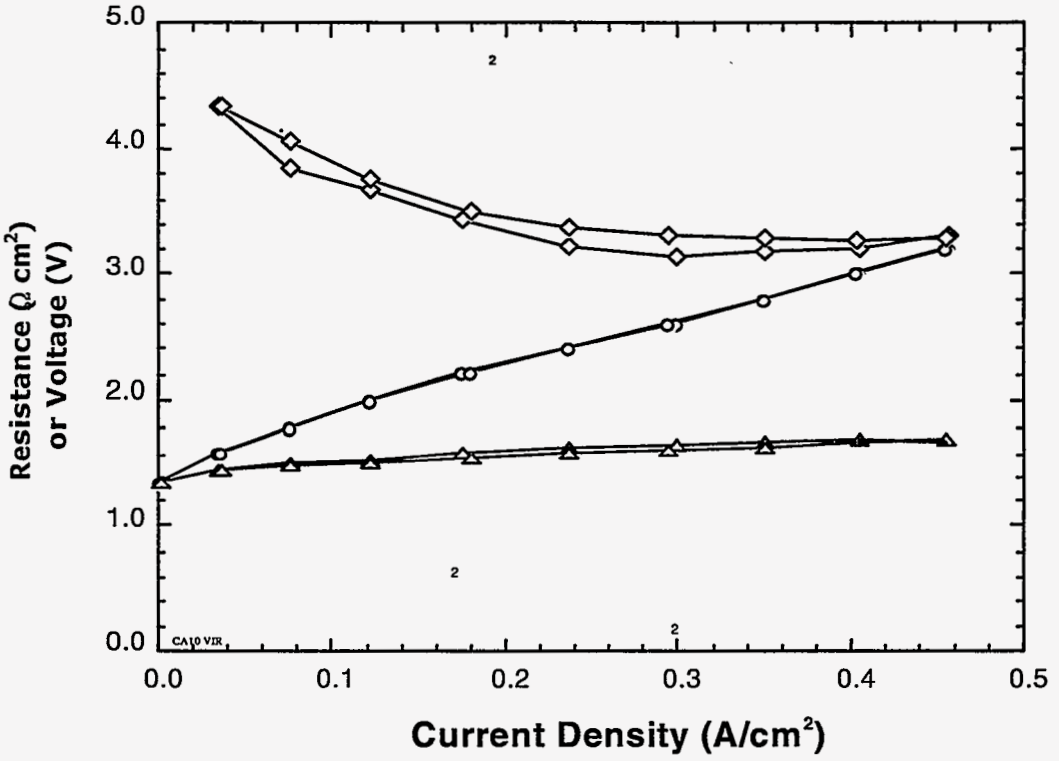

Figure 4. Cell polarization (middle curve), iR corrected polarization (bottom curve), and cell resistance (top curve) as function of cell current for a modified Dow test cell with an oxygen electrode.

Additional experimentation has indicated that the transport properties and cell resistance are closely linked to cathode properties. Work is thus continuing in developing satisfactory current collector configurations and in optimizing the cathode structure to attain lower cell resistances in this industrial type cell configuration.

As to current efficiency, we run the cells with a 30-32% product concentration at measured current efficiencies on the order of 96-98% which is equal to or better than current efficiencies obtained in chlor-alkali ECRs with hydrogen evolving cathodes.

INDUSTRIAL INPUT and TECHNOLOGY TRANSFER

CRADA with Dow Chemical

A Cooperative Research and Development Agreement Amendment (CRADA) between UC (LANL) and Dow Chemical was executed on June 18, 1997, to include the collaborative effort on chlor-alkali ECRs of lowered electric energy consumption. The LANL effort in this collaboration is the continuation of our project under the AIM program on ECRs of lowered energy consumption.

Final Dow management approval for the Joint Work Statement (JWS) was obtained at the end of April, based on technical approach described in a JWS. The JWS includes materials, components and cell configuration optimization efforts to be pursued at LANL; techno-economic evaluation of the merit of this concept as function of plant location which affects cost of power and marketability of hydrogen; and, pilot plant testing to be performed in the third year of the project to the degree justified by preceding life tests in smaller cells, employing materials and cell structure optimized by LANL work during the first two years.

We had excellent opportunities during FY 1997 to interact with Dow Chemical. They visited Los Alamos three times during this year. We have visited twice their central chlorine production facility to establish contact with production engineers. We had a good opportunity during the visit to discuss in-depth a strategy for demonstration of the concept at pilot plant level.

HIGHLIGHTS

• Utilizing fuel cell hardware, we demonstrated the operation of a chlor-alkali cell at target voltage level (0.4 A/cm^2 at 2.0V) with a LANL oxygen cathode and a commercial chlor-alkali membrane of high current efficiency (>95%). Lowering cell voltage for a chlor-alkali ECR from the ordinary level of 3.2 V to 2.0 V at constant, commercial throughput level, corresponds to savings of 38% in electric energy invested per-unit-weight of product. This is of special significance in an industry that consumes about 2% of all of the electric power generated in the US. There would be a corresponding percentage of reduction in CO_2 emissions associated with this major industry.

• We adapted a standard 58 cm^2 cell, of the type employed by Dow Chemical for lab testing, to routinely test ECRs with oxygen cathodes.

• We redesigned and rebuilt our chlor-alkali ECR lab testing system. The new system has accommodates continuous operation of three test cells in parallel. Several engineering controls were included such as water make-up to the brine and to the caustic, a chlorine scrubber system to safely convert chlorine gas to ordinary "bleach" for disposal, and a brine purification system.

• We ran our oxygen cathode cells with a 30-32% product concentration at measured current efficiencies on the order of 96-98% which is equal to or better than current efficiencies obtained in chlor alkali ECRs with hydrogen evolving cathodes.

• Introduction of an oxygen cathode in an industrial type cell which employs minimal mechanical pressure across cell elements results in contact resistance and some cathode structure issues that need to be further resolved. Appropriate cell configurations for resolving such performance limitations are being implemented.

PROJECT INVESTIGATORS

NAME	ACTIVITIES	FTE
Gottesfeld	Principal Investigator Planning and Supervision	0.25
Christine Zawodzinski	Reactor Fabrication and Testing	0.50
Mahlon Wilson	Reactor Design and Testing	0.30
Chuck Derouin	Technical Assistance	0.20
Don McMurray	Technical Assistance	0.15

POLYMERIZATION AND PROCESSING OF POLYMERS IN MAGNETIC FIELDS

M. E. Smith and B. C. Benicewicz

Polymers and Coatings Group
MST-7, MS E549
Los Alamos National Laboratory
Los Alamos, NM 87545

INTRODUCTION

The ability to align polymers in magnetic fields presents a unique opportunity to improve the mechanical properties of epoxy thermosets for lightweight structural applications. The material under study is the diglycidyl ether of dihydroxy a-methylstilbene, crosslinked with sulfanilimade. Under the proper thermal profile during the epoxy cure, the material forms a smectic liquid crystalline structure that dramatically increases it's tensile strength. This material and its successful processing show great promise in meeting the continuing national need for advanced lightweight materials.

TECHNICAL PROGRESS - FY 1997

The project entered FY 1997 with the demonstrated ability to increase the tensile modulus of the epoxy system nearly a factor of three through the use of magnetic fields in the 4 to 7 Tesla range. Advances in the reduction of time necessary for field exposure had also been achieved through the selective use of B-staging, or partially reacting the material prior to magnetic field processing.

The advances in FY 1997 were focused upon scale-up to demonstrate commercial viability of structural part production; reduction of field strength needed to produce the mechanical property enhancements and study by deuterium NMR to better understand the orientation mechanism and structural results within the network.

Plaques of 8" x 8" x 0.125" were successfully produced through the use of a large magnetic field similar to those used in medical MRI facilities (see Figure 1). The static field strength applied was 1.5 Tesla. The plaques produced had a 50% increase in the modulus as compared to unoriented plaques. Measurements of the thermal expansion coefficients were consistent with the tensile results.

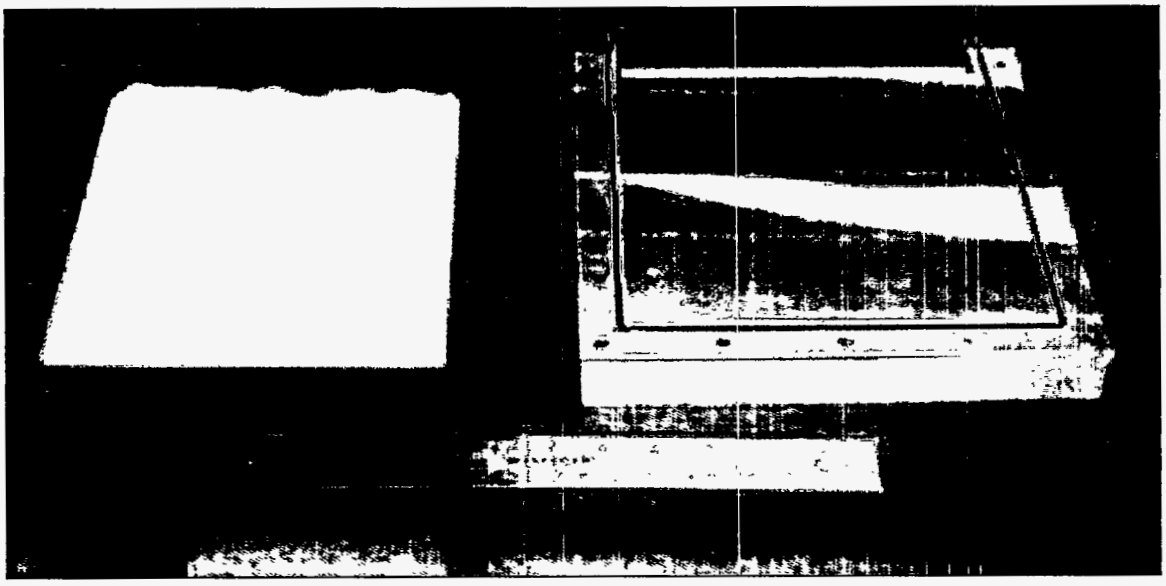

Figure 1. Plaque and mold face employed in magnetic field processing. The ruler shown is a standard 12" length. The plaque (left) is 8" x 8" with a 0.125" thickness. In this sample, the orientation of the material is horizontal (left-right as pictured). The mold (right) is fabricated from aluminum to minimize interaction with the magnetic field.

The mold design was kept as simple as possible while still allowing for the determination of transverse and tensile properties. Excellent uniformity of the sample was found, therefore edge effects of the walls and open top surface are not present with the magnetic process. These effects are typically rather pronounced for shear flow orientation processes.

Continuing research is focused on the ability to produce thicker parts, and evaluate the time during the thermoset cure when the efficiency of the magnetic field is most significant on the orientation rate of the molecules. The experimental design of these areas has been completed and the experimental schedule is currently being evaluated.

Curing in the magnetic field orients the molecules parallel to the field and allows the phenyl rings to undergo ring cooperative ring flips at much lower temperatures. This response is shown in Figure 2. As the chemical species of the molecules become isotropic in their mobility and environments, the spectral peaks narrow. This effect is seen in the lower spectra collected at elevated temperatures.

The NMR studies have shown that there exists mobility of the epoxy structure in the cured parts; however this mobility is highly restricted due to the liquid crystalline packing. The crosslinking agent, sulfanilamide, does not orient but rather serves as the boundary between the stacked smectic layers.

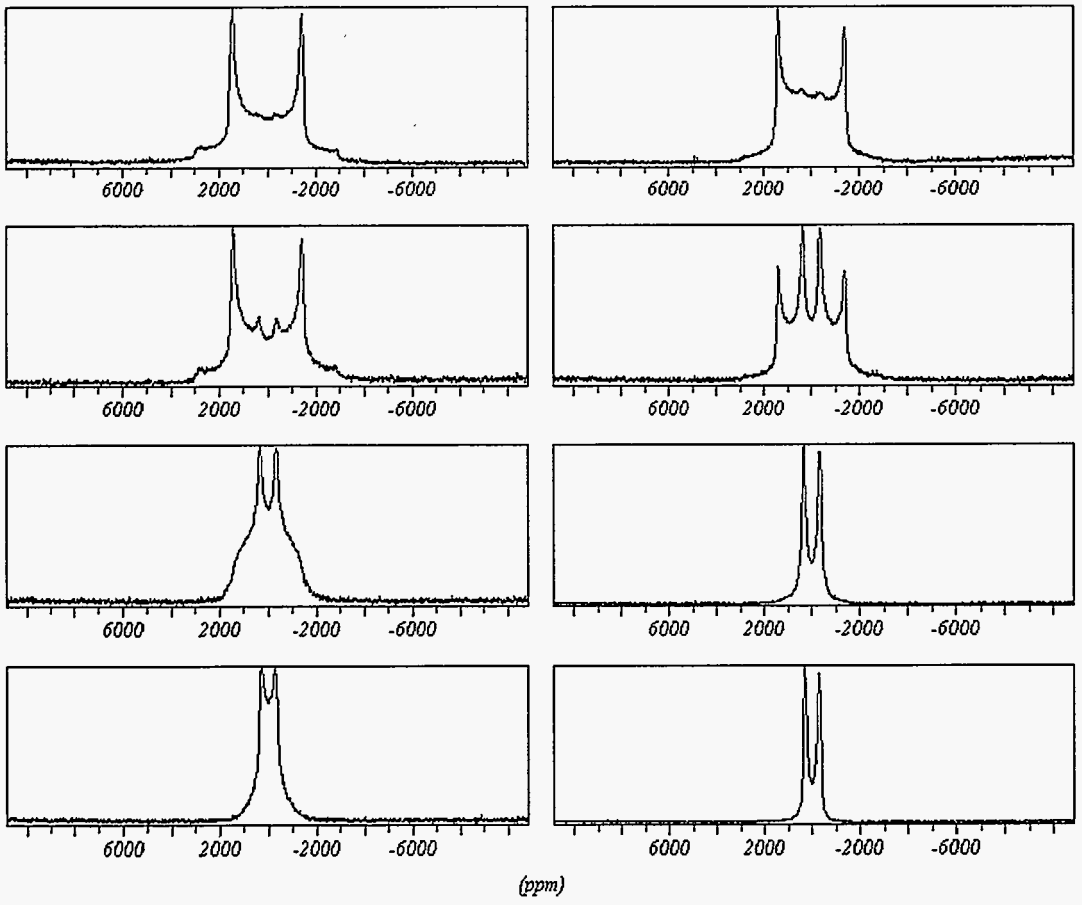

Figure 2. Deuterium NMR Spectra of Dow's DGEHAMS thermosetting epoxy. Left column are spectra of a sample cured outside of the magnetic field at the temperatures (top to bottom) 173°K, 273°K, 373°K and 473°K. The spectra on the right are of a sample cured in a field of 7.2 Tesla, collected at the same temperatures. The protons on the epoxy monomer phenyl rings were replaced with deuterons for these spectra.

MILESTONES

• Successfully produced large plaque samples or excellent uniformity as determined by visual inspection and mechanical property analysis.

• Demonstrated feasibility of using magnetic fields in the 1-2 Tesla range as provided with commercially available equipment.

• Determined the nature of the molecular packing structures as aligned in the magnetic field by NMR.

PUBLICATIONS

Journals

Magnetic Field Processing of Liquid-Crystalline Thermosets, B.C. Benicewicz, M.E. Smith, J.D. Earls, R.D. Priester, Jr., and E.P. Douglas, Chemtec, **1997**, 27(8), 44-48.

Properties of Liquid Crystal Thermosets and their Nanocomposites, D.A. Langlois, M.E. Smith, B.C. Benicewicz, R.P. Hjelm, and E.P. Douglas, Applications of High Temperature Polymers, CRC Press, Boca Raton, FL, **1997**, 79-96.

Effect of High Magnetic Fields on Orientation and Properties of Liquid Crystal Thermosets, M.E. Smith, B.C. Benicewicz, E.P. Douglas, J.D. Earls, and R.D. Priester, Jr., Polym. Prepr. **1996**, 37(1), 50-51.

Phase Behavior of Liquid Crystalline Thermosets, D.A. Langlois, M.E. Smith, B.C. Benicewicz, and E.P. Douglas, Polym. Mat. Sci. Eng. **1996,** 74, 135-136.

PRESENTATIONS

M.E. Smith, E.P. Douglas, B.C. Benicewicz, J.D. Earls, and R.D. Priester, Jr., High Modulus Liquid Crystalline Thermosetting Resins Through Novel Processing Techniques, Materials Research Society Meeting, San Francisco, CA (April 1996).

B.C. Benicewicz, M.E. Smith, and E.P. Douglas, Recent Developments in Liquid Crystalline Thermosets, ACS Meeting, ACS Industrial and Engineering Award Symposium, New Orleans, LA (March 1996) (invited).

D.A. Langlois, M.E. Smith, B.C. Benicewicz, and E.P. Douglas, Phase Behavior of Liquid Crystalline Thermosets, ACS Meeting, Polym. Mat. Sci. Eng. Div., New Orleans, LA (March 1996).

M.E. Smith, B.C. Benicewicz, E.P. Douglas, J.D. Earls, and R.D. Priester, Jr., Effect of High Magnetic Fields on Orientation and Properties of Liquid Crystalline Thermosets, ACS Meeting, Polym. Div., New Orleans, LA (March 1996).

HONORS AND AWARDS

Los Alamos National Laboratory, "Excellence in Industrial Partnerships Award," 1996

PATENTS/DISCLOSURES

High Magnetic Field Processing of Liquid Crystalline Polymers, Application No. 08/608,343

LICENSES

None.

INDUSTRIAL INPUT and TECHNOLOGY TRANSFER

This project is continuing under a CRADA agreement, initiated in FY 1994. The industrial partner has been the material supplier and collaborator in the processing and evaluation of the material performance. Quarterly meetings are held at both Los Alamos National Laboratory and The Dow Chemical Company, Freeport, TX.

ESTIMATED ENERGY SAVINGS

Significant energy savings exist through the magnetic processing technique presented for the production of high-strength, lightweight, structural components. Additional energy savings would result from the use of self-reinforcing liquid crystalline resins with faster cure times, as the faster time requires less energy per part in a continuous production scheme. Additionally, liquid crystalline materials do not require reinforcing fillers, mechanical compounding, or excessive handling in a manufacturing process.

INTERNAL DISTRIBUTION

1-2. Central Research Library
3. Document Reference Section
4-5. Laboratory Records Department
6. Laboratory Records, ORNL RC
7. ORNL Patent Section
8. P. Angelini
9. B. R. Appleton
10. G. A. Aramayo
11. R. L. Beatty
12. P. F. Becher
13. T. M. Besmann
14. E. E. Bloom
15. C. A. Blue
16. R. A. Bradley
17. K. Breder
18. C. R. Brinkman
19. G. M. Caton
20. R. H. Cooper, Jr.
21. D. F. Craig
22. S. A. David
23. R. B. Dinwiddie, Jr.
24. J. R. DiStefano
25. G. M. Goodwin
26. H. W. Hayden, Jr.
27. L. L. Horton
28. C. R. Hubbard
29. T. J. Huxford
30. M. A. Janney
31. D. R. Johnson
32. R. R. Judkins
33. M. A. Karnitz
34. J. R. Keiser
35. R.J. Lauf
36. C.T. Liu
37. K.C. Liu
38. Gail M. Ludtka
39. Gerald M. Ludtka
40. P.J. Maziasz
41-42. J.O. Mynatt
43. T.A. Nolan
44. A.E. Pasto
45. F.L. Paulauskas
46. S.J. Pawel
47. B. A. Pint
48. B. Radhakrishnan
49. M.L. Santella
50. A.C. Schaffhauser
51. V.K. Sikka
52. S. Simunovic
53. P.S. Sklad
54. R.W. Swindeman
55. T.N. Tiegs
56. S. Viswanathan
57. X.L. Wang
58. A.Wereszczak
59. C.G. Westmoreland
60. T. Zacharia
61. H.W. Foglesong (Consultant)
62. E.L. Menger (Consultant)
63. J.G. Simon (Consultant)
64. K.E. Spear (Consultant)

EXTERNAL DISTRIBUTION

65. ABB-Combustion Engineering, Inc., P.O. Box 568, 200 Great Pond Dribe, Windsor, CT 06095-0568

Mark LeBel

66. ABB-CE Power Products Manufacturing Combustion Engineering, Incorporated, 1119 Riverfront Parkway, Chattanooga, TN 37402

Jeff Henry

67. ABB-Combustion Engineering, Inc., 911 West Main Street, Chattanooga, TN 37402

Domenic Canonico

68-69. ABB C-E Services, Inc., 200 Great Pond Drive, P. O. Box 568, Windsor CT 06095-0568

Hank Arenstam
Reddy Ganta

70. ABB Combustion Engineering, Inc., P.O. Box 500, 200 Day Hill Rd.,Windsor, CT 06905

Thomas Gibbons

71-72. ACuPowder International, LLC, 901 Lehigh Avenue, Union, NJ 07083

Edul M. Daver
Krishna Patel

73. Acutus Gladwin, Airport Office Park, Bldg 1, 410 Rouser Rd., 5th Floor, Corapolis, PA 15108

James B. Sears, Jr.

74. Advanced Refractory Technologies, Incorporated, 699 Hertel Avenue, Buffalo, NY 14207

Keith A. Blakely

75. Advanced Technology Group, Incorporated, 14 Wellesley Place, Fairfield, OH 45014

Charlie E. Guzi

76. Advanced Technology Group, Incorporated, 989 Ehlers Road, Neenah, WI 54956

Jim Gustafson

77. AFFCO, 6th & Jefferson, P.O. Box 1071, Anaconda, MT 59711

Jim Liebetrau

78. AFG Industries, PO Box 929, Kingsport, TN 37662

Ed McCullah, Jr.

79-80. Ahlstrom Recovery, Incorporated, 10745 Westside Parkway, Alpharetta, GA 30004

James P. Martin
Jorma Simonen

81. AHT, Inc, 1024 Kittanning Pike, P.O. Box U, Chicora, PA 16025-0491

Gary Hudson

82. Alabama Pine Pulp Company, Inc., Po. O. Box 100, Perdue Hill, AL 36470

Sunil Chandnani

83. Alcon Industries, Inc., 7990 Baker Avenue, Cleveland, OH 44102

William S. Habansky, Jr.

84-85. Alfred University, Center for Advanced Ceramic Technology, Alfred, NY 14802

Richard M. Spriggs
Harrie J. Stevens

86. Alfred University/NYSCC, 2 Pine St., Alfred, NY 14802

Doug Korwin

87. Allegheny Ludlum Steel Corporation, Research Center, Alabama & Pacific Avenue, Brackenridge, PA 15014

Gerald L. Houze, Jr.

88. Allied-Signal Aerospace Company, Garrett Ceramic Components Division, 19800 S. VanNess Avenue, Torrance, CA 90509

Maxine L. Savitz

89. Allied-Signal, Incorporated, Ceramics Program, P.O. Box 1021R, Morristown, NJ 07960

Clifford P. Ballard

90. Allison Engine Co., 2001 South Tibbs Ave., Indianapolis, IN 46206-0420

Ray Xu

91-92. Alloy Engineering & Casting Co., 1700 W. Washington Street, Champaign, IL 61821

James R. Lytle
David Robinson

93. Allvac, P.O. Box 5050, Monroe, NC 28111-5030

Kathy Davis

94. Alstrom Machinery, Incorporated, 10745 Westside Parkway, Alpharetta, GA 39201

Peter Collins

95. American Axle and Mfg., 1840 Holbrook Avenue, Detroit, MI 48212-3488

Michael E. Stevens

96. American Forest & Paper Association, 1111 19th Street, NW, Suite 800, Washington, DC 20036

David Cooper

97-98. American Spring Wire Corp., 26300 Miles Road, P.O. Box 46510, Bedford Heights, OH 44146-1410

William C. Mack
Todd Pickett

99. American Video Glass Company, 777 Technology Drive, Mt. Pleasant, PA 15666

Keith Congleton

100-104. Ames Laboratory, Iowa State University, 214 Wilhelm, Ames, IA 50011-3020

L. S. Chumbley
H. Mahmood
K. L. Pauwels
P. P. Pulvirenti
R. Bruce Thompson

105. Ames Laboratory, Iowa State University, 206 Wilhelm Hill, Ames, IA 50010

Lavonne J. Carson

106. Ames Laboratory, Iowa State University, 204 Metals Development, Ames,IA 50011-3020

D. C. Jiles

107. Ames Laboratory, Iowa State University, 107 Metals Development, Ames, IA 50012

Dan Sordelet

108. Ametek, Rt 519, P.O. Box 427, Eighty Four, PA 15330

John H. Reinshagen

109-114. Amoco Chemical, 150 West Warrenville Road, Naperville, IL 60563-8460

Martin Carrera
Charles Scouten
Bill Huber
Dickson Ozokwelu
Nari Calamur
Joe Golab

115. Anaconda Foundry Fabrication Co., Inc., Sixth and Jefferson, Anaconda, MT 59711-2658

Robert Mackey

116-117. Anchor Glass Container, One Anchor Plaza, MP 27, 4343 Anchor Plaza Parkway, Tampa, FL 33634-7513

Samuel Wilson
Michael Nowson

118. Andritz Sprout Bauer, Sherman Street, Muncy, PA 17756

Ronald L. Musselman

119. AP Green Industries, 1 Green Blvd., Mexico, MO 65265

John Conrad

120. ARCO Aluminum, Inc., 2900 National City Tower, Loiusville, KY 40232

Gyan Jha

121. Argonne National Laboratory, 9700 South Cass Avenue, Argonne, IL 60439

Bobby Dunlap

122. Arizona State University, Mechanical and Aerospace Engineering, Tempe, AZ 85287-6106

Dusan Krajcinovic

123. Army Research Office, P.O. Box 12211, Research Triangle Park, NC 27709

Andrew C. Crowson

124. Army Materials Technology Laboratory, Watertown, MA 37919

Robert N. Katz

125. ASM R&D Comm Tocco, Inc., 30100 Stephenson Highway, Madison Heights, MI 48071-1630

George Pfaffmann

126. Associated Technical Consultants, 2375 Dorr Street, Suite 1, Toledo, OH 43607-3406

Ray S. Richards

127. Aviation Components Services, Dallas, TX 75380-1092

Arnold Prill

128-129. Babcock & Wilcox, 20 S. Van Buren Avenue, P.O. Box 351, Barberton, OH 44203-0351

Joan Barna
J. William Smith

130-131. Babcock & Wilcox, 2302 Parklake Drive, NE, Suite 300, Atlanta, GA 30345

Robert Larsen
Thomas F. Roberts

132. Babcock & Wilcox, Pulp & Paper Projects, 90 East Tuscarawas Avenue, Barberton, OH 44203-0665

Gregory M. Pifer

133. Ball-Foster Glass Container Co., PO Box 4200, Muncie, IN 47307

Marv Gridley

134-135. Battelle Pacific Northwest Laboratories, Department of Materials Science, P.O. Box 999, Richland, WA 99352

Gary L. McVay, K2-45
Gregory J. Exarhos, K2-44

136. Battelle, 505 King Avenue, Columbus, OH 43201-2693

Jeffrey Colwell

137-138. Bethlehem Steel Corporation, P.O. Box 248, Chesterton, IN 46304

Dan Elwood
Anthony Simola

139-140. Black & Decker, Incorporated, 701 East Joppa Road, TW 460, Towson, MD 21286

Nick Achterberg
Stephen R. Crosby

141-143. Boeing Aerospace, Material Lobby, Renton, WA 98124-2499

K. Y. Blohowiak, Building 7-20, Mail Stop 73-09
Thomas S. Luhman, Building 7-20, Mail Stop 73-09
M. S. Strasik, Building 7-20, Mail Stop 73-09

144. Boeing Company, P.O. Box 516, MS S276-1009, St. Louis, MO 63166-0516

S. Eric Baldini

145. Boise Cascade Corporation, 1111 West Jefferson Street (83702), Boise, ID 83728-4933

Len Erikson

146-147. Bowater, Inc., 5020 Highway 11 South, Calhoun, TN 37309

John E. Griffey
LeRoy Hershey

148. Brown University, Division of Engineering, Box D, 182 Hope Street, Providence, RI 02912

K. Sharvan Kumar

149. Cal Poly State University, 39 Rafael Way, San Luis Obispo, CA 93405

Richard L. Thomas

150. Callaway Golf, 2285 Rutherford Road, Carlsbad, CA 92008-8815

Herb Reyes

151. Canspec Group, Incorporated, 7450 - 18th Street, Edmonton, Alberta, Canada T6P 1NB

Brian K. Beresford

152. CarboMedics, 1300 East Anderson Ln., Austin, TX 78752-1793

Gregory Hofmann

153. Cardinal FG, 2200 Parkway Drive, Menomonie, WI 54751

Mark Piper

154-155. Carpenter Technology Corporation, 101 West Bern Street, P.O. Box 14662, Reading, PA 19612-4662

Bradford A. Dulmaine
Nicholas Fiore

156. Carpenter Technology Corporation, 92 Burning Tree Lane, Reading, PA 19607

Robert L. Caton

157. Caterpillar, Inc., Technical Ctr. - E/8 54, P.O. Box 1875, Peoria, IL 61656-1875

Kaichu Hsieh

158. Caterpillar, Incorporated, Engineering and Research Materials, Technical Center, Building E, P.O. Box 1875, Peoria, IL 61656-1875

Michael H. Haselkorn

159. Ceradyne, Incorporated, 3169 Redhill Avenue, Costa Mesa, CA 92626

Joel P. Moskowitz

160-162. Ceramatec, Incorporated, 2425 South 900 West, Salt Lake City, UT 84119

Raymond Cutler
Ronald S. Gordon
David W. Richerson

163. CeramTec North America, P.O. Box 89, One Technology Place, Laurens, SC 29360-0089

Fred Wilson

164. CertainTeed, PO Box 1100, Blue Bell, PA 19446

Terry Berg

165. Champion International Corporation, W. Nyack Road, W. Nyack, NY 10994

Dave Bennett

166. Chevron Research and Technology Co., 100 Chevron Way, P.O. Box 1627, Richmond, CA 94802-0627

Brian L. Jack

167. Cincinnati Milacron, 4701 Marburg Avenue, Cincinnati, OH 45209

David M. Suprock

168. Cincinnati Milacron, 4165 Halfacre Road, Batavia, OH 45103-3247

Dean Reber

169. Colorado School of Mines, 1500 Illinois Street, Colorado School of Mines, Golden, CO 80410

George Krauss

170. Columbia Falls Aluminum Company, 2000 Aluminum Dr., Columbia Falls, MT 59912

David Wilkening

171. Combustion Tec, Inc., 2501 Clark Street, Apopka, FL 32703-2112

Scott Anderson

172. Conrex, Incorporated, 1050 Crown Pointe Parkway, Suite 1440, Atlanta, GA 30338

Pekka Eskelinen

173. Coors Glass - RMBC, 10619 W. 50th Ave., Wheatridge, CO 80033

Maurice Hanavan

174. Core Star International Corporation, 1044 Sandy Hill Road, Irwin, PA 15642

Matthew B. Wolf

175. Corhart Refractories, 1600 West Lee St., Louisville, KY 40210

Michael Nelson

176. Cornell University, School of Mechanical and Aerospace Engineering, 196 Rhodes Hall, Ithaca, NY 14853

Paul Dawson

177-178. Corning Corporation, Sullivan Park FR-02-5, Corning, NY 14831

Thomas P. DeAngelis
Frank E. Murphy, Jr.

179. Corning Incorporated, HP ME-2 E-5, Corning, NY 14830

John Wosinski

180-182. Cummins Engine Co., 1900 McKinley Ave., Columbus, IN 47201

Cheryl Klepser
Yong-Ching Chen
Thomas M. Yonushonis

183-185. Cummins Engine Company, Incorporated, P.O. Box 3005, Columbus, IN 47202-3005

Paul C. Becker, Mail Code 50183
Magan J. Patel, Mail Code 50183
James W. Patten, Mail Code 50183

186. Dartmouth College, Thayer School of Engineering, Tuck Drive, Hanover, NH 03755

Ian Baker

187. DELPHI Saginaw Steering Systems, 3900 Holland Road, Saginaw, MI 48601-9494

David M. Hitz

188. Delta M Corporation, 525 Warehouse Road, Oak Ridge, TN 37830

Reginald W. McCulloch

189. Diemakers, P.O. Box 278, Monroe City, MO 63456

Harold Berry

190. Doehler-Jarvis Technologies, Inc., P.O. Box 902, Toledo, OH 43691

H. Brucher

191-192. Dow Chemical Company, Incorporated, 1776 Building, Midland, MI 48674

David A. Dalman
Richard D. Varjian

193-196. Dow Chemical Company, 2301 N. Brazosport Blvd, Freeport, TX 77541-3257

Jim Earls, Building 1210
Chris Kneupper, B-251
Tom Patterson, MST-7, MS E-549
Mark Smith, MST-7, MS E549

197. Dow Corning Corp., 4770 Highway 42 East, Carrollton, KY 41008

Charles A. Hall

198. DSF Refractories & Minerals Ltd., Friden, Newhaven, NR Buxton, Derbyshire SK17 0DX, England, UK

Paul Hutchinson

199. DuPont Central Research and Dev., Mater. of Construction, Experimental Station, MS E323/158, Route 141, P.O. Box 80323, Wilmington, DE 19880-0323

J. J. Barnes

200. DuPont Lanxide Composites, Inc., 1300 Marrow Road, Newark, DE 19714-6077

Craig Shumaker

201-202. Duraloy Technologies, Inc., 120 Bridge Street, Scottsdale, PA 15683-1748

Roman Pankiw
Alan Paris

203. Dynamet Technology, Incorporated, 8 "A" Street, Burlington, MA 01803

Walter Bergler

204. E. R. Johnson Associates, Inc., 9302 Lee Highway, Suite 700, Fairfax, VA 22031-1214

Govind Hira

205. Eaton Corporation, Truck Components of the Americas, P.O. Box 4013, Kalmazoo, MI 49003

Ralph Ralph

206. Eaton Corporation, Corporate Research & Development, Milwaukee, Center, 4201 North 27th Street, Milwaukee, WI 53216

John W. Kroll

207. Eaton Corporation, Manufacturing Technologies Center, 32500 Chardon Road, Willoughby Hills, OH 44094-9137

Alvin M. Sabroff

208. Eckart America L.P., 4101 Camp Ground Road, Louisville, KY 40211-2157

Norbert F. Koopman

209. Edison Wedling Institute, 1250 Arthur E, Adams Drive, Columbus, OH 43210

Z. Feng

210. Electric Power Research Institute, 2000 L Street, Suite 805, Washington, DC 20036

W. Eugene Eckhart

211-212. Electric Power Research Institute, Nuclear Plant Corrosion Control, 3412 Hillview Avenue, Palo Alto, CA 94303

Ben Banerjee
Mohamad M. Behravesh

213. Energetics, Incorporated, 7164 Gateway Drive, Columbia, MD 21046

Aziz Azimi

214. Ervin Industries, Inc., 3893 Research Park Drive, P.O. Box 1168, Ann Arbor, MI 48106-1168

William L. Rhodaberger

215. EXXON R&D Labs, P.O. Box 2226, Baton Rouge, LA 70821

R. C. Schucker

216-219. A Finkl and Sons Co., 201 1 Southport Ave., Chicago, IL 60614-4079

Guy Brada
Bruce C. Liimatainen
Carl Manthe
Algirdas Underys

220-222. FM Technologies, Incorporated, Patriot Square, 10529-B Braddock Road, Fairfax, VA , 22032

Richard S. Silberglitt
P. Columbo
G. A. Danko

223. FMC Corporation, Corporate Technology Center, 1205 Coleman Ave. Box 580, Santa Clara, CA 95052

Michael T. Orillion

224. Ford Motor Company, Glass Technical Center, 25500 West Outer Drive, Lincoln Park, MI 48146

Vincent I. Henry

225-227. Ford Motor Company, P.O. Box 2053, Dearborn, MI 48121-2053

John E. Allison, Mail Drop 3182
William E. Dowling, Jr., MD3135/SRL
Kenneth Hass, Room S3028

228. Ford Motor Company, 35500 Plymouth Road, Box 13, Lovonia, MI 48150

Mark G. Shapona

229. Ford Motor Company, P.O. Box 1899, Room 354, Dearborn, MI 48121

Vello Arrak

230. Ford Motor Company, 21500 Oak Wood Boulevard, POEE Building, Mail Drop 53, P.O. Box 2053, Dearborn, MI 48121

Peter Y. Chen

231. Forging Industry Association, 25 Prospect Avenue West, Suite 300, Cleveland, OH 44115

George F. Mochnal

232. ForMat Industries, Inc., 10512 Lexington Dr., Suite 100, Knoxville, TN 37932

Thomas Reddoch

233. Foster Wheeler Development Corporation, 12 Peach Tree Hill Road, Livingston, NJ 07039

Jeffrey L. Blough

234-235. Foster Wheeler Energy Services, 9539 Stein Street, Custer, WA 98240

Neil Solomon
Mike Place

236. General Electric Aircraft Engines, 1 Newman Way, Cincinnati, OH 45215

Sule Jain

237. General Electric Company, Research & Development, Met Building, Room 263, P.O. Box 8, Schenectady, NY 12301

Alan I. Taub

238-239. General Electric Company, One Newmann Way, Cincinnati, OH 45215

Ram Darolia, Mail Drop M-89
James Williams, Mail Drop H-85

240. General Electric Lighting, Nela Par Noble Rd., East Cleveland, OH 44112

Ken Hyrcik

241. General Motors Tech Center, Composite Section Manufacturing Building, A/MD-24, 30300 Mound Road, Warren, MI 48090-9040

I. E. Poston

242-245. General Motors Powertrain Division, 1629 North Washington Avenue, Saginaw, MI, 48605-5073

Ron Cafferty
Paul N. Crepeau
Mark E. Hoover
Dennis Meyers

246-247. General Motors Powertrain Division, 895 Joslyn Road, Pontiac, MI 48340-2920

Ramesh Shah
Robert Wiltse

248-252. General Motors Corporation, Saginaw Division, 3900 Holland Road, Saginaw, MI, 48601-9494

Steven L. Avery
Randy P. Bal
Madhu S. Chatterjee
James Fargo
David H. Hitz

253-256. General Motors Corporation, 30500 Mound Road, Warren, MI 48090-9055

M. S. Rashid
Edward F. Ryntz
James G. Schroth
Michael M. Shea

257. General Motors Corp.- Technical Center, 30500 Mound Rd., Mail Code: 480-103-001, Warren, MI 38090-9055

Anil Sachdev

258. General Motors Corporation, 1660 L Street N.W., Suite 400, Washington, DC 20036

Bo Campbell

259-262. General Motors Corporation, AC Rochester, 1300 North Dort Highway, Flint, MI 48556

R. F. Beckmeyer
Lawrence A. Carol
W. LaBarge
Carl E. Miller

263-264. George Mason University, 4400 University Drive, Fairfax, VA 22030

W. M. Black
R. F. Cozzens

265-270. Georgia Institute of Technology, School of Materials Engineering, 778 Atlantic Drive, Atlanta, GA 30332-0245

Steve Antolovich
W. Brent Carter
Joe K. Cochran, Jr.
S. Lee
Thomas L. Starr
S. R. Stock

271. Georgia-Pacific Corp., 133 Peachtree Street, N.E., 11th Floor, Atlanta, GA 30303

Karl T. Morency

272. Georgia-Pacific Corporation, Recovery/EVAP Area, Ashdown, AR 71822-0496

Jeff Bazarow

273. Glass Industry Consulting, P.O. Box 6730, 1 Park Paseo, Laguna Niguel, CA 92677

Philip Ross

274. Glenshaw Glass Company, 1101 William Flynn Highway, Glenshaw, PA 15116

Steve Hutchins

275-277. Golden Technologies Company, Incorporated, Research & Development, 17750 West 32nd Avenue, Golden, CO 80401

Rick Kleiner
Dean Rulis
Jack Sibold

278. Goldendale Aluminum Corp., 85 John Clay Dam Rd., Goldendale, WA 98620

Robert J. Barnett

279. T. M. Grace Company, Incorporated, 2517 S. Harmon Street, Appleton, WI 54915

Thomas Grace

280. Gray-Syracuse, 901 E. Genesse St., Chittenango, NY 13037

Jack Zheng

281. Guardian Industries Corp., 2300 Harmon Rd., Auburn Hills, MI 48326

Charles Cocagne

282-283. Harbison-Walker Refractories Company, 600 Grant St., Pittsburgh, PA 15219

Peter Antimarino
David V. Stiles

284. C.I. Hayes, Inc., 800 Wellington Ave., Cranston, RI 02910

Stephen Balme

285. Herty Foundation Development, P.O. Box 7798, Savannah, GA 31418

James Anderson

286. Holcroft, 12068 Market Street, Livonia, MI 48150

Jack Titus

287. Holophane Corporation, PO Box 3004, 214 Oakwood Avenue, Newark, OH 43058-3004

Kimball Lombardi

288. Hoskins Manufacturing Company, 10776 Hall Road, Hamburg, MI 48139

Forrest Hall

289. Hoskins Manufacturing Company, 600 Buhl Building, Detroit, MI 48226

Jerome L. Reinke

290-292. Hughes Research Laboratories, 3011 Malibu Canyon Road, Malibu, CA 90265

Jesse Matossian
John McLendon
Robert Schumacher

293-296. Idaho National Engineering Laboratory, EG&G Idaho, P.O. Box 1625, Idaho Falls, ID 83415-2218

Elmer Fleischman
D. Kunerth
E. S. Peterson
Thomas D. Foust

297-300. INCO Alloys International, 3200 Riverside Drive, Huntington, WV 25705-1771

Vernon Hartmann
Gaylord D. Smith
Pasupathy Gancsan
Brian A. Baker

301-302. Institute of Gas Technology, 1700 S. Mt. Prospect Road, Des Plaines, IL 60018

Hamid Abbasi
Laurence M. Feder

303-307. Institute of Paper Science and Technology, 500 10th Street, NW, Atlanta, GA 30318

Preet Singh
Maclin S. Hall
Robert H. Horton
Thomas McDonough
David Orloff

308. International Paper, P. O. Box 160707, Mobile, AL 36616

Russell S. Andrews

309. International Paper, 6283 Tri-Ridge Boulevard, Loveland, OH 45140-7910

Subhash Pati

310. IPST, Pulping and Bleaching Group, Chemical and Biological Sciences Division, 500 10th St., Atlanta, GA 30318-5794

Cheryl Rueckert

311. Irving Pulp and Paper, Limited, Postal Station B, Saint John, N.B., E2M 3H1, Canada

Walter Bursey

312-313. J&L Specialty Steel, Inc, One PPG Place, P.O. Box 3373, Pittsburgh, PA 15230-3373

Paul Grandy
Donald Hadfield

314. Jaakko Poyry Fluor Daniel, 100 Fluor Daniel Drive, Greenville, SC 29607-2762

Bo Oscarsson

315. James River Corporation, HC66, Pennington, AL 36916-9499

John Clifton

316. James River Corporation, P.O. Box 2218, Richmond, VA 23217

Ronald Estridge

317. James River Corporation, 1915 Marathon Avenue, P. O. Box 899, Neenah, WI 54957-0899

Bill Steed

318. Jeffrey Chain Corporation, 2307 Maden Dr., Morristown, TN 37813-2898

David L. King

319. Johns Hopkins University, Center for Nondestructive Evaluation, Maryland Hall 107, Baltimore, MD 21218

Robert E. Green, Jr.

320. Johns Manville, P.O. Box 625005, 10100 West Ute Avenue, Littleton, CO 80162-5005

Walter A. Johnson

321-322. Johnson Controls, Inc., 507 East Michigan Street, P.O. Box 423, Milwaukee, WI 53201

Carl F. Klein
Bryan L. McKinney

323. Kaiser Aluminum & Chemical Corporation, P.O. Box 870, Pleasanton, CA 94566

S. C. Carniglia

324-325. Kennametal, Inc., Corporate Technology Center, Route 981 South, Latrobe, PA 15650-0231

Ed Conley
Russ Yeckley

326. Kimball Glass Inc., 537 Crystal Avenue, Vineland, NJ 08360

Jim Ceriani

327. Knauf Fiber Glass GmbH, 240 Elizabeth St., Shelbyville, IN 46176

Mike Carroll

328-333. Kvaerner Pulping, 8008 Corporate Center Drive, Charlotte, NC 28226

Joe Barsin
Markku Isoniemi
Jussi Mantyniemi
Pertti Petane
Steve Koviack
Eric L. Wasson

334. Kyocera, 5713 East Fourth Blvd., Vancouver, BC 98661

Ray Bralton

335. Lancaster Glass Corporation, 240 West Main St., PO Box 70, Lancaster, OH 43130-0070

August Link

336. Lawrence Berkeley Laboratory, 1 Cyclotron Road, MS-62-203, Berkeley, CA 94720

Joel Ager

337-338. Lawrence Livermore National Laboratory, P.O. Box 808, Livermore, CA 94550

M. Fluss, Mail Stop L-326
Jeffery Wadsworth, Mail Stop L-353

339. Libbey Inc., PO Box 919, Toledo, OH 43616

James McGaughey

340. Lightpath Technologies, Inc., 6820 Academy Parkway East, Albuquerque, NM 87109

Robert Wade

341. Lincoln Electric Company, 22801 St. Clair Ave., Cleveland, OH 44117-1199

John McLane

342-372. Los Alamos National Laboratory, P.O. Box 1663, Los Alamos, NM 87545

P. G. Apen, D453
Tom Archuleta, E549
R. S. Barbero, E549
A. H. Bartlett, G770
B.C. Benicewicz, E549
D. P. Butt, G755
D. W. Carroll, E549
R. G. Castro, G770
D. J. Devlin, E549
E. P. Douglas, E549
F.D. Gac, G756
S. Gottesfeld, D429
P. J. Hay, B268
T.W. Hegwer, D453
K. J. Hollis, G770
W.R. Howell, J586
E.L. Joyce, D453
J. D. Katz, G771
H. H. Kung, G755
R. Leipens, E549
R. LeSar, K765
J. Mercer-Smith, E549
M. A. Miller, C331
M. Nastasi, K765
Y. Park, G755
J. J. Petrovic, G771
A. Redondo, D429
K. N. Siebien, MST-7, MS E549
M.E. Smith, E549
Paul W. Stanek, MS G770
G. J. Vogt, G771
K. C. Walter, K762

373. LTV Steel Company, Technology Center, 6801 Brecksville Road, Independence, OH 44131

F. J. Barchfeld

374. M-C Power Corp., 8040 S. Madison St., Burr Ridge, IL 60521-5808

Diane Erikson

375. MacMillan Bloedel Packaging, Inc., Hwy 10, P. O. Box 336, Pine Hill, AL 36769

Wallace Baxter

376. Martec, Inc., 50 W. Techne Center Drive, Suite C, Milford, OH 45150

Ronald D. Markle

377. Massachusetts Institute of Technology, 77 Massachusetts Avenue, Rm 35-229, Cambridge, MA 02139-4307

Jung-Hoon Chun

378. Materials Technology, Inc., 179 Avenue at the Common, Suite 2, Shewsbury, NJ 07702

Ira Friedman

379. Mechanical Consulting Services, Augusta, GA 30917

Frank Sosnin

380. Memtec America Corporation, 1750 Memtec Drive, DeLand, FL 32724-2045

Robert Malanga

381 Metal Experts International, 7440 Mason Falls Drive, Winston, GA 30187

John L. Mihelich

382. Minteq International, Inc., PO Box 446, Dover, OH 44622

Larry Stover

383. National Aeronautics & Space Administration, Materials & Structures Division, Code RM, 600 Independence Avenue, S.W., Washington, DC 20546

Samuel L. Venneri

384. National Forge Company, Irvine, PA 16329

Ashok Khare

385-386. National Institute of Standards and Technology (NIST), Gaithersburg, MD 20899

Edwin R. Fuller, Jr., Ceramics Division, Room, A256, Building 223
Richard E. Ricker, Depart. of Commerce, Materials Bldg., Room B254

387. National Refractories & Minerals, 41738 Esterly Drive, PO Box 47, Columbiana, OH 44408-0047

Jim Houp

388-393. National Renewable Energy Laboratory, 1617 Cole Boulevard, Golden, CO 80401-3393

Helena L. Chum
Robert J. Evans
Gregory Glatzmaier
Neil Kelley
Stephen S. Kelley
Deb Satyen, MS-3221

394-395. National Science Foundation, 4201 Wilson Blvd., Arlington, VA 22230

Alex Schwarzkopf
Liselotte J. Shioler

396. National Thermospray, Inc., 20810 Magnolia Brook Ln, Cypress, TX 77429

Ken Norris

397. Naval Research Laboratory, Building 43, Room 212, Code 6000, 4555 Overlook Avenue, SW, Washington, DC 20735-5341

Bhakta B. Rath

398. North American Refractories, 3127 Research Dr., State College, PA 16801

Robert Antram

399. North Carolina A&T State University, Department of Mechanical Engineering, Greensboro, NC 27411

V. S. Avva

400-401. North Carolina State University, Department of Materials Science and Engineering, Box 7907, Raleigh, NC 27695-7907

Carl C. Koch
Nkadi Sukidi

402. Northeastern University, Department of Mechanical, Industrial & Manufacturing Engineering, 334 Snell Engineering Center, Boston, MA 02155

Teiichi Ando

403. Norton Company, Goddard Road, Northboro, MA 01532-1545

Normand D. Corbin

404. Ohio State University, 210 Baker Systems, 1971 Neil Avenue, Columbus, OH 43210

Richard Allen

405. Oregon State University, Oregon Street, Rog 414 OSU, Corvallis, OR 97331

Michael Kassner

406. Osram Sylvania Inc., 1000 Tyrone Park, Versailles, KY 40383

Tom Hoffman

407. Osram Sylvania Inc., 71 Cherry Hill Dr., Beverly, MA 01915

William Rhodes

408-411. Owens Corning, Science & Technology Center, 2790 Columbus Rd., Granville, OH 43023

Christopher Jian
John Petreanu
Gary Shuster
Manoj Choudhary

412. Owens-Brockway Inc., 1 Seagate 30L/GC, Toledo, OH 43666

Al Poolos

413. Oxford University, Department of Materials, Parks Road, Oxford, Oxfordshire, OX1 3PH, United Kingdom

Adam M. Baker

414. P. H. Glatfelter Company, Spring Grove, PA 17362-0500

Mike Fremont

415. Park Ohio Transportation Group, 1441 Chardon Road North, Cleveland, OH 44117-1582

Timothy Dunagan

416-417. Parsons and Whittemore, Inc., Monroeville Office, P. O. Box 65, Perdue Hill, AL 36470

Adam Melton
Raoul Fenelon

418-422. Pennsylvania State University, Department of Materials Science and Engineering, Metals Science and Engineering Program, 221 Steidle Building, University Park, PA 16802

John Hellman
Paul R. Howell
George L. Messing
William A. Pratt
Richard E. Tressler

423. Philips Lighting Co., 320 Vaksdahl Ave., Danville, KY 40422

Ken Enos

424. Philip Morris, P.O. Box 26583, Richmond, VA 23261-6583

Mohammad R. Hajaligol

425-426. Philip Morris U.S.A., P.O. Box 26603, Richmond, VA 23261

John Dawson
Richard N. Webb

427-428. Pilkington LOF, 1701 East Broadway, Toledo, OH 43605

Peter Gerhardinger
Dan Lubelski

429. Pittsburgh Corning, 800 Presque Isle Dr., Pittsburgh, PA 15239-279

Dennis Kauser

430. Polymet Corporation, 10073 Commerce Park Drive, Cincinnati, OH 45246

William C. Mosier

431. Postle Industries, Inc., P.O. Box 42037, Cleveland, OH 44142

Chris North

432-433. Potlatch Corporation, Lewiston, ID 83501-1016

Larry Butts
Gerald Cran

434. Powdermet, 416 Trinity Court, Petaluma, CA 94954

Animesh Bose

435-438. PPG Industries, Inc., Glass Technology Center, PO Box 11472, Harmarville, PA 15238-0472

Warren Curtis
Ganjiang Feng
Amar Mishra
George A. Pecoraro

439. PQ Corporation, Corporate Headquarters, PO Box 840, Valley Forge, PA 19482

Paul DeHoff

440-441. Precision Castparts Corporation, 4600 SE Harney Drive, Portland, OR 97206-0898

David A. Chang
Larry J. Watland

442. Process Simulations Ltd., (CFD consultant for Weyerhauser), Box 1125, Station A, Delta, BC V4M 3T2

Zia Abdullah

443. Pulp and Paper Research Institute of Canada, Vancouver Laboratory, 3800 Westbrook Mall, Vancouver, B.C. V6S 2L9

Robert Prescott

444. Quaker Alloy, Inc., Planning Dept., 200 E. Richland Ave., Myerstown, PA 17067

Hong Ouyang

445-446. Rapid Technologies, Incorporated, P.O. Box 368, 170 Werz. Ind. Blvd., Newnan, GA 30264

Ed Dailey
Andrew Tomys

447. Rennsselaer Polytechnic Institute, School of Engineering, Materials Engineering Department, 8th Street, Troy, NY 12180-3590

N. S. Stoloff

448. Reynolds Metals Company, Manufacturing Technology Laboratory, 3326 East Second St., Muscle Shoals, AL 35661-1258

Ray Peterson

449. Reynolds Metals Company, Corporate Research and Development, 4th & Canal Streets, P.O. Box 27003, Richmond, VA 23219

Paul Tretina

450. Rhenium Alloys, Inc., P.O. Box 245, 1329 Taylor St., Elyria, OH 44036

Boris Bryskin

451. Riverwood International, 1000 Jones Road, West Monroe, LA 71294-5800

Don Jordan

452. Riverwood International Corporation, Macon, GA 31205-3215

Phil Hardin

453. Rohr, Inc., P.O. Box 878, Chula Vista, CA 91912-3646

Brian Norris

454. Rouge Steel Company, 3001 Miller Rd., P.O. Box 1699, Dearborne, MI 48121-1699

Dennis Crosby

455-461. Sandia National Laboratories, P.O. Box 969, 7011 East Avenue, Livermore, CA 94551-0969

Mark D. Allendorf, MS-9052
S. M. Ferko, MS-9052
S. Griffiths, MS-9042
D. R. Hardesty, MS-9052
A. H. McDaniel, MS-9052
R. Nilson, MS-9042
G. A. Samara, MS-1421

462-465. Sandia National Laboratory, University of New Mexico, Advanced Materials Laboratory 1708, 1001 University Boulevard, SE, Suite 100, Albuquerque, NM 87106

J. Brinker
W. G. Fahrenholtz
Ronald E. Loehman
A. P. Tomsia

466-479. Sandia National Laboratory, P.O. Box 5800, Albuquerque, NM 87185-0710

C. S. Ashley, Mail Stop 1405
T. V. Bohuszewicz, MailStop 1349
A. V. Chavez, Mail Stop 0710
B. Damkroger
Bob Eagan, Division 1800
Kevin G. Ewsuk, Mail Stop 1349
Kay Hays, Mail Stop 1709
K. S. Johnston
J. B. Kelley, Mail Stop 1134
A. Martino, Mail Stop 0710
T. M. Nenoff, Mail Stop 0710
P. I. Pohl, Mail Stop 0720
R. D. Skocypec, Mail Stop 0835
Alan P. Sylwester, Mail Stop 0710

480-483. Sandusky International, 615 W. Market Street, Box 5012, Sandusky, OH 44871-8012

John C. Rogers
Edward R. Ryan
Dan Scott
Greg Michel

484-485. Sandvik Steel Co., P. O. Box 1220, Scranton, PA 18501-1220

Jim Noble
Gary Boberick

486. Schuller Intol, Inc., Moutain Technical Ctr., 10100 West Ute Ave., Littleton, CO 80162-5005

S.C. Ghorpade

487. Schuller International, Inc., PO Box 517, Toledo, OH 43697-0517

Don Shamp

488. SCM Metal Products, Inc., 2601 Weck Drive, P.O. Box 12166, Research Triangle Park, NC 27709-2166

Gerard Reverri

489. Seagate Technology, 10323 W. Reno Avenue, Oklahoma City, OK 73157

Mukund Rao

490. Smelter Service Corp., Arrowmines Drive, Mt. Pleasant, TN 38478

Victor Hovis

491. A. O. Smith Corp., Corporate Technology Center, P.O. Box 23990, Milwaukee, WI 53223-0990

B. N. Ranganathan

492-494. Southern Illinois University, Department of Mechanical Eng. and Energy Process, Carbondale, IL 62999

Rasit Koc
D. B. Hodge
C. Meng

495. Southwire Co., One Southwire Drive, Carrollton, GA 30117

Ronald D. Adams

496. St. George Crystal, Brown Ave., PO Box 709, Jeannette, PA 15644

Jerry Kynik

497. Starmet Powders, 2229 Main Street, Concord, MA 01742

Steven A. Miller

498. Steel Manufacturers Association, 1730 Rhode Island Avenue, N.W., Washington,DC 20036-3101

Thomas A. Danjczek

499. Stone & Webster Engineering Corporation, 1430 Enclave Parkway, Houston, TX 77077-2023

Joseph M. Gondolfe

500-501. Stone Container Corporation, 8170 South Madison Street, Burr Ridge, IL 60521

Max Moskal
Chuck Timko

502. Stoody Deloro Stellite, 101 S. Hanley Road, St. Louis, MS 63105

James B.C. Wu

503. Stoody Company, 5557 Nashville Road, Bowling Green, KY 42101-7546

Ravi Menon

504. Tampella Power Corporation, 2300 Windy Ridge Parkway, Suite 1125, Atlanta, GA 30339

Markku Isoniemi

505. Techneglas, 727 E. Jenkins Ave., Columbus, OH 43207

Jim Shell

506. Tennessee Technological University, Center for Manufacturing Res. & Tech. Util. College of Engineering, P.O. Box 5014, Cookeville, TN 38505

Joseph T. Scardina

507-508. The Carborundum Company, P.O. Box 187, Keasbey, NJ 08832

Craig L. Dillman
Stanley Gursky

509. Thermo Electron Technologies, 85 First Avenue, Waltham, MA 02254

Peter Reagan

510-512. Timken Company, 1835 Dueber Avenue, S.W., Canton, OH 44706-2798

Mark Carlson
Robert L. Leibensperger
Jeffrey C. Moscsari

513. Torrington Steel Company, Shiloh Plant, 1510 U.S. Highway 221 South, Rutherfordton, NC 28139

Harry Walton

514. Trinity Forge, 947 Trinity Drive, Mansfield, TX 76063

Muhammed Abbas

515. Truecast, 6761 Cane Run Rd, P.O. Box 58610, Louisville, KY 40258

David Hubbard

516. TRW, Incorporated, 23555 Euclid Avenue, Cleveland, OH 44117

A. L. Bement, Jr.

517-518. U.S. Air Force, Wright Patterson AFB, Dayton, OH 45433-6533

Dennis M. Dimiduk, WRDC Material Laboratory
Allan Katz, AFWAL/MLLM Material Laboratory

519-522. U.S. Department of Energy, 19901 Germantown Road, Germantown, MD 20585

Fred Glaser, FE-72
Robert J. Gottschall, ER-13
Helen Kerch, ER-13
F. W. Wiffen, ER-52

523. U.S. Department of Energy, 9800 South Cass Avenue, Argonne, IL 60439

Jill E. Jonkouski

524. U.S. Department of Energy/Albuquerque, P.O. Box 5400, Albuquerque, NM 87115

D. Morton

525-555. U.S. Department of Energy/Headquarters, 1000 Independence Avenue, SW, Washington, DC 20585

David J. Boron, EE-23
Rolf F. Butters, EE-24
Joseph Carpenter, EE-32
H. Bruce Cranford, EE-21
Sidney Diamond, EE-34
Sara Dillich, EE-22
Douglas L. Faulkner, EE-21
Deborah A. Haught, EE-23
Marvin E. Gunn, Jr., EE-60
M. P. Hoffman, EE-23
Ramesh Jain, EE-22
Gobind Jagtiani, EE-22
Theodore Johnson, EE-21
Douglas E. Kaempf, EE-22
Hank Kenchington, EE-21
William P. Parks, Jr., EE-23
Marsha L. Quinn, EE-24
Scott L. Richlen, EE-21
Valri Robinson, EE-21
Charlie Russomanno, EE-22
Peter H. Salmon-Cox, EE-20
Kurt Sisson, EE-21
M. A. Smith, EE-21
Charles A. Sorrell, EE-23
Louis Sousa, EE-20
Denise F. Swink, EE-20
B. G. Volintine, EE-22
Daniel E. Wiley, EE-21
F. W. Wilkins, EE-21
Stanley M. Wolf, EM-54
Harvey Wong, EE-21

556. U.S. Department of Energy/Oak Ridge, Building 4500N, Mail Stop 6269, P.O. Box 2008, Oak Ridge, TN 37831-6269

Mary Rawlins

557. U.S. Department of Energy/Idaho, 785 Dow Place, Idaho Falls, ID 83402

Joanne Malmo

558. U.S. Department of Energy, 850 Emery Drive, MS-1225, Idaho Falls, ID 83401

Jenya Macheret

559-560. U.S. Department of Energy, Office of Scientific and Technical Information, Office of Information Services, P.O. Box 62, Oak Ridge, TN 37831

Robert Costas Hammerton
Debo Aichbhaumik

561. U.S. Department of the Interior Bureau of Mines, 2401 "E" Street, NW, Washington, DC 20241

Garrett R. Hyde

562-563. UES, Inc., 4401 Dayton-Xenia Road, Dayton, OH 454231-1894

Hal Gagel
Mark Sammons

564. UK Software Services Inc., 30 Hemlock Drive, Grand Island, NY 14072

Steve Winder

565. Uniform Metal Technologies, LLC, 12689 N. W. Logie Trail, Hillsboro, OR 97124

Christopher Brown

566. Unifrax Corporation, 2351 Whirlpool Street, Niagara Falls, NY 14305-2413

Douglas J. Bailey

567. Union Camp Corporation, Research and Development Division, P. O. Box 3301, Princeton, NJ 08543-3301

Dave Crowe

568-573. United Defense, Steel Products Div., 2101 West 10th St., Box 1030, Anniston, AL 36202

John Boggan
Chien-Hua Chen
Elmer L. Doty
Gary E. Hudson
John Orth
Nectar L. Ramirez

574. United Technologies Research Center, East Hartford, CT 06108

Vincent C. Nardone

575. United Technologies Pratt & Whitney, 1700 Beeline Highway, Jupiter, FL 33478

Donald R. Clemens

576. Universal Energy Systems, Inc, 4401 Dayton-Xenia Road, Dayton, OH 45432-1894

Young-Won Kim

577. University of Alabama at Birmingham (UAB), 1016 15th St. South, Birmingham , AL 35294-4552

Harry Littleton

578. University of Alabama, Metal Casting Technology Center, P.O. Box 6374, Tuscaloosa, AL 35487

Thomas S. Piwonka

579. University of California, San Diego, Department of AMES, 1801-EBU1, La Jolla, CA 92093-0411

Bimal Kad

580. University of Cincinnati, 408 Rhodes Hall, Cincinnati, OH 45221-0012

Oswald Uwakweh

581. University of Idaho, Institute for Materials and Advanced Processes, Mines Building, Room 321, Moscow, ID 83844-3026

F. H. Froes

582-583. University of Maine, 5737 Jenness Hall, Orono, ME 04469-5737

Joseph Genco
Marquita Hill

584. University of Missouri at Rolla, 224 McNutt Hall, Rolla, MO 65401

Robert E. Moore

585-586. University of New Mexico, 1001 University Blvd, S.E., Suite 100, Albuquerque, NM 87106

Bill Fahrenholtz
Thomas P. Swiler

587. University of Pennsylvania, Department of Mechanical Engineering, 111 Towne Building, 220 South 33rd Street, Philadelphia, PA 19104-6315

David Pope

588-590. University of Tennessee, Department of Materials Science & Engineering, Knoxville, TN 37996-2200

C. R. Brooks
Ben F. Oliver
Jeongguk Kim

591. University of Toronto, 200 College Street, Toronto Canada M5S 1A4

Honghi Tran

592. Valimet, Inc., P.O. Box 6186, 431 Sperry Road, Stockton, CA 95206

George T. Campbell

593. Vander Linden & Associates, 5 Brassie Way, Littleton, CO 80123

Carl R. Vander Linden

594. VGT-DYKO Industrial Ceramics Inc., 7002 Graymoor Rd., Louisville, KY 40222

D. J. Thomas

595-597. Virginia Polytechnic Institute and State University, 213 Holden Hall, Blacksburg, VA 24061-0237

B. J Love
Michael Stawovy
S. B. Desu

598. Wagner Castings Co., 825 N. Lowber St., Decatur, IL 62521

James Quintenz

599. Waukesha Electric Systems, 400 South Prairie Ave., Waukesha, WI 53186-5940

Bruce Sielen

600-601. Weirton Steel Corporation, 400 Three Springs Drive, Weirton, WV 26062

Debo Aichbhaumik
James J. Brinsky

602. Welding Services, Incorporated, 2110 Pebble Beach Drive, Suite 100, Carmel, IN 46032

George Lai

603-604. Welding Services, Incorporated, 2225 Skyland Court, Norcross, GA 30071

Mike Jirinec
David A. Joiner

605. Wescast Industries, Inc., P.O. Box 1930, 799 Powerline Road, Brantford, ON N3T 5W5

Richard W. Williams

606-607. Westinghouse Electric, 4400 Alafaya Trail, Orlando, FL 32826

Steve Breitenbach
Mahmood Choudry

608-611. Westvaco, Laurel Technical Center, 11101 Johns Hopkins Road, Laurel, MD 20723-6006

Abbie Alavi
Lad Falat
Greg Makar
Sandy Sharp

612-613. Weyerhaeuser Paper Company, Columbus Pulp and Paper Complex, P. O. Box 1830, Columbus, MS 39703-1830

Joe May
Rob Barker

614-619. Weyerhaeuser Paper Company, Research and Development, WTC 2H22, Tacoma, WA 98477

Dick Ericson
Margaret Gorog
Peter Gorog
Jules V. Gommi
Denny Hunter
Dick Shenk

620-621. Willamette Industries, Incorporated, Hawesville, KY 42348

R. Byron Alvey
William C. Mack

622. Worcester Polytechnic Institute, Department of Mechanical Engineering, 100 Institute RJ, Worcester, MA 01609

Robert N. Katz

623. Wyman-Gordon Forgings, P.O. Box 40456, Houston, TX 77240-0456

Ronald A. Wallis

624. Wyman-Gordon Company, 244 Worcester Street, P.O. Box 8001, North Grafton, MA 01536-8001

Sanjay N. Shah

625. X Form, Inc., 100 North Mohawk Street, Box A-9, Cohoes, NY 12047

Karl Shaw

626. 3M Industrial & Electronic Sector, Research Laboratory, Building 201-4N-01, 3M Center, St Paul, MN 55144-1000

Ross H. Plovnick

627. 127 West View Lanes, Oak Ridge, TN 37830

James Wessell

628-629. 14390 W. 30th Avenue, Golden, CO 80401

Richard Kleiner
David G. Wirth

630. 225 Linden Court, Sewickley, PA 15143

William E. Dennis

631. 2375 Dorr Street, Suite 1, Toledo, OH 43607-3406

Ray S. Richards

632. 715 Freeman Lake Road, Elizabethtown, KY 42701

John DuPlessis

633. 9208 Burning Tree Road, Bethesda, MD 20817

Samuel Goldberg